



**EXPERIMENTAL INVESTIGATION AND MATHEMATICAL
MODELLING OF MECHANICAL PROPERTIES OF SHOOKS
AND FINGER JOINTED TIMBER**

HOW SEOK SEAN

A thesis submitted in fulfillment for the Degree of
Doctor of Philosophy in
Chemical and Process Engineering

Department of Chemical Process and Engineering
University of Canterbury
New Zealand

2015

Table of Contents

Table of Contents	i
List of Tables	v
List of Figures.....	vi
Acknowledgement	x
Abstract.....	xi
1 Introduction.....	1
1.1 An Overview of the Potential of Wood Industry	1
1.2 Potential of Timber Industry in New Zealand with Special Reference to Radiata Pine	1
1.3 Challenges in Radiata Pine Timber Supply.....	2
1.4 Research Motivation	3
1.5 Research Challenge	4
1.6 Scope of study and limitation.....	6
1.7 Research Objectives	7
1.8 Organisation of the Thesis.....	9
2 Background and Summary of Literature	11
2.1 Background Information	11
2.1.1 Structural glulam and finger jointing	11
2.1.2 An Overview of Processing of Finger jointing	12
2.1.3 Stress Graded Feedstock for Glulam Making.....	14
2.1.4 Relating the Overall MOE of Glulam with the MOE of Glulam Laminates	14
2.1.5 Bending MOE and Relationship between MOR and MOE	19
2.1.6 Joint Strength in Finger Jointed Timber	20
2.2 An Overview of Modelling of Local MOE Variability, Laminating Stock and Glulam	21

3	Development of Relationship between Dynamic and Static MOE	22
3.1	Background and Justifications	22
3.2	Literature Review	22
3.2.1	Brief history on Non-Destructive Testing (NDT).....	22
3.2.2	Fundamental concepts of acoustics.....	23
3.2.3	The Fundamentals of Dynamic Stiffness	24
3.2.4	Relationships between Dynamic MOE, Static MOE and Static MOR	26
3.2.5	Modification and Transformation of Linear Regression Models	27
3.2.6	Factors Affecting Correlation between Dynamic and Static Properties	29
3.3	Experimental Methods	32
3.3.1	Considerations in the Experiment Design.....	32
3.3.2	Static Flexural Test	36
3.3.3	Modulus of Rupture (MOR)	37
3.3.4	Experiment I: Relationship between Dynamic and Static MOEs for Lower and Higher l/d Ratio Shook Specimens	38
3.3.5	Experiment II: Effect of the Number of Finger Joints on the Overall Dynamic MOE of Finger Jointed Timber.....	38
3.3.6	Experiments on Development of Relationship between Dynamic MOE of Shooks and Overall Dynamic MOE of the Corresponding Finger Jointed Member	42
3.4	Results and Discussions	45
3.4.1	Experiment I: Relationship between Shook MOEs at Lower and Higher l/d Ratios	45
3.4.2	Experiment II: Dynamic MOE of Sawn Timber and Corresponding Finger jointed Timber.....	49
3.4.3	Dynamic MOE at Different Shook Lengths vs. Overall Dynamic MOE for Solid Wood	56
4	Development of Models to Predict Finger Jointed Timber Mechanical Properties	58
4.1	Literature Review	58

4.1.1	Modelling of the Overall MOE based on Local MOE Variability in A Piece of Timber or Laminates	58
4.1.2	Modelling Glulam Properties	70
4.1.3	Simulation on End-joint Properties	74
4.2	Summary of models	74
4.2.1	Static Bending Stiffness	75
4.2.2	Relationship between Global MOE and Local MOE in Selected Standards	76
4.2.3	Effects of Length-to-depth Ratio and Challenges in Experimental Design	77
4.2.4	Digital Image Correlation (DIC)	79
4.3	Derivation of Elastic Curve in pure bending	80
4.3.1	Fundamentals on MOE in Tension and Compression	80
4.3.2	Theoretical Derivation for Transverse Deformation in Pure Bending	82
4.3.3	Location of the Neutral Surface of the region	86
4.4	Modelling of overall MOE in a Finger Jointed Timber under Bending	91
4.4.1	Modelling Discrete Variations in (i) Shook MOE and (ii) Shook Length along the Span using Moment-Curvature Analysis Approach	92
4.4.2	Modelling Assumptions	93
4.5	Modelling Moment-curvature Equation in a Single-point Loading System	97
5	Relationships between Local MOE of Shook, Overall MOE and MOR of Finger Jointed Member	100
5.1	Test Sequence – An Overview	100
5.2	Test Equipment	101
5.2.1	Test Method 1: Third-point Loading for Shook Specimens	101
5.2.2	Test Method 2: Single-point Bending for Finger Jointed Member	103
5.2.3	Deflection Measurement	105
5.2.4	Digital Image Correlation (DIC)	107
5.3	Preparation and Testing of Shooks	109
5.3.1	Pre-classification based on Industry Grading of Sawn Timber	109

5.3.2	Determination of Moisture Content	110
5.3.3	Testing on Shooks' MOEs	110
5.4	Results and Discussion - Shooks' MOEs.....	111
5.5	Experimental Design	113
5.6	Preparation and Testing of Finger Jointed Timber.....	116
5.6.1	Preparation of Finger Jointed Timbers	116
5.6.2	Testing on the Overall MOE of Finger Jointed Timbers	117
5.6.3	Testing on the Overall MOR Finger Jointed Timbers	118
5.6.4	Results and Discussion	119
5.6.5	Modulus of Rupture (MOR)	134
5.7	Economic Analysis.....	142
5.7.1	Shooks Costing Guide.....	142
5.7.2	Economic Analysis	143
6	Conclusions and Recommendations.....	147
6.1	Conclusions	147
6.2	Recommendations for Future Studies	150
	References.....	152
	Appendices.....	160

List of Tables

Table 3.1: Comparison between different types of Pythagorean Means	28
Table 3.2: Number of specimens cut from MSG8 radiata pine from the first cutting	40
Table 3.3: Number of finger joint per finger jointed timber and the number of replicates tested for dynamic MOE	40
Table 3.4: Combination of shooks to examine effect of shook length and location.....	43
Table 3.5: Combination of shooks to investigate effects of shooks' MOE and locations in a finger jointed timber	44
Table 3.6: Maximum and minimum MOE and the discrepancy between dynamic and static MOE at different dynamic MOE range from 4.0-10.0 GPa	45
Table 3.7: Results from Z-Test for correlations of $E_{\text{dyn}36}$ vs. $E_{\text{stat}15}$ and $E_{\text{dyn}15}$ vs. $E_{\text{stat}15}$ at alpha level 0.05 and 0.10, respectively	46
Table 3.8: Assessment of significance in correlations between E_{stat} and E_{dyn} with stepwise grouping of data based on nominal $E_{\text{dyn}36}$ from the lowest value of 4 GPa to different upper limit values.....	48
Table 3.9: Linear regression coefficients of determination (R^2) for the relationship between $E_{\text{stat}15}$ and E_{dyn} with consideration of sawing patterns	49
Table 3.10: Explanations for abbreviations used as predictor Y	49
Table 3.11: Explanations for abbreviations used as variable x	50
Table 3.12: Statistical T-tests on R^2 values between varies finger joint combinations	52
Table 3.13: Numerical modelling for all MSG8 specimens	52
Table 3.14: Numerical modelling on MSG8 specimens with shooks MOE combinations having standard deviation ≤ 0.6	53
Table 3.15: Numerical modelling on MSG8 specimens with shooks MOE combinations having standard deviation ≤ 0.5	55
Table 5.1: List of the number of shooks from Group G5 to Group L, arranged based on measure MOEs in the respective range of MOEs	111
Table 5.2: Experimental design matrix for research Objective 3	115
Table 5.3: The 4 mm finger joint profile	116
Table 5.4: Summary of range of model errors and Arithmetic mean error for Group B to O	133
Table 5.5: Linear regression for correlations between finger jointed MOR and overall MOE	138

Table 5.6: Publications for linear correlations between MOR and MOE.....	141
--	-----

List of Figures

Figure 2.1: Processing flow diagram for finger jointed wood (the processing flow is based on a case study at Niagara Sawmill, Invercargill, New Zealand	13
Figure 2.2: Glulam member made of different grades of laminations.....	16
Figure 3.1: Longitudinal wave in the direction parallel to the direction of displacement of a particle in compression and rarefaction. (adapted from Science Desk Reference[1])	24
Figure 3.2: Transverse wave travels in the direction perpendicular to the direction of displacement of a particle. (adapted from Science Desk Reference[1]).....	24
Figure 3.3: Effect of length-to-depth on fundamental frequency [71].....	31
Figure 3.4: An overview of experimental flow for dynamic-static tests.	33
Figure 3.5: Determination of sawn type according to growth ring orientation on the end grain section	34
Figure 3.6: Test setup for resonance frequency test	35
Figure 3.7: Excitation of vibration on a finger jointing shook to measure resonance frequency	36
Figure 3.8: First harmonic frequency peak detected by the FFT analyser.....	36
Figure 3.9: Test setup for a Third-point static MOE	37
Figure 3.10: Resonance excitation on 3600 mm untreated MSG8 radiata pine	41
Figure 3.11: The first harmonic resonance frequency received and calculated by the B&K FFT analyser	41
Figure 3.12: Shooks derived from the MSG8 radiata pine	41
Figure 3.13: Finger jointed MSG8 radiata pine	41
Figure 3.14: Finger jointed wood with Resorcinol Formaldehyde (R15) ready for heat curing	41
Figure 3.15: Excitation of vibration on finger jointed specimens tested in stages at reduced number of finger joints.....	41
Figure 3.16: Correlations and regressions for static MOE and dynamic MOE without sorting on sawn pattern	47
Figure 4.1: <i>Lag-k</i> serial correlation between segment A, B, C and D. <i>Lag 1</i> is the correlation between A and B; <i>Lag 2</i> is the correlation between A and C	64

Figure 4.2: Bending moment diagram describing the beam as a system made of 8 elements. The bending moment due to action denoted as M_s and M_R as the moment capacity. (Figure adapted from an unpublished article by Isaksson [96]).	65
Figure 4.3: A beam section with combination of low stiffness and higher stiffness (adapted from Kass (1975)[36])	67
Figure 4.4: The effects of E_l/E_h and L_l/L_g on the predicted overall MOE represented as percentage to the lowest MOE [36]	67
Figure 4.5: Weighting function for a simply-supported, centre-loaded bending span of length L . (Excerpt from F. Bechtel[43])	69
Figure 4.6: Illustration of a glulam beam made of different grades of laminating stock and each layer being segmented into different zones according to mechanical behaviour in bending application	71
Figure 4.7: Illustration of a Third-point bending	76
Figure 4.8: Linear relationship between stress and strain in the elastic region. Figure adapted from [119], pp. 39	80
Figure 4.9 : Illustration of changes in strain (Δx) in exaggeration.	82
Figure 4.10: Magnified mechanical illustration on Δx differentiates stress distributions across section Δx .	82
Figure 4.11: Illustration of stress distribution (adapted from Piter [2])	87
Figure 4.12: A graphical illustration of the total area under the integrands $f(x_l)$ to $f(x_5)$, representing independent integrands for shook elements A to E constituted in the finger jointing system	91
Figure 4.13: A finger joint member made of shooks with same shook length. Each shook has the measured E_i obtained individually prior to testing of the overall MOE of the finger joint member. The E_i values for shooks 1 to 5 (counting from left to right) are represented by E_1 , E_2 , E_3 , E_4 and E_5 . The location of x is referring to any point within the testing span, from L_0 to L . The finger joint member is subjected to static bending in a free-free boundary condition	93
Figure 4.14: Illustration of loading deflection at any point x along the test span. The red dotted line represents the imaginary neutral axis before P is exerted. The blue dotted inverse parabolic line is an exaggerated illustration of the imaginary neutral axis during loading. Maximum y deflection occurs at mid-span at $x=L/2$. The first section $0 \leq x \leq L/2$ is represented in orange cells, the second section $L/2 \leq x \leq L$ is represented in the yellow.	95

Figure 4.15: Single-point loading on a finger joint member made of segment of shooks with the corresponding MOE's from A to E.....	97
Figure 5.1: Tests sequence for static bending tests.....	100
Figure 5.2: A typical test setup for the Third-point static bending.....	103
Figure 5.3: Side view and aerial view for Single-point MOE bending test for finger jointed member at 120mm x 20mm x 2m.....	104
Figure 5.4: Third-point bending test configuration and bending moment diagram.....	106
Figure 5.5: An example for one of the image frame running on the Digital Image Correlations (DIC) analysis	108
Figure 5.6 (a) to (e): Shooks' MOE distributions displayed in groups G5, G6, G7, G8 and L. The frequency distributions were accompanied with mean, SDs and total number of samples in each group.....	112
Figure 5.7: Technical drawing of a 4mm finger joint.....	116
Figure 5.8: A typical single-point loading on a homogeneous beam and the corresponding bending-moment diagram	118
Figure 5.9: Distributions of the integrated segments of Shook 1 to Shook 5 for Group B to Group O	122
Figure 5.10: Displacement for Group B Sample B10 at y-displacement pixel 100.....	124
Figure 5.11: Displacement for Group J Sample J07 at y-displacement pixel 100.....	124
Figure 5.12: Displacement for Group L Sample L09 at y-displacement pixel 100	125
Figure 5.13: Displacement for Group E Sample E08 at y-displacement pixel 100	125
Figure 5.14: Displacement for Group N Sample N09 at y-displacement pixel 100	126
Figure 5.15: Displacement for Group I sample I01 at y-displacement pixel 100.....	127
Figure 5.16: Displacement for Sample M03 at y-displacement pixel 100.....	127
Figure 5.17: Single point loading on five finger jointed shooks denoted as Shook 1 to Shook 5 with shook MOE - E_1 to E_5 , respectively (recalled from Figure 4.15)	128
Figure 5.18: Comparison of MOE deviations between PhD model and arithmetic mean.....	133
Figure 5.19: Linear regression for relationship between MOR and overall MOE of finger jointed wood for Group B to S.....	139
Figure 5.20: (a) MOR test before loading for Group I and (b) during loading before rupture	140
Figure 5.21: Relationship between the average overall MOE and average MOR for Group B to Group O	141

Figure 5.22: Relationship between the projected overall MOE and gross profit in Scenario A and Scenario B.	146
---	-----

Acknowledgement

I am thankful to the Lord Almighty for this priceless walk and opportunity in His provision during the journey of this PhD. His grace is always sufficient.

*“I lift up my eyes to the hills – where does my help come from? My help come from the Lord,
the Maker of heaven and earth”*

~Psalms 121: 1-2

First and foremost, I wish to extend my gratitude to the government of Malaysia for the funding and support especially the Ministry of Natural Resources (NRE) and Forest Research Institute Malaysia (FRIM). To Mr Alan Hartley and the team from Niagara Sawmill, this project will not be accomplished without your support and assistance.

Special gratitude is extended to my senior supervisor Prof. Shusheng Pang for his patience and mentoring effort. I would like to thank the supervisory team - Dr. David Carradine, late Dr. Tan Yu Eng, and Dr. Chris J. Williamson for their guidance and support. Thanks to the technical staff at the Model Structures Laboratory Mr Alan Poynter for technical support and assistance. I would like to extend special thanks to Dr. Jason Cambridge and Dr. Brian Donohue for their relentless help and advice given during times in need. To Dr. Ong Wen Eng and Ms Tew Xiao Wei, thanks to their unconditional support and kind assistance. Thanks to the technical support and many pleasant sharings from the technical teams at the Chemical and Process Engineering. Not to forget, thanks to the supports given by many friends throughout the period of study.

For my parents and parents-in-law, thank you for your support and understanding. Last but not least, my deepest gratitude to my dearest hubby - John Koo Kong Ming for his patience, sacrifices, understanding, and has always been there for me.

I dedicate this thesis to my beloved hubby for his unconditional love and in celebrating the arrival of our little baby Joshua Koo.

Abstract

The issue on variability of mechanical properties within wood has found to be increasingly prominent in recent years. On the other hand, it is known that uniformity of wood properties is essential in quality control in the timber manufacturing such as manufacturing of Glued Laminated (Glulam) timber. The AS/NZS 1328 P2 specified that the overall mechanical properties of Glulam timber can be estimated based on the MOE of the finger jointed laminates and the arrangement of the corresponding laminates. In relating to the above standard, optimisation in the arrangement of shooks' location along the finger jointed laminate will enable determination of the overall MOE of laminates, as well as optimise the utilisation of feedstocks. In this study, a deterministic model was developed in relating the local shook's modulus of elasticity (MOE) with the overall MOE of the corresponding finger jointed timber based on the principle of the Moment of Curvature. The projected overall MOE is calculated as a function of lengths and MOEs of individual shooks in the finger joint timber. The effect of shooks' location can also be determined from the model. Numerical derivation of the model was addressed and the analyses of the relationships between the local shook MOEs, the overall MOE, and bending strength (MOR) were assessed. Experimental results showed that the model can effectively predicts the overall MOE, particularly on shook combinations with random and large standard deviations in shook MOEs. The errors of the predictive model were ranged from -8.17% to +0.81%. Results from the assessment on the relationships between the overall MOE and bending MOR indicated that wood failure in the combinations of small standard deviations shook MOEs was most likely to occur at the weakest point, however, wood failures may not necessarily occur in the shook with the lowest MOE in the asymmetrical MOE arrangements. This also applies to the finger jointed timber with combinations of shooks with large standard deviations for local MOEs.

In addition, the relationship between dynamic MOE of shooks and the static bending overall MOE were assessed. A linear regression has been suggested for the adjusted shooks dynamic MOE at 36 mm thickness. The predictability of the model could further improve when the shook MOEs were sorted according to sawing pattern and the proposed model for quarter sawn is suggested.

Lastly, economic analysis was performed based on the models available in literature and the developed model in this study. Models reported in the literature including the

arithmetic mean model and model based on the shook's minimum MOE. The results from economic analysis showed that the study's model was most cost effective in predicting the cost of shooks based on the predicted overall finger jointed MOE using the model as compare to the arithmetic mean and the minimum shook MOE method. In conclusion, the proposed model has demonstrated to be unique, simple, effective and robust in predictive applications.

1 Introduction

1.1 *An Overview of the Potential of Wood Industry*

The demand of timber and wood products for structural and non-structural use has called for the expansion of forest plantations especially in the last few decades. The increase in public awareness and acceptance towards plantation wood as a sustainable and renewable material has been the driving force for development and commercialisation of new wood products and corresponding processing technologies.

Wood and wood based products have gained their reputation in the building construction industry due to aesthetic beauty, higher strength-to-weight ratio, workability, better insulation, sustainability and renewability. Recently the application of wood as building material has also been highlighted for its flexibility to be used during disasters and for future buildings due to its capability to survive in natural disasters [3]. With better understanding of the advantages of timber application in construction, particularly in the seismic prone regions, the application of wood products are and will be of great potential as a natural material in meeting the current and future construction demand.

However, there are some limitations and restriction in applications of wood. For example, the application of wood in high-rise building is often limited as compared to its counterparts such as steel and concrete. In addition, wood in some cases, is regarded to be unreliable due to variability in mechanical properties (specifically in strength) and difficulty in maintenance. On the other hand, the ability and modularity of engineered wood products is often being overlooked. Nonetheless, development of new engineered wood products have been developed and applied in construction sector such as the glulam beam, plywood and laminated veneer lumber (LVL).

1.2 *Potential of Timber Industry in New Zealand with Special Reference to Radiata Pine*

Radiata pine (*Pinus radiata*), as the major exotic commercial plantation species in New Zealand, has been an essential commodity to the country. The harvested log volume has been around 20 million m³ p.a. since 2000 and 90% of the logs are radiata pine harvested from 1.7 million hectares under the sustainable forest management practice [4]. Radiata pine has been used for timber, pulp and paper, and engineered wood products, predominantly

plywood, LVL, MDF and glued-laminated (Glulam) timber. Approximately 75% of the timber grade radiata pine logs have been used for laminating stock in the country [5]. It is also noted that over 40% of the annually harvested wood was exported as logs due to the variable wood properties and processing limitation in New Zealand.

Looking at the potential of timber demand and the importance of radiata pine timber industry in New Zealand, it is evident that the industry has great potential to expand the production of engineered wood products. However, there are still plenty more melioration needed for the wood processing industry to gain greater confidence in the manufacturing sector.

1.3 Challenges in Radiata Pine Timber Supply

In last decades, New Zealand forest industry has transformed the wood supply chain from conventional plantation rotation to intensive forest management. This has promoted faster growth rate in reaching commercial log sizes, significantly improving the growth rate from 50 years or more to approximately 25 years [6-8]. The consequence of harvesting logs at a younger age has resulted in problems and difficulties in wood processing as a result of greater variability in strength, stiffness and stability due to large proportion of core wood (or juvenile wood), large knot sizes and high knot proportion [9]. The core wood has lower density and lower strength than the normal wood [10]. It has been reported that the concerned properties (strength, stiffness and stability) varied between trees and within the same tree - both along the radius and height of the tree. The above properties are closely related to the variability of wood density within a standing tree mainly attributed to the resource age [8]. The effect of inferior quality of the core wood in radiata pine has been exacerbated when plantation forests have shorter rotation especially those with less than 35 years [11, 12]. This is confirmed by measurements for trees harvested below 30 years which have a higher proportion of low-stiffness juvenile wood [13].

Research on lengthwise variability in wood properties such as bending stiffness and strength along a full sized timber is not new. The first research report was published in 1965 [14]. Modelling studies to describe and predict the variability properties have been reported extensively.

Another common challenge faced by most of the wood processing industry is the progressive increment in the overall production costs for the products to meet quality compliance and stringent customers' specification. The overall raw material costs (notably

the price of adhesives and feed stocks) can be volatile. Therefore, alternative solutions have been sought for keeping the industry being competitive.

1.4 Research Motivation

Finger jointed timber is a commercial engineered wood product which can enhance the overall wood properties by removing defect portions and re-gluing the defect-free portions (shooks) of a piece of wood. Production costs can be reduced by optimising the cutting and arrangement of the defect-free shooks. This requires comprehensive understanding on how the localised properties of the finger jointing shooks would affect the global properties after finger jointed. By having a good understanding on the mechanical behaviour of the individual components with respect to the overall performance of a full size jointed member, we could subsequently suggest optimum arrangements of shooks for desired mechanical performance in finger jointed member.

The finger jointed member can be used alone as an enhanced timber or can be glued together to form a large sized beam, termed as glulam. The glulam making requirements stipulated under the Australia/New Zealand standard [15] specifies that feedstock for structural grade glulam beam can either be preselected from machine stress grading or timber that has been docked free of defects. In the current industrial and timber design practice, the arithmetic mean or the minimum local MOE of the stress graded timber is used in determining the overall stiffness of the same piece of wood. Research studies in the past decades indicated greater variability of mechanical properties present within the same timber; as such the estimated overall stiffness of the timber could no longer be accurate. In view of estimating the mechanical properties specifically the overall MOE of a Glulam beam is based on the magnitude of MOE of the constituted finger jointed laminates [15], a reliable and accurate predictive method is necessary in determining the overall MOE of each laminate.

In addressing the aforementioned challenges as well as in choosing the viable type of feedstock, there are possibilities of undergraded or overgraded finger jointed feedstocks. On the other hand, upgrading laminates made of shooks from lower timber grades is possible in making the process more attractive in terms of economic viability. In doing so, the first-hand knowledge of the material properties in commercial mills is critical. Therefore, in this study, a finger joint timber processor in New Zealand North Island was firstly approached, whereby industry samples of the finger jointing blocks were obtained and tested before joining together to make finger jointed member. However, it was quickly found that this attempt was

not practical in achieving the optimum arrangement using statistic correlations solely based on experiments due to considerable variability of the raw wood material. Therefore, it was motivated that a theoretical model should be developed to simulate the overall properties based on the known sizes and properties of individual shooks. The model was then validated using results from experiments.

The end-user application of finger jointed timber can be structural and non-structural. Examples of the non-structural use are fascia wood and furniture whereas the structural examples are housing studs and glulam. The target of this project is on the structural application with focus on glulam. It is hoped that a cost-effective decision making model is established which can be used for making decision on optimum combinations of shooks with different lengths and stiffness. Ultimately the highest overall stiffness of the finger jointed timber is achieved using the available feedstock shooks. A cost analysis was performed to compare the prices of timber to be derived based on the study's model, arithmetic mean, and the minimum shook MOE criteria. The analysis was performed to demonstrate the economic benefits in the application of the model as compared to conventional prediction method in determining the overall MOE based on information on the corresponding local MOEs.

From literature review performed in this study, there are limited studies on simulation of the overall performance of the finger jointed timber and the processes involved. Most of the published modelling and simulation studies in finger jointing were mainly focused on establishing empirical correlations or modelling of the localized behaviour of end-products based on given shooks [16, 17]. There is little information available concerning the sensitivities of shook lengths and stiffness, and the effects of shooks combination on the overall properties of the jointed members.

1.5 Research Challenge

There are three main research challenges addressed as below and these challenges have been taken into account in the present study during the process of experimental design.

i. Length-to-depth Ratio

The bending deflection can be affected by shearing stress and it should be taken into consideration when the specimen has a small length-to-depth ratio geometrical dimension

[18]. Such phenomenon affects the bending stress as well. As the length-to-depth ratio decreases, the maximum load due to rupture is increased as a result of greater resistance activity taken place in perpendicular to the grain, also known as the horizontal shear stress. Besides, the compliance having high length-to-depth ratio specimen is also required during measurement of flexural waves in acoustic testing. A more in-depth discussion on length-to-depth ratio can be found in Chapter 2 and Chapter 5.

In a finger joint mill, the geometrical dimensions of finger jointing stocks (shooks) are often limited by available lengths of the defect free shooks. Considering the decision in complying with a suitable length-to-depth ratio specimen and the shook dimensions available in the processing mills, the present study has used shook dimensions of 400mm (length) x 20mm (depth) x 120mm (width) for the final phase of finger joint manufacturing and testing.

ii. Acoustic Measuring Device and Complexity in Acoustic Measurements

In the first phase of the study, it was planned that bending MOE of both the finger jointing shooks and the finger jointed specimens was measured using a resonance tool. The correlation relationships between the dynamic and static MOE's were then established using the statistical regression method at an acceptable confidence level. The bending strength of the finger jointed specimen was to be measured from static bending tests. Lastly, a regression correlation between static bending strength and dynamic MOEs was proposed which could be used as a predictive model.

The challenge in maintaining good repeatability in dynamic measurements was later found to have posed greater unexpected obstacles after initial attempts in experimentation. In addition, it was also identified that the movements of bending frequencies along the finger jointed span made of shooks with mixed of MOEs were obstructed by a few factors: i) variability in elasticity, ii) being diverged and obstructed due to dampening by multilayers of finger joint adhesives, and iii) being shifted with the grain orientations due to the change in geometry in the finger joints. The direction pursuing with using dynamic tool at that juncture was vague. From initial trials, it was concluded that specimen hanging during the dynamic measurement was implausibly unfeasible and questionable.

A change in experimental modification was then performed during the transitional phase. It was eventually decided that the mechanical static bending would be less complicated, achievable, and more straight forward especially in postulating the relationships

between shook MOE and the corresponding overall MOE of the finger jointed specimen. Therefore, the predictive modelling approach for overall MOE has been led into a different pathway - from a statistical modelling method to theoretical modelling.

iii. Selection of Appropriate Measurement Method for Static Bending MOE

Choosing a suitable boundary condition and test setup in acquiring the desired measurement outcome has been by far demanding. Each type of test configuration and boundary condition presents its pros and limitations. The selection process requires careful weighing between the pros and cons, therefore a certain degree of compromise was necessary. For instance, a Third-point loading has been chosen for measuring the bending MOE properties of shooks, a single-point bending was chosen for finger jointed wood, and a Third-point loading for bending MOR. The details and justifications for each test configuration and modifications are presented in Chapter 5.0.

1.6 Scope of study and limitation

The present study is focused on developing relationships between the bending stiffness of finger jointing shooks and the corresponding overall MOE and MOR of the finger jointed timber. The finger jointed timber will eventually be used for horizontally laminated glulam in structural application.

The experimental design for manufacturing and testing on finger jointed specimen has confined the number of shooks to five and the finger jointed timber length to 2 m. Therefore the theoretical modelling is based on the five segments of finger jointing shooks. The reason for not recruiting greater number of finger joints or having wider varieties of finger jointing matrix was limited by the number of suitable shooks available after screening. The preparation process prior to finalising the experimental matrix involved intensive screening process to ensure uniformity in specimens by excluding undesirable additional variables or defects. Furthermore, bending MOE of the shook specimens can only be identified after completion of shook bending tests. The last stage in sample screening and design of finger jointing matrix can only be finalised after that. There was already sizable number of shooks being excluded after screening, thus the initial draft for the finger jointing matrix was revised by limited resources. It was also apparent that expanding the experimental tests or increasing

the number of replicates would be infeasible, requiring prolonged time, and it is beyond the scope of study.

The final finger jointing matrix is catered to encompass both the common and extreme scenarios in MOE groupings. This is supported by test results which appeared to be sufficient for the scope of study.

The study has included bending strength in determination of the strength properties of finger jointed member. As mentioned earlier, the experimentation design was limited by available resources. There was only a single type of mechanical destructive test machine in the laboratory that can be used for testing. It has been noted that performing the tensile strength tests was difficult and may put the accuracy of test results at stake. Lastly, it would be plausible to share similarity in test configurations for an “apple-to-apple” comparison.

1.7 Research Objectives

The overall aim of the project is to develop a predictive model that can describe how different combinations of shooks with different lengths and stiffness (Modulus of Elasticity, or MOE) will influence the overall stiffness of a finger jointed member. The model will be validated with experimental results and used in the future for optimisation of finger joint manufacturing. The objectives of this PhD study are:

- Objective 1: To establish relationships between static MOE and dynamic MOE for individual shooks based on experimental results
- Objective 2: To develop a theoretical model to find the relationships between the MOEs of individual shooks and the corresponding overall MOE of the constituted finger jointed timber
- Objective 3: To validate the predictive model by performing experiments on finger jointed member made with combinations of different shook lengths and stiffness

From literature review, there are no deterministic models that can predict the overall finger jointed timber MOE based on individual shooks' MOE and lengths with various arrangements. It is envisaged that the models that quantify the effect of individual shooks' MOEs, lengths and locations on the overall MOE of the finger jointed member will be able to predict the total MOE, thus can be used to find the best finger joint shooks arrangements

prior to the finger joint processing. Once these models are developed and validated, utilisation of raw wood resources can be optimised for finger joint manufacturing and the overall production costs can be reduced.

To determine the MOE of individual shooks, both static bending technique and non-destructive technique (NDT) can be used. Due to the convenience and non-destruction nature, the NDT is preferred. However, a reliable correlation is needed to ensure that the NDT gives accurate MOE. The relationship between dynamic MOE and static MOE has been established in past researches, most of which were focused on samples such as full size timbers, beams and logs that have high length-to-depth ratio. The subject of this study is to firstly determine the MOE of finger jointing shooks/blocks [19] before jointing them. As the defect-free shooks normally have low length-to-depth ratio, model(s) is required to compensate the shear effect that could be introduced during excitation. In addition to MOE correlations, the relationship between dynamic and static MOE with the corresponding Modulus of Rupture (MOR) will also be investigated. Lastly, the sawing pattern of individual shooks may also affect the MOE correlation which has not been reported elsewhere before. This study will also examine the effect of sawing pattern on the models and how it can be improvised when the sawing pattern is included in the models.

In finger jointing processing, the optimum use of finger jointed shooks can be achieved by quantifying the localized mechanical properties of shooks as well as the effect of these individual shooks' properties on the overall finger jointed timber properties after they are jointed. Once this is known, shooks were sorted and jointed to achieve the maximum overall MOE. In order to achieve this target, a mathematical model has been developed in relating the individual shook properties with the overall MOE of the finger jointed property. This model can be integrated into a processing model for manufacturing glulam in the future.

1.8 Organisation of the Thesis

Chapter One provides an overview of the potentials of wood industry and issues with special reference to radiata pine in New Zealand. Following this overview, objectives of this study are listed and discussed.

Chapter Two is a collection of selected background information and an overall review of literatures on wood industry, finger joint processing and glulam processing while literature review on specific topic is extended in the following chapters. This chapter presents the overall review on finger jointing process, the Law of Mixture for optimisation in laminates arrangement in the processing of structural glulam, related standards on finger jointing for structural glulam, a brief discussion on selected researches on modelling of localised MOE and glulam. The chapter also discusses the importance of laminates MOE in glulam making and how bending MOE of laminating stocks is related to Glulam making. Lastly, the research assumptions, challenges, scope of study and limitations, and the research plan for the study are also presented.

The project has attempted using dynamic tests to ascertain the shooks' MOE profile prior to finger jointing using selected acoustic tools available in the university. A resonance-based acoustic tool and an ultrasonic device have been selected and the execution of the tests is explained in **Chapter Three**. The objective is to study the feasibility in utilising the tools on a noncompliant span-to-depth ratio shook dimension. Comparisons between the results from the acoustic tools and the static bending are discussed. The chapter concluded the feasibility and potential of the dynamic tools in finger jointing.

The emphasis of **Chapter Four** is to presents the theoretical modelling based on the principle of pure bending. Detailed literature review is presented including fundamental principle of the stress-strain theory incorporated with explanations on how the model is “retrofitted” based on case study in finger jointed lamella.

Chapter Five presents the experiments on validation of the rendered model developed in Chapter 4. Static bending of individual shooks was firstly tested to find MOEs of the shook pieces that will be used for finger jointing. Then the shooks were sent to a finger jointing company to manufacture finger jointed timbers. Finally the finger jointed timbers were tested in the lab to determine the overall MOE of each timber. The relationship between localised MOE values measured from segment of shooks and the overall MOE after finger jointing was established and compared with model predictions. The process of conducting experimentation is detailed in this chapter. These including preparation of raw material,

experimentation design, testing challenges, test configurations and justifications are detailed. Results from the modelling and the experimentations are presented.

In addition to having variable MOE's combination in the finger jointed matrix, variable in shook lengths has been introduced into the study. **Chapter Five** examined a range of lengths commonly found in finger jointing in the design matrix with fixed stiffness. Observations on how different combinations of shook lengths would affect the overall MOE of a jointed member are analysed and discussed. The relationship between MOR and MOE for varied shook lengths is also examined and discussed. Lastly, the economic analysis with different combinations of shooks MOE's in finger jointing was presented and the cost effectiveness of using the model as compared to using the arithmetic mean and the minimum of shook MOE within a finger jointed member was compared and discussed.

Lastly, **Chapter Six** presents the conclusion and recommendations for future studies.

2 Background and Summary of Literature

2.1 Background Information

2.1.1 Structural glulam and finger jointing

Glued laminated timber (glulam) was initially developed in early 1930's [20] and, in the following years, extensive research and development have been performed to improve its performance and manufacturing process including new adhesives, designs of edge-joint or end-joints, and the design factors assigned based on end-uses. One of the many advantages of glulam over solid timber is the flexibility in customising various grades of laminates at different layers in a glulam assembly based on design requirements. With optimum design and manufacturing, lamella of low grade materials can be used in combination of lamella of high grade materials to obtain and meet the required high strength and stiffness of the glulam.

There are two main categories of glulam – non-structural and structural glulam. The types of glued-joints in both categories can be subdivided into edge-joint (or edge-to-edge) and end joint (or face-to-face). The selection of the type of a glued-joint is dependent on its end-use. Lamination of edge-jointing is necessary when the available material is not sufficiently wide. On the other hand, the end joint is used in laminations of long materials and provides greater flexibility in making curved assembly. Some of the common subcategory of end-glued joints includes scarf joint, butt joint, and finger joint. Given the account that finger joint laminates is commonly used in laminated beams, it has been chosen as the focus in the present study. Different configurations and types of glulam beams, such as the horizontally laminated glulam, vertically laminated glulam, and curved laminated beam, are all dependent on the end uses accompanied with the respective working stress design. Horizontal lamination is referred to glulam with wide face of laminations laid parallel to the neutral axis with applied loads normal to the wide face of the lamination. The vertically laminated glulam stands loads parallel to the wide of the laminations. The primary use in horizontal lamination is for bending purpose while the latter type is often used in axial loading. In the context of this study, we have chosen finger jointed timber to be used as horizontal lamination for horizontally laminated glulam beam.

2.1.2 An Overview of Processing of Finger jointing

A typical processing flow diagram for manufacturing of structural and non-structural finger joint timber is shown in Figure 2.1 (A. Hartley, personal communication, 7th August 2009 and 18th Jul 2012). This processing flow is adapted from the industry partner.

In the production of structural finger jointed laminates, it has been specified in AS/NZS 1328.1 [21] that solid timbers for structural grade are required to be stress graded. The existing mill setup uses a resonance-based tool to measure the density and stiffness of a timber. Subsequently the timber is sorted into groups and the grouped timbers will go through a defect detector scanner known as Woodeye®. The location of the identified defects are marked and registered into the system. The Woodeye® system will decide the location of the defects based on input setting and docked accordingly. The clear finger jointed blanks (known as shooks) are sent for finger profiling, glue spreading, and finger jointing, and curing. Structural finger jointed timbers are sent for batch testing for stiffness bending to check on the overall MOE.

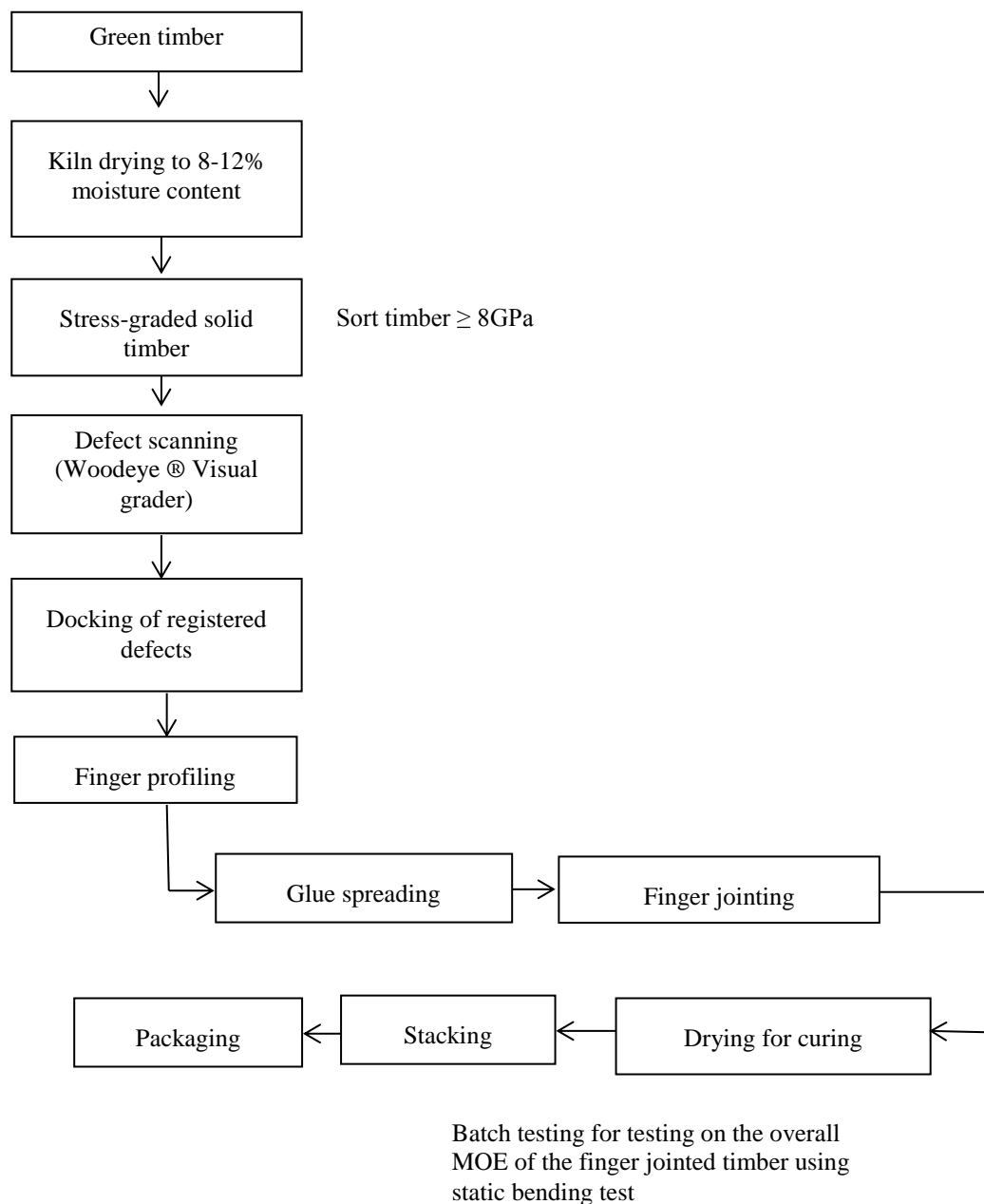


Figure 2.1: Processing flow diagram for finger jointed wood (the processing flow is based on a case study at Niagara Sawmill, Invercargill, New Zealand)

2.1.3 Stress Graded Feedstock for Glulam Making

The requirements of the Australia/New Zealand standard (AS/NZS 1328.1) for manufacturing of structural grade glued laminated timber has specified that timber feedstock has to be pre-stress graded before sending to finger jointing process to ensure reliability and durability. The standard has given provision to conduct stress grading in conformity with either of the specified grading methods including AS/NZS 1748, NZS 3631, AS 2082 and AS 2858 [15, 21]. The first standard listed above specifies the mechanical stress grading while the latter three standards (NZS 3631, AS 2082 and AS 2858) specify the visual grading for hardwood and softwood timber. It is documented that finger joints have the potential to reach at least 75% of the strength of clear wood in many species [22] and this is acceptable as most graded timbers have been allowed for at least 25% in strength reduction than that of in clear wood.

The Australia/New Zealand standard, AS/NZS 1748 version 2006, has defined stress grading as a classification system for structural timber which provides the characteristic properties for design purpose. Provision in the 2006 edition [23] specifies that stress grading of solid timber for structural glulam is subjected to non-destructive mechanical bending test about its minor axis. The stress graded timber is sorted according to the tested MOE. This can be achieved by means of visual, machine, mechanical or by other method of assessments. Each piece of the stress graded timber will be graded at a maximum length interval of 1200 mm and each piece can only have one single grade. In the case where there is more than one value of stress grading on a piece, the stress grade of the piece will be based upon the lowest indicated stress-grade.

2.1.4 Relating the Overall MOE of Glulam with the MOE of Glulam Laminates

i. Law of Mixtures based on Effects of End Joints in Various Parts of a Member

The Law of Mixtures is a mathematical expression which gives a property of a composite based on properties, quantities and arrangement of its constituents. In glulam manufacturing, this method is often used in optimising the arrangement of laminates to achieve the optimum property of the glulam. The laminates may have different properties and different thickness. The glulam made of laminates with varying properties responds towards

the external loads in a different manner. The principle of mechanics that lays the foundation in the composite arrangements is based on the stress distribution and the maximum stress location.

It is known that in a simple Three-point bending test on a beam, the maximum bending moment occurs at mid-span loading point. Bending moments decrease progressively away from the mid-span loading point towards the two end-supporting points, becoming zero at these two points. In a simple bending theory when constant bending moment is applied at a given point, the stress is linearly proportional to the distance from the neutral layer or axial layer. The maximum stresses occur at both faces, one on tension and the other on compression.

It is noteworthy that the maximum tension or the maximum compression of a beam is a dominant factor in the design of a beam [20]. Essentially under load, the beam starts failing at the outer lamination layers while layers inside have low stress which would not be sufficiently high to cause failure.

Likewise in a glulam beam design, consideration in satisfying the above physical phenomenon is required. The above understanding introduces an opportunity in optimising the arrangement of laminates to achieve the maximum strength of the glulam beam. For a bending member, it has well been known that a third of the total thickness of the beam is normally catered for higher strength and stiffness laminates at the upper and lower zone, while two-thirds of the inner laminates near the neutral axis can be allocated with lower strength and stiffness laminates without compromising the overall beam strength and stiffness. Therefore, finding laminates with suitable tensile/compression strength for the outermost layers of the member is required [24].

A new opportunity arise when considering the distribution of the bending moments along the beam length, where there is a possibility in optimising arrangements of shooks by using the lower quality ones in certain length locations where the moments are low while using high quality shooks where the moments are high [20]. However, the exact arrangements of shooks with variable properties and lengths on how that would mechanically affect the overall properties of a finger jointed timber require a quantitative description. Such knowledge is unavailable in literature and will require extensive study. Apart from having reliable mechanical effective properties of the jointed laminates, the understanding on how inner laminations in a glulam member are required to be staggered in relative to those of the adjacent layers is also essential for optimised performance of the finger jointed member. The transverse distance between one joint and the adjacent layer must be at least equal to the

lamination thickness [24]. Figure 2.2 shows the cross section of a typical horizontally laminated glulam member made with different grades of laminations.

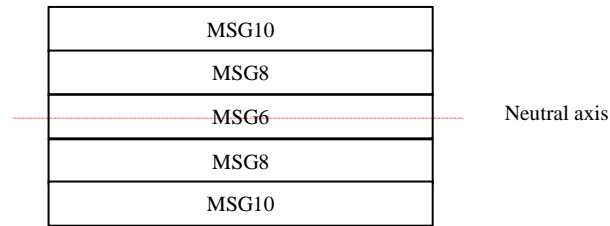


Figure 2.2: Glulam member made of different grades of laminations

ii. *Effects of Stressed Graded Finger Jointed Laminates MOE on the Glulam Performance*

The Australian/New Zealand standards have set guidelines for structural glulam grades as specified in AS/NZS 1328.1 (Part 1)[21] and 1328.2 (Part 2) [15]. The standards define the structural graded glulam timber in the form GL_{xx} , where xx is approximately the same as the characteristic modulus of elasticity in GPa.

AS/NZS 1328 Part 2 describes arrangement of laminated timbers based on graded MOE properties [15]. Formula in Equation 2.1 is proposed to determine the outer layers' MOE grades based on the inner layers' MOE, the desired ratio of mixed inner to the overall layers, and the target MOE of glulam to be manufactured. Despite that the actual use of the formula is for the case where members of GL grades is higher than the lowest in the given range in a listed table, the formula can be used as a guide in determining lamination matrix.

$$MOE_{outer} = \frac{MOE_{GLgrade} - p^3 MOE_{inner}}{1 - p^3}$$

Equation 2.1

Here, we have p as the ratio of number of inner laminations to the total number of laminations. The standard suggested a ratio of 0.7 for radiata pine with GL grades ranging from $GL8$ to $GL12$. In AS/NZS 1328 Part 1[21], the ratio between the outer and the inner laminations zones in a horizontally laminated beam that has been defined 30:70. The suggested ratio appeared to be in consistent with Freas and Selbo [20], whereby “one-third” rule of thumb has been allocated for the inner and outer laminating zones.

Other Modelling Methods for Glulam Properties:

More precise description of the relationship between the overall glulam properties and the individual laminates' properties requires a mathematical model. Most of the common modelling attempts in predicting the performance of glulam can be classified into three categories: (a) the empirical I_k/I_g modelling, (b) finite element modelling (FEM), and (c) transformed section method [25].

The I_k/I_g method is currently being adopted in the American standard - ASTM D3737 [26]. I_k represents the moment of inertia of the areas occupied by all knots within 6 in. of the critical cross section and I_g is the gross moment of inertia of the beam. The modelling method considers using the effect of strength reducing knots as a function of moment of inertia. The allowable design stresses in bending for a glulam member can be determined by multiplying bending stress indices by strength ratios for each lumber grade.

The FEM model determines the distribution of glulam beam strength and stiffness accurately by using the finite element method. Each lamination in the intended glulam design is divided into small elements known as cells. The input requirement of detail information such as the clear wood density, knot sizes and location are assigned into each cell. Finally, the probabilistic distribution of the intended characteristics is predicted using Monte Carlo simulation.

The third method adopted by the American Standard ASTM D3737 calculates the allowable load-bearing capacity known as the transform section method. The ASTM D3737 has adopted this method in conjunction with the I_k/I_g method.

The transformed section method considers glulam as a composite beam and made transformation of surface area analogous to a composite beam. The aim of this method is to transform different layers of laminates having varying moduli (MOE's). Laminations having lower MOE values are replaced by lesser areas of wood having the same MOE as the outer laminations using the force equilibrium concept so that simple elastic formula ($\sigma = \frac{My}{I}$) can be applied. In general, the transformed section formula for a member having two types of laminates, for example, Laminate 1 (inner laminate) and Laminate 2 (outer laminate) can be represented as follow:

$$\frac{E_1}{E_2} \cdot b_1 = b_2$$

Equation 2.2

where E_1 and E_2 are the moduli for the corresponding Laminate 1 and Laminate 2, respectively. b_1 is the width (or breadth) of Laminate 1 and b_2 is the transformed width of Laminate 2. Essentially this method transformed the width of Laminate 1 into Laminate 2 by multiplying the modulus ratio between E_1 and E_2 , known as the modular ratio, with the width of Laminate 1. Having the new transformed area for Laminate 2 results a new gross moment of inertia. From there on, we may calculate the stress and strain of the transformed section using the normal flexural formula.

Equation 2.2 explicitly entails how the MOE values of the laminates at different grades are converted to a common transformed area so that the effective stress and strain of the glulam beam can be calculated using the common flexural formula. In addition to Equation 2.2, Equation 2.1 can be referred to as a guide as to how the beam configuration can be dealt with.

With prior knowledge on allocation of laminates based on the stress profile explained in Section 2.1.5 (i) and (ii), it is known that laminations having lower MOE values can be allocated as the inner zone laminates near the neutral axis while those having stronger MOE should be placed at the outer region. This is analogous to the transformed section method in an irregularly glued section. The stress in the outer laminations under bending load can be computed using the moment of inertia value of the transformed section in the flexure formula, $\sigma = \frac{M y}{I}$. The stresses in weaker laminations can be computed by multiplying the

ratio of $E(\text{inner})/E(\text{outer})$ given by the transformed section $\frac{M y}{I}$ [24]. Rearranging Equation 2.2, the glulam beam with j -th number of laminate layers, the MOE of the beam can be represented as follow [27]:

$$E_b = \frac{\sum (e_j I_j + e_{aj} I_{aj})}{I}$$

Equation 2.3

where E_b is the MOE of glulam, I is the moment of inertia the glulam, e_j and I_j the MOE and moment of inertia of the j^{th} layer of laminate, respectively, e_{aj} and I_{aj} are the MOE and moment of inertia of the adhesive layer, respectively.

2.1.5 Bending MOE and Relationship between MOR and MOE

In glulam processing, laminate stiffness is used as the input parameter in predicting the overall performance of the glulam produced. From Equation 2.2, the configuration of a glulam beam is designed based upon the MOE value of each laminate layer. This principle is possible when the glulam is considered as a composite member made of different grades of laminations with different MOE values. A number of combinations of lamination is allowed to produce a given bending stress level. As such, the accuracy in predicting the effective MOE of the laminates has become the key importance in glulam processing.

The strength properties of these laminates can be predicted from the strength ratio (SR) using the “ I_k/I_g ” model from the transformed section method [28]. Note that strength properties used in Equation 2.2 can only be measured via destructive measurements. The measurement of laminates’ MOEs has become part of the essential parameters in predicting lamina strengths and in preserving its reusability. The MOE of the laminates can be measured using non-destructive methods such as by using mechanical stress grading.

Deflection is regarded as one of the most important design considerations for wood framing especially in longer span application [29]. It is used as a basis in determining how the finger jointed lamellae should be arranged in glulam application. Bending MOE is relatively easier to be obtained through flexural loading than the axial MOE which can be measured either via compression or tension tests. Accurate axial MOE is difficult to be obtained and the test itself is difficult to be performed. In addition, the mechanical modelling of the work is based upon stress-strain model from bending. Therefore, the MOE measurement represented in the present study is referred to bending MOE.

In the process in determining the bending MOE of a specimen, apparent MOE is often used as the measure of approximate variation of the local MOEs along the span. Correlation between MOR and MOE, by far, is one of the most common avenues in MOR predictive modelling. It was reported that the predictability of the MOR-MOE relationship can be improved when strength was compared with the lowest localized MOE value [30]. There are two conventional methods in determining the overall MOE of a finger jointed laminate: (a)

conservatively assuming the lowest local MOE value as the overall MOE of the jointed beam, and (b) the arithmetic mean of all the local MOE values [31, 32].

The efficiency of MOE as a strength predictor can be improved with condition whereby local MOEs are measured and these values could reflect point-to-point variation along the span. In relating this to glulam application, the accuracy of prediction for glulam performance is known dependable upon the evaluation methods of lamella MOEs.

In review of the relationships between MOR and the other mechanical parameters, it has been known that MOR, tensile strength parallel-to-grain and compressive strength parallel-to-grain are positively correlated with MOE in wood. These parameters are required for structural reliability analysis of wood frames [33]. In 1968, Orosz [34] initiated a study relating MOR using estimated strength ratio and found that strength ratio alone had not been able to effectively predict the strength property when no significant defects existed in the specimen. Another important discovery by Orosz is that when there is present of significant destructive defect, the defect would act as the weakest link in a chain primarily responsible for the failure.

Bending properties of a glulam beam is considered as a function of the knot size, MOE and MOR for each lumber laminate. While there is no better available alternative method in getting strength values, it is often obtained from predicted regression method or by finite element analysis.

2.1.6 Joint Strength in Finger Jointed Timber

The Weibull theory suggests that the number of finger joints will affect the overall tensile strength of a finger jointed member. The greater the number of finger joints, the lower the tension strength. In contrast, Frese's study [35] has found that finger joints were not a point of weakness and his results suggest the possibility of recovering grade strengths of wood by removing local defects. Nevertheless experiments were performed in the present study shows that the failure points were not commonly found at the finger joints. Therefore, in this study, the joints are considered to have the same MOE and MOR as adjacent shooks, and its effect is not included in the modelling.

2.2 An Overview of Modelling of Local MOE Variability, Laminating Stock and Glulam

Approaches in modelling of glulam and glulam laminates can be generalised as (i) statistical modelling, (ii) other stochastic modelling methods, and (iii) deterministic modelling. The scope of this study has targeted glulam as the end product. As such, related references in glulam modelling has been cross-referenced and included.

Studies on modelling of localised MOE in timber have been reported since early 70's. Most of the initial modelling studies were based on statistical correlations using local variability of MOE in relation to mechanical properties such as tensile strength [14],[36] and [37].

Meanwhile, there have been considerable interests in modelling and simulation of variability of stress graded timber performance based on local constituents. Most of these studies adopted various form of statistical modelling together with stochastic modelling such as Monte Carlo in their modelling approach [31, 38] and [39]. The aim of these researches is to simulate local MOEs based on statistical distributions of local MOEs. In addition, other models such as "Karlsruhe Method" by Ehlbeck *et al.* [40, 41] and model by Foshi [42] had included finger joint strength in the modelling of glulam beam. Further discussions on various modelling approaches are extended in Chapter 4.1.

Most of the undertaken studies were relating the localised properties with its overall properties and these models have been confined to stochastic methods. It is apparent that there is a lack of theoretical modelling studies that could explain the interest of the present study on how the individual constituents of bending stiffness in shook segments would affect the overall bending properties when these segments are jointed together. By far, there are two most closely related deterministic modelling by Bechtel [43] and Govindarajoo [32] of which models were derived from mechanical phenomena. Nonetheless these models are not readily applicable for the current research interest. It is hoped that the findings from this study would be able to contribute in filling in the knowledge gap of the aforementioned relationships. Hence, the feedstock resources could be optimised and the economic benefits finger jointed laminates in glulam processing.

3 Development of Relationship between Dynamic and Static MOE

3.1 Background and Justifications

Non-Destructive Testing (NDT) has been widely used in wood and timber related field for determination of wood properties. For example, it has been used as an inspection tool for on-site tree defects evaluation, assessment of mechanical resonance of a building for earthquake damage, in-service testing tool for infrastructures such as timber pole and wooden bridges [44, 45], determination of strength performance in timbers [46, 47] and wood composites.

The original plan for this study was intended to attain shooks MOE and finger jointed overall MOE using resonance frequency. Tests of static MOEs of shooks were conducted in a bending machine (flexural) for comparison with the dynamic MOEs. Tests of bending MOE and MOR of the finger joint timber were also conducted on the bending machine to establish statistical model(s) which relates the static bending MOR to the corresponding overall MOE.

Considering the fact that the length-to-depth (l/d) ratio of the shooks in finger jointing in practical operation was less than that specified in the standard, validation on the reliability of frequencies on smaller l/d was necessary. The validation tests were described in [Section 3.4.3](#) to ensure frequencies measured from the lower l/d ratio specimens were acceptable and reliable. Calibration models were suggested to improve the predictability of overall MOE of finger jointed member on the basis of the corresponding dynamic shooks MOEs. Lastly, the relationship was established between the overall dynamic MOEs and the corresponding static bending strength (MOR) for the finger joint timber.

3.2 Literature Review

3.2.1 Brief history on Non-Destructive Testing (NDT)

Development of Non-Destructive Testing (NDT) began in the 17th century using the Bernoulli beam deflection theory. This was followed by the development of Bernoulli-Euler beam theory by Euler, who introduced the elastic-curvature and flexural vibration. Timoshenko advanced the theory in 1921 by including shear and rotary inertia. The solutions

of vibration theory for a free-free beam including the influence of shear and rotatory inertia was fine-tuned a decade later by Goens. In 1948, Hearmon conducted resonance tests on wood according to the pre-existing measuring method which was later modified in 1961. The author explained the rationality of vibration experiment of beam that could be applied similarly in wood [48].

3.2.2 Fundamental concepts of acoustics

Acoustics is an interdisciplinary sciences involving propagated oscillation from a vibration source referred as wave. There are two ways in classifying waves based on: a) the ability to transmit energy through a vacuum, and b) the wave motions based on the direction of vibration of the medium relative to the direction in which the wave is moving [49].

The ability of the waves to be transmitted across a medium can be broadly sub-categorised into the mechanical waves and the electromagnetic waves. The mechanical system vibrates when oscillations and resonance are created through applied mechanical force, known as natural frequency [1]. It requires a medium to carry the transmitting energy and to travel through but it does not transfer the matter. Meanwhile, transmission of electromagnetic waves does not necessarily require a medium, hence can be transmitted in a vacuum condition. As transmission of energy on electromagnetic waves is beyond the context of this study, discussions on this subject have been excluded.

There are two types of wave motions that are measureable in a solid medium, namely the longitudinal and flexural waves. The longitudinal waves travel across the medium by vibrating back and forth in the direction of travel. The waves experience a series of compressions (high density) and rarefactions (low density) during travelling along the same place as the direction of wave propagation across the medium (Figure 3.1).

As oppose to the longitudinal waves, flexural or transverse waves moves in the direction of vibration of the medium perpendicular to the direction of the wave that is propagated through the medium (Figure 3.2). It is characterised by particles of the medium moving in the direction perpendicular to the direction of the wave travels. Flexural wave (also known as bending waves) is more likely to resemble static bending, hence is often related to static bending. It is easier to excite in a transverse manner than side way for longitudinal wave. Hence it is easier to obtain stiffness in a transverse plane and this suggests better practicality in a processing environment [50].

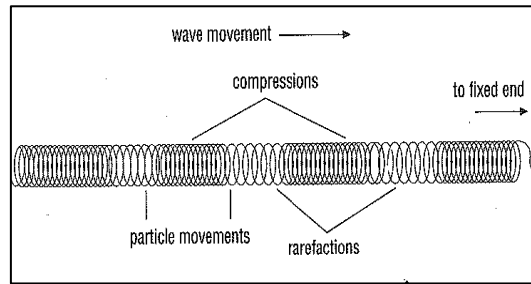


Figure 3.1: Longitudinal wave in the direction parallel to the direction of displacement of a particle in compression and rarefaction. (adapted from Science Desk Reference[1])

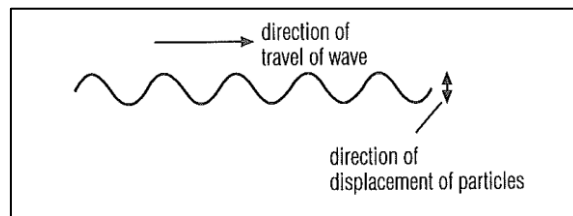


Figure 3.2: Transverse wave travels in the direction perpendicular to the direction of displacement of a particle. (adapted from Science Desk Reference[1])

3.2.3 *The Fundamentals of Dynamic Stiffness*

Elasticity is considered a property enabled recovery after distortion is applied by force and transmitted through a medium. All matters including gaseous, liquid or solid undergo distortion of shape or volume or both when force is applied. For most solids, the distortion can disappear and the distorted shape can be recovered once the external force is removed. The elasticity limit is the limit when the applied force has exceeded the recovery stage. In a compressed air environment it has a higher density when air molecules are compacted. The restoring force that returns the air molecule to its pre-existed density formation is known as dynamic elasticity [49].

Dynamic MOE value for solid materials can be equated as a function, based on either the frequency-domain measurement (i.e. frequency), or time-domain measurement from pulse response of a system (e.g. ultrasonic pulses). There are various NDT technologies available including tomography, near infrared scanning, acoustic-ultrasonic, stress wave, laser and ultrasound.

The acoustic measurement techniques can be broadly classified as frequency-domain measurements, and time-domain measurements. In a resonance-based system, oscillating force is applied to localise the resonant frequency where the acoustic waves travel within the medium back-and-forth repeatedly, from end-to-end resonating strongly at various frequencies, i.e. the fundamental frequency and its overtones. The velocity is calculated based on the first harmonic and the length of the medium. Predicting dynamic MOE by means of resonance using mechanical excitation method (hammer or other hitting tools) to generate vibrations is common and the tools are commercially available. The mechanism of the operation includes a hammer or other means to excite resonance waves and the magnitude of frequencies will be picked up by an accelerometer (e.g. piezoelectric transducer). The spectrum of frequencies is then analysed by a Fast Fourier Transform (FFT) spectrum analysing software from which the dynamic elasticity value of the testing sample is then calculated. Meanwhile, the time-domain measurement (or the Time-of-Flight (TOF) system) measures the time for the acoustic waves travel along the length of the medium between two points known as the path length. The pulse response of a system is an essential indicator of material characteristics. Velocity is used as the measured parameter [51].

Most resonance vibration methods are based on the Euler-Bernoulli theory applicable to slender beam with high length-to-depth (l/d) ratio (details on l/d are elaborated in Section 4.2.3). The models used in deriving dynamic MOE for longitudinal and flexural waves were developed from the Elementary Rod Theory, and Bernoulli-Euler Beam Theory used in relating a beam. These theories assumed long slender member and neglects any shear deformation due to it [52]. Kirchhoff theory is normally used for plates where both the Bernoulli-Euler and Kirchhoff theories are interchangeably used.

Concise descriptions on the model derivation of dynamic elasticity on wood specimens was first published by Hearmon[53, 54] who found that constant elasticity could be computed from frequency of vibrations, density and the radius of gyration of the cross section of wood specimen. Although the properties of wood depart from assumptions in the fundamental theory where homogeneous and perfect elasticity are expected, Hearmon argued that the above theories could be used in wood with some modification. In fact the dynamic elasticity methods provide reliable MOEs in most situations [54].

The origin of the elastic modulus from bending waves (or flexural frequency) was derived from Equation 3.1 which can be elaborated as Equation 3.2 under a free-free support measured on the first harmonic ($n=1$). The derivation details can be referred to

$$E_{f_Dym} = \frac{4\pi^2 L^4 f^2 \rho}{m^4 k^2}$$

Equation 3.1

where E_{f_dyn} is the dynamic elasticity of bending waves, ρ is the density, l the length of specimen, $m = \frac{(2n+1)\pi}{2}$, and k is the radius of gyration of the cross-section.

$$E_{f_Dym} = \frac{0.9464 l^4 f^2 \rho}{d^2}$$

Equation 3.2

From Equation 3.2, the magnitude of frequency in an object is determined by its density and length. The speed or velocity of sound is a constant. It is also dependent on the wave length (λ) which is related to the length of specimen (l).

3.2.4 Relationships between Dynamic MOE, Static MOE and Static MOR

Extensive research can be found in literature on acoustic wave propagation in clear wood, timber and logs [51], and most of these studies used longitudinal frequency. In the reported studies, longitudinal frequency were more commonly used than the flexural frequency as the former produces strong signals for predicting the bending strength [55]. Nevertheless, it has been found that concentrated knot diameter ratio (CKDRm) is the most important factor in determination of the tensile strength.

Correlations between the flexural vibration MOE and the static bending MOE can be found in the reports of Halabel [56], Ayarkwa [57] and Vikram [58]. The study by Vikram [58] has shown that Douglas fir had a more significant correlation between the dynamic transverse MOE and static MOE ($R^2 = 0.83$) than the southern pine species ($R^2 = 0.70$) [56]. The study conducted by Ayarkwa [57] used three African species to predict the static bending MOE from dynamic MOE using the longitudinal vibration. The author suggested dynamic MOE could be used for sorting short lengths timber during finger jointing instead of using density [59]. In relation to that, Hirakawa reported there was no relationship between MOE and wood density despite strength had a linear relationship with density [60]. However, a

contradictory finding was reported by Ayarkwa where the correlation between dynamic MOE and density in three African species were found to be very strong ($R = 0.97$).

Despite that there have been sizable number of studies indicated strong relationships between dynamic MOE and static bending MOE with acceptably well fitted regression models, it is crucial in discerning the discrepancies between measurements from types of waves motions and measurement techniques. The differences between acoustic measurements have been analysed as follows.

In general, dynamic MOE from resonance tests were usually found to be higher by 5 to 15% than the static bending MOE. Ayarkwa [57] reported that the dynamic MOE was 10% higher than the counterparts of static MOE. The MOE based on the TOF measurements were approximately 10% higher that derived from resonance [58]. A wide range of coefficients of determinations ($R^2 = 0.09-0.81$) were observed on the correlations between MOE measured with TOF tools and static MOE [51]. Studies reported by Weyerhaeuser Ltd. shows a reasonable predictive strength at $R^2=0.64$ [58]. Meanwhile, it was reported the strength of correlation between stress waves and static bending was slightly lower than between transverse waves and static bending [58].

In addition, reports also showed that there were differences between dynamic MOEs derived from longitudinal vibrations and that from flexural vibrations. The transverse dynamic MOE is usually less than the longitudinal dynamic MOE by approximately 1/5 to 1/3 [22]. Ayarkwa [61] also found that the dynamic MOEs measured using longitudinal frequencies were 5% to 8% higher than the flexural MOE [62]. Meanwhile the flexural resonance in Ayarkwa's study with 1% to 2% discrepancy compared static flexure [61]. A much greater discrepancy for the longitudinal dynamic MOEs (12-20% higher than the static MOEs) was reported in the study of Hossein *et al.* [63]. Considering the discrepancies and uncertainties in the NDT measurements, the statistical models correlated from these measurements need validation and modification in order to give reliable and accurate prediction of the wood properties.

3.2.5 Modification and Transformation of Linear Regression Models

i. Pythagorean Means

In the wood property measurements, the data can be arranged in different ways to obtain mean values for a given property. One of them is categorised as the Pythagorean

means and was selected for computation of variable X in the regression modelling. Arithmetic Mean (AM), Harmonic Mean (HM), and Geometric Mean (GM) are grouped as the Pythagorean means.

Table 3.1: Comparison between different types of Pythagorean Means

Arithmetic Mean (AM)	Harmonic Mean (HM)	Geometric Mean (GM)
$AM = \frac{1}{n} \sum_{i=1}^n x_i$	$HM = \frac{n}{\sum_{i=1}^n \frac{1}{x_i}}$	$GM = (\sum_{i=1}^n x_i)^{1/n}$
The Arithmetic Mean (AM) of a data set is the summation of the numerical values in the data set divided by the number of sample (n).	Referred as the reciprocals of arithmetic means. It is essentially useful in determine the average of rates.	The n^{th} root of the product of the numbers. It is used as indicator of the central of tendency or the typical value of a set of numbers by using the product of their values instead of summation of the set of numbers.

ii. Combining and Averaging Sound Levels

The formula used in the summation of sound pressure levels with n incoherent radiating source [64] can be referenced in Equation 3.3. This formula is applicable in combining different levels of sound pressures, sound intensity, or sound powers in a logarithmic scale which compresses these values into a manageable range.

$$L = 10 \log_{10} \left(\sum_{i=1}^n 10^{\frac{L_i}{10}} \right)$$

Equation 3.3

In relation to the present study which relates the overall MOE with its constitutional shocks at different MOEs, Equation 3.3 has been inspired to be applied in the context with slight modification by replacing the individual sound intensity (L_n) with shook dynamic MOE values (MOE_i). Hence, the variable MOE in the linear regression is included as in the following equation:

$$x = 10 \log_{10} \left(\sum_{i=1}^n 10^{\frac{MOE_n}{10}} \right)$$

Equation 3.4

3.2.6 Factors Affecting Correlation between Dynamic and Static Properties

i. Location in a tree

It was found that the speed of stress waves in red pine decreased with increase in tree diameter at the same tree age. This was presumably due to the high growth rate that lower stiffness wood is produced in the faster-grown trees. The same was true for static MOE values which, however, decreased at a slower rate with diameter compared to the dynamic MOE. This deviation between the dynamic and static MOE values can explain the increased discrepancies for wood cut from large diameter logs. The observation was attributed to the tendency for stress-waves to follow the high density and stiffness path through the log. The multivariate regression model which had included the diameter effects, acoustic speeds and density was found to be more accurate in predicting the static MOE than that of only with fundamental frequency. This was further explained by Wang that the multivariate regression model had inevitably reduced the errors in density and MOE measurements by taking into account on the stem form and geometrical imperfections [65].

ii. Knots

The presence of knots and the knot size affect the acoustic wave propagation in wood. This observation was validated by systematically removing whorls from logs in which case the acoustic speeds were found to be increased [65]. It was known that there is a significant negative correlation between velocity and knot area ratio (KAR). The speed of wave transmission decreased with higher KAR. In the cases that the size of larger knots constitutes a larger part of the total volume of the wood member, lower overall stiffness and strength are expected from the dynamic measurements. This can be explained by the grain deviation around the knot which is more significant for larger knots [65]. During the wave propagation across the locations where grain deviation is high, the waves travel through a “less parallel” segment than across a straight-grained sample [66]. Another form of explanation was given

by Gerhards (1982) that the possibility of lagging in stress-waves timing through knots due to irregular waveform caused by the wave lagging behind the knot. Therefore, the measured static MOE values were reduced and the acoustic speeds were slower when knots were present [65].

Hossein et al. (2011) [63] in their study examined the discrepancy in modes of vibrations from which knot-free logs were found to have clear symmetry peaks while knot-containing logs yielded asymmetrical spectra, resembling a twin-peak in the frequency spectrum. Similar observation was discussed by Yang et al. (2003) [67] that one or sometimes two major peaks occurred in flexural resonance testing.

Wood temperature and moisture content will also affect wave propagation. In general, higher moisture content and temperature of the test specimen result in decrease in the acoustic speeds [68, 69]. In a separate study [48], moisture content was found to negatively affect the dynamic MOE when the moisture content was increased from 5 to 35%.

iii. Length-to-depth (l/d) ratio

As discussed in Chapter 2, the length-to-depth (l/d) ratio of the test specimen is an important factor in dynamic measurements of wood properties [70]. The fundamental theory of dynamic elasticity is based on the thin-wall theory where large l/d ratio in the specimen is required. Dynamic measurements became smaller as the l/d increases as a result of interference from the shearing waves.

There are limited studies on dynamic MOE using small wood specimens. The rationale behind the unpopularity of resonance testing using small wood specimens was discussed by Nakai [71] who proposed that the minimum l/d ratio was to be larger than 6. Nakai demonstrated that for wood specimens having l/d ratio less than 5 (value of length by height as shown in Figure 3.3), it is impossible to detect the fundamental vibration frequency because such relatively short specimen could not be regarded as a bar for vibration.

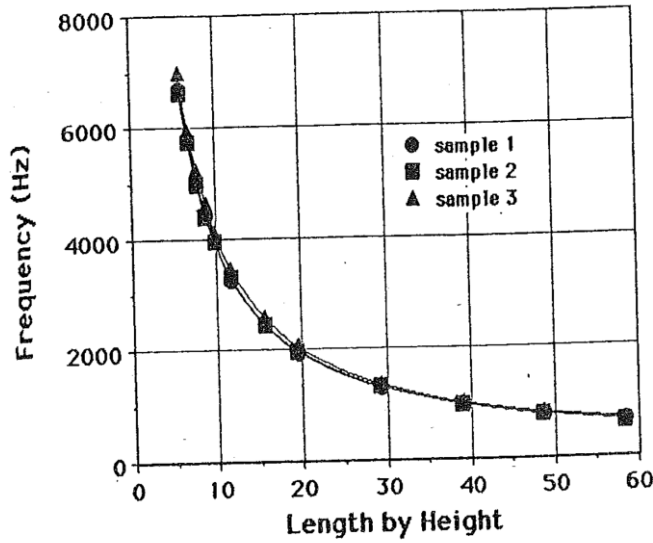


Figure 3.3: Effect of length-to-depth on fundamental frequency [71]

Other studies have been found in literature on small clear specimens to evaluate the reliability of dynamic MOE. Amongst these studies is that by Haines et al. [62] who used $1(d) \times 5(w) \times 30(l)$ mm spruce wood specimens on flexural vibrations. Machek et al. [72] in a separate study used specimen at $10 \times 5 \times 100$ mm and Ilic [73] used specimens of $1.6 \times 20 \times 120$ mm. However, the dynamic MOE values obtained from the above studies were in reasonable agreement with those from the larger specimens and static bending MOEs. Ilic's study achieved remarkably high correlations between dynamic and static MOEs for 55 different species ($r = 0.96-0.98$). The author commented that in order to obtain consistent dynamic MOE on short clear small beams, the uniformity in width and thickness of the sample was crucial, especially with flexural vibrations [73]. Despite that results from the above studies had showed promising correlations using small clear specimens, ones should bear in mind that the l/d ratio has significant effect on the dynamic MOE measurement.

3.3 *Experimental Methods*

3.3.1 *Considerations in the Experiment Design*

i. Overview and Challenges

The nominal shook dimension at 120 x 36 x 300 mm is typical in New Zealand finger jointing manufacturing. However, this dimension has a relatively low l/d ratio, i.e. approximately 8. Considering that the recommended l/d ratio specified in the first version in ASTM D198 [74] was between 11 and 15, there is a possibility that the dynamic MOE would include the effect of shear stresses. In order to investigate the effects of the l/d ratio on the experimental results, specimens with l/d ratios from 8 to 15 were used in the dynamic MOE measurements. In producing high l/d ratio for the matching specimens, the original specimens with a low l/d ratio were plane to reduce thickness. The details of this part of experiments are described in Section 3.3.4.

After the above tests on examination of slender ratio (l/d) effect, the dynamic MOE of shooks were correlated with that of the corresponding overall MOE of finger jointed member. Prior to finger jointing, shook specimens with greater varieties in dynamic MOEs were grouped and combined to produce the test finger jointed timber. In this part of study, a small scale study was designed using MSG8 untreated radiata pine as control for comparison with more detailed studies to establish more rigorous models to relate overall MOE of finger joint timer with individual shooks used in the corresponding timber. The details of this part of experiment are described in Section 3.3.5

After the above study, shooks were re-arranged based on designed combination of shooks with various dynamic MOEs and lengths. The purpose was to determine the effect of shook's MOE, length and location in the finger joint timber. The experimental results are also used to validate a mathematical model that would relate shook MOE with the corresponding overall MOE in finger jointed specimen. Nevertheless, the experimental design and the mode of shook MOE measurements had been changed due to circumstances explained in Section 3.4.3. The following flow chart (Figure 3.4) depicts an overview of the experimental sequence. Note that the dotted box in the flow chart represents planned experimentation in earlier stage but has been dropped as a result of lacking of good repeatability due to complexity in acoustics measurements in finger jointed samples. Modelling approach is replaced with theoretical modelling and validated using mechanical testing.

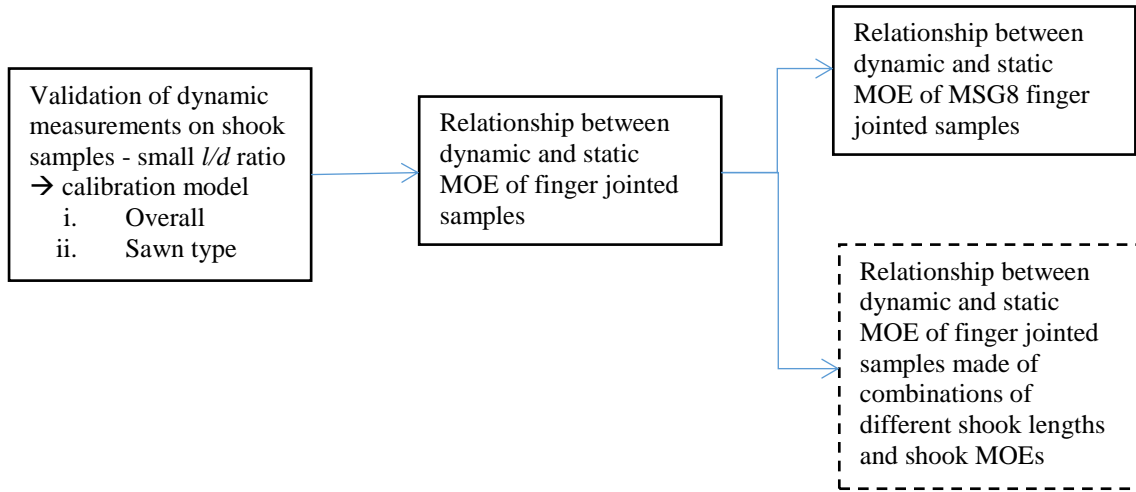


Figure 3.4: An overview of experimental flow for dynamic-static tests.

ii. Preparation of Test Specimens

New Zealand radiata pine samples with nominal dimension 120 x 36 x 290 mm were used in dynamic and static bending tests. All radiata pine testing specimens were cut to nominal size 120 x 36 x 290 mm and delivered to the Structural Lab at University of Canterbury by the industry collaborator. Samples received were firstly conditioned at 65% relative humidity (RH) and 21.1°C to achieve 12% moisture content prior to testing. Basic profiles for each sample including density and moisture content were measured and recorded.

iii. Sample Profiles and Determination of Sawing Pattern

Specimens after conditioning were grouped according to sawing pattern, namely flat sawn, quarter sawn and semi sawn. Determination of the sawing pattern using end-face cross section visual sorting can be difficult in some cases when the growth ring curvature may change from one ring to another. Therefore, growth ring profiles on the specimen's end-face cross section were pre-screened with visual sorting and this was followed by quantitative sorting using modified method of Olson [75]. In Olson's method, the requirement of sawing pattern grouping is based on growth ring orientation on the end-face cross section or end grain of a test piece. There are two steps in determination of the sawing pattern. Firstly, growth ring angles of each ring on the end face cross section are measured. If the angle is

equal to or greater than 45° , then this ring is considered to be quarter sawn while otherwise it is flat sawn. After this, the area percentage of flatsawn and quarter sawn on the sample's cross section computed. The sample is regarded as a certain sawing pattern when this pattern area is over 50%. In this study, Olson's concept was adopted but the second step is modified. Test piece is regarded as the semi-sawn if a sawing pattern area is less than 70% or the competitive sawing pattern area is more than 30% (Figure 3.5). For example in Figure 3.5 by using a 5° protractor running across the horizontal line of the cross section of an end grain surface we will be able to mark growth rings that meet the tangent line of the protractor. Therefore we will be able to compute the percentage of coverage of sawn type and conclude sawn type category based on the definition above.

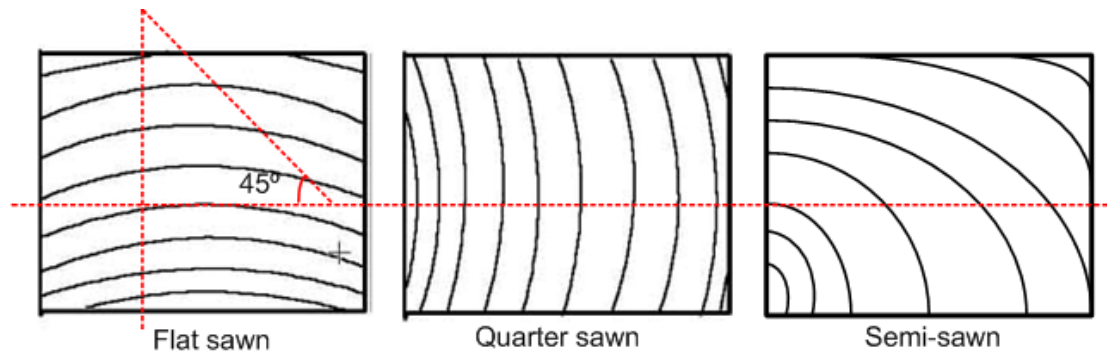


Figure 3.5: Determination of sawn type according to growth ring orientation on the end grain section

iv. Dynamic Tests

The experiment was carried out on a commercial *Brüel & Kjær Handheld 2260 Investigator* Fast-Fourier Transform (FFT) analyser. The FFT analyser measured and computed the discrete Fourier transform and the frequency. The first mode fundamental frequencies were measured from which the dynamic MOE for each specimen was estimated. The analyser was set at frequency of 5 kHz and speed of vibration of 3.112m/s^2 . The FFT analyser is connected to a piezoelectric sensor (Accelerometer *B&K 4507*) as receiver.

In the test, the wood specimen was supported by bubble-wrapped supports. The idea was to create air-support to simulate a “free-free” boundary condition. The test setup is illustrated in Figure 3.6. A plastic cable cord as the impact hammer was used to lightly tap on the plane surface during testing. The fundamental vibration frequencies were recorded from the FFT analyser (Figure 3.7).

Pilkey [76] suggests that the two nodes under a free-free support should be at $0.224 l$ and $0.776 l$, respectively, measured from left end of the specimen. l is the specimen length. These node locations are similar to those recommended by Timoshenko [77] who located the nodes at 20% of the length from each end. In the present study, Pilkey's suggestion has been adopted. A *Deltatron*® piezoelectric accelerometer was used as a sensor to pick up the magnitude of the resonance frequencies. The FFT analyser was set with full scale at 3.270 m s^{-2} . The accelerometer is placed on the estimated first harmonic of the antinodes (that will be between the two supports) for optimum reception while the two supports were placed on the nodes positions.

The location of tapping has to be approximately at the antinode position (refer to Figure 3.6). Specimen was impacted and excitation was generated to obtain flexural resonance created in the state of free support condition. The resonance was detected using piezoelectric transducer that was brought in contact with the front face (tangential plane) of the specimen and the resonance frequency was then determined with a spectrum analyser. The transducer was placed in close proximity to a second antinode to receive the radiated sound from the specimen due to excitation of the hammer. The electrical signal generated in the transducer was sent to a digital storage oscilloscope with fast Fourier transform processing capability. The frequency of the strongest resonance displayed on the screen of the FFT analyser was the resonance frequency to be used for calculation of MOE.

The weight of the hammer for excitation must be sufficient to deliver enough energy to excite the vibrations, meanwhile shall not be too heavy to avoid delivering too much momentum to carry the specimen with it as a rigid body. From this consideration, a light elastic plastic cable was selected. Flexural resonance was determined by tapping lightly on the radial face at mid-length (tangential direction) of the specimen.

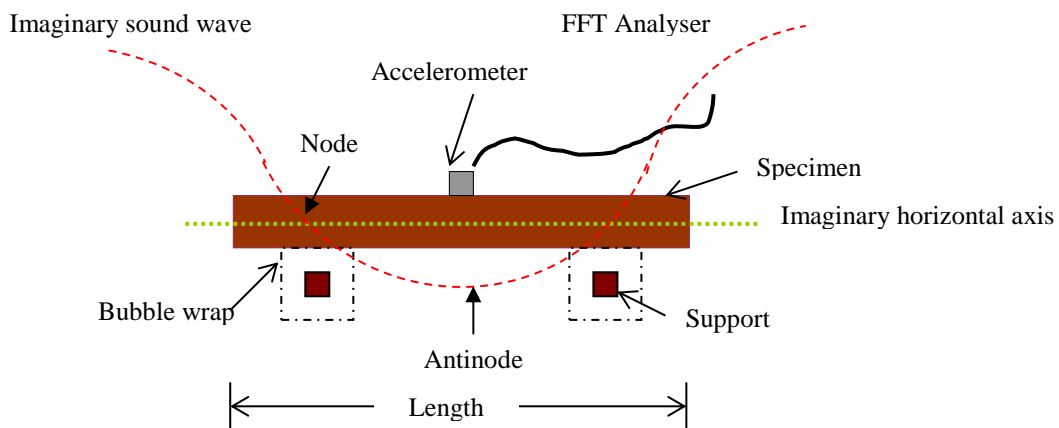


Figure 3.6: Test setup for resonance frequency test

The expected first harmonic frequency range can be estimated using Equation 3.2 based on assumption of an arbitrary MOE. The computed frequency can later be used as a guideline as to which frequency range and location of the peak would be expected. Following that, the frequency from the peak was selected to calculate the actual dynamic MOE.

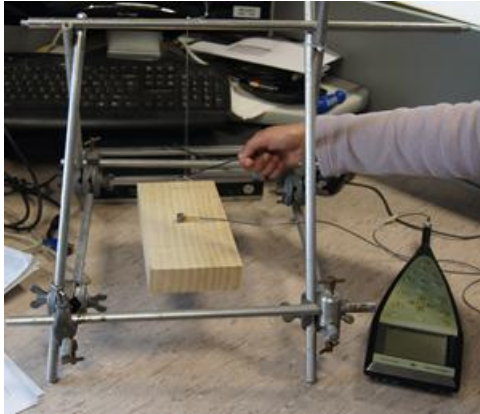


Figure 3.7: Excitation of vibration on a finger jointing shook to measure resonance frequency

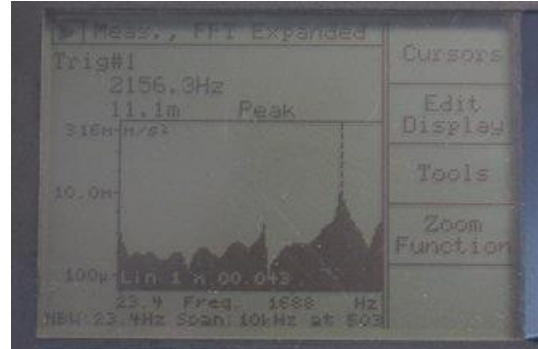


Figure 3.8: First harmonic frequency peak detected by the FFT analyser

3.3.2 Static Flexural Test

Third-point loading static bending was carried out to measure the static MOE of the shook specimens following the standard ASTM D198-5a [74]. The test setup for flexural bending is shown in Figure 3.9. Tests were conducted on an Instron of UTM Model A212-201 with a load cell Type 2511-308. The maximum load for the sample with dimension of 25 x 15 x 256 mm was calculated to be 1 kN. The loading speed was set at a constant rate of 1.0 mm/min. 8 mm linear potentiometer was used to measure the displacements of each side of the wood sample. The linear potentiometers were attached on a “U” shaped yoke deflectometer hanging on both sides of the wood sample. Displacement at the neutral axis between the shear-free loading zones was measured and used in computation of static MOE.

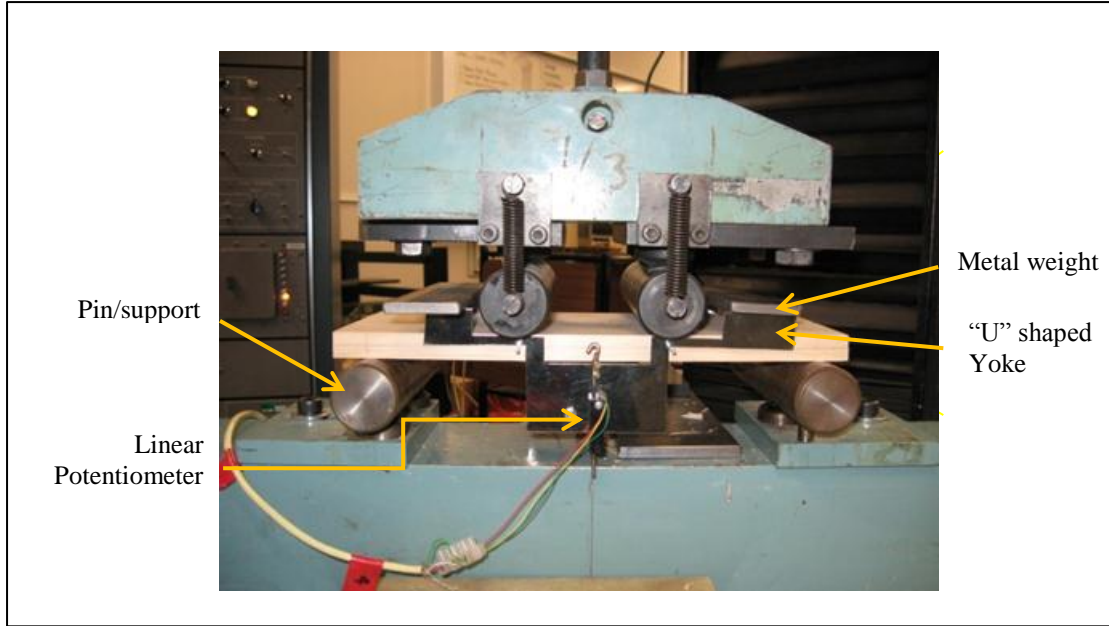


Figure 3.9: Test setup for a Third-point static MOE

3.3.3 Modulus of Rupture (MOR)

Flexural Modulus of Rupture (MOR) is defined as the maximum load carrying capacity of a member in bending and proportional to the maximum moment on the specimen. MOR is commonly used as an accepted criterion of strength [78]. In this study, the same set of samples undergone dynamic MOE measurements were used MOR tests based on AS/NZS4063.1:2010 [79]. The relationship between the corresponding dynamic MOE, static MOE and static MOR were assessed. Equation 3.5 and was used to compute the static MOR under the two-point bending.

$$MOR = \frac{P_{\max} L}{bh^2}$$

Equation 3.5

where P_{\max} is the maximum load borne by the specimen to failure, L is the span of the specimen between the two supporting points, b the width and h the thickness.

3.3.4 Experiment I: Relationship between Dynamic and Static MOEs for Lower and Higher l/d Ratio Shook Specimens

All shook samples were visually sorted prior to dynamic testing and this was followed by sawing pattern sorting using the criteria and methods described in section of “*Sample Profiles and Determination of Sawn Type*”. 74 samples were selected and divided based on the sawing patterns into three groups of flat sawn (45 pieces), quarter sawn (12 pieces) and semi-sawn (17 pieces). All samples were then conditioned to targeted 12 % moisture content in a conditioning room; the density of each sample was measured thereafter.

For comparisons between dynamic MOE and static MOE, tests were conducted in for the same samples with two thicknesses. Firstly, shook samples with thickness of $d = 36$ mm were used for measurement of dynamic MOE (denoted as E_{dym36}). After this, the thickness of the same set of specimens were reduced to 15 mm ($d = 15$ mm) and the resonance frequencies were re-measured. The computed dynamic MOE at $d = 15$ mm was denoted as E_{dym15} . The purpose of the thickness reduction was to assess if the span to depth ratio has any effect on the correlation between dynamic MOE and static MOE. The 36 mm thick shooks are commonly used in industry but the span to depth ratio in this case is around 7.1 ($=256/36$) which is less than the specified values in standards. However, this ratio is increased to 17 when the thickness is reduced to 15 mm ($= 256/15$).

After measurements of dynamic MOEs, all of the 15 mm thick samples were tested for static MOE and MOR subject to Third-point loading in the Instron described above. The static bending MOE is denoted as E_{stat15} .

From the above experiments, MOE_{dym36} and MOE_{dym15} were compared with MOE_{stat15} . Regression analysis was firstly performed to assess the correlation between E_{dym36} and E_{dym15} . Effect of sawing pattern was also assessed using linear regression method. Finally the correlations between E_{dym} , E_{stat} and MOR were assessed.

3.3.5 Experiment II: Effect of the Number of Finger Joints on the Overall Dynamic MOE of Finger Jointed Timber

In this part of study, full size finger joint timber were tested to measure the dynamic MOE and the results are used to assess the effect of the number of finger joints on the overall dynamic MOE of the finger joint timber. All of the shooks were cut from untreated MSG8 kiln-dried radiata pine sawn timber.

Firstly, the sawn timber boards with nominal size of 90 x 45 x 3600 mm were selected from local retailers. These boards were measured for the resonance frequency. A lifting fabric strop cord was used to hang the board on a gantry crane and the two ends of the strop was tied to the ends of the testing member (Figure 3.10) simulating a free-free support system. The positions of the specimens where the cord ends were tied onto were based on 0.224 and 0.778 of the total length [76]. A T086C01 Impact hammer with force sensor and super soft rubber impact cap was used for excitation of vibration. Figure 3.10, Figure 3.11 and Figure 3.15 illustrate the test setup and testing for the resonance frequencies using the *B&K* FFT analyser.

After the tests, the sawn boards were cut to shooks of three different lengths: 900mm, 600mm and 300 mm. Some of the 900 mm and 600 mm lengths were further cut to 300 mm lengths. The number of the overall 300 mm shook length specimens from a piece of full size member was dependent on the number and position of knots in the full size board, thus all 300mm shooks were carefully produced to ensure they are defect free. The number of specimens of different lengths cut from the full size boards is summarised in Table 3.2. Specimens were labelled based on the corresponding original full size member number so that the origin of full size member could be traced and related to during analysis.

Resonance frequency tests were conducted in each stage as soon as the specimens were cut to shorter length. When the specimens had reached the desired shook length 300mm, resonance frequencies of these specimens were obtained from the FFT analyser and were tested on the test setup mentioned in [iv\) Dynamic Test Setup](#) (Figure 3.8).

Table 3.2: Number of specimens cut from MSG8 radiata pine from the first cutting

<i>Sample at original 3600 mm</i>	Number of specimens derived		
	<i>900mm</i>	<i>600mm</i>	<i>300mm</i>
1	1	0	5
2	2	1	1
3	1	2	1
4	1	2	1
5	1	1	2
6	0	1	5
7	1	2	2
8	0	0	4
9	1	1	1
10	1		Lost in processing

All of the shooks prepared in the above section were sent to the industry partner mill for finger jointing. Each finger jointed specimen was made of 5 shooks that were originally derived from the same piece of full size board. The shooks were finger jointed with micro-joint and glued with Resorcinol Formaldehyde (*R15*). There were a few samples that were made of random mix of different length shooks due to discontinuation in finger jointing and some unavoidable processing errors. However, the shooks to make one finger jointed timber were cut from one MSG 8 full size timber board.

After the finger joint timber boards were manufactured, the overall dynamic MOE for the finger jointed members were measured with the same test setup described earlier (Figure 3.15). Resonance frequencies were measured in stages as the finger jointed members were reduced from 5 finger jointed wood to various segments which were then measured for dynamic MOE as summarised in Table 3.3.

Table 3.3: Number of finger joint per finger jointed timber and the number of replicates tested for dynamic MOE

<i>Number of segments cut from a finger jointed timber board</i>	<i>Total number of segments tested</i>
5	10
4	14
3	15
2	14



Figure 3.10: Resonance excitation on 3600 mm untreated MSG8 radiata pine

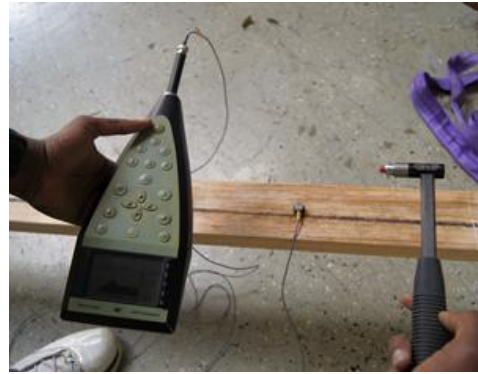


Figure 3.11: The first harmonic resonance frequency received and calculated by the B&K FFT analyser



Figure 3.12: Shooks derived from the MSG8 radiata pine



Figure 3.13: Finger jointed MSG8 radiata pine



Figure 3.14: Finger jointed wood with Resorcinol Formaldehyde (R15) ready for heat curing



Figure 3.15: Excitation of vibration on finger jointed specimens tested in stages at reduced number of finger joints

3.3.6 Experiments on Development of Relationship between Dynamic MOE of Shooks and Overall Dynamic MOE of the Corresponding Finger Jointed Member

The last part of the experimentation in this chapter was to examine the effect shook combinations on global MOE. The measurements are as follows:

Experimentation was the same as presented before except for using E-longitudinal waves to deduce the dynamic E. The dynamic MOE profile for each shook was first measured, and these shooks were then finger joint to produce full size timber. The full size finger jointed timber static MOE was determined with bending tests. Dynamic MOE of the finger joint member was also measured but only for probing purpose.

Experiment design, constants and assumptions:

- The respective lengths of the shooks were 260mm, 240mm and 200 mm.
- The thickness of the shooks was set at 36 mm.
- The width of the shooks was 125 mm.
- Each finger joint member consisted of 5 shooks. The 5 shooks were carefully selected and located in the finger jointed member as given in Table 3.4 and Table 3.5.
- To determine the effect of different lengths of shooks, shooks with similar MOEs were selected (the replicate for each finger jointed timber was 5).
- To determine the effects of shook's MOE and location, 260mm shooks were carefully selected and used.
- Finger joint strengths were assumed to be uniform and stronger than the strength of wood.

Table 3.4: Combination of shooks to examine effect of shook length and location





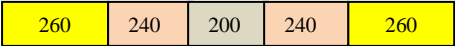
Shook lengths combination	No. of Replicates
 <p>To include some longer lengths amongst shorter pieces</p>	5
 <p>Control group: only include shortest shooks</p>	5
 <p>Reverse of row 1: include some shorter pieces among the longer ones.</p>	5
 <p>Additional of 240 mm: the longer ones in the middle (240 mm and 260 mm) and include some short ones at the end.</p>	5
 <p>The longer/longest ones at the edges while the shortest is arranged at the mid-span</p>	5

Table 3.5: Combination of shocks to investigate effects of shocks' MOE and locations in a finger jointed timber

Groups	S1	S2	S3	S4	S5	Standard Deviations
A1	5	5	5	5	7	0.89
A2	5	5	7	5	5	0.89
B1	5	5	6	6	7	0.84
B2	5	6	7	6	5	0.84
C1	6	6	8	6	6	0.89
C2	6	6	6	6	8	0.89
Control	7	7	7	7	7	0.45
E1	6	6	6	8	8	1.10
E2	8	6	6	6	8	1.10
E3	6	6	8	6	6	0.89
E4	6	8	8	6	6	1.10
E5	8	6	6	8	8	1.10
G1	7	7	7	7	5	0.89
G2	7	7	5	7	7	0.89

Note: The above matrix has only considered samples with dynamic MOE up to 8 GPa. Samples having MOE greater than 8 GPa were excluded.

3.4 Results and Discussions

3.4.1 Experiment I: Relationship between Shook MOEs at Lower and Higher l/d Ratios

i. General

74 full size sawn timber boards were selected in this part of experimentation with four regarded as outliers and thus being discarded from analysis. Hence, 70 boards were used to prepare shook specimens. All shook specimens were conditioned to the targeted 12% moisture content. The range of measured moisture contents were between 11% and 12.9% ($11.76 \pm 0.08\%$ at 95% confidence interval). The range of dry density was between 360 kg/m^3 and 560 kg/m^3 with most of the samples falling in the range of 400 kg/m^3 and 500 kg/m^3 ($451.24 \pm 10.78 \text{ kg/m}^3$ at 95% confidence interval).

Table 3.6 gives a summary of classified results for dynamic MOE and static MOE for shook specimens with thickness 36mm and 15mm. The minimum and maximum measured MOE values were divided into five categories (A to E) based on $E_{\text{dym}36}$ values. These values did not take into account the effect of sawing pattern. The difference between $E_{\text{dym}36}$ and $E_{\text{stat}15}$ and the difference between $E_{\text{dym}15}$ and $E_{\text{stat}15}$ were computed to identify the discrepancies between dynamic stiffness and the corresponding static stiffness. Increment in discrepancies between dynamic and static MOE at thickness 15 mm and 36 mm appeared indiscriminately increased as the magnitude in dynamic MOE groups increased from A to E.

Table 3.6: Maximum and minimum MOE and the discrepancy between dynamic and static MOE at different dynamic MOE range from 4.0-10.0 GPa

Dynamic MOE Group	Dynamic MOE Range Sorted by $E_{\text{dym}36}$ (GPa)			MOE-difference based on Data Sorted by $E_{\text{dym}36}$ (GPa)	
	$E_{\text{dym}36}$	$E_{\text{dym}15}$	$E_{\text{stat}15}$	$E_{\text{dym}15} - E_{\text{stat}15}$	$E_{\text{dym}36} - E_{\text{stat}15}$
A: 4.0-6.0	4.81 - 5.99	4.77 - 6.85	4.03 - 6.74	(-)0.92 – (+)0.81	(-)0.83 – (+)0.78
B: 6.1-7.0	6.32 - 6.80	6.44 - 7.69	6.18 - 8.75	(-)1.60 – (+)0.69	(-)1.95 – (+)0.16
C: 7.1-8.0	7.10 - 7.99	7.33 - 9.55	7.40 - 10.79	(-)2.58 – (+)1.40	(-)3.10 – (-)0.02
D: 8.1-9.0	8.07 - 8.99	7.08 - 10.70	7.83 - 12.52	(-)3.23 – (+)0.58	(-)4.33 – (+)1.17
E: 9.1-10.0	9.78 - 10.98	8.50 - 10.17	9.37 - 14.27	(-)4.10 – (-)0.10	(-)3.71 – (+)1.33

ii. Comparison of Results between E_{dym36} and E_{dym15} with E_{stat15}

Statistical analyses were conducted using Z-test at alpha levels of 0.05 and 0.10 to assess the significant difference in the means between E_{dym36} and E_{stat15} and the difference in the means between E_{dym15} and E_{stat15} . The Z and P values as given in Table 3.7 indicate that the null hypothesis could not be rejected and that the difference in means of E_{dym36} vs. E_{stat15} and in those between E_{dym15} vs. E_{stat15} were statistically insignificant. The relationship between dynamic MOE at thickness 36 mm and 15 mm is considered to be valid, suggesting the correlation between E_{dym36} and E_{dym15} can be used to determine the static MOE.

Table 3.7: Results from Z-Test for correlations of E_{dym36} vs. E_{stat15} and E_{dym15} vs. E_{stat15} at alpha level 0.05 and 0.10, respectively

	Alpha level 0.05		Alpha level 0.10	
	E_{dym36} vs. E_{stat15}	E_{dym15} vs. E_{stat15}	E_{dym36} vs. E_{stat15}	E_{dym15} vs. E_{stat15}
Mean	1.0664	0.8261	1.0664	0.8261
Z value	1.0402			
Z critical two-tail	1.9600		1.6449	
P-value	0.2982		0.2982	

In most cases (approximately 60%), E_{stat15} values were slightly higher than those of E_{dym36} and E_{dym15} . On average, E_{stat15} values were approximately 11% and 6% higher than those of E_{dym36} and E_{dym15} , respectively. The difference was consistent with the findings of Haines *et.al.* [62]. In the present study, a comparison was made for MOE measurements of flexural resonance, longitudinal resonance and longitudinal ultrasound. It was found that the flexural resonance was merely 1 to 2% higher than the corresponding static flexure values. Considering that different FFT analysers may give different resolutions to the frequency readings, this range of discrepancy were considered to be within acceptable experimental error.

Correlations between E_{stat15} vs. E_{dym36} and E_{stat15} vs. E_{dym15} were fitted to assess the reliability of the measured dynamic MOE. When all data were compiled and correlated without taking into consideration the effect from sawing pattern, the data showed the linear regressions are generally closely related and well fitted with R^2 value of 0.73 for E_{stat15} vs. E_{dym36} and 0.80 for E_{stat15} vs. E_{dym15} (Figure 3.16). This observation is in agreement with findings from the Z-test. However, there is significant data scattering from the regression

lines observed for E_{dym} ranging from 7 to 9 GPa. The correlation strength starts to diminish as E_{dym36} greater than 8GPa, i.e. Group IV and Group V (Figure 3.16 and Table 3.8).

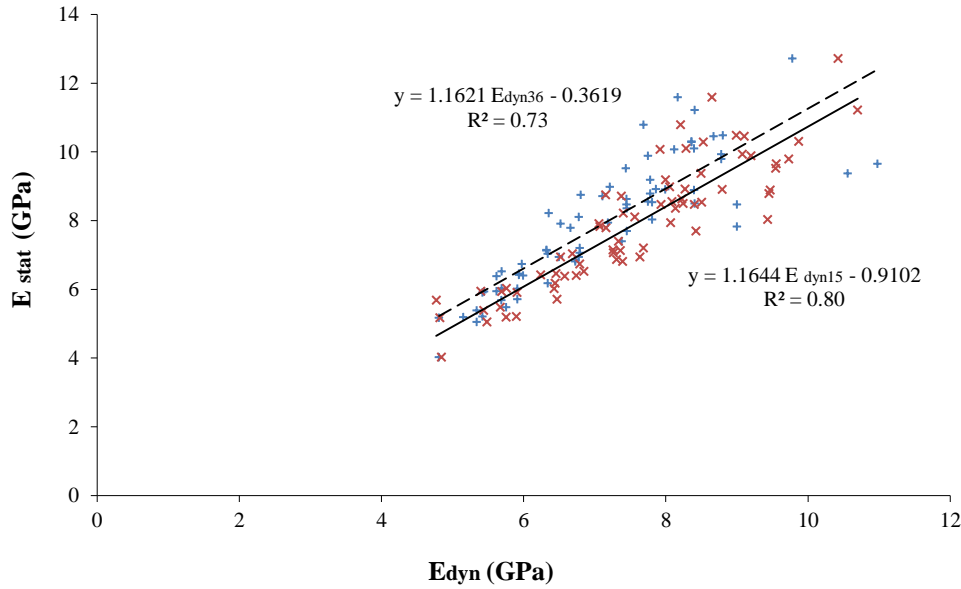


Figure 3.16: Correlations and regressions for static MOE and dynamic MOE without sorting on sawn pattern

Verification on the predictability of the trend lines was explored using stepwise grouping on E_{dym36} at different lower and upper limit values and the results are presented in Table 3.8. In general, segmentation of dynamic MOE into Groups I to V show a slight improvement in correlation strength between E_{dym36} and E_{stst15} as compared to that without sorting and grouping except for Group I. The stiffness range in Group III (4.0 – 8.0 GPa) for E_{dym36} vs. E_{stat15} has the highest strength in correlation (R) and coefficient of determination (R^2). The predictive linear equation for this range is suggested to be used as the calibration model for shooks with l/d ratio = 8 at 36 mm thickness. Although the differences in correlation strengths between Group IV and V were fairly small, the number of shook specimens with E_{dym36} greater than 8.0GPa was only 27% of the total. Greater discrepancy in correlation strength could be taken place. Hence, a more conservative measure in specifying the calibration model application was preferred for the range 4.0 - 8.0 GPa.

Table 3.8: Assessment of significance in correlations between E_{stat} and E_{dyn} with stepwise grouping of data based on nominal E_{dyn36} from the lowest value of 4 GPa to different upper limit values

Dynamic MOE group (GPa)	Sort by E_{dym36}				Sort by E_{dym15}			
	No. of samples	Reg. Coeff.	Intercept β	R^2	No. of Samples	Reg. Coeff.	Intercept β	R^2
I : 4.00- 5.99	20	0.44	+3.01	0.66	12	0.34	+3.63	0.20
II : 4.00- 6.99	35	0.50	+2.79	0.74	23	0.73	+1.69	0.62
III : 4.00- 7.99	53	0.57	+2.45	0.82	41	0.61	+2.51	0.73
IV : 4.00- 8.99	67	0.59	+2.38	0.79	58	0.60	+2.65	0.78
V : 4.00-10.99	70	0.63	+2.16	0.73	70	0.69	+2.15	0.80

iii. *Effect of Sawing Patterns on E_{dym} and E_{stat}*

The effect of sawing pattern on E_{stat} and E_{dym} was examined and the coefficients with the coefficients of determinations (R^2) for the respective sawn type are summarised in Table 3.9. The correlations for E_{stat15} vs. E_{dym36} and E_{stat15} vs. E_{dym15} may be further improved by taking into account the effect of sawing pattern. In general, all three sawing patterns had provided favourable correlation coefficients with acceptably well linear regression fittings.

Correlation of coefficients in the table indicates the highest R^2 was achieved in quarter sawn specimens. Improvement in predictability in the quarter sawn model can be explained by the formation of its growth ring orientation where they were mostly aligned at $> 45^\circ$. The quarter sawn specimens appeared to be anatomically more “homogeneous” than other sawn groups and thus less impedance to the resonance of flexural waves. Despite that l/d ratio is lower in the 15 mm thickness shooks, the correlation strength in quarter had slightly improved.

Application of calibration models based on sawing pattern may improve in predictability of the regression when mass identification on sawing patterns and sorting are available. The calibration model for quarter sawn samples at thickness 36 mm is proposed as Equation 3.6. Nevertheless sorting shook based on end-face growth rings may still be problematic in the current state of the local processing mill.

$$E_{stat} = 1.57 E_{dym_Quarter\ sawn} - 3.15$$

Equation 3.6

Table 3.9: Linear regression coefficients of determination (R^2) for the relationship between E_{stat15} and E_{dyn} with consideration of sawing patterns

Sawing Pattern	E_{stat15} vs. E_{dym36}			E_{stat15} vs. E_{dym15}		
	Regression Coefficient	Constant β	Coefficient of Determination (R^2)	Regression Coefficient	Constant β	Coefficient of Determination (R^2)
Quarter	1.57	-3.15	0.92	1.51	-3.55	0.86
Flat	1.17	-0.18	0.71	1.09	-0.16	0.77
Semi	0.93	+0.83	0.71	1.12	-0.50	0.79

3.4.2 Experiment II: Dynamic MOE of Sawn Timber and Corresponding Finger jointed Timber

This part of study attempted to examine the effects of number of finger joints on the overall MOE of the finger jointed timber. Modelling were established in three stages, including statistically modelling on all specimens, followed by analysis of data set with standard deviations less than 0.6 and eventually on lesser than 0.5.

Correlation fitting was conducted on predictor (overall MOE) and regressand (local MOEs) in statistical modelling. Assorted numerical expressions were produced accordingly as defined in Table 3.10 and Table 3.11. Descriptions on the numerical manipulations on regressand x are summarised in Table 3.11. Manipulations on the shooks dynamic local MOE_i in terms of variable MOE_i were based on simple linear equation variable x . The summary of the proposed equations with corresponding coefficients of determination (R^2) as a measure of the predictability of the model is tabulated in Table 3.13, Table 3.14 and Table 3.15 where Y is the predictor, m the coefficient for the variable MOE_i , and C the constant.

Table 3.10: Explanations for abbreviations used as predictor Y

Terms for Predictor	Abbreviations	Descriptions
Overall MOE	Y	Measured overall dynamic MOE for the finger jointed specimens
Global Class	Y_{class}	Measured dynamic MOE of specimens that has been classified as the MSG grades value according to the measured value and there were no rounding up of the measured values were conducted.
Global Class	Y_{r_class}	Measured dynamic MOE of specimen that has been classified as the MSG grades according to its measured value. The measured values were round up and classified into MSG grade value according to the rounded up to the

		nearest integer.
	$\log_{10} Y$	$\log_{10} Y$ where Y is the predictor.
	$\frac{1}{Y}$	The reciprocal of predictor Y

Table 3.11: Explanations for abbreviations used as variable x

Terms for Regressands	Abbreviations	Descriptions
Shooks MOE	MOE	Measured dynamic local MOE for the shook specimens
Assigned Class for local MOEs	MOE_c	Measured dynamic MOE of specimens that has been classified as the MSG grades value according to the measured value and there were no rounding up of the measured values were conducted.
	$\log_{10} MOE_i$	$\log_{10} MOE_i$ where MOE_i is the dynamic local MOE for shook i .
Reciprocal local MOE		$\frac{1}{MOE_i}$ The reciprocal of predictor MOE_i for the dynamic local MOE in shook i . The value of the MOE can be minimum($\frac{1}{MOE_{min}}$), maximum ($\frac{1}{MOE_{max}}$), or the arithmetic mean ($\frac{1}{MOE_{mean}}$) of the constituted shakes
Arithmetic mean	A	$A = \frac{1}{n} \left(\sum_{i=1}^n MOE_i \right)$ where n is the number of specimens
Harmonic mean	H	$H = \frac{n}{\sum_{i=1}^n \frac{1}{MOE_i}}$
Geometric mean	G	$G = (MOE_i!)^{\frac{1}{n}}$
Quadratic mean (root mean square)	Q	$Q = \left(\frac{\sum_{i=1}^n MOE_i^2}{n} \right)^{\frac{1}{2}}$
	MOE_i^2	Squared of the shakes MOE in a finger jointed specimen
Akin to sound intensity formula		$\left(\frac{1}{m} \right)^{(\frac{1}{n})^m}$ where n is the number of specimens and m can be 1, or 2.

The overall results in Table 3.13 indicate the strongest predictability in linear regression is attainable with higher number of finger joints. Findings show that 5 FJ had the highest R^2 values but the strengths of predictability decreased with decrease in the number of finger joints. The R^2 range for 5 FJ is acceptable (0.61 to 0.87) but the R^2 values decreased to

a range of 0.4 - 0.67 in 4 FJ, which were further decreased to a range of 0.30 – 0.58 for 3 FJ. The lowest R^2 values were found for 2 FJ (0.30 - 0.47).

The average R^2 values for 2 FJ and 3 FJ were found to be similar between 0.30 and 0.47. This is confirmed with statistical T-test analysis where no significant difference in R^2 was found between 3 FJ and 2 FJ (Table 3.12). The same applied to 4 FJ and 3 FJ with borderline P-value which indicates no significant difference in R^2 .

The occurrence of poor correlation in 2 FJ suggests greater sensitivity of standard deviations due to small number of shook pieces, thus enforced greater influence on the predictability of the models. This conjecture is further substantiated with observation in elimination of data with finger jointed specimens made of shook MOEs having standard deviations greater than 0.6 and 0.5. The predictability of the tabulated models had not improved despite removal of combination with unwanted standard deviation. This observation is apparent in 5 FJ, 4 FJ and 3 FJ. In contrast, the R^2 values had significantly improved in 2 FJ combinations giving an average R^2 at 0.71.

The overall predictability of the identified statistical models in the tables remained similar when compared with one another. The predictability of the model using Global MOE as a function of arithmetic mean of the shook MOEs appeared to be consistent throughout 5 FJ to 2 FJ, hence giving least deviations in R^2 values among variety numbers of finger joints. In this instance, arithmetic mean appeared suffice in predicting the overall stiffness of a finger jointed specimen with shooks MOE having standard deviation greater than 0.6. However, when shooks combinations having standard deviations greater than 0.6 were screened, results in Table 3.14 predominantly in Table 3.15 indicated arithmetic mean is no longer the best parameter in describing the function. Instead, parameter $[10\log_{10}10(\sum_{i=1}^n 10^{MOE_i/10})]$ appeared to be most efficient and consistent in predictability across 5 FJ to 2 FJ; hence giving least difference (SD in $R^2=0.7$) across assorted shooks combinations.

At this juncture, standard deviations in the constituted shook MOEs were apparently low as the shooks were derived from a single MSG grade and from the same piece of full size timber. The pursuance in identifying a single model that could describe the overall stiffness of finger jointed member made of shook MOE with various levels of standard deviations is necessary regardless of number of shooks involved in a constituted specimen. Nevertheless there is yet a conclusive and satisfying model that could be derived from using the aforementioned statistical modelling approach.

Table 3.12: Statistical T-tests on R^2 values between varies finger joint combinations

Comparison between	P-value at α 0.05
5FJ and 4FJ	1.98×10^{-23}
4FJ and 3FJ	0.0005
3FJ and 2FJ	0.97
5FJ and 3FJ	4.90×10^{-30}
4FJ and 2FJ	4.09×10^{-5}

Table 3.13: Numerical modelling for all MSG8 specimens

Model Description	Model	R^2				R^2 SD
		5FJ	4FJ	3FJ	2FJ	
Overall E vs. $MOE_{\max/\min/\text{mean}}$	$Y = m MOE_{\max} + C$	0.75	0.43	0.40	0.41	0.17
	$Y = m MOE_{\min} + C$	0.75	0.51	0.57	0.42	0.14
	$Y = m MOE_{\text{mean}} + C$	0.84	0.66	0.57	0.45	0.16
Global Class vs. $MOE_{\max, \min, \text{mean}}$	$Y_{\text{class}} = m MOE_{\max} + C$	0.77	0.44	0.40	0.37	0.19
	$Y_{\text{class}} = m MOE_{\min} + C$	0.76	0.41	0.39	0.52	0.17
	$Y_{\text{class}} = m MOE_{\text{mean}} + C$	0.85	0.59	0.40	0.47	0.20
Global Class vs. $MOE_{\max, \min, \text{mean}}$ class	$Y_{\text{class}} = m MOE_{c_{\max}} + C$	0.61	0.40	0.32	0.46	0.12
	$Y_{\text{class}} = m MOE_{c_{\min}} + C$	0.72	0.53	0.38	0.51	0.14
	$Y_{\text{class}} = m MOE_{c_{\text{mean}}} + C$	0.74	0.61	0.38	0.44	0.16
Global E vs. $[10 \log_{10} 10(\sum_{i=1}^n 10^{MOE_i/10})]$	$Y = m [10 \log_{10} 10(\sum_{i=1}^n 10^{MOE_i/10})] + C$	0.83	0.63	0.56	0.46	0.16
Global E class vs. $[10 \log_{10} 10(\sum_{i=1}^n 10^{MOE_i/10})]$	$Y_{r_class} = m [10 \log_{10} 10(\sum_{i=1}^n 10^{MOE_i/10})] + C$	0.85	0.57	0.40	0.45	0.20
Global E class vs. $[10 \log_{10} 10(\sum_{i=1}^n 10^{MOE_i/10}) - n]$	$Y_{r_class} = m [10 \log_{10} 10(\sum_{i=1}^n 10^{MOE_i/10}) - n] + C$	0.85	0.59	0.40	0.45	0.20
Overall E vs. $\frac{1}{MOE_{\max, \min, \text{mean}}}$	$Y = \frac{m}{MOE_{\max}} + C$	0.73	0.46	0.42	0.41	0.15
	$Y = \frac{m}{MOE_{\min}} + C$	0.76	0.51	0.55	0.55	0.11
	$Y = \frac{m}{MOE_{\text{mean}}} + C$	0.84	0.65	0.56	0.49	0.15
Reciprocal overall MOE $\frac{1}{Y}$ vs. $\frac{1}{MOE_{\max, \min, \text{mean}}}$	$\frac{1}{Y} = \frac{m}{MOE_{\max}} + C$	0.72	0.50	0.44	0.42	0.14
	$\frac{1}{Y} = \frac{m}{MOE_{\min}} + C$	0.76	0.51	0.53	0.56	0.12
	$\frac{1}{Y} = \frac{m}{MOE_{\text{mean}}} + C$	0.84	0.67	0.57	0.51	0.14
Global E class vs. $\frac{1}{MOE_{\max, \min, \text{mean}}}$	$Y_{r_class} = \frac{m}{MOE_{\text{mean}}} + C$	0.77	0.47	0.30	0.41	0.20

	$Y_{r_class} = \frac{m}{MOE_{min}} + C$	0.78	0.41	0.38	0.53	0.18
	$Y_{r_class} = \frac{m}{MOE_{mean}} + C$	0.86	0.59	0.40	0.48	0.20
$\log_{10} Y$ vs. $\frac{1}{MOE_{max, min, mean}}$	$\log_{10} Y = \frac{m}{MOE_{max}} + C$	0.73	0.49	0.43	0.42	0.15
	$\log_{10} Y = \frac{m}{MOE_{min}} + C$	0.77	0.51	0.54	0.56	0.12
	$\log_{10} Y = \frac{m}{MOE_{mean}} + C$	0.85	0.66	0.57	0.50	0.15
Y vs. MOE^2	$Y = m x_{max}^2 + C$	0.75	0.42	0.38	0.34	0.19
	$Y = m x_{min}^2 + C$	0.74	0.51	0.57	0.57	0.10
	$Y = m x_{mean}^2 + C$	0.83	0.65	0.58	0.47	0.15
$\log_{10} Y$ vs. $MOE_{max, min, mean}$	$\log_{10} Y = m MOE_{max} + C$	0.74	0.46	0.41	0.38	0.17
	$\log_{10} Y = m MOE_{min} + C$	0.75	0.51	0.56	0.56	0.11
	$\log_{10} Y = m MOE_{mean} + C$	0.83	0.66	0.58	0.49	0.14
Reciprocal overall MOE $\frac{1}{Y}$ vs. $MOE_{max, min, mean}$	$\frac{1}{Y} = m MOE_{max} + C$	0.71	0.47	0.42	0.38	0.15
	$\frac{1}{Y} = m MOE_{min} + C$	0.74	0.50	0.54	0.56	0.11
	$\frac{1}{Y} = m MOE_{mean} + C$	0.81	0.66	0.58	0.49	0.14
$\log_{10} Y$ vs. $\log_{10} MOE$	$\log_{10} Y = m \log_{10} MOE_{max} + C$	0.73	0.47	0.42	0.40	0.15
	$\log_{10} Y = m \log_{10} MOE_{min} + C$	0.76	0.51	0.55	0.56	0.11
	$\log_{10} Y = m \log_{10} MOE_{mean} + C$	0.84	0.66	0.57	0.49	0.15
Y vs. Harmonic mean	$Y = m H + C$	0.85	0.66	0.57	0.51	0.15
Y class vs. Harmonic mean	$Y_{class} = m H + C$	0.87	0.59	0.40	0.49	0.20
Y vs. Geometric mean	$Y = m G + C$	0.84	0.66	0.58	0.49	0.15
Y vs. Quadratic mean	$Y = m Q + C$	0.83	0.65	0.36	0.47	0.21

Table 3.14: Numerical modelling on MSG8 specimens with shooks MOE combinations having standard deviation ≤ 0.6

Model Description	Model	R ²				R ² SD
		5FJ	4FJ	3FJ	2FJ	
Overall E vs. $MOE_{max/min/mean}$	$Y = m MOE_{max} + C$	0.75	0.64	0.64	0.71	0.05
	$Y = m MOE_{min} + C$	0.75	0.49	0.56	0.63	0.11
	$Y = m MOE_{mean} + C$	0.84	0.69	0.68	0.71	0.07
Global Class vs. $MOE_{max, min, mean}$	$Y_{class} = m MOE_{max} + C$	0.77	0.60	0.64	0.70	0.07
	$Y_{class} = m MOE_{min} + C$	0.76	0.40	0.38	0.60	0.18
	$Y_{class} = m MOE_{mean} + C$	0.85	0.62	0.47	0.69	0.16
Global Class vs. $MOE_{max, min, mean}$ class	$Y_{class} = m MOE_{c_max} + C$	0.60	0.50	0.48	0.73	0.11

	$Y_{class} = mMOE_{c_min} + C$	0.71	0.51	0.41	0.64	0.13
	$Y_{class} = mMOE_{c_mean} + C$	0.73	0.67	0.40	0.51	0.15
Global E vs. $[10\log_{10}10(\sum_{i=1}^n 10^{MOE_i/10})]$	$Y = m[10\log_{10}10(\sum_{i=1}^n 10^{MOE_i/10})] + C$	0.83	0.69	0.68	0.71	0.07
Global E class vs. $[10\log_{10}10(\sum_{i=1}^n 10^{MOE_i/10})]$	$Y_{r_class} = m[10\log_{10}10(\sum_{i=1}^n 10^{MOE_i/10})] + C$	0.85	0.62	0.47	0.69	0.16
Global E class vs. $[10\log_{10}10(\sum_{i=1}^n 10^{MOE_i/10}) - n]$	$Y_{r_class} = m[10\log_{10}10(\sum_{i=1}^n 10^{MOE_i/10}) - n] + C$	0.85	0.62	0.47	0.69	0.16
Global E vs. $\frac{1}{MOE_{\max, \min, mean}}$	$Y = \frac{m}{MOE_{\max}} + C$	0.73	0.63	0.63	0.69	0.05
	$Y = \frac{m}{MOE_{\min}} + C$	0.76	0.49	0.54	0.62	0.12
	$Y = \frac{m}{MOE_{mean}} + C$	0.84	0.69	0.67	0.69	0.08
$\frac{1}{Y}$ vs. $\frac{1}{MOE_{\max, \min, mean}}$	$\frac{1}{Y} = \frac{m}{MOE_{\max}} + C$	0.72	0.64	0.61	0.65	0.05
	$\frac{1}{Y} = \frac{m}{MOE_{\min}} + C$	0.76	0.48	0.51	0.60	0.13
	$\frac{1}{Y} = \frac{m}{MOE_{mean}} + C$	0.84	0.69	0.64	0.66	0.09
Global E class vs. $\frac{1}{MOE_{\max, \min, mean}}$	$Y_{class} = \frac{m}{MOE_{mean}} + C$	0.77	0.60	0.43	0.67	0.14
	$Y_{class} = \frac{m}{MOE_{\min}} + C$	0.78	0.40	0.36	0.60	0.19
	$Y_{class} = \frac{m}{MOE_{mean}} + C$	0.86	0.62	0.45	0.68	0.17
$\log_{10} Y$ vs. $\frac{1}{MOE_{\max, \min, mean}}$	$\log_{10} Y = \frac{m}{MOE_{\max}} + C$	0.73	0.64	0.62	0.67	0.05
	$\log_{10} Y = \frac{m}{MOE_{\min}} + C$	0.77	0.49	0.53	0.61	0.12
	$\log_{10} Y = \frac{m}{MOE_{mean}} + C$	0.85	0.69	0.65	0.68	0.09
Y vs. MOE^2	$Y = mx_{\max}^2 + C$	0.75	0.63	0.64	0.72	0.06
	$Y = mx_{\min}^2 + C$	0.74	0.49	0.56	0.63	0.11
	$Y = mx_{mean}^2 + C$	0.83	0.69	0.68	0.72	0.07
$\log_{10} Y$ vs. $MOE_{\max, \min, mean}$	$\log_{10} Y = mMOE_{\max} + C$	0.74	0.64	0.62	0.70	0.06
	$\log_{10} Y = mMOE_{\min} + C$	0.75	0.48	0.54	0.61	0.12
	$\log_{10} Y = mMOE_{mean} + C$	0.83	0.69	0.66	0.69	0.08
$\frac{1}{Y}$ vs. $MOE_{\max, \min, mean}$	$\frac{1}{Y} = mMOE_{\max} + C$	0.71	0.64	0.61	0.68	0.04
	$\frac{1}{Y} = mMOE_{\min} + C$	0.74	0.48	0.53	0.60	0.11
	$\frac{1}{Y} = mMOE_{mean} + C$	0.81	0.68	0.65	0.68	0.07

$\log_{10} Y$ vs. $\log_{10} MOE$	$\log_{10} Y = m \log_{10} MOE_{\max} + C$	0.73	0.64	0.62	0.69	0.05
	$\log_{10} Y = m \log_{10} MOE_{\min} + C$	0.76	0.49	0.53	0.61	0.12
	$\log_{10} Y = m \log_{10} MOE_{mean} + C$	0.84	0.69	0.66	0.69	0.08
logY vs X	$\log_{10} Y = mX_{\max} + c$	0.74	0.64	0.62	0.70	0.06
	$\log_{10} Y = mX_{\min} + c$	0.75	0.48	0.54	0.61	0.12
	$\log_{10} Y = mX_{mean} + c$	0.83	0.69	0.66	0.69	0.08
Y vs. N/xi	$Y = m(N/xi) + c$	0.85	0.69	0.66	0.69	0.09
Y vs. Geometric mean	$Y = mG + C$	0.84	0.69	0.67	0.71	0.08
Y vs. Quadratic mean	$Y = mQ + c$	0.86	0.69	0.67	0.71	0.09

Table 3.15: Numerical modelling on MSG8 specimens with shooks MOE combinations having standard deviation ≤ 0.5

Model Description	Model	R ²				R ² SD
		5FJ	4FJ	3FJ	2FJ	
Overall E vs. $MOE_{\max, \min, mean}$	$Y = m MOE_{\max} + C$	0.75	0.61	0.52	0.72	0.11
	$Y = m MOE_{\min} + C$	0.75	0.50	0.58	0.70	0.11
	$Y = m MOE_{mean} + C$	0.84	0.69	0.61	0.74	0.10
Global Class vs. $MOE_{\max, \min, mean}$	$Y_{class} = m MOE_{\max} + C$	0.77	0.58	0.52	0.72	0.12
	$Y_{class} = m MOE_{\min} + C$	0.76	0.41	0.35	0.71	0.21
	$Y_{class} = m MOE_{mean} + C$	0.85	0.61	0.38	0.74	0.20
Global Class vs. $MOE_{\max, \min, mean}$ class	$Y_{class} = m MOE_{c_max} + C$	0.61	0.49	0.37	0.72	0.15
	$Y_{class} = m MOE_{c_min} + C$	0.72	0.56	0.38	0.71	0.16
	$Y_{class} = m MOE_{c_mean} + C$	0.73	0.66	0.26	0.62	0.21
Global E vs. $[10 \log_{10} 10 (\sum_{i=1}^n 10^{MOE_i/10})]$	$Y = m [10 \log_{10} 10 (\sum_{i=1}^n 10^{MOE_i/10})] + C$	0.83	0.68	0.61	0.74	0.09
Global E class vs. $[10 \log_{10} 10 (\sum_{i=1}^n 10^{MOE_i/10})]$	$Y_{r_class} = m [10 \log_{10} 10 (\sum_{i=1}^n 10^{MOE_i/10})] + C$	0.85	0.61	0.38	0.75	0.20
Global E class vs. $[10 \log_{10} 10 (\sum_{i=1}^n 10^{MOE_i/10}) - n]$	$Y_{r_class} = m [10 \log_{10} 10 (\sum_{i=1}^n 10^{MOE_i/10}) - n] + C$	0.85	0.61	0.38	0.74	0.20
Global E vs. $\frac{1}{MOE_{\max, \min, mean}}$	$Y = \frac{m}{MOE_{\max}} + C$	0.73	0.61	0.51	0.68	0.10
	$Y = \frac{m}{MOE_{\min}} + C$	0.76	0.50	0.56	0.68	0.12
	$Y = \frac{m}{MOE_{mean}} + C$	0.84	0.68	0.59	0.71	0.10
$\frac{1}{Y}$ vs. $\frac{1}{MOE_{\max, \min, mean}}$	$\frac{1}{Y} = \frac{m}{MOE_{\max}} + C$	0.72	0.62	0.50	0.65	0.09
	$\frac{1}{Y} = \frac{m}{MOE_{\min}} + C$	0.76	0.50	0.56	0.68	0.12
	$\frac{1}{Y} = \frac{m}{MOE_{mean}} + C$	0.84	0.68	0.59	0.70	0.10

Global E class vs. $\frac{1}{MOE_{\max, \min, mean}}$	$Y_{class} = \frac{m}{MOE_{mean}} + C$	0.77	0.58	0.30	0.68	0.20
	$Y_{class} = \frac{m}{MOE_{\min}} + C$	0.78	0.39	0.34	0.70	0.22
	$Y_{class} = \frac{m}{MOE_{\max}} + C$	0.86	0.60	0.37	0.72	0.21
$\log_{10} Y$ vs. $\frac{1}{MOE_{\max, \min, mean}}$	$\log_{10} Y = \frac{m}{MOE_{\max}} + C$	0.73	0.62	0.51	0.67	0.09
	$\log_{10} Y = \frac{m}{MOE_{\min}} + C$	0.77	0.50	0.56	0.68	0.12
	$\log_{10} Y = \frac{m}{MOE_{mean}} + C$	0.85	0.68	0.59	0.70	0.11
Y vs. MOE^2	$Y = m x_{\max}^2 + C$	0.75	0.61	0.53	0.73	0.10
	$Y = m x_{\min}^2 + C$	0.74	0.51	0.59	0.71	0.11
	$Y = m x_{mean}^2 + C$	0.83	0.68	0.62	0.75	0.09
$\log_{10} Y$ vs. $MOE_{\max, \min, mean}$	$\log_{10} Y = m MOE_{\max} + C$	0.74	0.62	0.51	0.69	0.10
	$\log_{10} Y = m MOE_{\min} + C$	0.76	0.50	0.57	0.69	0.12
	$\log_{10} Y = m MOE_{mean} + C$	0.84	0.68	0.60	0.72	0.10
$\frac{1}{Y}$ vs. $MOE_{\max, \min, mean}$	$\frac{1}{Y} = m MOE_{\max} + C$	0.71	0.62	0.51	0.68	0.09
	$\frac{1}{Y} = m MOE_{\min} + C$	0.74	0.50	0.57	0.68	0.11
	$\frac{1}{Y} = m MOE_{mean} + C$	0.81	0.67	0.61	0.71	0.08
$\log_{10} Y$ vs. $\log_{10} MOE$	$\log_{10} Y = m \log_{10} MOE_{\max} + C$	0.74	0.62	0.52	0.70	0.10
	$\log_{10} Y = m \log_{10} MOE_{\min} + C$	0.75	0.50	0.58	0.70	0.11
	$\log_{10} Y = m \log_{10} MOE_{mean} + C$	0.83	0.68	0.61	0.73	0.09
Y vs. Quadratic mean	$Y = mQ + C$	0.86	0.68	0.62	0.74	0.10

3.4.3 Dynamic MOE at Different Shook Lengths vs. Overall Dynamic MOE for Solid Wood

It was found that all dynamic measurements on subsequent batches of random shooks at different lengths that were originally prepared for final dynamic testing phase were poor in repetitions. Very often the measured first harmonic frequencies for a sizable number of shooks were out of the expected range, thus giving unacceptable magnitude of dynamic MOEs. Furthermore, the previous testing phase in Experiment II and modelling using the statistical approach in relating the MSG8 radiata pine shooks with the corresponding full size dynamic measurements were non-conclusive and unsuitable. An alternative modelling

method and mode of measurements had been changed and continued in Chapter 4 and Chapter 5.

4 Development of Models to Predict Finger Jointed Timber Mechanical Properties

4.1 Literature Review

Research has been conducted in the past decades to investigate the variability in wood mechanical properties both between trees and within a tree and, consequently, in a piece of timber [38] since 1965 [14]. In recent years, growing interests have been reported on the modelling of wood mechanical properties to predict the performance of woods and engineered wood products. These models are directly and indirectly related, collated and cited as modelling references for the current study. The modelling studies are reviewed and discussed in the following categories.

- a. Modelling of local MOEs and strength properties based on MOE in timber or laminates using probabilistic and deterministic approach
- b. Modelling of Glulam properties
- c. Modelling of finger joint strength

4.1.1 Modelling of the Overall MOE based on Local MOE Variability in A Piece of Timber or Laminates

It has been known that the wood properties in a tree vary along the tree height and in radius directions. The wood properties in a piece of timber also changed along the length direction. In general, the modelling approach can be divided into two categories, namely probabilistic and deterministic. The probabilistic method can be further grouped as the statistical correlation method and the stochastic method.

1) Probabilistic modelling

i. Statistical Correlation

Early researches on prediction of the overall MOE based on the local MOEs were conducted using the correlation approach. Most of these studies aimed to relate material strength with different mechanical properties using correlation method such as linear regression. One of the earlier correlation studies was conducted by Orosz [80] and the author has incorporated span length as an additional affecting parameter. The study evaluated the

effect of shorter span MOE on the predictability of the overall tensile strength and found that MOE measured over a short span was a better predictor. The predictability was further improved when individual MOEs over short spans were measured with bending strength ratio. The author had also found that flatwise overall MOE on shorter gage length was correlated significantly with tensile strength [81].

Corder [14] studied the western hemlock and found that the overall MOE was closely correlated to the minimum local MOE within a piece of timber. For glulam, tensile failure is a crucial factor in determining its performance in application [37], [15, 21]. Therefore, strong interests have been developed to relate the local MOEs and the other strength properties to the glulam tensile strength.

The strength of correlations (correlation coefficient) between the MOE and bending strength was highly dependent on how the non-destructive test was conducted. The range of a typical MOE correlation coefficient were between 0.65 and 0.70 [82] when MOE was determined from static bending. The correlation coefficient can be improved when the minimum local MOE is compared with bending strength. Foshi [82] highlighted the importance of determining the local MOEs and strength with lengthwise variability and using the results to predict the overall performance of the timber. The author found that it was much more reliable to predict the timber failure than using the measured overall MOE and strength.

Similar studies [83],[80], [84] were also found in literature where the minimum local MOE was found to be a better predictor in correlating with the tensile strength tested at a shorter testing span and refinement was continued by Kim et al. [85].

On the other hand, most of the modelling studies related the overall MOE of a pre-graded full size timber to its local MOEs measured at various intervals or with other mechanical properties. Statistical modelling was frequently used to express the relationship between the overall MOE and other variables.

Although the overall MOE can be predicted from the local MOEs, measuring the local MOE distribution along the timber length using a stress grading machine has been a challenge. The stress grading machine was initially designed to produce consecutive average measurements to minimise the effect of concentrated zones due to low and high stiffness. The possibility of missing out low MOE sections by the machine is inevitable. Foshi [82] demonstrated that by using the Fourier transform method a close approximation to the true minimum MOE was achievable. The proposed approximation procedure was based on truncation of the transform $K(f)$ at a certain frequency f_{\max} disregarded of the amplitudes

corresponding to the frequencies that were greater than f_{\max} . The end result showed improved correlation between stiffness and strength.

In recent study, Nocetti [86] presented regression modelling on localised MOE of different species and local defects in predicting the overall MOE from local MOEs in a piece of timber. The author conducted theoretical analyses on relationship between local MOEs and the overall MOE based on DIN EN408-2003 [87] and suggested the relationship between the two should be in the form of polynomial. The study selected the overall MOE as dependent variable and local MOE as the predictor.

The author also investigated the effect of species and the effect of defects and their location relative to loading point. Interestingly species was found to have insignificant contribution towards accuracy of the model prediction.

1) Correlation between Tensile Strength and High and Low MOEs with Weighted Least Square Regression

Woeste et al. [88] used a classic regression method in developing correlations to predict tensile strength based on long span MOE in full-size Southern pine timber. The author performed curve fitting and found that MOE had a 3-parameter Weibull distribution. Subsequently, tensile strength was modelled as a function of the long span MOE using the weighted least square regression. Random MOE values were generated from the Weibull distribution from distribution fitting and tensile strength was calculated using the developed correlations.

During curve fitting Woeste realised tensile strength did not follow the normal distribution pattern, hence the developed correlations may need further improvement. The author then suggested using the logarithmic transformation for the fitting improvement. This model was later discussed in-depth by Bender [89] who also included the effect of end-joints on the local MOE by assuming the end joint MOE to be the average of MOEs between the two adjacent end joints.

Other studies also indicated that the correlation between the bending MOE and the strength could be improved when measured shorter span MOEs were used as proposed by Burk and Bender ([38]&[90]) who adopted Woeste's [88] concept on Douglas-fir finger jointed wood. The study was conducted by measuring the local MOE on each finger joint at a 2-feet timber segment and finger joint segment, respectively. The locally measured MOEs were correlated with the overall MOE and the tensile strength of the finger joint member

using multiple regression analysis. The bending tests were conducted flatwise on single-point load. The model is presented as follow:-

$$MOE_j = \beta_0 + \beta_1 MOE_L + \beta_2 MOE_H + \gamma$$

Equation 4.1

$$T_j = \beta_3 + \beta_4 MOE_j + \varphi$$

Equation 4.2

where MOE_j is the global finger joint MOE, T_j the global finger joint tensile strength, MOE_L and MOE_H are the lower and higher localised MOEs of the jointed laminates, respectively, $\beta_0, \beta_1, \dots, \beta_4$ are the linear regression parameters, γ and φ are the error terms distributed normally with mean zero and variance equal to the residual variances, γ^2 and φ^2 respectively.

The correlation strength for the overall MOE as a function of the lower and higher localised MOE using multiple regression was strong ($r = 0.93 - 0.97$). The correlation for tensile strength models, however, was much weaker ($r = 0.40 - 0.48$). The authors suggested that strong correlations in the former relationship could be due to the normal distribution pattern of finger joint MOEs as oppose to tensile strength distributed in a skewed *Weibull* distribution. The authors speculated that the above regression expression may not be as effective when the distribution of tensile strength was skewed.

Taylor and Bender [91] pointed out the limitations present in Woeste's approach and commented that the flexibility of the suggested method would be limited by the choice of transformation which can be subjective. As a result, improper modelling of distribution could lead to adverse effect in structural reliability. Taylor and Bender (1988) presented an algorithm using a modified multivariate normal approach for simulating correlated random variables which could preserve the marginal distribution of each variable and the correlation between the variables. Each point of measurement of interest in an autocorrelation model was assumed to be related to the next measured point spaced by a specified k^{th} step. Therefore, the similarity between two observations was a function of time lag (typical in time series correlation) between the two. Considering the local MOE of a full size timber can be serially correlated, Taylor and Bender (1988) substituted time lag using the local MOE measured along the span of a full size member. The model appeared to be more reliable when the local MOE values were in sequential order and when the departure of the local MOE values were

not too far apart to ensure the correlation between the *lag-k* values fell in sequence. The model was valid only when the local MOE profile follows the normal distribution pattern. This model appeared to be highly depending on the consistency of quality within a piece of timber of the same grade. Other factors such as size, species, grading method, and simulation on segment less than the prescribed segment length (30 inch) were not addressed in the study. Nevertheless, the contribution of the modelling approach played an important role and had become the predecessor to many subsequent statistical modelling [92].

Showalter et al. [92] has expanded Kline's [31] model by combining Woeste's regression model [88] and correlated tensile strength with MOE. The author used Kass's method in finding the local MOEs so that the distribution of strength in the test groups can be closely matched. Later, Showalter adopted Kline's approach by using the second-order Markov process to model the lengthwise variability of MOE at a 30 inch segment along the timber length. The authors refined the regression model which described the relationship between tensile strength parallel to grain and the independent MOE. The model was based on the "weakest link theory" and was able to predict tensile strength taking into the effects of timber length. Tensile strength was predicted using serial correlation weighted least-square regression model in which the MOEs were randomly generated from *3-Parameter Weibull* distribution. The study of Showalter et al. showed that tensile strengths were significantly lower in longer specimen (3 m) than the shorter specimens at 2 m and 0.7 m by 70 to 88 percent.

2) *Improved Method using Multivariate Statistical Approach*

Taylor and Bender [93] identified the importance of modelling local variability of material properties within a piece of wood referred to as spatial variability where the local MOE and tensile strength within timber can be spatially correlated. Thus, a multivariate statistical method was used to determine local MOE and tensile strength. The authors conducted transformation on the multivariate normal distribution to generate local properties on an 8-ft long timber. The multivariate statistical analysis (MANOVA) was used to model the local MOE and tensile strength properties. It was assumed that each segment has its own independent distribution of properties (MOE and strength) obtained from best fitting. Hence, each pair of MOE and strength in a given segment was treated as the correlated variable. Last, the authors used the model as an input for Monte Carlo models to predict the structural reliability of glulam beams. Richburg and Bender attempted to simulate longer timber in

1991 by extrapolating the MOE-Tensile strength correlation matrix based on the third-order and first-order autoregressive models for serial correlations in MOE and tensile strength, respectively. Later in 1992, Richburg and Bender [37] extended the research of Taylor and Bender (1991) by including E-rated grades laminating timber.

ii. *Stochastic Modelling*

1) *Lag-k Serial Correlation*

Kline et al. [31] developed a simulation method in simulating the local MOE (lengthwise variability in MOE) using the *Lag-k* serial correlation method. The mechanical properties of laminates were predicted based on a series of MOEs measured over a short bending span. The assumption of the model is that timber exhibits serial correlation attributes, hence the research problem could be run on “serial autocorrelation model”. Each local MOE was segmented at an equal interval, followed by autocorrelation between the MOE with the MOE in the previous n^{th} segment. This was referred to as the *lag-k* serial correlation. Explanation on *lag-k* serial correlation is illustrated in Figure 4.1.

The author performed a second order Markov *lag-2* serial correlation (Equation 4.3) on a 30 inch segment over a full size member based on available mechanical properties distributions on selected timber dimensions and grades. The overall MOE of the timber was considered as a function of the local MOE measured at 30 inch segment and calculated using arithmetic mean (Equation 4.4). The segment MOEs were obtained from Equation 4.3. Later, MOE indexes were generated using Equation 4.5. These MOE indexes were used to generate segment MOE values from Equation 4.3. The simulated global MOE of a piece of timber was generated based on a prescribed probability distribution of the desired size and timber grade. Finally, the simulated lengthwise MOE values were generated by multiplying the simulated timber MOE with the MOE indexes from Equation 4.5. The overall MOE of a simulated piece was determined from arithmetic mean using Equation 4.4 and MOE_i were computed from the simulated lengthwise MOEs or the simulated local MOE's.

$$X_{i+1} = \beta_1 X_i + \beta_2 X_{i-1} + \sigma_{i+1}$$

Equation 4.3

where X_i is the observed data values, β is the multiple regression coefficients, σ_i is the measurement errors

$$X_{overall} = \frac{1}{n} \sum_{i=1}^n MOE_i$$

Equation 4.4

where $X_{overall}$ is the average MOE or overall MOE of timber, MOE_i is the segment MOE and n is the number of segments per timber.

$$MOE_{Index} = \frac{\text{Generated segment MOE value}}{X_{lumber}}$$

Equation 4.5

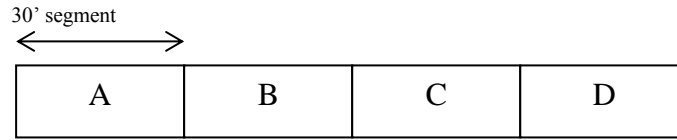


Figure 4.1: *Lag-k* serial correlation between segment A, B, C and D. *Lag 1* is the correlation between A and B; *Lag 2* is the correlation between A and C

Govindarajoo [94] adopted the above method in developing a model for determination of local MOEs within timber. A series of correlations were proposed for the local MOEs by using the second-order Markov and regression model to simulate the overall MOE and strength of the timber.

Isaksson [95] has developed a model that describes the bending strength within and between timber. The author has made assumptions that the distance between weak sections, length of weak sections, and the strength of weak sections as the stochastic variables.

The model was able to describe the variability within and between timber in the bending mode subject to span length and load configurations. The study claimed that the strength of a beam could be improved by 10% by optimisation of cutting and loading configurations based on the model prediction. The author highlighted the definition of element used in the context of his study, where element was referring to the volume of material made of the member and beam was considered to be a system built up by elements.

As such, the variability within a member was due to variability between elements assembled to a member [96].

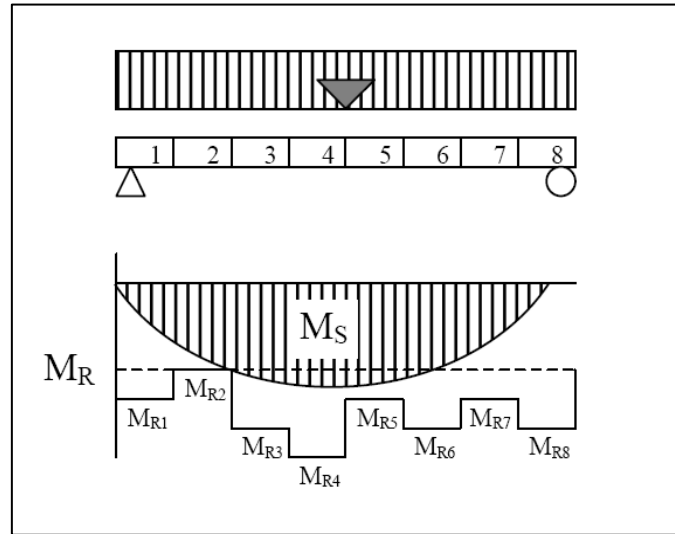


Figure 4.2: Bending moment diagram describing the beam as a system made of 8 elements. The bending moment due to action denoted as M_s and M_R as the moment capacity. (Figure adapted from an unpublished article by Isaksson [96]).

Another model was presented by Ehlbeck [97] for laminated lumber whereby correlations were fitted between the lamella tensile strength and the overall MOE, density and knottiness of the lamella using the Multiple Logarithmic Regression. Assumption on the maximum tensile and compression strengths on the two surfaces are the same and equal to the material strength were made in the modelling. The overall MOE ($E_{overall}$) of the lamellae was calculated using Equation 4.6 and was used to correlated with the lamella tensile strength.

$$E_{overall} = \frac{n}{\sum_{i=1}^n \frac{1}{E_i}}$$

Equation 4.6

where n is the number of finger joint segments, and E_i is the MOE of the finger joint segment.

Another related study was conducted by Ehlbeck [98] and he had developed a model known as “Karlsruhe model” which paved the foundation to many subsequent modelling studies for predicting glulam strength. Linear regression was used to model the tensile

strength of laminate as a function of the lower density of two finger jointed shooks. The regression model considered density, occurrence and the frequency of knots, and species in various models. However, the study did not take into account the size effects, species, and finger joint strength.

2) *Deterministic modelling*

a. Arithmetic Mean and Minimum MOE

Many deterministic modelling studies had chosen using the arithmetic mean of the measured local MOEs (Equation 4.4 and Equation 4.6), or the minimum local MOE in predicting the overall MOE of the same piece of wood.

One of the early studies related to wood variability in bending MOE was conducted by Kass [36] who used a middle ordinate instrument to measure continuous discrete MOEs. In that study, the MOE values were derived based on assumption that wood was homogeneous and complied with Hooke's Law. Kass explained how the overall modulus of a beam was affected by low and high stiffness regions within the beam. In the study, Kass derived a relationship to predict the overall MOE of using two MOE values and the corresponding lengths. The test setup is summarised in Figure 4.3 for a beam span between 203 mm to 610 mm. The correlation is given as follows for the overall MOE prediction. However, the correlation became weaker when tested on shorter span.

The overall modulus of elasticity E_{mo} is given by the equation below,

$$E_{mo} = \frac{E_l}{1 - (1 - \frac{E_l}{E_h})(1 - \frac{L_l}{L_g})^2}$$

Equation 4.7

where E_l is the low stiffness in a length containing defect wood, E_h is the high stiffness of clear wood, L_l is the length of the low stiffness length and L_g is the gage length (span).

However, the author found that middle ordinate MOE of a span was influenced by the relative proportion of clear (high stiffness) and defective area (low stiffness). Therefore,

Equation 4.7 was suggested to be a deterministic model applicable to test specimens with high variability in local MOEs. Kass (1975) also examined the ratios of E_l/E_h and L_l/L_g on

the predicted overall MOE represented as the percentage to the lowest MOE as shown in Figure 4.4 from which it is found that the overall MOE is reduced to be close to E_l when L_l is over half of the span ($L_l/L_g > 0.5$). However, the model was determined for a beam in which the low MOE wood was adjacent to the high MOE wood, and only the effect of the lowest and highest MOE elements was considered to predict the overall MOE. The effects of the other elements with MOE in between the highest and the lowest values were not taken into account.

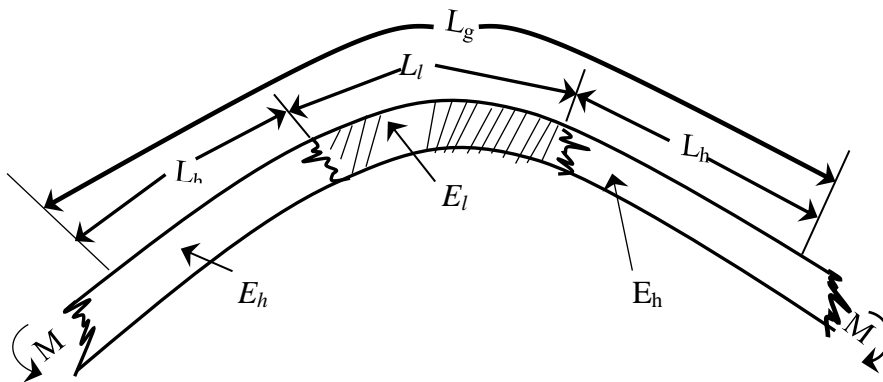


Figure 4.3: A beam section with combination of low stiffness and higher stiffness (adapted from Kass (1975)[36])

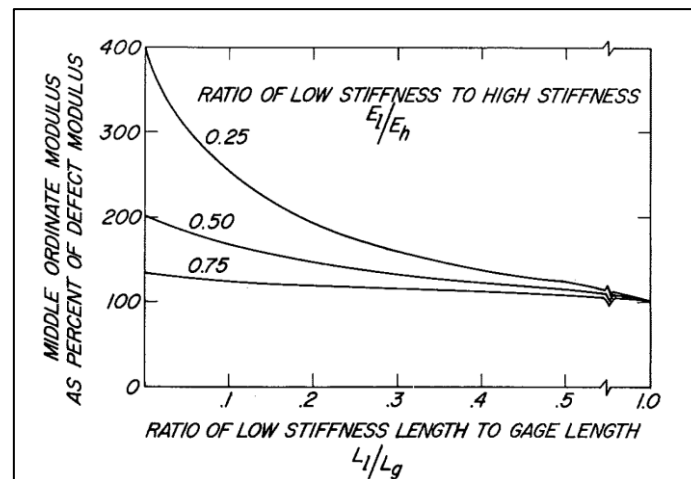


Figure 4.4: The effects of E_l/E_h and L_l/L_g on the predicted overall MOE represented as percentage to the lowest MOE [36]

b. Modelling Local MOE based on Flexural Stress-Strain Relationship

Bechtel [43] derived a predictive model that predicts the overall MOE from local MOEs using the double integration method as given in Equation 4.8. The author introduced “the change of integration order” method during integration.

The work of Bechtel is closely related to the present study as the equation between local MOE and overall MOE were derived from theoretical analysis based on moment profile in flexural bending and local wood properties. The intention of the derivation was to resolve issues rose from the machine stress grader and the model was dedicated for a simply-supported Three-point loading system.

In the modelling, the weighting function ‘ w ’ was used in the double integration over a bending span which has uniform MOE in the cross section. . The weighting function varied in quadratic manner, i.e. from zero at one beam end to the maximum at the adjacent beam end. Effectively, the weighting function illustrated the relative influence of each cross-sectional MOE on the overall MOE. From these correlations, the influence of local MOEs at each cross-section along the span on the bending characteristics of the span can be examined. In deriving the above correlations, a bending moment diagram was used as the basic loading distribution as illustrated in Figure 4.5.

In validation of Equation 4.8 the overall MOE was physically measured from mid-span load-deflection measurement and the local MOE values from the machine stress grader. The output from the rearrangements had explicitly expressed the overall MOE with the local MOE at each point of the cross-section with the assigned weighting function (Equation 4.8). Details on the derivation of Bechtel’s model can be found in Appendix 4.1.

$$C_{overall} = \frac{12}{L^3} \left[\int_0^{L/2} v^2 C(v) dv + \int_{L/2}^L (L-v)^2 C(v) dv \right]$$

Equation 4.8

where $C_{overall} = \frac{1}{E_{overall}}$ and $C(v) = \frac{1}{E(v)}$.

The weighting function w was defined as:

$$w(v) = \begin{cases} \frac{12v^2}{L^3} & , 0 < v < L/2 \\ \frac{12(L-v)^2}{L^3} & , L/2 < v \leq L \end{cases}$$

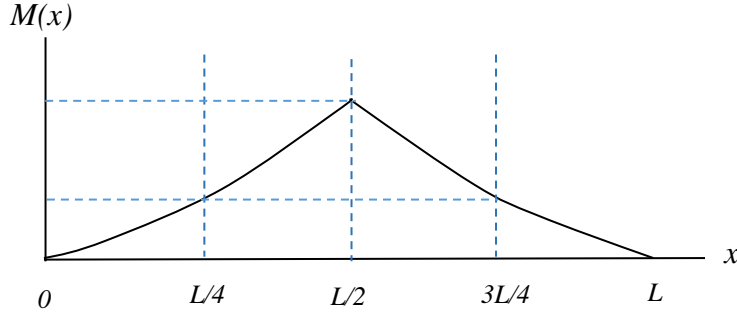


Figure 4.5: Weighting function for a simply-supported, centre-loaded bending span of length L . (Excerpt from F. Bechtel[43])

Foshi [82] proposed a simplified equation to calculate the maximum deflection as given in Equation 4.9 from detailed analysis of beam bending. In the equation, local MOE was a function of x and the local load, $P(x)$, varied along the bending span. The local coordination α was measured from the left support of the test span.

$$\Delta = \frac{P(x)}{4I} \left\{ \int_0^{L/2} \frac{\alpha^2}{E(x - L/2 + \alpha)} d\alpha + \int_{L/2}^L \frac{(L - \alpha)^2}{E(x - L/2 + \alpha)} d\alpha \right\}$$

Equation 4.9

Foshi noted that $P(x)$ in Equation 4.9 can be used to determine the “average” MOE over the bending span at any location x . However, the author commented that in a set of largely varied local MOEs or $E(x)$, the distribution of $E(x)$ from measurement of loads $P(x)$ over short span was numerically difficult and described that as ill-condition. This can be reflected in the case of having a set of very different functions $E(x)$ corresponds to a set of very close functions $P(x)$ for the same deflection. Determination of approximate $E(x)$ would require extremely accurate measurement of $P(x)$ which is practically impossible.

A similar predictive modelling was conducted by Govindarajoo [32] using the flexural strain energy theory. The author incorporated the model using the weighting function and assumed the moment of inertia of the contained segments to be uniform across entire

beam. The shear-strain energy was considered negligible and the influence of each segment on the overall MOE was considered uniform (Equation 4.6). The author suggested Equation 4.4 as an alternative in predicting the overall MOE. By incorporating Equation 4.6 and the quadratic weighting function w into the flexural-strain energy equation, the equation was simplified as follow (Equation 4.10):

$$MOE_{overall} = \frac{L^3/12}{\left\{ \int_0^{L/2} \frac{w}{E_x} dx + \int_{L/2}^L \frac{w}{E_x} dx \right\}}$$

Equation 4.10

where

$$w = \begin{cases} x^2, & 0 \leq x \leq L/2 \\ (L-x)^2, & L/2 \leq x \leq L \end{cases}.$$

Govindarajoo highlighted that the model in Equation 4.10 was only valid for static bending. It is noteworthy that the above model [32] and the model by Bechtel [43] (Equation 4.8) were derived from theoretical analysis without experimental validations.

4.1.2 Modelling Glulam Properties

i. Overview

The constitution of a glulam beam is made of layers of laminates which can be optimised via different grades of laminations. In manufacturing and research practices, optimising the arrangements of laminating stocks facilitates utilisation of resources and promotes recovering of wastes from the offcuts.

Figure 4.6 is an illustration of a cross section of glulam beam made of 3 different laminating grades. Each zone represents a region within the laminated cross section which comprised a specific grade. Referring to

Figure 4.6, laminating stock in zone C should have strong tensile properties while zone A with strong compression properties. Layers with lower MOEs can be placed at zone B. In

the case of an unbalanced layups, the allowable stress on the compressed zone has been specified in ASTM (2009) [26] to be increased by a factor of 1.4.

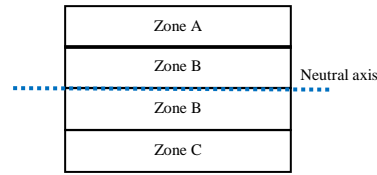


Figure 4.6: Illustration of a glulam beam made of different grades of laminating stock and each layer being segmented into different zones according to mechanical behaviour in bending application

In symmetrical cross section of laminations, the neutral axis that is presumably at the centre of a glulam beam cross section. However, if the laminating layers have different properties, the neutral axis may shift of which this is likely to result in unbalance combination of laminating grades termed as the unbalance grades. Investigations on shifting of the neutral axis and its implication upon strength and stiffness were discussed in-depth by Govindarajoo [28]. The author explained how shifting of neutral axis and other factors (knots, end joint and cross grain) could affect the expected glulam strength and stiffness. The allowable stress for the compression side of laminates can be increased by factor of 1.4. The mathematical derivations were explicitly explained in detail. The author explained that if I_1 , I_2 and I_3 were the transformed moment of inertia in terms of E_1 , E_2 and E_3 respectively, thus $E_1 I_1 = E_2 I_2 = E_3 I_3$. This assumption enabled I_k/I_g to be related to the equivalent MOE of the entire glulam beam (E_g) as in Equation 4.11.

$$E_g = E_1 \cdot \frac{I_k}{I_g} \times 0.95$$

Equation 4.11

where E_g is equivalent MOE of the entire beam, E_1 is the top layer MOE and 0.95 is the reducing factor for unbalance layup in a Glulam beam.

Hence,

$$E_g \cdot I_g = E_1 \cdot I_1 \times 0.95$$

Equation 4.12

where E_g is the overall MOE, E_l the top layer MOE, I_l the moment of inertia of the top layer laminate, I_g the gross moment of inertia of the entire beam and 0.95 is the reducing factor for unbalance layup in a Glulam beam (ASTM D3737) [26].

ii. Modelling of Glulam Properties

Extensive modelling researches have been reported in literature to predict and improve the mechanical performance of glulam beams. The ultimate goal of these researches was to simulate and optimise the strength and stiffness of the glulams.

One of the earliest studies on Glulam modelling was based on lamination properties using Finite Element (FE) method by Foshi and Barrett [42]. The author proposed a model to predict the strength and stiffness of a glulam beam by including basic information such as the knots frequency and tensile stress of laminating stocks. In the analysis, the beam was divided into cells. Each layer of lamination was assigned with varying number of cells in equal length with MOEs being obtained from stress grading. Equation 4.6 was used to calculate the composite MOE for a series of cells. The computed composite MOE was assumed to be the same as that from tensile tests or longitudinal stress-wave MOE. In addition, each cell was allocated with the corresponding strength profile based on presence of knots and tensile stress. One of the setbacks of the model was the exclusion on finger joint strength due to lacking of information. The author highlighted that the model was not intended for predicting the strength of a particular glulam beam but to estimate the statistics for similar beams and derived data for design purpose.

Ehlbeck [98] extended Foshi and Barrett [42]'s model and established a modified model known as the "Karlsruhe model". The model adopted the similar approach using the FE analysis. In addition, the authors included the end-joint effects which were based on tension tests of individual end-jointed timber. The model was able to simulate progressive failure by in the remaining adjacent cells after the first cell failed, thus this model accommodated the occurrence of redistributed stresses. The Karlsruhe model has strong influence on many other later researches such as Hernandez et al. [99], Aasheim et al. [16], and Colling and Falk [100].

iii. Statistical Correlations between Glulam MOE and MOEs of Laminating Stocks

Several related researches have been reported on development of probabilistic modelling using different assumptions and model refinements (Foschi-Barrett, 1980) [42], D.A. Bender, and Govindarajoo [28], Hernandez et al. [99]&[101], Aasheim et al. [16] Govindarajoo [28] developed a model as given in Equation 4.13 for relationship among the overall MOE of a glulam, the MOEs on the outer layer and the inner layer laminates, and the ratio of inner laminates to the total laminates. The objective of this equation was to determine the required MOE and the laminate number of the outer layers to meet the requirement of the overall MOE of the glulam. However, by re-arrangement, this equation can be used to determine the overall MOE when the laminate arrangement and MOEs of each laminate are known.

The Australian / New Zealand standard - AS/NZS 1328.2 (1998) [15] adopted Equation (4.14) for expected combination of MOE's using a value of 0.7 for the ratio of the inner laminations to the total number of laminations in a Glulam.

$$MOE_{outer} = \frac{MOE_{GLgrades} - p^3 MOE_{inners}}{1 - p^3},$$

Equation 4.13

where $MOE_{GLgrades}$ is the MOE of the expected Glulam grade based on species, MOE_{outers} is the MOE of the outer laminations, MOE_{inners} is the MOE of the inner laminations and p is the ratio of number of inner laminations to the total number of laminations.

The above standard has specified that only MOEs for the inner and outer laminations are required for glulam beam design. The requirement for laminations in the outer 0.15D (where D= thickness) tension zone should pass the proof test.

Equation 4.13 was developed based on deterministic characteristic in transformed section analysis. The “ I_k/I_g ” method, however, is probabilistic whereby the input parameters have to be prescribed as random variables to be used in a probabilistic simulation. Once the properties are generated, strength and stiffness of the beam can be analysed using the transformed section model or FE model [28].

4.1.3 Simulation on End-joint Properties

Ehlbeck [98] extended Foshi's work by including end-joint effects into the model. The authors utilised the individual tensile test of end-jointed timber to develop the joint properties as a function of the lower density of two jointed boards by using the regression method.

Simulation on end-joint properties was continued by Burk and Bender [38] relating the end-joint MOE with the MOEs of adjacent 61 mm segments. A predictive model was then developed which predicted the end-joint MOE and the segment tensile properties for determination of overall MOE of the laminating timber using linear regression.

Hooper [102] expanded the Burk and Bender's model by using the recursive transformation to predict the highly skewed distribution of end-joint MOE and tensile properties within each E-rated timber grade.

4.2 Summary of models

There are two selection of shooks options in the current finger jointed timber manufacturing practice. The first practice is randomly select shooks for jointing together without taking account on the individual shook's MOE. The second practice uses the same grade shooks for a structural grade finger jointed timber, assuming insignificant discrepancy in individual shook's MOE for each grade.

Considering that both options are common in Australia and New Zealand, modelling the overall MOE using serial correlation method appeared to be less appropriate as deviation in the MOEs among shooks can be highly random with large discrepancy. The correlations between the neighbouring MOEs may not be sufficiently strong and this explains why modelling with serial correlations is less practical.

The predictability of a statistical model is highly dependent on sampling and choosing the right model for getting a good correlation coefficient. In the case of wood, deviation from normality is not uncommon and inevitable as the distribution of one property to another is often not identical. [88].

The current industry practice and design practice use either the arithmetic mean [31] or the lowest measured local MOE as the rule of thumb indicating the stiffness of the whole piece of timber (the overall MOE). On the other hand, some other advanced stochastic models such as Kline's method [31] simulates local MOEs based on populated sampling

using probabilistic method. Nevertheless there were no further expanded studies predicting the overall MOE based on the simulated local MOEs. Furthermore, the simulated local MOEs were performed based on populated sampling on selected species and timber grades and this may restricts the flexibility in application. In addition, greater properties variability within wood may affect the validity of the suggested model. Thus, serial correlation using second-order Markov may not be suitable modelling approach in meeting the current research objective.

A good understanding on the mechanical properties and related factors is essential. From literature review, it is found that there are limited studies on deterministic modelling in predicting the overall stiffness of a finger joint member based on local stiffness properties of the corresponding finger jointing shooks. There are also many existing models which focused on modelling the local behaviour of glulam beam [16],[103],[101], and [17] and not the local properties of glulam laminates while others focused on statistical modelling correlating one properties to another based on likelihood relationship.

In corresponding to the knowledge gap, the present study intended to develop a deterministic model that could predict the overall MOE based on local MOEs of the corresponding finger jointing shooks. The effects of end-joints were found to be negligible during preliminary tests and have thus been excluded from the scope of study.

4.2.1 Static Bending Stiffness

Static bending stiffness refers to MOE of a beam determined from deflections due to gradually increase in load on the specimen under the region of proportionality of load and deflection [104]. There are two types of static bending tests – I) Single-point loading, and II) Two-point loading.

A single-point loading refers to bending on test specimen with a single load (P) applied at mid-span and supported by two reactions. The bending MOE (E_f) for Single-point loading is calculated from the following equation:

$$E_f = \frac{PL^3}{4bd^3\Delta}$$

Equation 4.14

In which L is the span (m), b and d are the width and thickness of specimens (mm), P is the loading (N) and Δ is deflection under load (mm).

Two point loading system comprised two loads and two reactions, hence is also known as four-point loading. The two-loading points can be spaced either at equidistance (known as the Third-point loading) or at equidistance from the reaction but at different distance on the loading span (two-point loading). The equation for a Third-point loading can be referred to Equation 4.15.

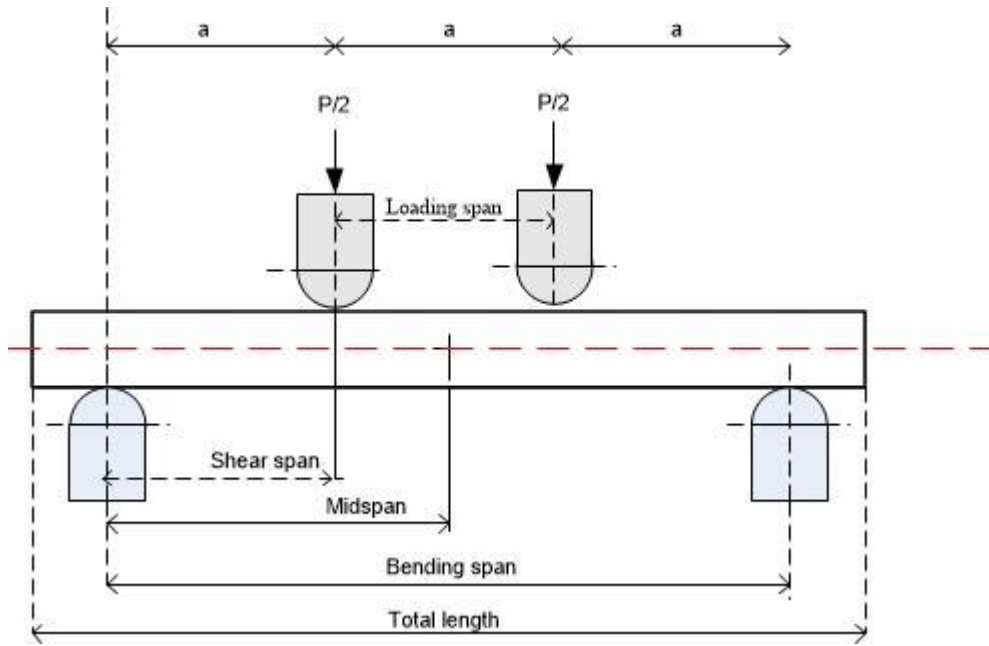


Figure 4.7: Illustration of a Third-point bending

$$E_f = \frac{23 PL^3}{108 b d^3 \Delta}$$

Equation 4.15

where E_f is the apparent MOE, P is the incremental load, L is the bending span, b and d is the respective width and thickness of specimen and Δ is the incremental deflection of beam's neutral axis measured at mid-span over distance L .

4.2.2 Relationship between Global MOE and Local MOE in Selected Standards

The apparent MOE (E_f) is commonly used in predicting the bending Modulus of Rupture (MOR). However, apparent MOE in short span includes shear distortion of the beam cross-section. This distinguished between the apparent MOE and true MOE.

The relationship between true MOE (categorised as the local MOE in BS/EN384:2010 [105]), apparent MOE (or overall MOE in BS/EN 384:2010 [105]) and shear modulus can be found in ASTM D198:2009 (X4.3) [106] in Equation 4.16. The equation suggests that true MOE is larger than the apparent MOE. This was supported by Grant [107] and Piter [2] with apparent MOE being 12% less than the true MOE when bending span was reduced from 900mm to 600mm. However, the correlations between MOE and MOR did not change because of the reduction in testing span. Observation by Piter et al. [2] shows that the mean of the true MOE was only 6 to 7% greater than the apparent MOE, thus it was concluded that the apparent MOE was more conservative and would be safer to be used as characteristic value in structural design.

$$\frac{PL^3}{48E_f I} = \frac{PL^3}{48EI} + \frac{PL}{4GKA}$$

Equation 4.16

where E_f is the apparent MOE in centre-point loading (or overall MOE), E is the shear corrected True MOE, G is the shear modulus, A is the area of the cross-section and K is the shear coefficient. For rectangular, $K = 5/6$, I is the moment of Inertia, and P is the increment of applied load below proportional limit. Calculation for the apparent MOE (E_f) and shear corrected True MOE (E) is defined in ASTM D198-09 [106] (Table X4.1).

4.2.3 Effects of Length-to-depth Ratio and Challenges in Experimental Design

i. Effect on Bending MOE

Length-to-depth ratio (l/d) is the ratio of length of a specimen to its thickness. In static bending, l/d has been found to be related to shear deflection thus l/d is used as a reference of pure bending [108]. A greater value of l/d is favourable which indicates that the occurrence of a primary failure is mainly caused by tensile and compressive stresses. On the other words, in a member with high l/d ratio, the influence of shear modulus on the measured deflection is minimal [109].

In the early years, the ASTM D198 (1928) testing standard specified test span for a third-point flexure test to be of minimum 15 feet (4.57m) and the l/d ratio was recommended

between 11 and 15. Test specimens for single-point loading bending was recommended not having thickness more than 4 inches and the l/d ratio lesser than 15. Nevertheless, there were no specifications on l/d ratio nor dimension in the ASTM standards since 1967. As to-date, ASTM D198-09 X5.3 has specified that determination of specimen length should be based on the purpose of the test [106]. In general l/d ratio of 16 should be acceptable for most materials [110]. In ASTM D3737-09 [26] clause 8.9, the MOE value for bending is calculated based on l/d ratio of 21:1. It has been assumed that the maximum deflection error due to shear (shear deflection) is accounted for up to 5% or less of the deflection with approximately 95% accounted for bending when loaded uniformly. Such assumption is applicable to load conditions with span-to-depth ratio greater than 14:1. Other standards such as the Japanese standard (JIS) suggested that the l/d ratios should be between 15 and 19 for bending stiffness tests and between 12 and 16 for bending strength tests [111]. Kubojima [108] recommended l/d ratio of 14 when one is juggled in choosing l/d between ASTM and JIS standards. Meanwhile, Lee and Kim [30] addressed the measurement challenge in setting local span for measurements of local MOEs in Glulam laminates.

Similar recommendations are made for specimens in resonance testing with different criterion. In the case of flexural resonance testing, the thickness of specimens should not be larger than one-sixth of the bending wavelength [112].

ii. *Effect on Bending Strength*

The effect of l/d on the measured bending strength of a specimen can be significant when *the* l/d ratio is too low due to influence on deflection caused by shearing stress [18]. As the l/d ratio decreases, the maximum load for rupture will increase as a result of greater resistance from the specimen in perpendicular to grain direction. In such a case, the deformation of the specimen is more significantly affected by small distances of supports. Subsequently, the relationship between the geometric and its neutral axis of the specimen are disrupted and eventually affecting the bending strength [113]. Sorn [113] reported that MOR was reduced by 1.8% and 0.43% for l/d ratio at 15 and 20, respectively; MOE reduced by 18.9 and 8.3%, respectively when both the l/d ratios were compared with $l/d \geq 20$. Despite of these reductions, the correlations between MOR and MOE remained the same. This observation was consistent with studies by Kass [36] and Grant [107].

4.2.4 Digital Image Correlation (DIC)

DIC is a technique in measuring strain (or displacement) of samples that are subject to gradually increasing load using photo-imaging. Strain can be calculated from a series of consecutive surface images of the specimens with sub-pixel resolution that can be obtained in digital images. It tracks the position of the same physical points shown in a reference image and deformed image. The digital mechanism is based on a square subset of pixels of the identified speckle pattern around the point of interest on a reference image and the corresponding location determined on the deformed image [114]. It uses mathematical correlation functions to analyse digital images of the subject of interest undergoing deformation. Digital image of the surface of deformation of the object is captured and the correlation between the deformed images and the un-deformed reference image are used.

There has been increased in interests on photogrammetry technique in measuring strain. This is known as the Digital Image Correlation (DIC) and has been broadly applied in wide range of disciplines in science and engineering. There has been many successful DIC applications in wood and wood-based material measured including measuring strain distribution in wood adhesive bonds [115], wood strands [116], on wooden knots[117]. The advantages of DIC application over other strain measuring approaches include its accuracy and its ability in fast data acquisition. It is claimed that this technology is well suited for characterization of material properties than the traditional method having extensometer or strain gauges being the major constrain in terms of practicality and difficulty in attaining strain information at challenging locations. In addition, DIC does not require installation of measurement probes, thus has made measurement over full-range of strain distribution via digital imagery possible [114].

However, the accuracy of the displacement in DIC is based on the resolution of the camera [118]. Amongst the setbacks in DIC application such as only surface images are used to evaluate the strain distributions, lacking in established application guideline, and requires sophisticated testing setup and specimen preparation to achieve reliable results [116].

4.3 Derivation of Elastic Curve in pure bending

4.3.1 Fundamentals on MOE in Tension and Compression

Stress (σ) can be defined as force per unit area while strain (ϵ) is the deformation caused by external forces, or the change in dimension in comparison to the original dimension. They can be mathematical defined by

$$\sigma = \frac{P}{A_0}$$

Equation 4.17

$$\text{and } \epsilon = \frac{(L-L_0)}{L_0} \text{ or } \frac{\delta}{L}$$

Equation 4.18

In a stress-strain (σ - ϵ) diagram, the ratio of stress to strain in a linear relationship is known as the proportional limit and we can deduce the Young's modulus, or Modulus of Elasticity (E) from the ratio of the two parameters where

$$\epsilon = \frac{\delta}{E}$$

Equation 4.19

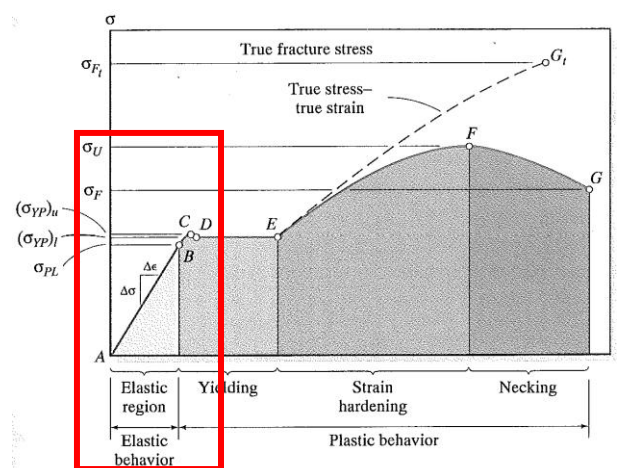


Figure 4.8: Linear relationship between stress and strain in the elastic region. Figure adapted from [119], pp. 39

The linear relationship between stress and strain along the x -axis can be described using the equation derived from Hooke's Law,

$$\sigma_x = E\varepsilon_x .$$

Equation 4.20

In Hooke's law it is assumed the uni-axial stress is applied to a homogeneous and isotropic member oriented along the x -axis. Hence the law is valid for uni-axial tension or compression within the linear portion of the stress-strain diagram. The material is considered isotropic when the mechanical properties of the material are independent of the direction considered.

Based on the theory of axial deformation along the x -axis to a member with constant Young's modulus, the stress and strain relationship can be reconstituted as follow:

From Equation 4.20 and Equation 4.18,

$$\sigma_x = E\varepsilon_x ,$$

$$\varepsilon_x = \frac{\sigma}{E} = \frac{P}{AE} ,$$

$$\frac{\delta}{L} = \frac{P}{AE} .$$

Equation 4.21

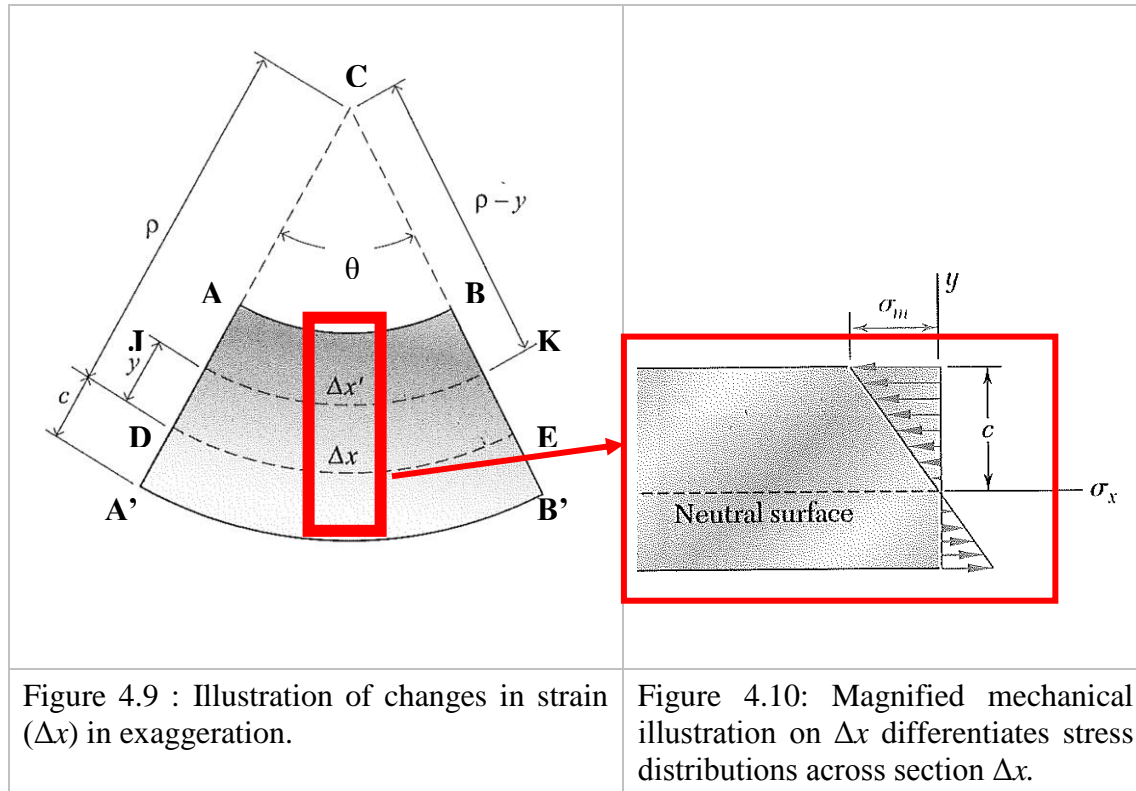
Thus, the total deformation δ of the sample over the length of L expressed in terms of dx can be denoted as

$$\delta = \int_0^L \frac{P(x) \cdot dx}{A(x)E} .$$

Equation 4.22

4.3.2 Theoretical Derivation for Transverse Deformation in Pure Bending

The mechanism of a member with a symmetrical cross section when subject to transverse loading in pure bending are illustrated in Figure 4.9 and Figure 4.10 in an exaggerated manner.



Figures 4.9 and 4.10 are adapted from Beer et al. [120]

Annotation for Figure 4.9 and Figure 4.10:

AB , DE , and $A'B'$ are the arcs of the circle at angle θ .

DE is the plane of neutral axis

ρ is the radius of arc DE .

θ is the central angle corresponding to AB , DE and $A'B'$.

The following is the standard assumptions [121] in pure bending for a member subject to transverse loading:

- The transverse section of the beam under bending remains plane during bending.
- The transverse section is perpendicular to circular arcs with the centre of curvature.

- The longitudinal elements of the beam are subjected only to simple tension or compression and there is no lateral stress (shear stress).
- The compression MOE and tensile MOE of the material are assumed to be the same.

Explanations:

The member subject to bending has a longitudinal plane of symmetry. The member remains in symmetry with respect to the plane when loaded, thus, the section remains plane and passes through C and the transverse section remains as a plane and is perpendicular to the deflection curve of the deformed member.

The arc of the upper surface of the member – AB , which is originally in a straight line will have a constant curvature with a circle around the centre C . During the bending, AB becomes shorter whilst the opposite lower surface $A'B'$ becomes longer.

According to the theory of elasticity the slender member has undergone a very small deformation. The deformation does not require any interaction between the elements of a given transverse cross section. With that, we assume that uniaxial stresses occur with values of σ_x .

The neutral layer is the layer which is parallel to the upper and the lower faces of the member and in which the stress (σ_x) and strain (ϵ_x) are zero as the member is deformed.

In pure bending, the transverse strains ϵ_y and ϵ_z are assumed to be negligible thus are not considered.

DE is the original position of neutral layer corresponding to the central angle θ . The neutral surface JK intersects the plane of symmetry along an arc of circle DE . The vertical deflection y is the difference of vertical distance between before and after deformation.

The length of arc DE corresponding to the central angle θ is denoted by the corresponding radius L prior to deformation. The new length of arc JK after deformation is denoted by new radius L' .

According to the Arc Length Theorem, the ratio of the arc length to the radius will be the radian of the central angle where the arc delimits.

Assume $DE = L$, then

$$L = \rho\theta .$$

Equation 4.23

Similarly, arc JK has moved a distance of y from the original neutral surface location DE after deformation; it is now denoted as L' ,

$$JK = L' ,$$

$$L' = (\rho - y) \theta .$$

Equation 4.24

The original length of arc DE was equal to L , the deformation of JK can be denoted as δ .

Therefore,

$$\delta = L' - L .$$

When Equation 4.23 and Equation 4.24 are substituted into δ :

$$\delta = (\rho - y) \theta - \rho \theta ,$$

$$\delta = -y\theta .$$

Equation 4.25

The longitudinal normal strain (ε_x) in JK is obtained by dividing δ with the original arc length JK :

$$\varepsilon_x = \frac{\delta}{L}$$

Substitute δ from Eq. 4.26 and L from Equation 4.23, we get:

$$\varepsilon_x = -\frac{y}{\rho}$$

Equation 4.26

The longitudinal normal strain ε_x is valid in anywhere as long as the transverse sections remained in plane. Identical deformation will occur in all planes parallel to the plane of symmetry.

The normal strain reaches maximum ε_m when y is the largest, herein known as c . This can be represented as an absolute value in the following form,

$$\varepsilon_m = \frac{c}{\rho}$$

Equation 4.27

The relationship between the normal longitudinal stress-strain and the maximum normal stress-strain as $\rho = \frac{c}{\varepsilon_m}$,

$$\varepsilon_x = -\left(\frac{y}{c} \cdot \varepsilon_m\right)$$

Equation 4.28

When Equation 4.28 is substituted into Equation 4.20, we get a normal longitudinal stress as a function of maximum normal longitudinal strain,

$$\sigma_x = E\left(-\frac{y}{c} \cdot \varepsilon_m\right)$$

Equation 4.29

Recall Equation 4.23,

$$\sigma_x = E\varepsilon_x$$

When the normal stress and strain reaches maximum, we get

$$\sigma_m = E \varepsilon_m$$

Equation 4.30

Substitute ε_m from Equation 4.29 into Equation 4.30, we get:

$$\sigma_m = - \left(\frac{\sigma_x}{\varepsilon_m} \cdot \frac{c}{y} \right) \cdot \varepsilon_m$$

$$\sigma_m = - \left(\sigma_x \cdot \frac{c}{y} \right) \quad \text{or} \quad \sigma_x = - \left(\sigma_m \cdot \frac{y}{c} \right)$$

Equation 4.31

Equation 4.31 presents the relationship in an elastic region, where the normal stress varies linearly with the distance from the neutral surface.

4.3.3 Location of the Neutral Surface of the region

The normal stress or strain of the member can be calculated at any point when the neutral surface in the member is identified.

From definition, the neutral axis can be determined by $\int y \cdot dA = 0$.

The first moment of area is defined as the summation of area multiply with the distance to an axis. It is commonly used to determine the centroid of an object. In this instance, the assumption that the neutral axis will pass through the centroid of the section is valid as long as the stresses remain in the elastic region.

The law of variation of flexural stress noted that the compression force (F_c) and tensile force (F_T) [12] in the x -direction must be zero.

When $F_c = F_T = 0$, couple M is formed,

$$M = - \int_{Area} y \cdot dF = - \int_{Area} y \cdot \sigma_x \cdot dA$$

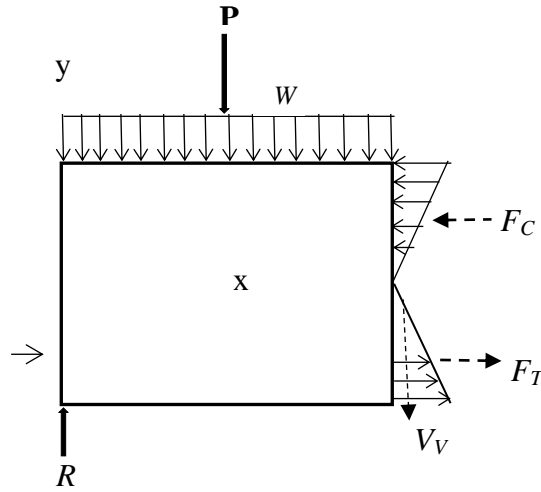


Figure 4.11: Illustration of stress distribution (adapted from Piter [2])

Under loading, if the moment over a given cross section is M , then the sum of the moments of the elementary forces must be equal to the bending moment and is represented as follow,

$$\int (-y \sigma_x \cdot dA) = M$$

Substitute σ_x from Equation 4.31, we get:

$$\int -y \cdot \left(\sigma_m \cdot \frac{y}{c} \right) \cdot dA = M$$

$$\frac{\sigma_m}{c} \int y^2 \cdot dA = M$$

Equation 4.32

where $\int y^2 \cdot dA = I$ is the second moment or moment of inertia I .

Solving Equation 4.32 for σ_m as a function of moment, distance y , and moment of inertia, we get

$$\sigma_m = \frac{Mc}{I}$$

Equation 4.33

This is the same as getting the normal stress (σ_x) at any distance y ,

$$\sigma_x = -\frac{Mc}{I},$$

Equation 4.34

where $\sigma_x < 0$ when the member undergone compression;

$\sigma_x > 0$ when the member undergone tension.

The deformation caused by bending moment can be found from the reciprocal of radius of curvature (ρ) in Equation 4.35.

$$\varepsilon_m = \frac{c}{\rho}$$

Equation 4.35

Thus,

$$\frac{1}{\rho} = \frac{\varepsilon_m}{c}.$$

Equation 4.36

The curvature of a member can be computed in a function of bending moment, modulus of elasticity, and moment of inertia

Substitute ε_m from Equation 4.35, where $\sigma_m = E\varepsilon_m$ into Equation 4.36, we get:

$$\frac{1}{\rho} = \frac{\sigma_m}{E \cdot C}.$$

Substitute σ_m from Equation 4.22, we get

$$\frac{1}{\rho} = \frac{M}{E \cdot I}.$$

Equation 4.37

To compute deflection of a *homogeneous beam* at any given point, the effective slope of a linearly elastic beam can be determined by using differential method.

From Equation 4.37, we have the following equation,

$$\frac{1}{\rho} = \frac{M}{E \cdot I}, \quad \text{or} \quad M(x) = \frac{E(x) \cdot I(x)}{\rho(x)}.$$

The equation of curvature ([122] & [119]) of a plane curve represented in the form of $y = f(x)$ can be referred as follow:

$$k = \frac{d^2 y / dx^2}{\left[1 + \left(\frac{dy}{dx} \right)^2 \right]^{3/2}}.$$

The radius of curvature $\rho(x)$ is related to the derivative of the deflection,

$$k \equiv \frac{1}{\rho} = \frac{\frac{d^2 y}{dx^2}}{\left(1 + \left(\frac{dy}{dx} \right)^2 \right)^{3/2}}.$$

where $\frac{dy}{dx}$ and $\frac{d^2 y}{dx^2}$ are the first and second derivatives of the function $y(x)$ represented by the curve.

Since the slope of the curvature is very small as compared to unity, $\frac{dy}{dx}$ become negligible, we have the following known as the *moment-curvature equation*:

$$\frac{1}{\rho} \approx \frac{d^2 y}{dx^2} = \frac{M(x)}{EI},$$

$$EI \cdot \frac{d^2 y}{dx^2} = M(x).$$

Equation 4.38

By integrating the moment-curvature equation, we can now determine the slope $\frac{dy}{dx}$ and deflection y at any point given in the expression in $M(x)$.

We know $\tan \theta = \frac{dy}{dx}$, let $\tan \theta$ be $\approx \theta(x)$.

$$EI \cdot \theta(x) = \int_0^x M(x) \cdot dx + C_1$$

Equation 4.39

Integrate Equation 4.39 to get the slope $\frac{dy}{dx}$ at any given point.

$$EI \cdot \frac{dy}{dx} = \int M(x) \cdot dx + C_1$$

$$\frac{dy}{dx} = \frac{1}{EI} \int M(x) \cdot dx + C_1$$

Equation 4.40

The deflection at any given point y can be determined with the following equation by second integration.

$$EI \cdot y = \int \left[\int M(x) dx + C_1 \right] dx + C_2$$

$$EI \cdot y = \int dx \int M(x) \cdot dx + C_1 x + C_2$$

$$y = \frac{1}{EI} \int dx \int M(x) \cdot dx + C_1 x + C_2$$

Equation 4.41

where C_1 and C_2 are the constants of integration.

4.4 Modelling of overall MOE in a Finger Jointed Timber under Bending

In the previous section, Equation 4.40 and Equation 4.41 were derived based on the basic kinematic assumptions in Bernoulli-Euler beam theory and it is valid for uniform and homogeneous member subject to pure bending. The theory may require some modification when subject to less homogeneous beam such as a finger jointed timber. Discussion of extending the original model will be discussed in the following sub-sections for the finger jointed timber.

The predicted total deflections and predicted overall MOEs will be compared with experimental results for validation of the modified models.

In essence, Equation 4.43 is derived based on the concept illustrated in Figure 4.12. The model comprises summation of the integrands over the finger joint member (or finger jointed system), represented by functions based on the measured MOE values of the shook elements. The overall deflection of the finger joint member, represented as the grand function $F(x_i)$, is the summation of those of individual shooks, the corresponding sub functions $f_i(x_i)$, under moment loading as functions $f_1(x_1)$ to $f_5(x_5)$ as shown in Figure 4.12.

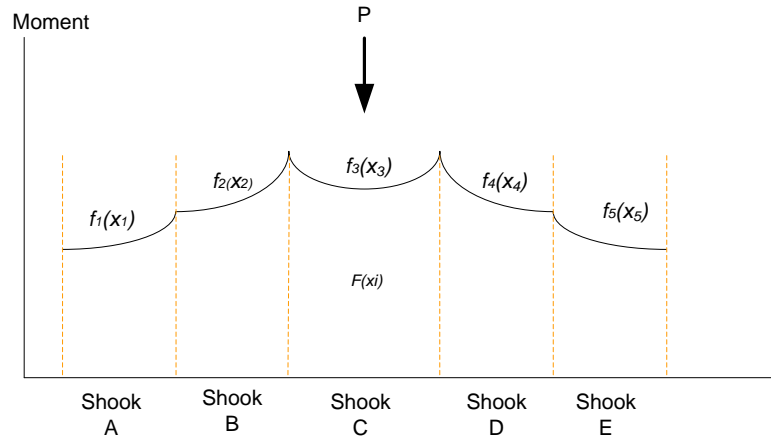


Figure 4.12: A graphical illustration of the total area under the integrands $f(x_1)$ to $f(x_5)$, representing independent integrands for shook elements A to E constituted in the finger jointing system

Note: The functions of the curves are merely for illustration and may not be representing the actual graph functions.

The lower and upper limits of each integrand L_0 to L_5 are differentiated by the distance of the corresponding shook element away from the point of bending moment, measuring from the starting point of the shook to its adjacent end within the loading span of the same finger jointing system. The lower and upper limits of the next shook element continue from the subsequent connection of the next piece in relative to the length of the finger joint member. The starting point of the first element having lower limit “0” would be depending on where the point of moment is considered. The location of the point of bending moment is important as this will determine where “0” would starts from, thus determine the magnitude of area covered under the constituted functions. Intuitively we know that contributions of shooks’ MOEs at the reaction pins would be less significant than the mid-span. A graphical representation is illustrated in Figure 4.12.

4.4.1 Modelling Discrete Variations in (i) Shook MOE and (ii) Shook Length along the Span using Moment-Curvature Analysis Approach

Modelling in the present study has confined the finger jointed member to be made of five finger jointing shooks as in Figure 4.13. However, the method can easily be extended to a finger jointed timber with different number of shooks. The testing span of a finger jointed member is made of segments of shooks with different stiffness represented as E_i . In this case, they are made of five finger jointing shooks with stiffness E_1 , E_2 , E_3 , E_4 and E_5 . These E values have been individually measured prior to finger jointing. The shooks have been pre-selected to be as uniform as possible by removing any undesirable defects and by isolating those that have significant grain deviations. The deviation of the shook’s mechanical properties caused by undesirable physical properties should be negligibly small and the measured MOE for each shook can be considered constant along the shook length. The mechanical properties across the testing span are, however, considered to be non-homogenous because of variance in stiffness along the length. Shearing stress is assumed to be negligible and the moment of inertia I is the same for each cross-section of the finger jointed beam.

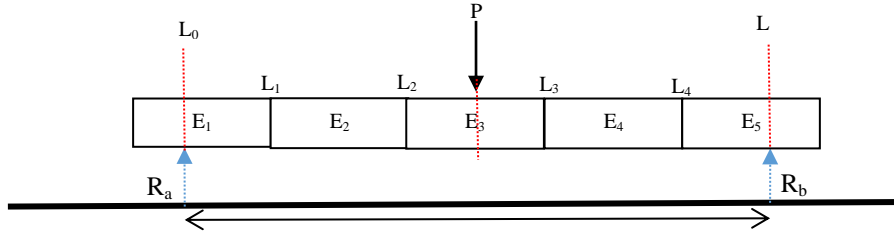


Figure 4.13: A finger joint member made of shooks with same shook length. Each shook has the measured E_i obtained individually prior to testing of the overall MOE of the finger joint member. The E_i values for shooks 1 to 5 (counting from left to right) are represented by E_1 , E_2 , E_3 , E_4 and E_5 . The location of x is referring to any point within the testing span, from L_0 to L . The finger joint member is subjected to static bending in a free-free boundary condition

The refined modelling has assumed the testing specimen subjected to bending complied with the Hook's elastic law whereby under the elastic region the specimen it would perform in stress-strain linearly. Since all selected shooks in the finger jointing have excluded the visible knots, the model assumes that deflection in anywhere of the finger jointed specimen has a continuous cross section moment of inertia.

4.4.2 Modelling Assumptions

The following assumptions are made in application and modification of the beam theory in static bending of the finger jointed timber. The ultimate objective is to establish a relationship to determine the overall MOE based on known individual shook's MOE.

- The MOE of a shook is assumed to be uniform across each element
- Stresses near the beam edge in a two-point loading are considered negligible
- The end-joint strength is stronger than wood. Joint failure is negligible and joint strength is not taken into account in modelling
- Each shook is considered to have the same MOE value as measured from separate tests

Considering that the length-to-depth (l/d) ratio of the specimen is large, effect of shearing stress in the bending is negligible, and the bending is considered to be pure bending. Since moment of inertia (I) for each shook is the same, the moment of inertia for the finger jointed wood across the testing span would be the same.

Recall Equation 4.38 where

$$\frac{1}{\rho} = \frac{M(x)}{EI}, \quad \text{and} \quad \frac{d^2 y}{dx^2} = \frac{M(x)}{EI}.$$

We can re-arrange the above equation as

$$I \frac{d^2 y}{dx^2} = \frac{M(x)}{E}.$$

In this instance the moment of area (I) remained constant along the length of the member. Bending moment at any point x is denoted as a function of $M(x)$. The slope $\frac{dy}{dx}$ can be found by integrating Equation 4.38.

Introducing the E_i for i^{th} shook counted from the left end, here we have:

$$I \cdot \int \left(\frac{d^2 y}{dx^2} \right) dx = \int \frac{M(x)}{E_i} \cdot dx.$$

Equation 4.42

Since MOE varies along length L , E_i is considered a discrete function of x .

Refer to Figure 4.8 and Figure 4.9, the maximum flexural deflection in a single-point bending under a free-free boundary condition occurs at the mid-span; the location x is at $L/2$. The y deflections at both reaction points R_a and R_b should be zero. To comply with the above presumptions, the functions for slope $\frac{dy}{dx}$ and the overall deflection y has been divided into two segments as illustrated in Figure 4.9 and Figure 4.10. The mathematical expression is given in Assumption 1 and 2.

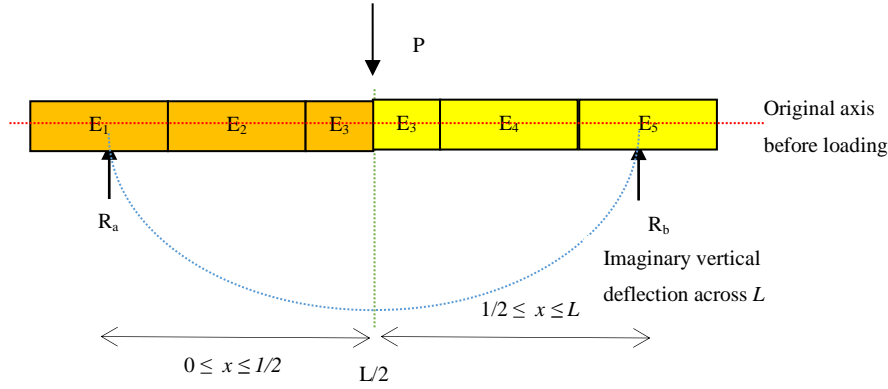


Figure 4.14: Illustration of loading deflection at any point x along the test span. The red dotted line represents the imaginary neutral axis before P is exerted. The blue dotted inverse parabolic line is an exaggerated illustration of the imaginary neutral axis during loading. Maximum y deflection occurs at mid-span at $x = L/2$. The first section $0 \leq x \leq L/2$ is represented in orange cells, the second section $L/2 \leq x \leq L$ is represented in the yellow.

In a single-point bending with a load of P , the reaction R_a and R_b are equal to each other at the value of $P/2$. The bending moment $M(x)$ as a function of x can be written as

$$M(x) = \begin{cases} \frac{Px}{2}, & 0 \leq x \leq \frac{L}{2} \\ \frac{P}{2}(L-x), & \frac{L}{2} \leq x \leq L \end{cases}.$$

By firstly integrating Equation 4.42 and introducing the local moments defined above as a function of x , the integral function $\frac{dy}{dx}$ would be indefinite resulting in an integral constant. Since integration is done in parts by addition, we will have the corresponding constants for each integrated segment.

$$I \cdot \frac{dy}{dx} = P \left[\int \frac{x}{2E_1} \cdot dx + \int \frac{x}{2E_2} \cdot dx + \int \frac{x}{2E_3} \cdot dx + \int \frac{x}{2E_4} \cdot dx + \int \frac{x}{2E_5} \cdot dx \right]$$

$$\frac{I}{P} \cdot \frac{dy}{dx} = \frac{x^2}{4E_1} + C_1 + \frac{x^2}{4E_2} + C_2 + \frac{x^2}{4E_3} + C_3 + \frac{x^2}{4E_4} + C_4 + \frac{x^2}{4E_5} + C_5$$

Equation 4.43

where C_1, C_2, C_3, C_4 and C_5 are the integral constants.

$$\text{Let } C = C_1 + C_2 + C_3 + C_4 + C_5 \quad ,$$

$$\frac{I}{P} \cdot \frac{dy}{dx} = \frac{x^2}{4E_1} + \frac{x^2}{4E_2} + \frac{x^2}{4E_3} + \frac{x^2}{4E_4} + \frac{x^2}{4E_5} + C \quad .$$

Equation 4.44

$$\text{Let } z = (L-x) \text{ at } x = L_3 \text{ to } L \text{ when } L/2 \leq x \leq L ,$$

$$\begin{aligned} \frac{I}{P} \cdot y = & \int_0^{L_1} \frac{x^2}{4E_1} \cdot dx + \int_{L_1}^{L_2} \frac{x^2}{4E_2} \cdot dx + \int_{L_2}^{L/2} \frac{x^2}{4E_3} \cdot dx - \int_{L/2}^{L-L_3} \frac{z^2}{4E_3} \cdot dz - \int_{L-L_3}^{L-L_4} \frac{z^2}{4E_4} \cdot dz \\ & - \int_{L-L_4}^0 \frac{z^2}{4E_5} \cdot dz + \int_0^L C \cdot dx \end{aligned} \quad .$$

Equation 4.45

This can also be simplified as follow,

$$\frac{P}{y} = \frac{I}{A} \quad .$$

Equation 4.46

where

$$\begin{aligned} A = & \frac{L_1^3}{12E_1} + \frac{(L_2)^3 - (L_1)^3}{12E_2} + \frac{(L/2)^3 - (L_2)^3 - (L-L_3)^3}{12E_3} - \frac{(L-L_4)^3 - (L-L_3)^3}{12E_4} \\ & - \frac{-(L-L_4)^3}{12E_5} \end{aligned}$$

and

$$I = \frac{bd^3}{12} \quad .$$

4.5 Modelling Moment-curvature Equation in a Single-point Loading System

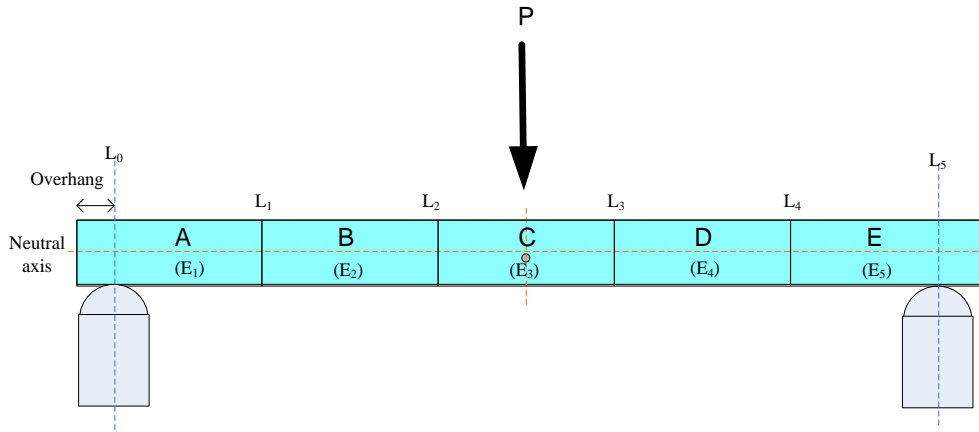


Figure 4.15: Single-point loading on a finger joint member made of segment of shooks with the corresponding MOE's from A to E

In Section 4.5, the Overall MOE was derived based on the Moment-Curvature equation. The original derivation of Moment-Curvature equation was accustomed for finger joint specimen made of five pieces of shooks at different MOEs values and different shook lengths. The equation was segmented into parts, based on i) the number of shooks to be finger joint, ii) the actual shooks' MOEs, and iii) the location of these MOEs along the finger joint member.

Each shook was visually screened for uniformity in properties with minimum visual grain deviation and knots removed prior to any testing. The MOEs of the shooks were individually measured prior to finger jointing. With that, assumptions on the measured MOE of the shook have been made to be constant across the element. The rational of the modelling is as follow:

The overall deflection and bending slope for finger jointed member loaded under a free-free single-point loading configuration can be represented by the maximum deflection and bending slope measured at mid-span, respectively. Refer to Equation 4.47, the overall deflection and slope are the product of summation of the integration functions obtained from individual shook, herein referred to as element. In each integration function, it is a representation of shook elements present in the finger jointed system and its corresponding MOEs that had been determined from determination of shook MOE tests. In this case, the MOEs of shook elements A, B, C, and D in Figure 4.15 is denoted as E_1 , E_2 , E_3 , E_4 , and E_5 , respectively.

From the first integration on Equation of Curvature result the overall bending slope ($\frac{dy}{dx}$). Equation 4.48 is simplified and made equivalence to Equation 4.43.

$$I \cdot \frac{dy}{dx} = P \left[\int \frac{x}{2E_1} \cdot dx + \int \frac{x}{2E_2} \cdot dx + \int \frac{x}{2E_3} \cdot dx + \int \frac{x}{2E_4} \cdot dx + \int \frac{x}{2E_5} \cdot dx \right] \quad \text{Equation 4.47}$$

$$I \cdot \frac{dy}{dx} = \sum \left[\left(\int_{L_0}^{L_1} \alpha \cdot dx \right) + \left(\int_{L_1}^{L_2} \beta \cdot dx \right) + \left(\int_{L_2}^{L_3} \gamma \cdot dx \right) + \left(\int_{L_3}^{L_4} \varpi \cdot dx \right) + \left(\int_{L_4}^{L_5} \tau \cdot dx \right) \right] \quad \text{Equation 4.48}$$

$$\text{where, } \alpha = \frac{M(x)}{E_1}; \quad \beta = \frac{M(x)}{E_2}; \quad \gamma = \frac{M(x)}{E_3}; \quad \varpi = \frac{M(x)}{E_4}; \quad \tau = \frac{M(x)}{E_5}.$$

Lastly, performing a second integration on Equation 4.47 gives us the overall deflection,

$$\frac{dy}{dx} = \frac{P}{4I} \left[\int_0^{L_1} \frac{x}{E_1} \cdot dx + \int_{L_1}^{L_2} \frac{x}{E_2} \cdot dx + \int_{L_2}^{L-\frac{L}{2}} \frac{x}{E_3} \cdot dx - \int_{L-\frac{L}{2}}^{L-L_3} \frac{z}{E_3} \cdot dz - \int_{L-L_3}^{L-L_4} \frac{z}{E_4} \cdot dz - \int_{L-L_4}^{L-L} \frac{z}{E_5} \cdot dz \right] \quad \text{Equation 4.49}$$

Let

$$A = \left[\int_0^{L_1} \frac{x}{E_1} \cdot dx + \int_{L_1}^{L_2} \frac{x}{E_2} \cdot dx + \int_{L_2}^{L-\frac{L}{2}} \frac{x}{E_3} \cdot dx - \int_{L-\frac{L}{2}}^{L-L_3} \frac{z}{E_3} \cdot dz - \int_{L-L_3}^{L-L_4} \frac{z}{E_4} \cdot dz - \int_{L-L_4}^{L-L} \frac{z}{E_5} \cdot dz \right]$$

Reshuffle Equation 4.49 as a function of load (P) per unit maximum deflection (y_{max}), we get

$$\frac{P}{y_{max}} = \frac{I}{A/4}, \quad \text{Equation 4.50}$$

where I is the second moment of inertia.

Ultimately, the Overall MOE of the finger jointed beam was derived by substituting the predicted deflection (Δ) into a standard Apparent MOE equation (Equation 4.51) [106].

$$E_{Apparent} = \frac{PL^3}{4bd^3 y_{\max}} = \left(\frac{P}{y_{\max}}\right) \cdot \left(\frac{L^3}{4bd^3}\right)$$

Equation 4.51

Equivalence is made based on the priori understanding of the overall deflection measured at mid-span representing the overall MOE of the bending specimen. Hence, Equation 4.51 can be equated to Equation 4.51 by substituting $\frac{P}{y_{\max}}$ into the equation.

Substitute Equation 4.50 into Equation 4.51, we have $E_{Apparent} = \frac{L^3}{12A}$.

When we examine Equation 4.48 and Equation 4.49, we can see that the overall apparent MOE ($E_{Apparent}$) is affected by the integration term A which is, in turn, a function of the local MOE and lengths of individual shooks. The integration of the same set of components i.e. A to E with shooks MOEs E_1 to E_5 , at different shook lengths or at different location in each integrated sub-component would essentially result in different value of total deflection. In another words, the location or position of a shook element, the lengths and MOEs of individual shooks will affect the overall MOE.

5 Relationships between Local MOE of Shook, Overall MOE and MOR of Finger Jointed Member

The tests samples in this part of study include shooks and finger jointed timbers. The shooks were prepared from sawn timbers which were supplied by a finger jointing mill in South Island, New Zealand. After the shook samples were received, these shooks were tested for MOEs in the Structural lab at this university, and were later sent to the finger jointing mill for manufacturing of the finger jointed timber samples. Finally the manufactured finger jointed timber samples were sent back to the laboratory for tests. The details of sample preparation for shooks will be described in Section 5.3.3, and those for the finger jointed timber samples are given in Section 5.6.1.

5.1 Test Sequence – An Overview

There were two phases of testing. In the first phase of testing, the MOE profiles of sawn timber and the MOE values of shooks were measured. The sawn timber MOEs were measured in the finger jointing mill and the individual shook's MOE was measured at the Structural Lab of this university. In the second phase, the MOE and MOR values of finger jointed timber samples were measured in the Structural Lab of this university. A flow diagram for a quick overview of the second phase test sequence is illustrated in Figure 5.1.

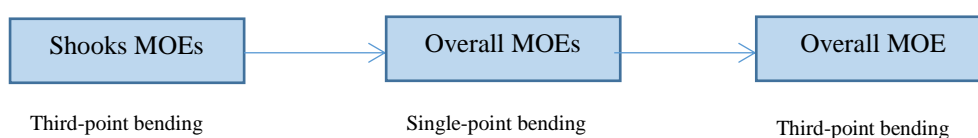


Figure 5.1: Tests sequence for static bending tests

Based on the sawn timber grading, the shooks were firstly sorted into different categories. After this, the MOEs of each shook were obtained using the Third-Point static bending test [106]. Then each piece of shook was re-sorted according to the value of the measured local MOE from which the combinations of shooks to be finger jointed were established as shown in Table 5.2. This design was based on the availability of shooks according to the values of the local MOE. The experimental design in Table 5.2 was drafted and finalised after information on the local MOEs was obtained.

The overall MOE of finger jointed members were obtained using the single-point loading test [106]. The relationship between local MOEs and the overall MOE of a jointed member were studied. Lastly, bending strength of a finger jointed member was ascertained from the single-point bending strength test and the relationship between bending strength of a finger jointed member and the corresponding shook MOEs was studied. Justifications on different types of MOE bending test configurations for shooks and finger jointed timber samples are explained in the following section of this chapter.

5.2 Test Equipment

5.2.1 Test Method 1: Third-point Loading for Shook Specimens

The third-point loading method was chosen for measuring the shook MOE and tests were conducted on an Instron Universal Testing Machine (UTM) Model 116. Figure 5.2 illustrates the test setup in the Third-point loading. The loading system comprised two loading anvils, each carrying half of the overall load (P) across the span between the two anvils (known as bending span). The stress was evenly distributed across the region within the bending span. The occurrence of lateral stress (shear stress) can be minimised with reduced concentrated stress (as compared to single-point loading). This can be explained in a bending-moment diagram in Figure 5.4 in which two vertical forces, each of $P/2$, were loaded symmetrically over the mid-span. In this case, the moment increased linearly from the support point to the loading position and maintained constant between the two loading points. The maximum deflection occurred at mid span and zero deflection at the reaction supports. The maximum deflection was measured at the mid span along the neutral axis assisted by the ‘U’ shaped yoke. In this way, shear deflection and indentation effect were considered negligible [123]. Besides, each anvil carried half the overall load. In this way it would incur less pressure and minimise indentation on the surface of specimen at the loading points. As such the measured local MOE would be less likely to be underestimated due to shear effect and overestimated due to indentation (crushing).

A 10% overhang was allocated for all the shook specimens. The reaction supports were equally spaced at one-third of the span length measuring from each support in the Third-point loading. The load was set at 10 kN at a constant loading speed of 1.0 mm/min.

A “U” shaped yoke deflectometer (Figure 5.2) made of aluminium sheet was suspended between the nails driven into the specimen along the neutral axis. The intention of

using a yoke deflector was to enable measurement of the deflection between the loading span along the neutral axis [106]. The yoke deflector was designed in a way so that it had sufficient weight to hold-on to the nails but would not exert unnecessary additional weight upon the suspended nails, meanwhile the form of the yoke deflector were ensured to be maintained over time. The dimension of the specimen was too small and had restricted movements during loading, hence the study had to exclude hanging the yoke deflector along the loading span but on the bending span. With that, apparent MOE was calculated for the local MOE of shooks.

The type of nail used on supporting the yoke deflector and the potentiometer in static bending test was a standard Panel Nail 25 mm (length) x 1.25 mm (diameter). The depth of the nail on each nailing point was controlled by a custom-made 15 mm depth gauge or jig-alike. This was to ensure the depth of the nails was uniformly driven into each point in each specimen.

The ASTM D198 [106] standard has suggested a concaved plate to be underlay between the pins (loading pins and reaction pins) and the surface of specimen to minimise potential crushing on specimens, thus minimising overestimation in MOE value. In the experiments, a 2 mm “slightly concaved” metal plate was under-laid between the anvils, the supporting reactions and the surfaces of the specimens.

In the Third-point bending, the apparent MOE of the sample can be deduced using Equation 5.1 [106].

$$MOE_{Apparent (3rd-pt)} = \frac{23 PL^3}{108 bh^3 \Delta}$$

Equation 5.1

where P is the increment of applied load below proportional limit (N), L is the span of beam (mm), b is the width of beam (mm), h is the depth of beam (mm), and Δ is the increment of deflection of beam's neutral axis measured at mid-span over distance L (mm) at corresponding P .

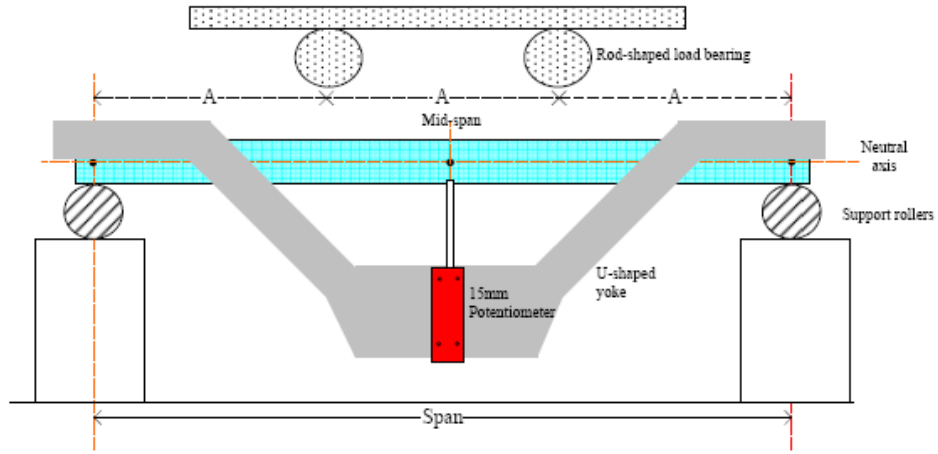


Figure 5.2: A typical test setup for the Third-point static bending

5.2.2 Test Method 2: Single-point Bending for Finger Jointed Member

The single-point bending tests were conducted on an Instron Universal Testing Machine (UTM) Model 116. The test setup for testing finger jointed member on the single-point loading is illustrated in Figure 5.3a and Figure 5.3b. A 20% overhang was allocated for all finger jointed members. A 1000 N load cell was loaded at a lower loading speed of 5.0 mm/min to accommodate the Digital Image Correlation (DIC) program. The loading was left to run and manually stopped at 300N to avoid any accidental rupture. The apparent MOE of the finger jointed specimen with the single-point bending was calculated using Equation 5.2.

$$MOE_{\text{apparent (Single-pt)}} = \frac{PL^3}{4bh^3 \Delta}$$

Equation 5.2

where P is the increment of applied load below proportional limit (N), L is the span of the specimen (mm), b and h are the respective width and depth of specimen (mm), and Δ is the increment of deflection of the specimen's neutral axis measured at mid-span over distance L and corresponding load P (mm).

In the single-point bending experiments (Figure 5.3), different potentiometers were placed at locations N1, N2 and N3 along both sides the finger jointed member. The identified sizes of suitable potentiometers along position at N1, N2 and N3 were 200mm, 200mm and

100mm potentiometers, respectively. The sizes of the potentiometers were determined based on the estimated deflections at points N1, N2, and N3 using the arbitrary MOE and MOR values.

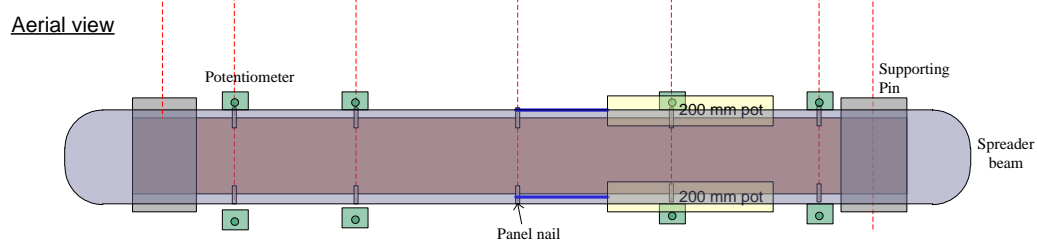
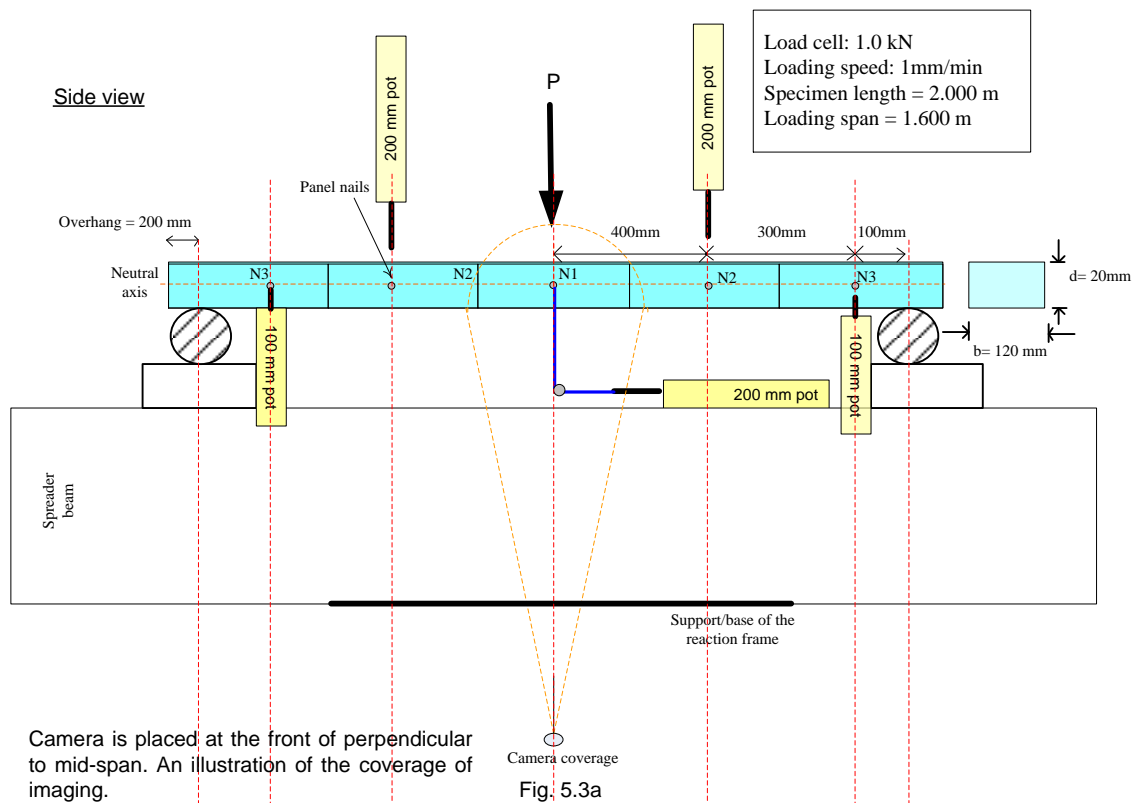


Fig. 5.3b

Figure 5.3: Side view and aerial view for Single-point MOE bending test for finger jointed member at 120mm x 20mm x 2m

5.2.3 Deflection Measurement

i. *Third-point Bending*

As shown in Figure 5.4, the vertical deflection in the third-point bending was measured at the neutral axis relative to the original position prior to loading. The vertical movements due to loading deflection were measured using a 15 mm deflection transducer (also known as potentiometer). It was the location where the shaft of the transducer was attached to the nail at mid-span along the neutral axis of specimen. The movement of the shaft was converted in analogue signals and later into digital by the Programmable Logic Controller (PLC) program and finally graphed in real-time on a computer. Simultaneous deflection measurements were made on both sides of the specimen during bending. The average of the maximum deflections measured from both sides of the shook was obtained and was used in computation of the apparent MOE. The apparent MOEs for the tested shooks were determined and sorted based on the MOE grouping declared in Table 5.2.

The estimated maximum load for the testing population was calculated to be approximately 10 kN at the elastic limit (Appendix A5.2). To ensure specimens were kept within its elastic limit, the maximum load during the bending tests was kept to be half of the calculated elastic limit load, which was 5 kN. The arithmetic mean of the load deflection measurements was used to determine the incremental deflection per unit incremental loads.

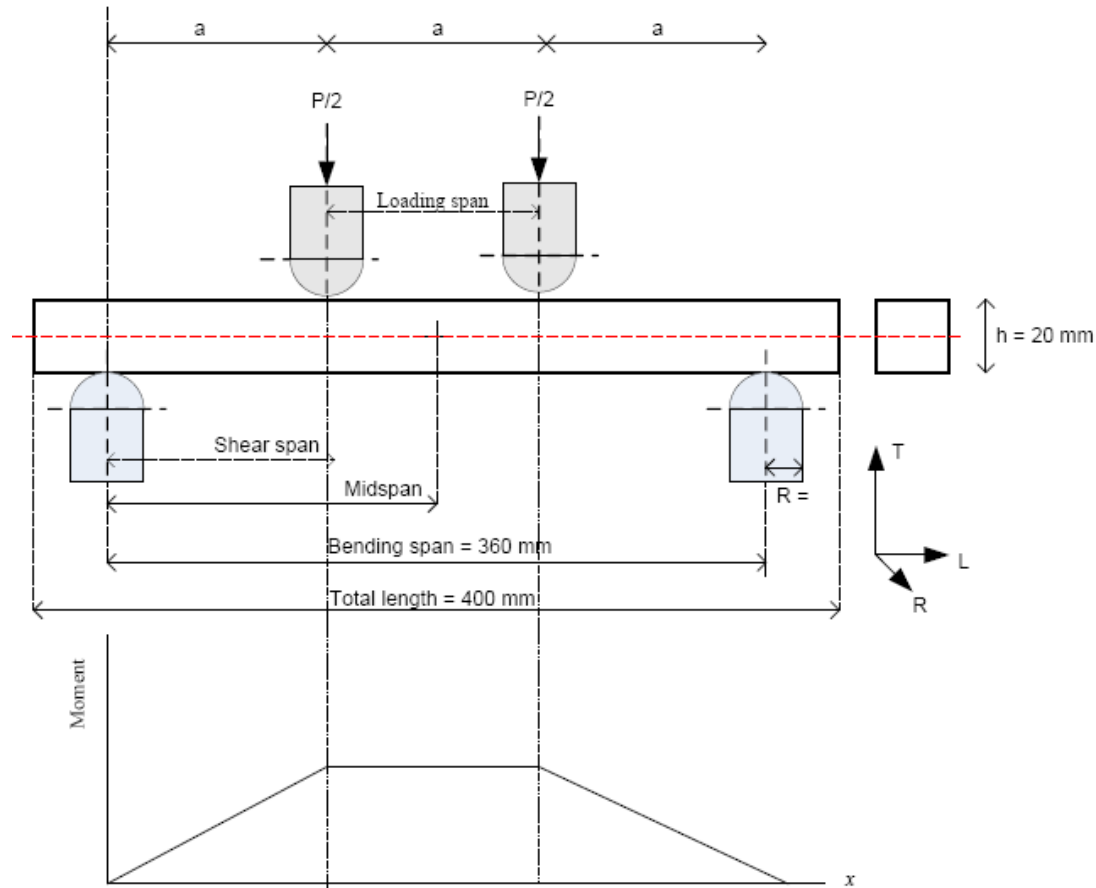


Figure 5.4: Third-point bending test configuration and bending moment diagram

ii. Single-point bending

In the single-point bending, the potentiometer at N1 location (Figure 5.3a) measured the mid-span deflection. Considering that the size of the UTM frame may restrict vertical travels of the 200mm potentiometer, the movement of the potentiometer was customised to be attached to a single pulley. The single pulley was attached between the potentiometer that was rested horizontally on the testing frame and the pulley's connector was connected to the vertical travels at N1 when P was loaded. This simple pulley system measured the vertical movements without interference of gravity forces and related displacement. Thus, the amount of vertical travels on the upper portion of the pulley would be the same as the amount of horizontal travels registered by the potentiometer. The displacements on the left and right sides at N2 and N3 locations measured the displacements at the corresponding points.

Potentiometers were placed across the loading span and a digital camera was placed at the right angle to the centre loading to capture the displacements at a fixed interval, thus the

bending MOE was calculated based on the captured maximum deflection. In this study, a Sony SLR camera was placed at a fixed distance that was sufficient to cover the bending deflection of the entire middle shoo (Figure 5.3). The camera could not be positioned to capture the entire loading span due to angle restriction by the UTM frame. To capture the deflection of the entire loading span at a macroscopic view, potentiometers at positions N2 and N3 were placed across the member and thus deflections across the entire beam was covered.

5.2.4 Digital Image Correlation (DIC)

The aim of capturing digital images was to characterise deflections in the vicinity of loading zone in replacement of potentiometers. Digital images were taken with a DSLR-SLR Sony Alpha A33 camera together with continuous capture of images taken at a set interval with an intervalometer during loading. The Sony SLR camera had been set fleshless at ISO 400. The shutter speed was set at 1/30 with aperture f 5.6. A manual focus setting was selected. Images were taken using a 3.5-5.6/18-55 SAM lens focus set at 55 mm. The lightning source was from an incandescent lamp with electromagnetic frequency at 50 Hz. A Timer Remote Controller was attached to the SLT unit to set at an interval time of 5 seconds per frame at a 100 exposure count. The intervalometer was set at 5 seconds per frame at 150 counts. Images were captured under incandescent lighting source at 50Hz. Images were taken simultaneously with static loading. The resolutions of the images were taken at 14.2MP and image format of ARW.

All images taken per specimen in the loading were compiled and processed using the Digital Image Correlation and Tracking application [124]. The output from the image processing tool was a graphical representation of displacements with respect to pixel points. The magnitudes of displacements were represented by the differences between the preselected points along the specimen image in pixels before and during loading between the first and the last image. The graphical plot of displacement can be used to explain whether a symmetrical bending had occurred and this information was crucial especially on combination of shooks with high standard deviation for MOEs.

The captured digital images were processed with the Digital Image Correlation and Tracking with Matlab (2010) application. The image processing software processed the input images to plot displacement starting from loading until at 100 to 150 exposures. Figure 5.5

depicts an example of one of the snaps. A plotted graph was generated by the application and will give an indication whether the bending of the specimen was symmetrical or otherwise.

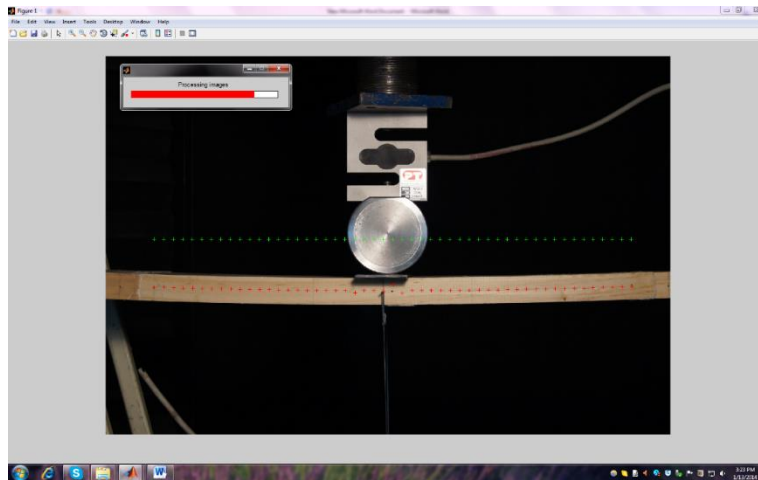


Figure 5.5: An example for one of the image frame running on the Digital Image Correlations (DIC) analysis

5.3 Preparation and Testing of Shooks

5.3.1 Pre-classification based on Industry Grading of Sawn Timber

Full size sawn timbers were kiln-dried and pre-tested for MOE characteristics at the collaborator's premises using the Third-point Loading test. The aim of pre-testing the MOE was to provide an estimate number of shooks available in each MOE group listed in the experimental design (Table 5.2).

The pre-tested timbers were sent for scanning of defects such as knots and other visible defects using the Woodeye® machine. Once defects had been detected and removed, the remaining lengths were docked into shook length of 400mm in the mill. Then the shooks were sent to the Structural Lab at the University of Canterbury for tests.

The existing finger joint manufacturing in New Zealand uses the thinnest shooks of 25 mm (Alan H., personnel communication, 2012 July 2). However, the shooks' thickness in this study was 20mm in which it was set to meet the requirement for sufficient high l/d ratio thus shear effects in the pure bending could be minimised.

Timbers used in the industry collaborator for preparing the test shooks were kiln-dried, MOE graded and then cut to finish shook size of 120 mm (width) x 20 mm (thickness) x 400 mm (length). The overall MOE of the full size timber was measured using the third-point bending test and the visually observed defects such as knots were removed in the shook preparation. The shooks were then sorted according to the timber MOE grade into groups of 5 GPa, 6 GPa, 7 GPa, and 8 GPa.

After careful check, 1082 pieces of shooks were selected for bending tests in this project at the university's Structural Lab to determine the local MOE of every piece of shook. After bending tests, a total of 807 shooks were selected to be finger jointed and the selection was based on the MOE criteria specified in the experimental design matrix with constant shook length of 400 mm (Table 5.2). The remaining 200 pieces had variable lengths and were grouped separately for finger jointing as group L (Table 5.2).

The dimension of each shook was measured using the height gauge and steel ruler so that actual dimension of each piece can be used in calculations. The thickness of shook specimens was measured using a 300 mm height gauge (resolution at 0.01mm) and the length was measured with a 500 mm steel ruler.

5.3.2 *Determination of Moisture Content*

The moisture contents of the shooks were determined using the Wagner moisture meter (resolution 0.1%). A small amount of wood specimens were pre-selected for calibration on the moisture meter using the oven-drying method. The discrepancies between the moisture content measured from Wagner moisture meter and that from oven-drying were plotted in linear regression and were for calibration. The adjusted moisture contents for the shooks was $11.5 \pm 2\%$.

5.3.3 *Testing on Shooks' MOEs*

There was no specific l/d ratio specified for the flexural test in ASTM D198-08 [106]. However the l/d ratio in the older version of the standard was recommended to be between 11 and 15 (span length to be 15ft). The l/d ratio for Compression Parallel to Grain was specified at 17. In our case, the l/d ratio of the shooks was 18 and was considered sufficient so that the shear stress was negligibly small.

Recall from [Section 2.4](#), the l/d ratio of shooks was limited by the availability of shook sizes in finger jointing as the standard shook dimension had to be considered to accommodate common processing sizes as well as the frequencies of knots occurrence. Due to this limitation, the third-point loading method was chosen to measure the local MOE of shooks. The bending moment span of a shook specimen was 360 mm with an acceptable l/d ratio of 18.

The idea for conducting a non-destructive test in identifying the local MOEs was to ensure the specimens were retained in the best form after test, hence it could be finger jointed for the next phase of experimentation. In the experimental design, care was taken on the loading so that the strain at anywhere of the specimen would be below the elastic limits of the specimen.

In the present study, an approximate 50% of the maximum deflection of the lowest possible shook MOE at the elastic limit was set as the boundary for the maximum loading to meet the above requirement.

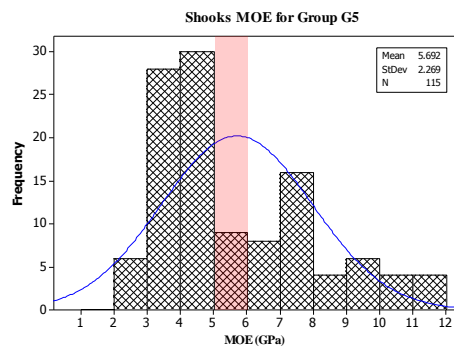
5.4 Results and Discussion - Shooks' MOEs

Based on the results of measured local MOEs, shooks were categorised into different groups with MOE ranging from 2.00 GPa to 13.99 GPa (Table 5.1). These MOE values of each group of shooks were compared with the MOEs assigned from the timber grading, namely G5, G6, G7, G8 and group L. For example, G5 represents the pretested shooks from the corresponding timber with expected MOE between 5.00 and 5.99 GPa, however, the measurements from shooks' MOEs indicated the actual MOE ranged from 2.00 GPa to 12.99 GPa.

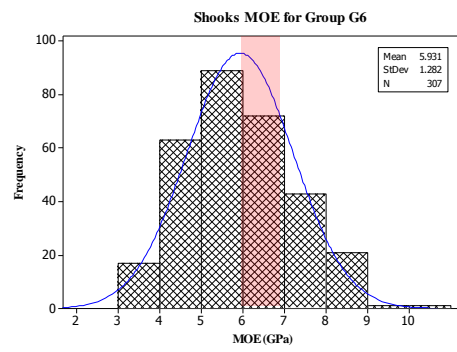
Figure 5.6 (a) to (e) are the distributions of measured shook MOEs for groups G5, G6, G7, G8 and L, respectively. The colour shaded bars denote the expected MOE range for the corresponding group. Blue curve represents the fitted normal distribution curve for the measured MOE frequency histograms. The results of comparison show that the shooks MOEs based on bending MOE conducted on full size timber were significantly different from the measured MOEs of individual shooks. Therefore, the grouping of shooks according to the actual measured shook MOE values was generally deviated from the grouping of shooks based on timber MOEs. Group G5 comprised the shooks with the highest number of shooks deviated from the 5 GPa range and with the highest standard deviation within the group, while group G7 had the least deviation of shook MOE from the 7 GPa range. In essence, grouping of shooks based on the overall MOE of a full size timber is less effective and thus some high MOE shooks may be under-utilised.

Table 5.1: List of the number of shooks from Group G5 to Group L, arranged based on measure MOEs in the respective range of MOEs

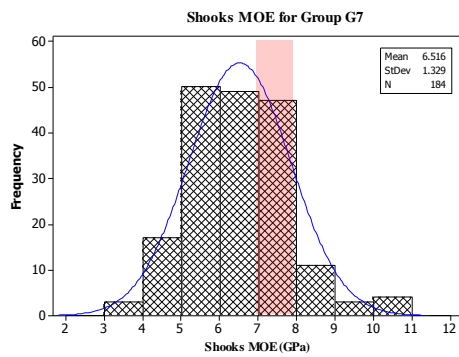
Groups	MOE Range (Gpa)												Total No. of shooks
	2.00	3.00	4.00	5.00	6.00	7.00	8.00	9.00	10.00	11.00	12.00	13.00	
	-	-	-	-	-	-	-	-	-	-	-	-	
	2.99	3.99	4.99	5.99	6.99	7.99	8.99	9.99	10.99	11.99	12.99	13.99	
G5	6	28	30	9	8	16	4	6	4	4	1	0	116
G6	0	17	63	89	72	43	21	1	1	0	0	0	307
G7	0	3	17	50	49	47	11	3	4	0	0	0	184
G8	0	1	11	26	32	38	42	29	16	5	0	0	200
L	0	0	0	9	21	28	46	52	67	36	15	1	275



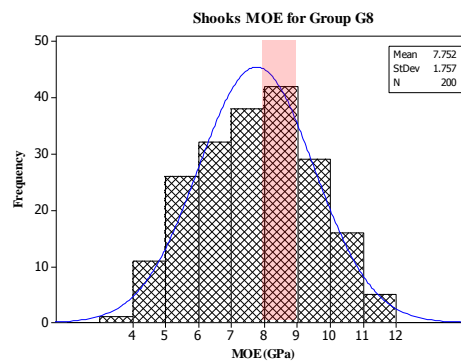
(a)



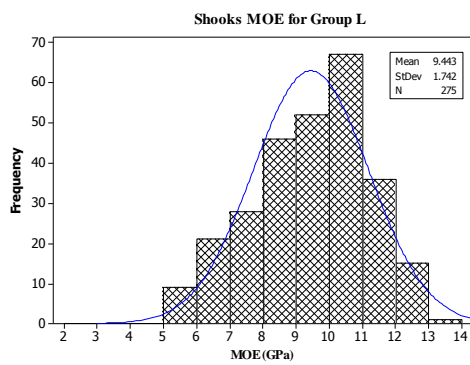
(b)



(c)



(d)



(e)

Figure 5.6 (a) to (e): Shooks' MOE distributions displayed in groups G5, G6, G7, G8 and L. The frequency distributions were accompanied with mean, SDs and total number of samples in each group

5.5 *Experimental Design*

Table 5.2 tabulates the experimental design for finger jointing. The shooks were grouped based on the measured shooks' MOEs with pre-set standard deviations from low to high. In this way, the sensitivity of the variation of shooks MOEs could be examined. In the experimental design, all of the shooks were identified by the nominal MOEs which had a scale of 0.5 GPa. For example, a 6.7 GPa sample would be assigned to the 6.5 GPa MOE range that comprised shooks with MOEs between 6.50 – 6.99 GPa. The standard deviation (SD) for the shook MOEs was used as a criterion in designing the experimental matrix. As each finger jointed member consisted of 5 shooks, Shook 1 to Shook 5 in Table 5.2 denoted as the arrangement of shooks in one finger joint member with MOE sequence from Shook 1 to Shook 5, respectively.

The experimental matrix shown in Table 5.2 include two types of arrangements: i) Groups of shooks with low SD of less than 1.1 GPa for the MOEs (Groups B, C, D, E, K, G, H), and ii) Groups of shooks with high SD between 1.5 and 3.7 GPa (Groups I, J, F, L, M, N, O).

In the first category of arrangement, there were 7 groups and the shooks in each group had SD between 0.5 and 1.1 GPa. Group B and C were designed with shook organisation based on the order of the convention in bending moment. The MOEs at the reaction points were lower and the MOE were progressively increased from the supporting ends toward the mid-span. In Group D and G, the organisations of shook MOE had no specific order. The range of shook MOE for Group D was between 4.0 GPa and 6.0 GPa while group G between 7.5 GPa and 9.0 GPa. The sequences of shook MOE in Group E and Group H were alternated between 7.5GPa and 9.5 GPa and between 7.0 GPa and 9.0 GPa, respectively. Lastly, Group K was arranged to model an asymmetric organisation with only 10.0 GPa shooks on the left and 8.0 GPa on the right.

In the second category of arrangement, the SD for each group ranged from 1.4 to 3.7 GPa. Group F, J and O shared the same convention order in bending moment, however, at different levels of MOE deviations. Group I and L shared similar trend by having high MOE on one side of the reaction point and the adjacent with a much lower shook MOE. The discrepancy of MOE between Shook 2 and Shook 3 in Group I was very large. Group L had the same shook MOE group arranged along the loading zone. Group M used the conventional order in bending MOE, however, it was arranged with a large discrepancy in shook MOE

between Shook 3 and Shook 4. Lastly, Group N was arranged with an asymmetrical organisation with high SD between shook MOEs ($SD = 1.917$).

Referred to one of the sub-objectives in Objective 3 was to examine the effect of shook lengths to the overall MOE of a finger jointed member. Two separate shook lengths were selected for this purpose. Length 1 was the 400 mm which was considered as the standard length in finger joint timber manufacturing. Length 2 was 320 mm which was considered as the shortest shook length in the finger joint timber manufacturing. The selection of shook lengths were limited due to the lacking of available shooks for this study.

In the preparation of finger jointed members made of shook with the same shook length, each group had 10 replicates and the results to be presented will be the average values of these 10 replicates. For groups with different shook lengths had only 5 replicates due to the lack of samples. However, there were a few cases where the replicates were less than the target number due to technical issue encountered during actual processing, and this will be discussed in the following section.

Table 5.2: Experimental design matrix for research Objective 3

	Category	FJ Group	Shook MOEs (GPa)					SD
			Shook 1	Shook 2	Shook 3	Shook 4	Shook 5	
Fixed shook length (Replicates in each group = 10)	Low SD Category	B	6.00	7.00	7.00	7.00	6.00	0.548
		C	5.00	6.00	7.00	6.00	5.00	0.837
		D	4.00	6.00	5.00	4.00	5.00	0.869
		E	7.50	9.5	7.50	9.50	7.50	1.095
		K	10.00	10.00	10.00	8.00	8.00	1.095
		G	9.00	8.50	8.00	9.00	7.50	0.652
		H	7.00	9.00	7.00	9.00	7.00	1.095
	High SD Category	I	9.50	3.50	10.50	11.50	4.50	3.647
		J	4.00	3.50	11.00	3.50	4.00	3.252
		F	4.50	5.00	8.00	5.00	4.50	1.475
		L	12.00	4.50	4.50	4.50	6.50	3.248
		M	3.50	11.0	10.50	6.50	4.50	3.421
		N	7.00	7.00	7.00	10.50	10.50	1.917
		0	7.50	11.00	9.50	10.00	7.50	1.557
			Shook lengths (mm)					Shooks' MOEs (GPa)
Fixed Shook MOE Range (Replicates in each group = 5)	Combination of Shook Lengths (mm)	P/M1/xx	400	320	320	320	400	5.50 – 5.99
		P/M2/xx	400	320	320	320	400	5.50 – 5.49
		Q/M1/xx	320	320	320	320	320	5.50 – 5.99
		Q/M2/xx	320	320	320	320	320	8.50 – 8.99
		R/M1/xx	320	400	400	320	320	5.50 – 5.99
		R/M2/xx	320	400	400	320	320	6.00 – 6.49
		S/M1/xx	320	400	320	400	320	8.50 – 8.99
		S/M2/xx	320	400	320	400	320	8.00 – 8.49

Note: xx in Objective denotes the number of identification for corresponding sample; SD denotes standard deviation.

5.6 Preparation and Testing of Finger Jointed Timber

5.6.1 Preparation of Finger Jointed Timbers

After testing and grouping, all shooks were sent to the finger jointed mill to make finger jointed timber samples according to the experimental design matrix in Table 5.2. Group B to Group S were manufactured in the second run and there were 10 replicates in other groups as initially planned due to manufacturing errors encountered in the first run.

All the shooks were finger-profiled using a 4 mm micro-joint cutter. Each shook were finger profiled running through the left hand knife and then the right hand knife. The descriptions on finger profile is listed in Table 5.3 and illustrated in Figure 5.7. The flat tip ends of the 4 mm finger were too delicate to be physically measured, thus the radius of the base of the fingers was considered. Two knives on the finger cutter generate the arcs and create a “slight” point at the fingertip as the shooks run through the knives. Thus, the design allowed a small space serving as tip gap when the finger tip of a finger touched the base of the adjacent shooks.

Table 5.3: The 4 mm finger joint profile

Descriptions	
Finger length (mm)	3.88
Pitch (mm)	1.60
Tip radius (mm)	0.18

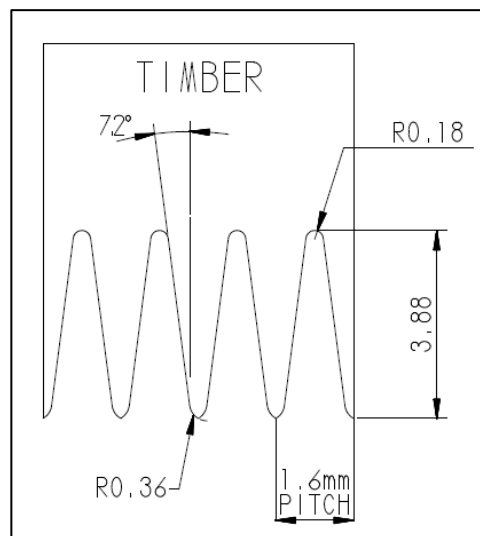


Figure 5.7: Technical drawing of a 4mm finger joint

The shooks were glue-jointed face-to-face with the thermosetting, one-component, ready-mixed Polyurethane adhesive of Henkel Purbond HB S029. The requirement for curing temperature was set at $20 \pm 2^\circ\text{C}$. Shooks were processed at ambient temperature (15°C). The finger profiled shooks were water-sprinkled before application of adhesives to ensure

sufficient of moisture was available for good bonding. Finally, they were assembled with end pressure clamps at 450 psi for 7 seconds and subject to curing for 5 minutes before packaging.

After having been received at the Structural Lab at this university, the bending span of each finger jointed member was measured and marked prior to bending. The width and thickness of the finger jointed members remained the same as the shooks, and were used in the calculations and modelling.

5.6.2 Testing on the Overall MOE of Finger Jointed Timbers

In the case of the third-point bending, constant bending moment was used to determine the overall MOE based on the deflection measured within the loading-span (refer to Figure 5.4). The modelling for such situation would therefore only take into account the local MOEs residing within the loading span. As such, the number of shooks taken into consideration would be depending on the length of the loading span. However, the objective of the study was to relate the contributions of all the shooks to the overall MOE of the corresponding finger jointed member. Therefore, the third-point bending has serious disadvantages and limitation for this purpose. In contrast, the loading span covered in the single-point bending started from one reaction support to the other reaction support (Figure 5.8). The MOEs of all shooks in the finger jointed member were included in the calculation and modelling of the deflection and overall MOE of the finger jointed member. In this regard, the single-point loading test was chosen for measuring the overall MOE of a finger jointed system.

Furthermore, the theoretical modelling in relating shook MOEs with the corresponding overall MOE of finger jointed member was based on the fundamental derivation of Moment-Curvature equation originally derived based on the Single-point loading system. The modelling process in the present study involved modifications on the Moment-Curvature equation using the same boundary condition in loading so that the process in modelling can be inferred analogous.

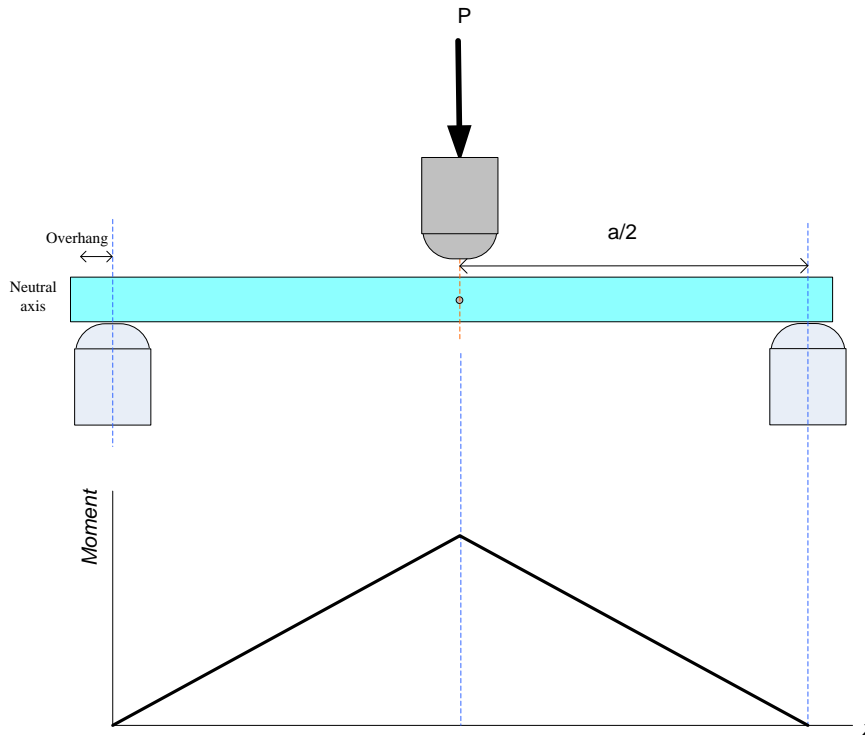


Figure 5.8: A typical single-point loading on a homogeneous beam and the corresponding bending-moment diagram

5.6.3 Testing on the Overall MOR Finger Jointed Timbers

Bending MOR on finger jointed timbers was conducted separately after the bending tests for overall MOE had been completed. The correlations between bending MOR, bending overall MOE, and the modelled overall MOE of the finger jointed members were analysed.

The overall MOR measured using the third-point bending was considered more representatives in providing information on the location of rupture over the single-point loading. This is because in the single-point loading has the peak moment at the mid-span where was most likely to be the breaking point. On the other hand, the test setup in the third-point bending comprised two equal loads giving constant bending moment across the loading span. Furthermore, the maximum deflection measured from the single-point bending was expected to be larger and this could add unnecessary mechanical challenge during setup. As such the third-point bending had been used in testing the overall MOR of finger jointed member.

A constant loading at 20 mm/min were loaded until ruptured. For the MOR measurements, there were total of 165 specimens retained from the bending MOE tests. The

maximum load (P_{max}) was used to calculate the bending MOR using Equation 5.3. The position(s) of rupture(s) and mode of failure were noted for analysis.

$$MOR = \frac{P_{max} L}{bh^2}$$

Equation 5.3

where P_{max} is the maximum load borne by the finger jointed specimen (N), L is the bending span (mm), b is the width of the specimen (mm) and h is the thickness of the specimen (mm).

Observations on the trends of location of failures were important in providing information as to whether ruptures would have occurred at the weakest point according to the Weibull's theory, or if the sustained maximum load had been shared by the neighbouring shooks.

The shooks' MORs were estimated using the dynamic-static regression model and the correlations between the finger jointed MOE and finger jointed MOR were analysed.

5.6.4 Results and Discussion

i. Integrated Segments

The first part of the discussion is about the MOEs for Group B to O calculated using Equation 5.5 and Equation 5.6 (Appendix 5.1 and Appendix 5.2). The results from second integration on the integrated segments for Shooks 1 to Shook 5 in the respective groups are summarised in Appendix 5.1. Results from the predicted overall MOEs and the computed overall MOE using Arithmetic Mean were compared and benchmarked against the corresponding measured overall MOEs. Results between the groups were compared and explained as follows.

Table A5.1 (1) to Table A5.1 (14) list the analysed integrated segments in each finger jointed specimen for Group B to Group O. In general, it can be seen that the trends of the products of integrated segments are in agreement with the explanations in Section 4.1.1. The plotted integrations (Figure 4.2) for a finger jointed specimen resembled the parabolic shape similar to the one in the bending moment diagram. From here, the smallest integrated shook MOE can be observed which is located at the reaction points whilst the magnitudes of integration progressively increase towards the loading point. Thus, the largest integration values are found to be at Shook 3 (herein split into Shook 3a and Shook 3b). The values of

integration for Shooks 3a are the same as 3b across Group B to Group O. This is because all the shooks in the finger jointed systems had the same length across Group B to Group O.

Results in Table A5.1 (1) to Table A5.1 (14) can be divided into three categories. First, the products of the integrated segments in Group C, E, F, H, L and J have a symmetrical vertical reflection of the integrated results across the groups, which is referring as the reflection of half from the integrated magnitudes of Shook 1, Shook 2 and Shook 3a to the other half of the integrated magnitudes of Shook 3b, Shook 4, and Shook 5. The SDs for shook MOEs varied from 0.7 to 3.5 between the finger jointed groups, however, the trend of the integrated shook MOEs are all symmetrically reflected due to the type of shook MOEs arrangement. This observation is prominent when the shook MOEs for Shook 2 and its mirror Shook 4 are selected from the same MOE range. This finding suggests that the standard deviation as well as the arrangement of shook MOEs are important for the member deflection and consequently the overall MOE. The second category comprised experimental groups with an average vertical reflection, which include Groups B, G and O. Lastly, in the third category, Groups of D, I, M, N, and K have shown significant differences in the integrated segments and these groups demonstrate an asymmetrical parabolic vertical reflection.

The distributions of the integrated segments for Group B to Group O are graphically represented in Figure 5.9. Most of the groups (except Group J and Group I) display a highly symmetrical parabolic shape similar to the Gaussian distribution. The highest deflection always occurs at the mid-span on Shook 3. However, the distribution of the integrated segments in Group J is different. The distribution somewhat resembles an “M” shaped distribution, whereby lower integrated values are at the mid-span (shook MOE at 11.0GPa) while higher integrated values are at the neighbouring shooks (shook MOEs at 3.5 GPa). The contribution to the sharp decrement in the mid-span integrated value is a result of large variation in shook MOE between the three middle shooks.

On the other hand, Group I experiences a left-skewed distribution of integrated segments. According to Equation 5.6, a larger integrated value is generated from a lower shook MOE. Such eccentric phenomenon is expected as the arrangement of shook MOEs has the lowest shook MOE in Shook 2 and the variances of MOE in Shook 2 with the neighbouring shooks are the highest.

Despite that shook MOEs between Shook 2, Shook 3, and Shook 4 in Group L are the same at 4.5 GPa, the group presents the steepest “bell curve” distribution. In Group L, higher shook MOEs were intentionally placed at the reaction points to assess its effects. Despite that

the least MOE effects occurs at the reaction points, the product of integration for Shook 1 appeared to be twice that of in Shook 5 and this is in line with the magnitudes of the MOEs for Shook 1 and Shook 5. In application, the higher shook MOEs at the reaction points does not contribute any additional benefits and will be economically unsound.

Group F appears to be in opposite trend to Group L whereby Group F presents the least steep distribution curve. The distribution no longer resembles a bell shaped curve; however the shape is inclined towards an evenly distributed triangle. The shape of the dispersion is contributed by small divergence of MOE values between all shooks (4.5GPa, 5GPa, 8GPa, 5GPa, 4.5GPa in Shook 1 to Shook 5, respectively).

The result of the products of integration in Group K shows slightly skewed to the right as Shook 4 and Shook 5 were made of lower shook MOEs than the others. The opposite but similar situation in Group N can be observed where lower shook MOEs on the left hand side while Shook 4 and Shook 5 had higher MOEs.

The level of symmetry of the parabolic reflections amongst the groups in the third category can be further confirmed in the analysis using DIC images as shown in Figure 5.10 to Figure 5.16.

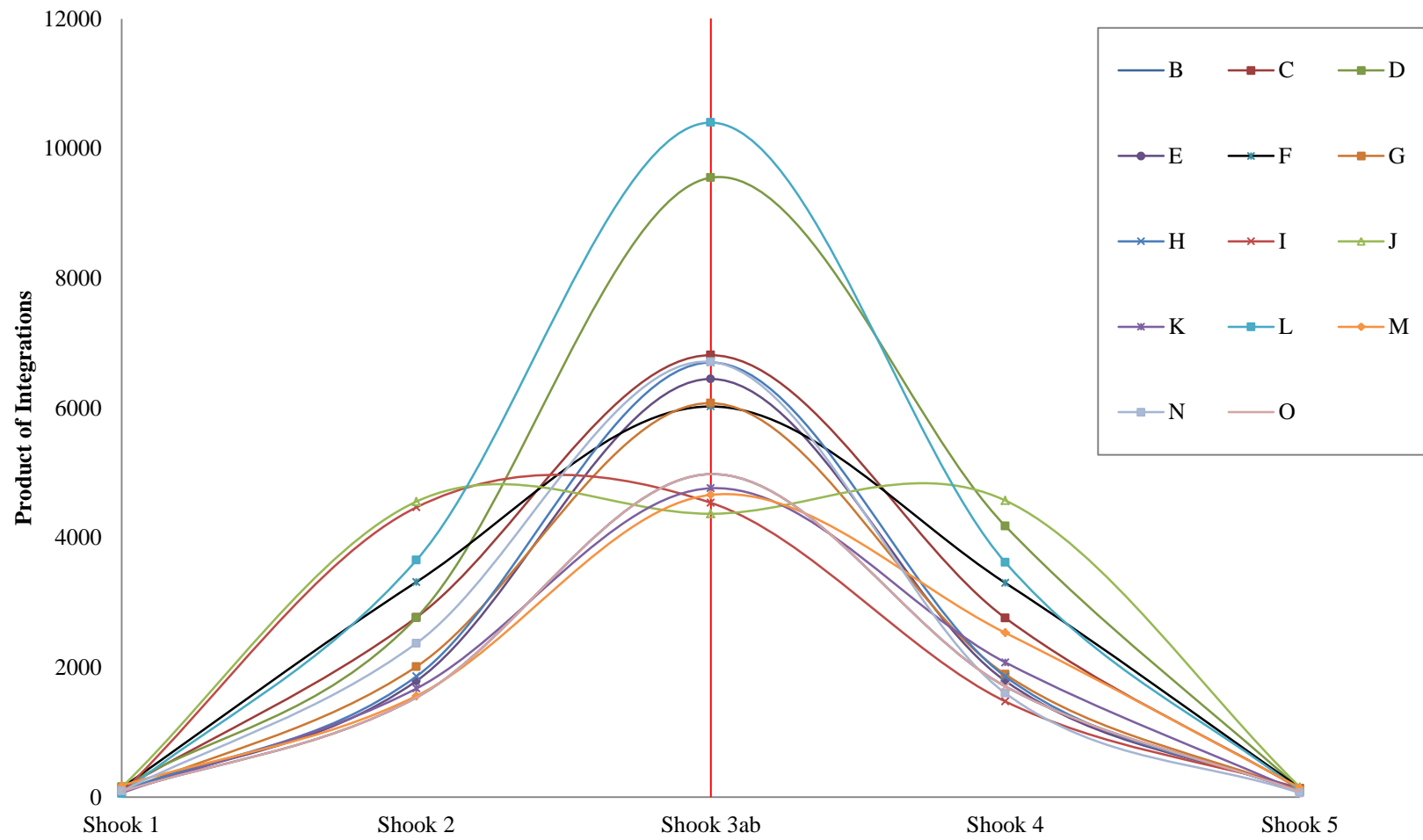


Figure 5.9: Distributions of the integrated segments of Shook 1 to Shook 5 for Group B to Group O

ii. *Shapes of Bending Deflections*

Digital images for selected groups of finger jointed timbers for Groups B, E, G, I, J, L, M, N and O were taken during testing and the “Digital Image Correlation and Tracking with Matlab software” were later used to ascertain the shape of deflection curves. The listed groups were selected to cover as many shook matching combinations as possible for image processing and analysis. Representations of the deflection shapes for the corresponding groups are shown in Figure 5.10 to Figure 5.16. The y -displacement on the ordinate denotes the vertical deflection represented in pixels while the abscissa represents the horizontal coordinates across the wood sample in pixels. The x -position at or near to 800 pixels refers to the mid-span of a specimen.

Among the selected groups in Groups B, J and L (Figure 5.10 to Figure 5.12), symmetrical deflections can be found at pixel number 100. Symmetrical deflection is expected in Group B as the shook MOEs surrounding the mid-span (S2, S3, and S4) were evenly distributed and follows the principle in bending moment. Similar observation is found in Group L except that it has slight deviation with higher deflection on the right end which can be explained by very high shook MOEs being placed on the left reaction point and half the shook MOE value on the adjacent reaction point. Nevertheless, the impact of asymmetrical deflections seems to be insignificant in terms of influence on the measured overall MOE as compared to the modelled overall MOE. Despite that the variances between the shook MOEs in Group J was large, the effects of the uneven distributions of shook MOEs appears to have dampened and presented symmetrical deflections. This can be explained by the arrangement of shook MOEs that were arranged in symmetrical order.

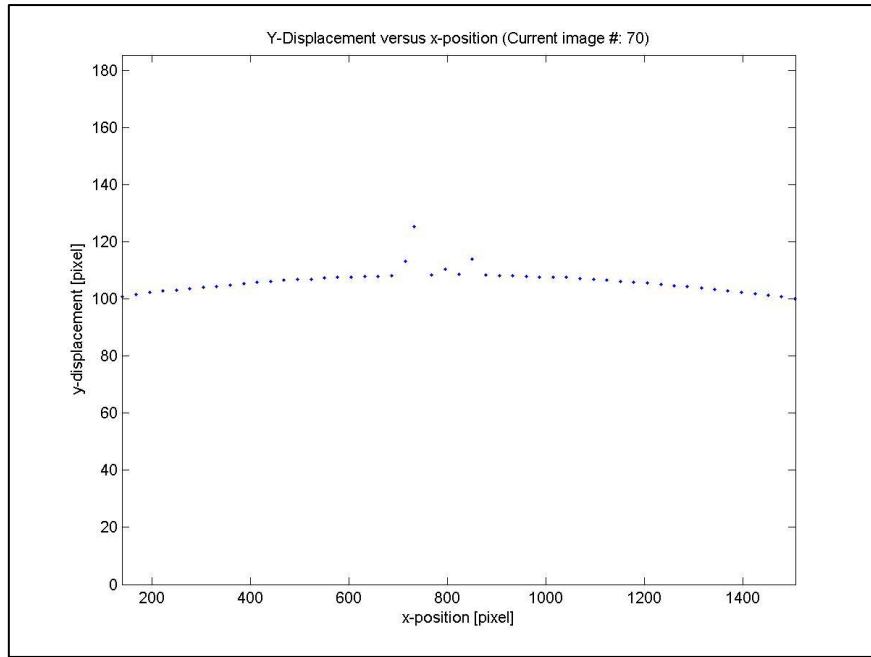


Figure 5.10: Displacement for Group B Sample B10 at y-displacement pixel 100

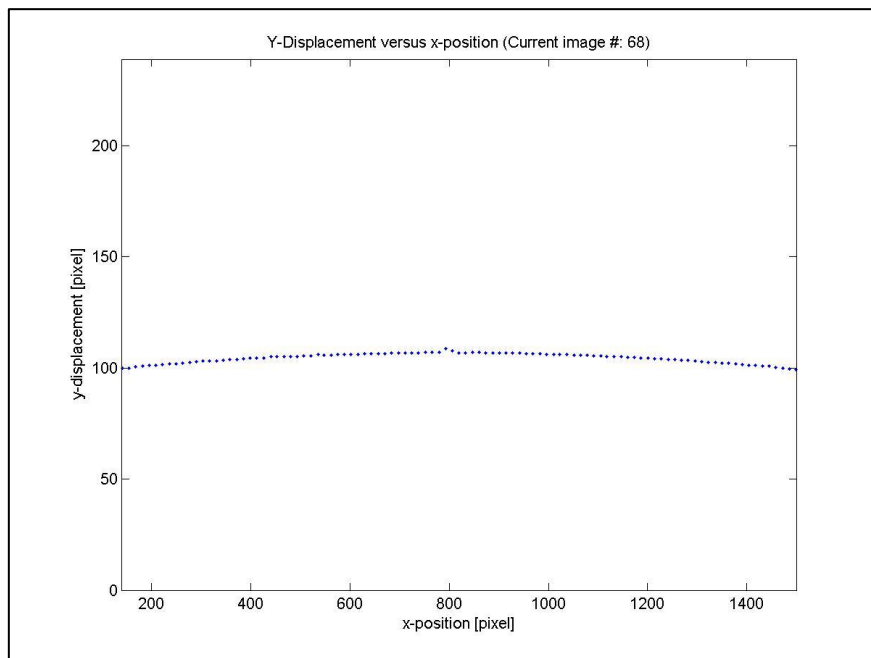


Figure 5.11: Displacement for Group J Sample J07 at y-displacement pixel 100

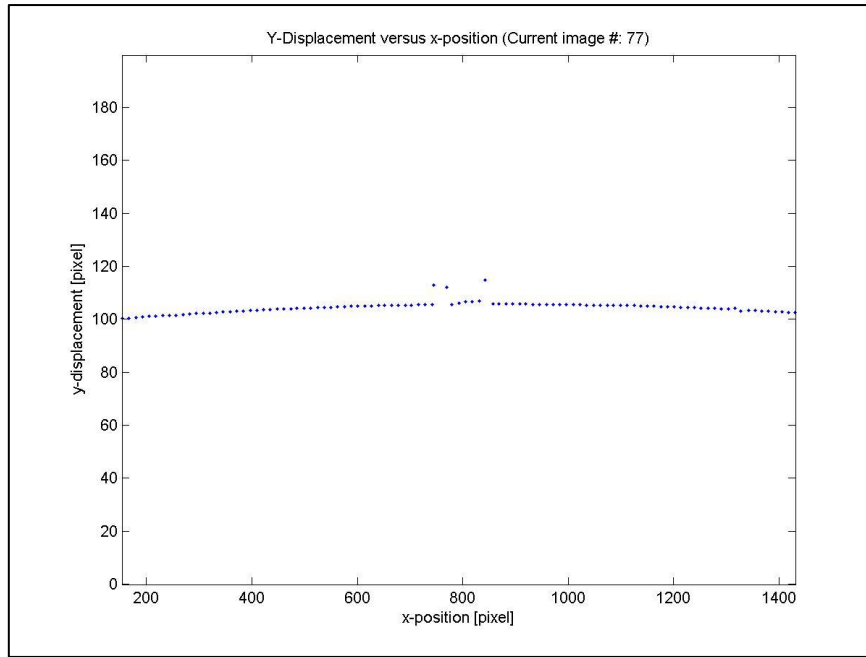


Figure 5.12: Displacement for Group L Sample L09 at y-displacement pixel 100

Groups E and N (Figure 5.13 and Figure 5.14) show slightly asymmetrical deflection with slightly higher displacement on the right hand side. The shook MOEs in Group E with an alternate MOE arrangement does not guarantee a symmetrical deflection. On the other hand, Group N that comprised asymmetrical arrangement in shook MOEs shows similar deflection profile as that for Group E.

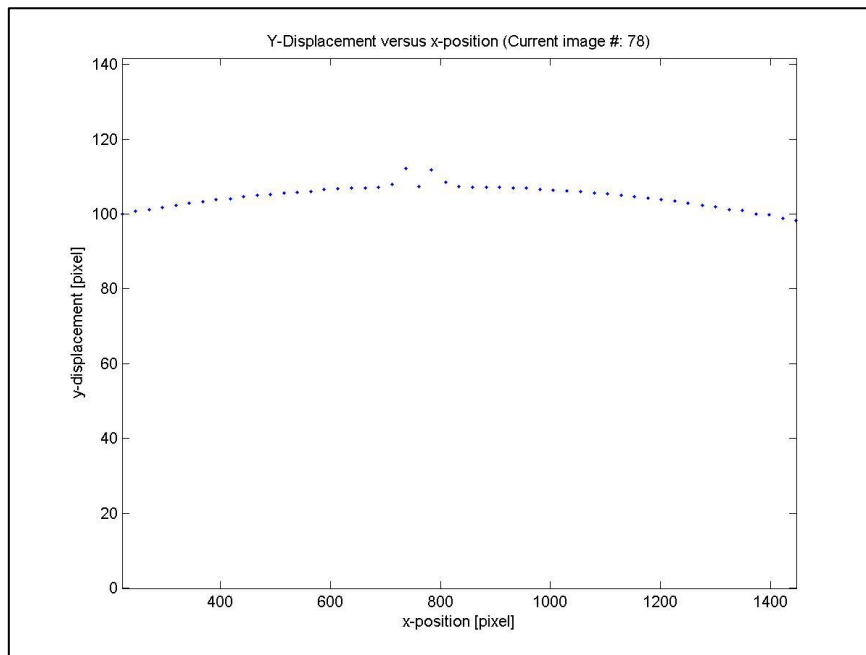


Figure 5.13: Displacement for Group E Sample E08 at y-displacement pixel 100

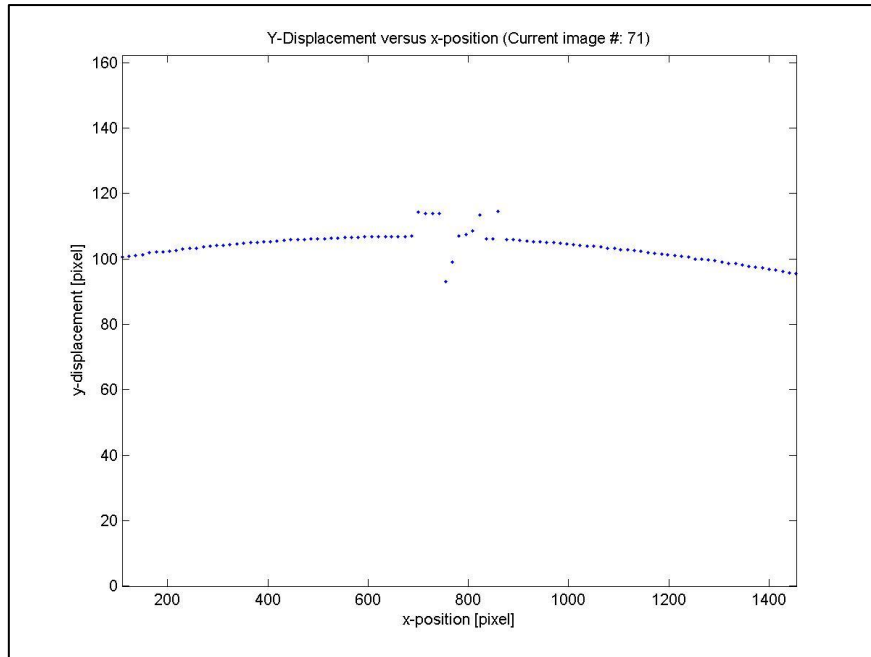


Figure 5.14: Displacement for Group N Sample N09 at y-displacement pixel 100

Groups that have experienced asymmetrical loading include Group I and Group M. Group I comprised shooks with highly deviated shook MOEs as well as with radical MOEs arrangements. Hence, asymmetrical deflection is expected in Group I (Figure 5.15) and this is consistent with distributions on integrated segments in Figure 5.9.

Figure 5.15 suggests that although the MOE difference between Shook 2 and Shook 3 was large, the asymmetrical loading shape was largely contributed by the lower MOE value at Shook 5 as compared to Shook 1, hence leading higher deflection on the right reaction point.

Similar observation can be found in Group M (Figure 5.16) with higher deflection occurring on the left hand side and this can be explained by a slightly lower shook MOE for Shook 1 in comparison with that of Shook 5. The observation is consistent with observation in Figure 5.9 on integrated segments where the bell shape curve Group M is slightly deviated to the right side compared to other groups. However, the difference in MOE values between Shook 1 and Shook 5 does not fully contribute towards the asymmetrical displacement like that of in Group L, which has large MOE difference between Shook 1 and Shook 5, yet the deflection curve is symmetrical. The other difference between these two groups is the MOEs arrangement of Shook 2 to Shook 4, whereby in Group L, Shook 2 to Shook 4 had similar MOEs. On the other hand, Group M has a much larger differences in MOEs among these three shooks hence has amplified the asymmetrical effect.

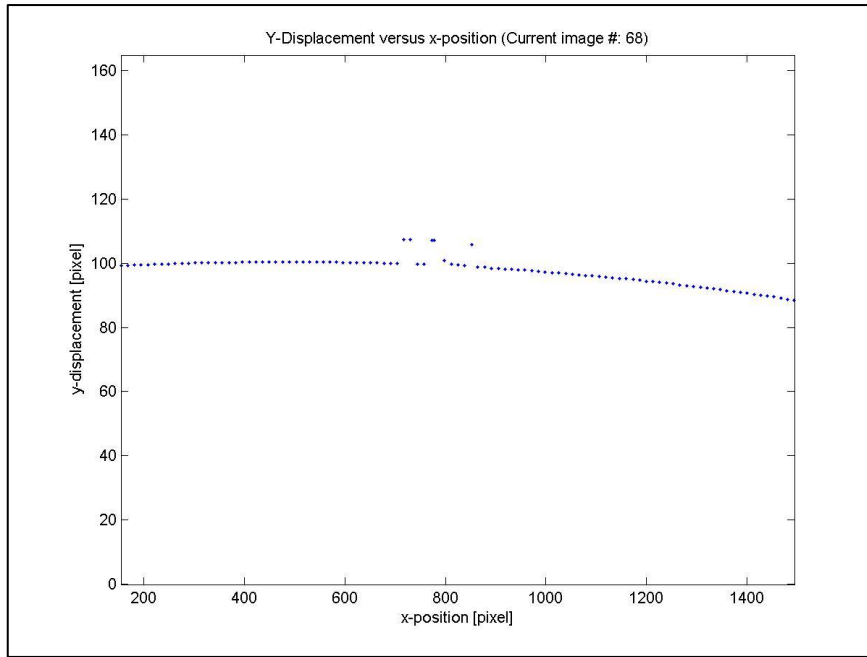


Figure 5.15: Displacement for Group I sample I01 at y-displacement pixel 100

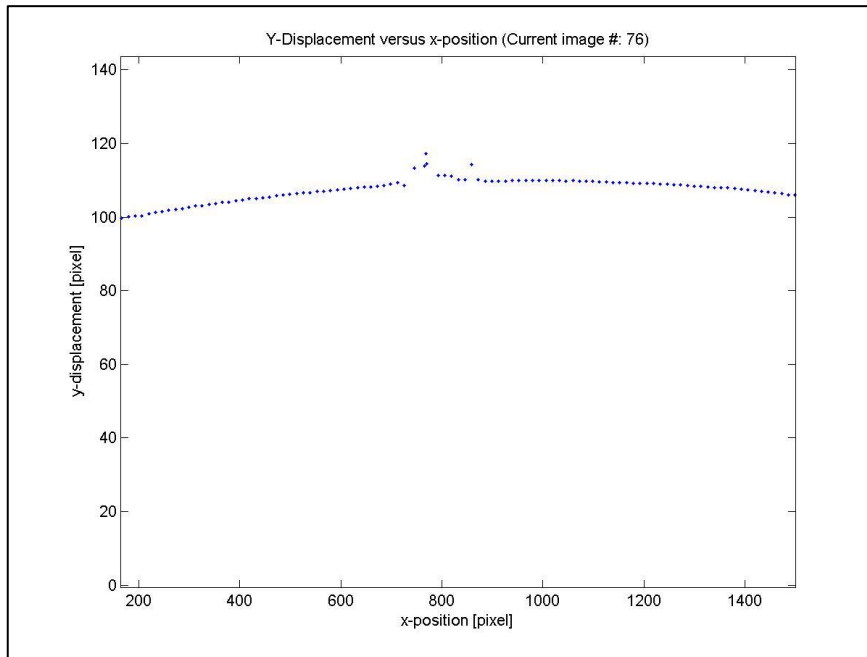


Figure 5.16: Displacement for Sample M03 at y-displacement pixel 100

iii. Application of Model in Case Study

The following section explains the application of the modified model from Equation 4.46 in the present study.

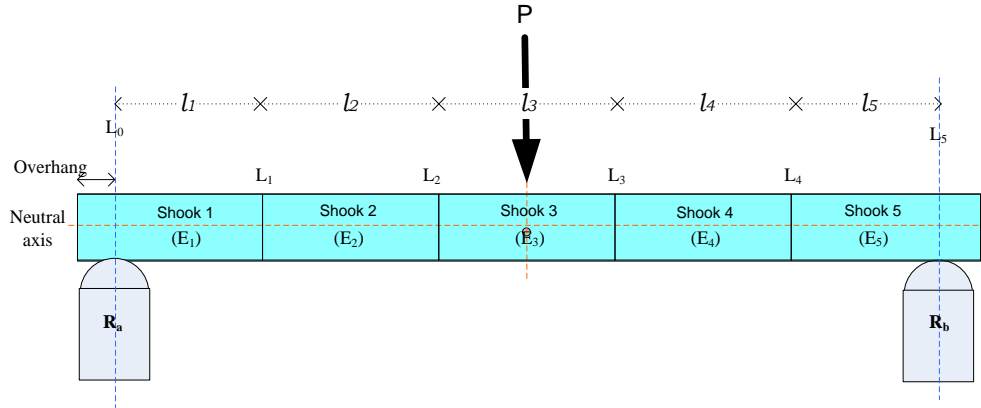


Figure 5.17: Single point loading on five finger jointed shooks denoted as Shook 1 to Shook 5 with shook MOE - E_1 to E_5 , respectively (recalled from Figure 4.15)

Recall from Section 4.5, the loading deflection in Equation 4.49 can be calculated from the second integration via integrating the slope of curve (or the angle tangent to the elastic curve with the horizontal axis).

$$\frac{dy}{dx} = \frac{P}{4I} \left[\int_0^{L_1} \frac{x^2}{E_1} \cdot dx + \int_{L_1}^{L_2} \frac{x^2}{E_2} \cdot dx + \int_{L_2}^{L_2+L_3/2} \frac{x^2}{E_3} \cdot dx - \int_{L_2+L_3/2}^{L_2+L_3} \frac{z^2}{E_3} \cdot dz - \int_{L_2+L_3}^{L_2+L_3+L_4} \frac{z^2}{E_4} \cdot dz - \int_{L_2+L_3+L_4}^{L_2+L_3+L_4+L_5} \frac{z^2}{E_5} \cdot dz \right]$$

Equation 5.4

Reshuffling Equation 5.4 to get a function of load (P) per unit deflection (y), we have

$$\frac{P}{y} = \frac{4I}{A}$$

Equation 5.5

where I is the second moment of inertia, and A is defined as

$$A = \left[\int_0^{L_1} \frac{x}{E_1} \cdot dx + \int_{L_1}^{L_2} \frac{x}{E_2} \cdot dx + \int_{L_2}^{L_2+L_3/2} \frac{x}{E_3} \cdot dx - \int_{L_2+L_3/2}^{L_2+L_3} \frac{z}{E_3} \cdot dz - \int_{L_2+L_3}^{L_2+L_3+L_4} \frac{z}{E_4} \cdot dz - \int_{L_2+L_3+L_4}^{L_2+L_3+L_4+L_5} \frac{z}{E_5} \cdot dz \right]$$

Equation 5.6

In the above equations, A is the summation of the integrated segments of the corresponding shooks used in a finger jointed member deemed as a system. In our case, we have fixed the finger jointed specimen made of 5 shooks at various combinations of shook MOEs. As such, there were 5 integrated segments described in the model.

The form of integrations upon A is a finite integration with the specified domain interval. The interval of the integration is defined as the boundary of the function variable x , which is also the point of location x . As shown in Figure 5.17, we have assigned the arbitrary values of shook lengths as l_i and the position of the joint between two shooks is denoted as L_i which is measured from the left-hand side reaction point along x direction.

The results from each integrated component of A are a representation of the bending moment diagram for the system which is made of 5 elements. In Figure 4.14 the shape of the bending moment diagram resembles an inverse parabola. The deflections at the point of reactions are zero and so the bending moments. The vertical deflections are progressively increasing from both reaction points towards the mid-span where the single-point load P is positioned. Based on this understanding, we conjectured the magnitudes of the integrated segments to inherit the same trend by having minimum integrated products on both reaction points and progressively increased from both sides of the reaction points towards the loading point. In this case, the loading point is at the mid-span where $x=L/2$.

When defining the lower and upper limit for an integrated segment, the interval for the integration limits is set from the distance of the starting point for a specific shook about the moment to the distance about the moment where the length of the shook length would end. Thus, the difference between the limits is the length of the shook. The boundary for a sub-function is necessary because different shook elements have different MOE values. Thus, different sub-functions are expected across the same system in A . Integration limits are assigned to explain the boundary for a particular sub-function. This explains the requisite for the integration limits to encompass the full length of a shook under a single sub-function, herein referred as the integrated segment. Refer to Figure 5.8, the first integrated segment has the lower interval known as $L_0 = 0$ at the left-hand side reaction point (Figure 5.17).

The integration segments for Shook 1, Shook 2, and Shook 3a (half of shook) ($0 < x < L/2$) have the following products of the respective integration segments:

For Shook 1, we have the lower limit 0 and the upper limit L_1 , where L_1 is the length of Shook 1 after subtraction from the length of the overhang at R_a . The second element of integration comprised integrating Shook 2 at E_2 . The lower limit for the second element is L_1

and the upper limit L_2 is the total length from point L_0 to L_2 , which is the summation of l_1 to l_2 . The third element comprised position x from L_2 to the loading point P at the mid-span at $L/2$. The lower limit for the third component is L_2 and the upper limit $L/2$.

The integration segments from the other half of Shook 3b, Shook 4 and Shook 5, where $L/2 < x < L$ have the following products of the individual integrations:

We have made assumption in Equation 4.45 where $z = (L-x)$ and $dz = d(L-x) = -dx$ when $L/2 < x < L$. The purpose of introducing $(L-x)$ in the region $L/2 < x < L$ is: i) to simulate the second half of the parabolic-alike bending moment, and ii) to eliminate negative functions generated from the smaller value of the upper limits, ranging from mid-span to the adjacent point of reaction (R_b). The reflection of the second-half parabolic segment may not necessarily resemble the mirror (symmetry) of the first half segment but it inherits the reflection alike in an opposite direction. Over here, the fourth integrated element involved the second half of Shook 3b. Recall that we have pre-defined z for the region $L/2 < x < L$, the lower and upper limit for this segment is from $L/2$ to $L-L_3$ which is also the subtraction of L from the summation of l_1 , l_2 , and l_3 . For Shook 4, the lower limit from $L-L_3$ to $L-L_4$ which is the subtraction of L from the summation of l_1 , l_2 , l_3 and l_4 . Lastly, the lower limit for Shook 5 is from $L-L_4$ to upper limit 0 , which is the subtraction of L from summation of l_1 to l_5 .

iv. Comparison of Computed Overall MOEs and Measured Overall MOE

In the present finger joint timber manufacturing, Arithmetic Mean has been widely used as the rule-of-thumb in finger jointing in determining the overall MOE when measurements of the local MOEs are available. Therefore, this method has been included in the modelling assessment as one of the measures for comparison and results are presented in Table A5.2 (1) to Table A5.2 (14). Errors of the overall MOE between the model and that of computed using the Arithmetic Mean are compared and discussed.

In general, the approximated errors derived from the modelled overall MOE for Group B to Group O are approximately $\pm 10.00\%$ (excluding outliers F/02, K/08, and J/10). The range of errors was between -8.17% and $+10.81\%$. However, the range of errors from Arithmetic Mean was much larger, ranging from -9.35% to $+42.50\%$.

The differences between the overall MOEs computed from the model and the measured MOE are less than 1.00 GPa ranging between 0.014 and 0.763 GPa. This indicates the overall predictability of the model is favourable, suggesting that the model can predict the

overall MOE of finger jointed timbers within an error of <1.00 GPa. However, the differences between the Arithmetic Mean and the corresponding measured overall MOEs are from 0.03 to 2.00 GPa, suggesting that the predictability of this method is less effective in certain cases. The summary of comparisons between the model's errors and the Arithmetic Mean's error can be found in Table 5.4 and the details for each group in Appendix 5.2. The difference between the experimentally measured MOE and the predicted MOE using the current study model method and arithmetic mean method are compared and illustrated in Figure 5.18.

Note that F/02 is considered as an outlier based on the value of model error (+21.926%) which has surpassed the range within the group (-4.7% to +3.595%). Similar occurrence is also observed from the Arithmetic Mean's errors having much lower percentage of error (+3.907%) than the others within the group (-19.588% to -12.646%). Similar observation can be found in J/10. The model's errors (-15.881%) and the Arithmetic Mean's errors (-25.195%) are remarkably away from the rests than those from the normal range between -8.565% and +7.742% and between -18.358% and -4.439%, respectively. As for K/08, only the model error for the specimen is exceptionally higher (+10.361%)) than others (-0.234% to +5.203%).

The differences in errors between the model and the Arithmetic Mean in groups of shooks with low MOE SD (Groups B, C, D and G with SDs <1.0) are insignificant, ranging from +1.5% to -6.0%. In this case, the differences in errors between the predictive model and the Arithmetic Mean do not appear to be significantly different. The differences of errors between the model and the Arithmetic Mean for groups with SD of MOEs from 1 to 2 (Groups E, F, H, K, O, and N) are comparatively larger than those for groups having low SD of MOEs. The range of the Arithmetic Mean errors are from -15.0% to +10.5%.

For the Arithmetic Mean method, the largest errors are found in most of the combination groups of shooks having high MOE SD (i.e. Groups I, J, L and M). Group L exhibits the highest error of +42.5% with the predicted overall MOE being almost twice that of measured. Nevertheless, the errors from the model and the Arithmetic Mean method for Group I are fairly low, 1.0% and 8.0% respectively. On the other hand, the errors from the Arithmetic Mean method are found to be significant for Groups F, J, L, M and N. Therefore, the errors are not solely affected by the magnitude of MOE standard deviation (SD) as the MOE SD across these groups were similar to or less than that of Group I. The errors from the Arithmetic Mean method can also be affected by the shook location in the finger jointed

timber. It is encouraging to note that the proposed model from the present study can predicts the overall MOEs more accurately in comparison with the Arithmetic Mean method for Groups with high SD in shook MOEs, namely Groups F, J, L, M and N.

There is no specific trend of whether the model and the Arithmetic Mean method have overestimated or underestimated the value of overall MOE. However, the overall MOEs of 64% of the groups were overestimated by the proposed model compared to the measured overall MOEs, suggesting that the model tends to overestimate the overall MOE of the finger jointed timbers. Results from the Arithmetic Mean method show an opposite trend that the overall MOEs of about 57% of the groups were underestimated.

For the groups to investigate the effects of shook length (Groups P, Q, R and S), the shakes' MOEs were relatively uniform with SD of less than 0.5 GPa as described in Table 5.2. Results computed from the proposed model and the Arithmetic Mean method are presented in Table A5.2 (1) to Table A5.2 (14) which show that the predicted overall MOE values from both methods are very similar and in close agreement with the measured values. The two methods tend to underestimate the overall MOEs with errors less than 10%. Since the SD between shook MOEs were controlled to be less than 0.5 GPa, the results indicate that the model retains favourable predictability for the variable of shook length. In the proposed model, shook length is an input parameter for the prediction of overall MOEs. The location and method in defining shook length i in respond to the horizontal position x is essential as x_i is a function of x at the point of shook i . In the case of varied lengths in Group P to S, x_i has to be accounted from the starting point to the end of shook; the location of the starting point for the subsequent shook will be the x_{i+1} until the end of the length of shook. The importance in defining shook lengths with its location across the bending span differentiates the present study model from models by Bechtel [43] or Govindarajoo's [32]. The location of shook x_i in this study model is being emphasised not as point-wise location considering it was not referred to at any point within the shook length.

Table 5.4: Summary of range of model errors and Arithmetic mean error for Group B to O

Group	Model Error			Arithmetic Mean Error		
	Min	Max	Mean	Min	Max	Mean
B	-4.49%	3.71%	-0.29%	-9.35%	-1.59%	-5.61%
C	-1.66%	5.82%	2.58%	11.50%	-5.30%	-8.42%
D	10.81%	0.23%	-4.62%	12.26%	-1.63%	-6.19%
E	0.35%	8.16%	2.89%	1.54%	9.56%	4.11%
F	-4.76%	3.96%	-1.79%	19.59%	3.91%	16.82%
G	-4.00%	5.14%	1.34%	-2.90%	7.71%	2.88%
H	-2.90%	7.71%	-1.19%	-1.55%	8.72%	2.85%
I	-0.95%	4.11%	1.29%	1.83%	7.89%	4.56%
J	8.66%	7.74%	0.44%	18.36%	-4.44%	10.50%
K	-0.23%	5.20%	1.81%	-3.24%	6.54%	-0.50%
L	10.45%	0.93%	-5.41%	24.76%	42.50%	32.25%
M	1.01%	6.93%	3.98%	20.72%	16.31%	18.35%
N	-8.17%	6.20%	0.33%	0.98%	18.30%	10.87%
O	0.85%	8.13%	3.76%	-7.39%	-0.68%	-4.07%

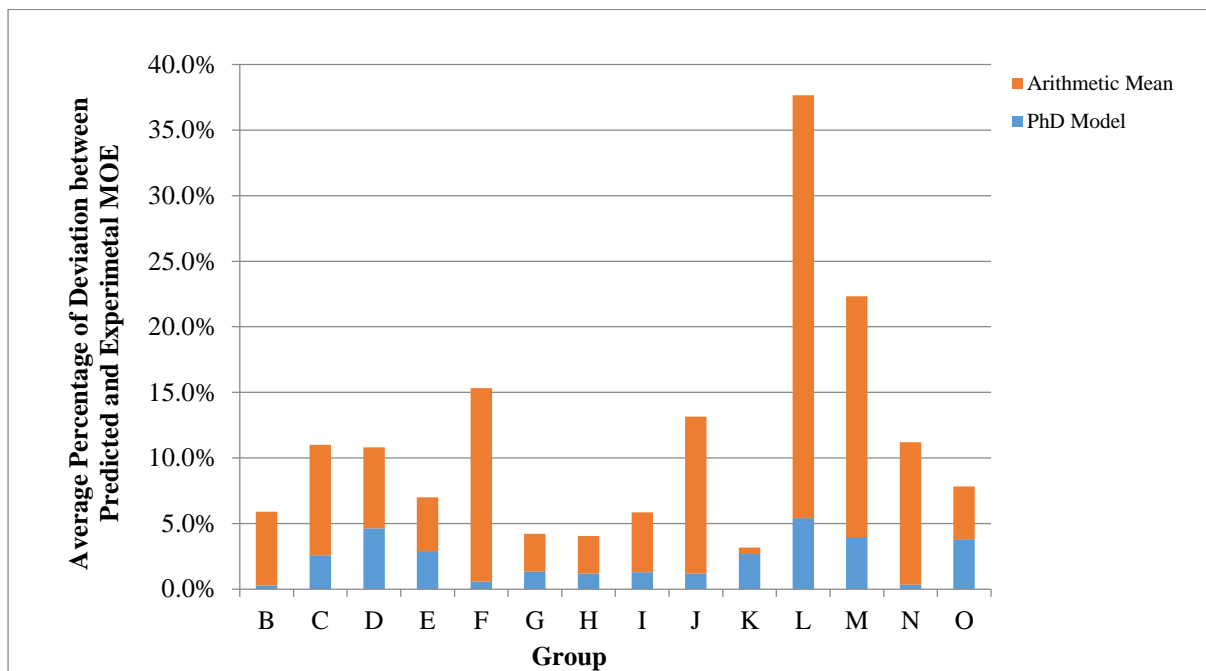


Figure 5.18: Comparison of MOE deviations between PhD model and arithmetic mean

5.6.5 Modulus of Rupture (MOR)

i. Overview

The Modulus of Rupture (MOR) for finger jointed wood specimens was determined using the Third-point bending test (Table 5.5). In this part of study, it is assumed that the MOR is uniform through a given shook while the joints do not have any effect, meaning that the MOR changes abruptly from one shook to the adjacent one. Considering the measured MOR for a finger jointed timber reflects the overall strength of the timber, as such it is termed as the overall MOR. The results of measured overall MORs for all finger jointed timbers are given in Table 5.5. The ranges of the measured overall MORs as given in Table 5.5 were calculated based on the maximum load exerted on the finger joint timber at the rupture.

ii. Relationships between MOE and Overall MOR

The relationship between shook MOEs and the overall MOEs of the corresponding finger jointed wood were correlated with the overall MOR. Correlation analyses were conducted to assess the significance in the correlation and linear regressions were generated and summarised in Table 5.5 and Figure 5.19.

The coefficient of determinations (R^2) in Table 5.5 and Figure 5.19 showed that there were no correlations between the overall MOE and MOR for Group B to Group O. Most of the R^2 values in Group B to Group O (except Group G) were less than 0.20. The strength of correlation in Group G was an average correlation with $R = 0.418$.

Findings in correlation strength (R) appeared to be much lower than the literatures (Table 5.6). One possible reason for having low correlations in the present study could be due to finger jointed wood is made of wide range of shook grades. In contrast, the testing materials listed in publications were solid wood or small clear specimens. Literature had cited that the MOR for finger joint specimens were lower than solid wood by 43% to 74% [125]. As such, low correlations between the overall MOE and overall MOR in finger jointed wood made of wide range of shook grades are not unexpected.

Interesting observations were observed in Group I and Group J, where these groups were made of large SDs shook MOEs having extreme shook MOEs combinations at the S2 to

S4 region (the critical loading zone). Extreme MOR values were found in these combinations and eccentric loading formation could be observed during loading (Figure 5.20 (a) and (b)). Figure 5.19 shows the measured overall MORs plotted against the corresponding overall MOEs for all of the samples. Figure 5.21 is the plot of the overall MOEs against the corresponding overall MORs for all of the groups listed in Table 5.5. In general, the measured overall MORs increased with the overall MOE except for the three groups on red-circles that appear to be outliers. However, the correlation is not significant and some groups may not follow that trend. A brief skimming on the correlation between the overall MORs and the overall MOEs based on the results given in Appendix 5.3 show that the overall MOR values have low predictability, especially for Group I (Table A5.3 (h)).

It appears that there is no consistent trend for a conclusive explanation. However, there is a possibility that in some instances shocks with higher shock MOE shared the load during loading and, contributed high MOR values.

iii. Location and Mode of failure

The objective in identifying the location(s) of failure is to validate the theory of constraint where failure would occur at the weakest link under consistent bending moment in the present finger jointing specimens. The location of rupture(s) and the mode of failure for specimens across Group B to Group O were observed and summarised in Appendix 5.3

ASTM D143-2009 clause 9 [126] were used as guide in determination of the mode of failure. The locations of failure(s) were referred to the order of shocks (from S1 to S5) as well as whether the failure(s) was located within or outside the loading zone. Refer to Appendix 5.3 majority of the mode of failures were observed at wood or at wood close to the finger joints. This confirms that the assumption of the joints has the same or higher strength as the adjacent shocks is valid. However, specimens B/10, E/09, E/10, M/02 were failed on the joints due to manufacturing fault and were disregarded from analysis. The finger jointed specimens were slender and the deflections under loading were large, thus the ruptures happened very quickly without any pre-warning. Identification on the initial mode of failure was nevertheless not possible.

It is observed that when the applied load exceeded the overall load resistance from the finger jointed wood, it would immediately snapped at the weakest spot at any point between the reaction points. The weakest spot means the local maximum stress at the spot is equal to

the material rupture stress and any increase in stress will result in material rupture. Therefore, the rupture may occur at the position where the material is the weakest, or when the stress is the highest, or the combination of the material strength and the stress.

In most of the groups, the location of wood failures occurs between the two loading points within the loading span. Under most of the shook MOEs combinations, the above phenomena is anticipated as wood failures is considered to follow the trend in the bending moment. Wood failures that occurred in the location within the constant bending moment zone are evident in Group H (SD shook MOEs =1.095), Group N (SD shook MOEs = 1.917) and Group O (SD shook MOEs = 1.557) in Table A5.3 (g), Table A5.3 (m) and Table A5.3 (n), respectively. Similar observation can be found in Group G (Table A5.3 (f)) and Group C (Table A5.3 (b)) where most of the locations of wood failure occurred at Shook 3, Shook 2 or Shook 4. In this instance, the impact of the location of wood failure on small discrepancy of shook MOEs between Shook 3, Shook 2 and Shook 4 are indiscriminate. Furthermore, it is observed that the location of wood failure within the loading span occur at the location of the lower shook MOE. This observation can be seen almost across all the groups and the observation is significant in Group I (Table A5.3 (h)) and Group J (Table A5.3 (i)). If ones were to relate higher shook MOE in higher shook MOR and vice-versa, we could deduce that the location of wood failure had occurred at the weakest spot within the loading span.

Similar observation is also evident in groups where the shook MOEs were being arranged in an asymmetrical order. For example, Group K (Table A5.3 (j)) and Group N (Table A5.3 (m)) are being arranged with shook MOEs higher on one side than the adjacent side in the finger jointing composition. Despite that asymmetrical deflection was observed during loading (Figure 5.20 (a) and (b)), almost all the samples in Group K and Group N experienced wood failure at the location within the loading span. However, the location of wood failure in Group K was at Shook 3 (10.0 GPa) instead of at the lower shook MOE at Shook 4 (8.0 GPa). This indicates Shook 3 at the mid-span has experienced the highest stress within the loading span.

However, there are a few instances in Groups D, F, G, I, J and M where wood failure occurred at the outer zone failure i.e. outside the loading pins (between Shook 1 and Shook 2, or between Shook 3 and Shook 4 beyond the span of the loading zone). For example in Group M, wood failure occurred at the location Shook 2 (shook MOE 11.0 GPa), Shook 4 (shook MOE at 6.5 GPa) and Shook 5 (shook MOE at 4.5 GPa) outside the loading zone. This indicates that regardless whether the bending moment at these areas are lower than that

within the loading zone, or when the MOE of shook at the ruptured area is high, rupture would occur at the spot where the local maximum stress is equal to or less than the rupture stress.

Table 5.5: Linear regression for correlations between finger jointed MOR and overall MOE

Groups	MOR Range		SD of MOR	Mean MOR (MPa)	Mean MOE (Gpa)	Shooks Combination					SD shooks	SD (S2/S3/S4)	Note	Linear Reg. R ²
	From	To				S1	S2	S3	S4	S5				
B	32.19	43.84	3.69	39.2	7.084	6.0	7.0	7.0	7.0	6.0	0.5	0.0		0.0073
C	23.95	43.68	5.76	36.45	6.607	5.0	6.0	7.5	6.0	5.0	1.0	0.9		0.0006
D	29.16	111.77	26.45	45.92	5.336	4.0	6.0	5.0	4.0	5.0	0.8	1.0	Two extreme MORs	0.0166
E	38.62	49.92	3.06	43.71	8.134	7.5	9.5	7.5	9.5	7.5	1.1	1.2		0.0014
F	32.01	43.24	3.40	38.62	6.593	4.5	5.0	8.0	5.0	4.5	1.5	1.7		0.0005
G	42.25	53.31	3.81	48.83	8.315	9.0	8.5	8.0	9.0	7.6	0.6	0.5		0.4918
H	35.07	49.72	4.14	44.44	7.907	7.0	9.0	7.5	9.0	7.0	1.0	0.9		0.167
I	35.04	130.33	31.46	55.22	7.887	9.5	3.5	10.5	11.5	4.5	3.6	4.4	Two extreme MORs	0.0701
J	22.39	59.47	11.08	34.55	6.288	4.0	3.5	11.0	3.5	4.0	3.3	4.3	One extreme MOR	0.0628
K	40.61	57.17	5.12	51.38	9.608	10.0	10.0	10.0	8.0	8.0	1.1	1.2		0.1767
L	25.8	38.78	4.12	31.92	5.072	12.0	4.5	4.5	4.5	6.5	3.2	0.0		0.0566
M	25.8	38.78	4.12	31.92	9.049	3.5	11.0	10.5	6.5	4.5	3.4	2.5		0.0566
N	35.51	45.56	3.76	40.7	7.861	7.0	7.0	7.0	10.5	10.5	1.9	2.0		0.0202
O	41.58	55.39	4.13	50.11	9.805	7.5	11.0	9.7	10.0	7.5	1.6	0.7		0.0894
P	35.82	36.14	0.23	35.98	5.608	5.0	5.0	5.0	5.0	5.0	0.0	0.0		0.0007
	32.3	41.03	4.88	37.92		5.5	5.5	5.5	5.5	5.5	0.0	0.0		0.1803
Q	40.07	60.32	8.72	44.93	7.412	5.5	5.5	5.5	5.5	5.5	0.0	0.0		-
	49.44	53.93	1.97	51.91		8.5	8.5	8.5	8.5	8.5	0.0	0.0		0.389
R	37.78	44.89	5.03	41.33	6.425	5.5	5.5	5.5	5.5	5.5	0.0	0.0		-
	34.73	43.81	3.99	38.56		6.0	6.0	6.0	6.0	6.0	0.0	0.0		0.6872
S	44.65	57.15	5.32	49.94	8.565	8.5	8.5	8.5	8.5	8.5	0.0	0.0		-
	39.68	-		39.68		8.0	8.0	8.0	8.0	8.0	0.0	0.0		0.389

Note:

- MOR is considered extreme when it has a mean error >50%
- SD is the standard deviation
- R^2 is the Linear Regression
- S1|S2|S3|S4|S5 denote Shook 1| Shook 2 | Shook 3 | Shook 4 | Shook 5 from left to right order in the finger jointed specimen

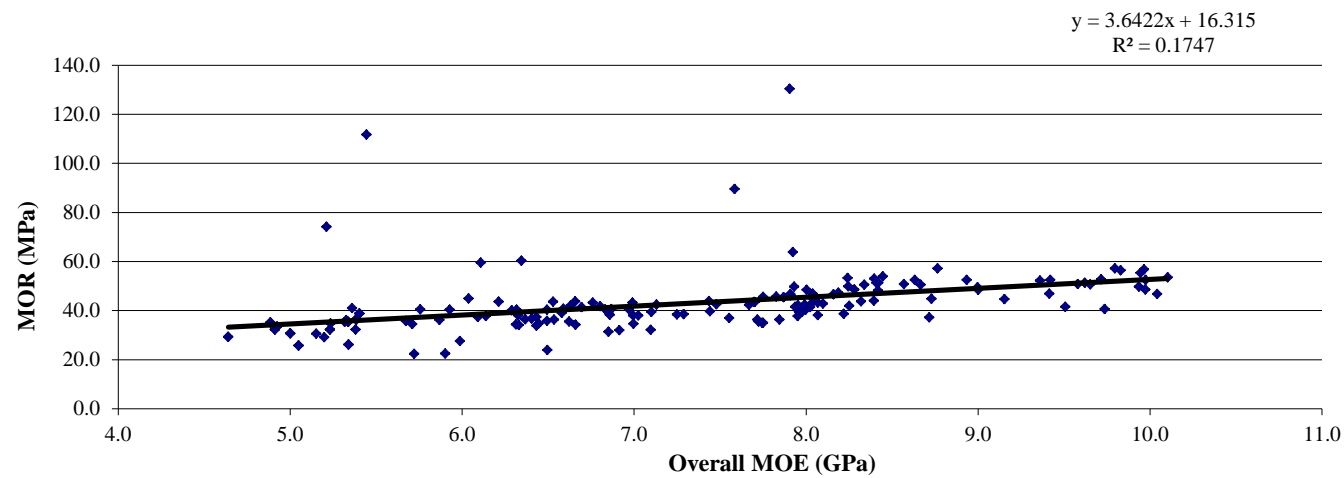
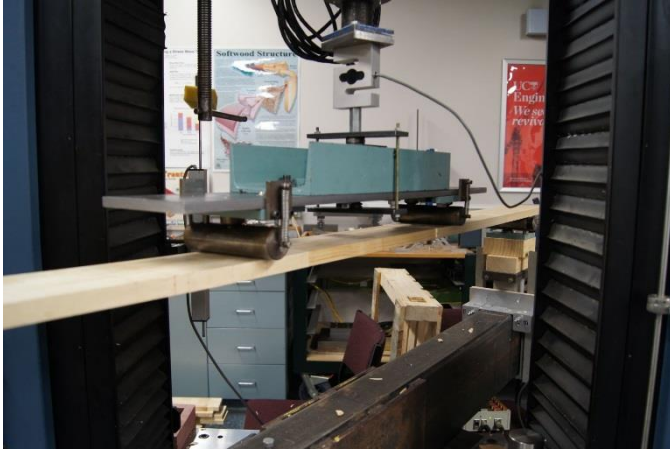
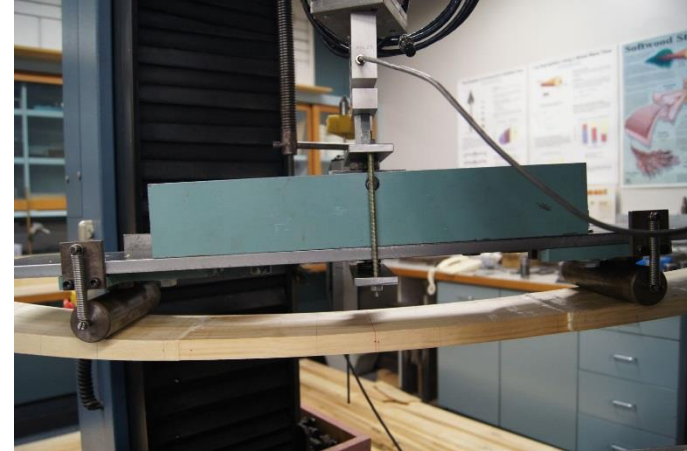


Figure 5.19: Linear regression for relationship between MOR and overall MOE of finger jointed wood for Group B to S.



(a)



(b)

Figure 5.20: (a) MOR test before loading for Group I and (b) during loading before rupture

Table 5.6: Publications for linear correlations between MOR and MOE

Material and References	Correlation coefficient MOR-MOE, r
Acetyled radiata pine [127]	0.45 – 0.82
Taiwan-grown Japanese Cedar [128]: Static MOE vs. MOR Static MOR vs. dynamic MOE	0.66 0.79
Radiata pine wood: MOR vs. MOE [129]	0.77 – 0.80
Spruce : MOR vs. MOE [130]	0.77 – 0.80
NZ radiata pine : MOR vs. MOE [131] Juvenile tree Mature tree	0.89 0.95
African species finger joint wood: MOR vs. density [61]	0.51-0.77
Finger joint wood: MOR vs. density [132]	0.42

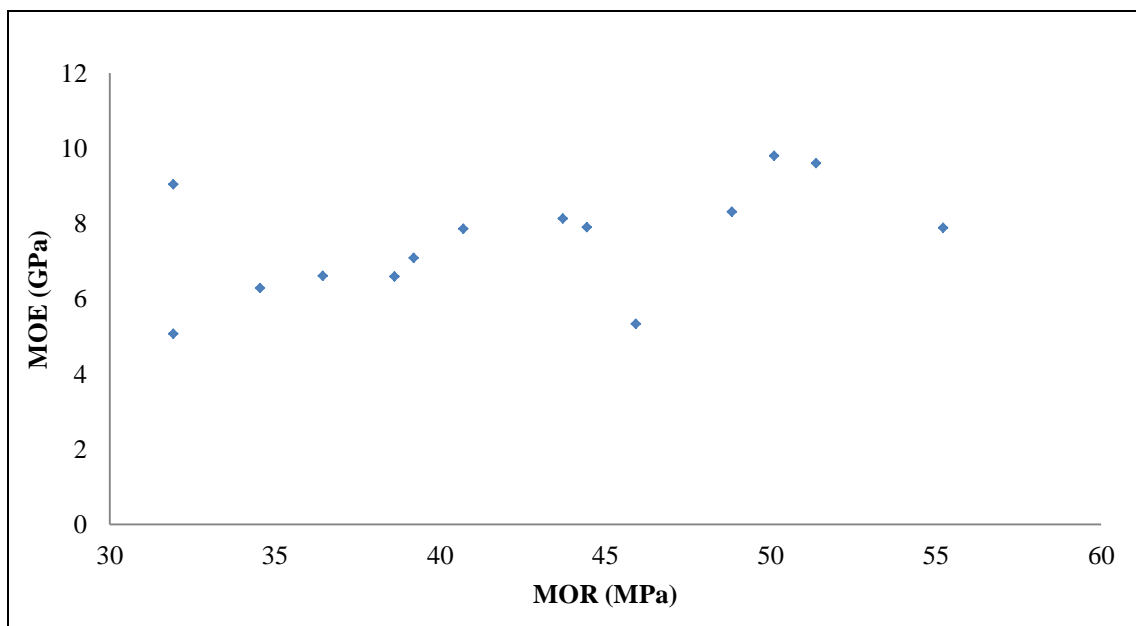


Figure 5.21: Relationship between the average overall MOE and average MOR for Group B to Group O

5.7 *Economic Analysis*

It is found that from the discussion in the previous section the developed model (Equation 5.5) can be used to predict the overall MOEs of a finger jointed timber based on individual MOEs of shooks contained in the finger jointed timber with satisfactory accuracy. The model can also be used to investigate the effects of shook length and location with the finger jointed timber. In this section, the model is further applied for economic analysis under different combinations of shooks with different MOEs. This analysis has considered the market prices of the graded and ungraded timber used as feedstock to be processed into shooks based on the MOE grades. The price of shooks from some of the required MOE grades that are not available in the market are estimated based on extrapolation from the pricing of the existing available grades. The overall MOEs of full sized finger jointed timbers are projected by using the proposed model, the mean and the minimum MOE which are still widely practiced in the area of Machine Stress Grading. The current practice in New Zealand machine stress grading assigned stress graded timber from the minimum local MOE [133]& [23].

Considering the distribution in the bending moment and the mathematical descriptions in Equation 5.5, it has found that the effect of shook MOEs at the reaction points is minimal while the maximum MOE shooks should be placed at the mid-span. In the economic analysis, the shook MOEs at S1 and S5 at 5.0 GPa are fixed as constant for the groups of AI to BV (Table A5.4 (a) to Table A5.4 (i)). The shook MOEs in Group BVI is arranged in random order. The shook length for the model simulation was fixed at 300 mm.

5.7.1 *Shooks Costing Guide*

The definition of predicted cost in this context is referring to the total cost of the projected shooks based on the corresponding grade prices. Revenue (in NZ\$) herein is referring to the projected selling prices of the finger jointed timber based on the grade of overall MOEs that were computed respectively using the proposed model, the mean of the corresponding combination of shook MOEs, and the minimum shook MOE in the finger jointed member. The selling prices for finger jointed wood were projected

according to the estimated combination costs of shooks. Other fixed processing costs such as adhesives and overhead costs had been excluded in the analysis.

A pricing guide for shooks with MOEs from 3.0 GPa to 12.0 GPa is listed in Appendix 5.4. The pricing of shooks was prepared based on the references made from several local retailers on kiln-dried untreated MSG8 radiata pine, kiln-dried untreated radiata pine for household grade, and kiln-dried dressed untreated radiata pine. The prices of the closest grades and dimensions of interest were cited and used with conversion when it is needed. The prices of shooks with MOE at 8GPa and above were based on the MSG timbers while the No. 1 Framing grade was used in determining the 7.0 GPa shooks. Prices for shooks with MOEs of less than 7.0 GPa were approximated from conversion (or approximated extrapolation). There were nine groups of shook combinations in the simulation. Table A5.4 (j) in Appendix 5.4 summarises the detailed combinations of shooks with different MOEs, the costs of shooks, and the overall MOEs of the finger jointed timbers based on i) the proposed model in the present study , ii) the mean of shook MOEs, and iii) the minimum shook MOE of the same finger jointed timbers. The selling prices of the three different overall MOEs were based on the calculated overall MOEs and were referenced to the pricing listed in Table A5.4 (a). The difference in selling prices among the overall MOEs were compared and discussed.

5.7.2 Economic Analysis

The tabulated gross profits were referred to the difference between the selling prices of the predicted finger jointed timbers and the costs of shooks constituted in a finger jointed member. Scatter graph in Figure 5.22 illustrates how the gross profits were affected by the overall MOE computed using the proposed model in the present study. The predicted MOEs were computed using the current study's model and the arithmetic mean method. The magnitude of the overall MOE of the finger jointed timbers is often dominated by the MOE of Shook 3 which is located at the mid-span. In general, lower overall finger jointed MOE resulted in lower revenue until to an optimum level in overall MOE. In this case, the overall MOE was predicted to be approximately between 7.0 GPa and 8.0 GPa. The percentage of gross profits at the overall MOE between 9.0 and 10.0 GPa diminished and remained at 60% to 70%. The

gross profits continued decreasing after 10.0 GPa and remained between 40% and 50% of gross profits.

From the economic analysis as given in Appendix 5.4 comparisons have been made between the overall finger jointed MOEs derived from the three methods as described above. It is found that, in general, better gross profits were attained from the proposed model in the present study. This model was able to fetch a better overall MOE than its counterparts virtually in all nine simulated case studies.

In general, the magnitude of shook MOE at Shook 3 strongly defined the overall MOE of the finger jointed member. The contributions of shook MOEs at other locations, i.e. at S1, S2, S4, and S5 have less levels of contribution towards the overall MOE, although S1 and S5 had the least impact. Therefore, it is important to include shooks with suitable MOEs at different locations for economic benefits in processing. The simulated results in Group AIII (Table A5.4 (d)) suggested that an effective combination of shook MOEs would favourably predict the overall MOEs. As a rule of thumb, for a given pool of shooks, the shooks with high MOEs should be placed at the mid-span (S3) while shooks with low MOEs should be placed at the reaction points (S1 and S5). The remaining shooks with medium MOEs should be located at S2 and S4 positions.

It is observed that the overall MOEs projected from the proposed model in the present study were higher than those using the mean or the minimum MOE methods. In some of these combinations, the overall MOEs projected from the model were significantly higher than the magnitudes of the calculated using the other two methods for the same shook combinations (e.g. Group AI, Group AII, Group AIII, Group BI, Group BII, Group BIII, and some combinations in Group BV).

The highest revenue among the nine simulated shook MOE combinations was from Group BV sample H1. The gross profit derived from the proposed model in the present study was as high as nearly 70%. However, the percentage of gross profit is diverse in Group BV, ranging from 15% to 70%. On the other hand, the gross profits in Group AI) and Group AIII (Table A5.4 (d)) are consistent in high profits ranging between 60% and 63%, and between 56% and 63%, respectively. The shook MOEs arrangements in Group AIII would enable attaining favourable profits is considered favourable. The combination of shook MOEs in Group AIII involved similar or lower

shook MOEs located at S2 and S4 than at S1 and S5, respectively, and the S3 MOE was the highest among the five shocks.

The combinations of sample G8 and G9 in Group BIV had the lowest gross profits in the simulated combinations. This was due to shook combinations that were arranged with low shook MOEs (5.0 GPa or less) for all of the shocks and as a result, the overall MOEs were low. As the value of the finger jointed members were dependent on the projected overall MOEs, hence the revenues were low.

However, the above findings cannot be predicted from the mean MOE method nor the minimum shook MOE method. These two methods cannot determine the effects of shook locations within the finger jointed timber thus are not as efficient as the proposed model in the present study. In the mean MOE and the minimum MOE method, the economic efficiency is solely determined by the calculated mean or the minimum of shocks' MOEs with the finger jointed timber. The minimum MOE method is the worst as the overall MOE of the finger jointed timber is dominated by the minimum MOE shook regardless of the location of the shook. Therefore, this method often results in the highest deficits for all combinations in comparison with the proposed model and the mean MOE method. The highest deficits were evident in most of the simulated groups except in Group BIV and BV. For example for sample A1 in Group AI, the projected price of the finger jointed timber from the proposed model was NZ\$12.15 but it was only NZ\$3.00 using the minimum MOE method (difference of 75%).

In conclusion, the study's model was identified to be economically efficient in determining the overall finger jointed MOE, thus was most effective for economic analysis for manufacturing of the finger jointed timber. The shook MOEs should be arranged orderly following the bending moment pattern rather than in random order. This means that the high MOE shocks should be located at the high bending moment position such as mid-span while the low MOE shocks should be located at the low bending moment positions such as reaction points. For combinations of shocks with small standard deviation for MOEs, the efficiency of the mean MOE method can achieve similar results as the proposed model. However, when the standard deviation of shook MOEs are large, the proposed model from the present study is more effective in comparison with both the mean MOE method and the minimum MOE method. The

minimum shock MOE method is least efficient and thus results in least profitable for the manufacturing of finger jointed timber.

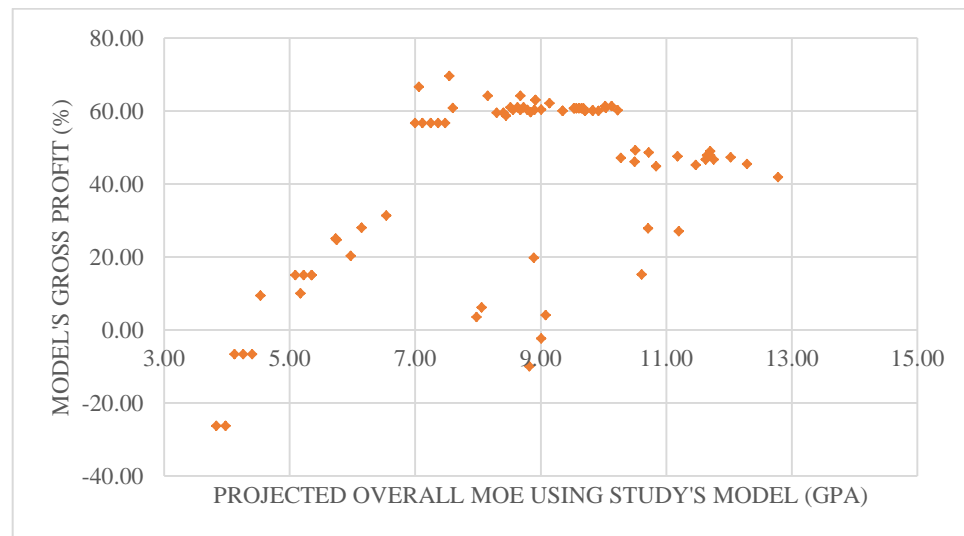


Figure 5.22: Relationship between the projected overall MOE and gross profit in Scenario A and Scenario B.

6 Conclusions and Recommendations

6.1 Conclusions

A deterministic model has been developed to predict the overall MOE of finger jointed laminates for horizontally laminated structural glued-laminated (glulam) beams. The developed model is based on inputs of the corresponding shooks constituted in the finger jointing laminates. Inputs of the shook MOEs and shook length were the two parameters in modelling.

The benefits from the model including maximising the use of feedstock from any timber grades regardless of shook lengths and shook MOE. The model is able to predict the overall MOE of a finger jointed member in any shook MOE arrangements including on eccentric arrangements. This would encourage improving resource management through optimising shook arrangements in finger jointed lamella.

There were four objectives accomplished in the study. The highlights of the research findings for each objective are summarised as follows.

Objective 1: To establish relationships between static MOE and dynamic MOE for individual shooks based on experimental results

- A statistical linear regression ($Adjusted\ Edym_{36} = 1.16 Edym_{36} - 0.36$) has been suggested in getting the adjusted dynamic MOE for shooks at 36 mm thickness. The strengths of correlation and the predictability of the model were strong and the model could further improve when the shook MOEs were sorted according to sawing pattern. The model for quarter sawn ($Adjusted\ Edym_{36} = 1.57 Edym_{36QuarterSawn} - 3.15$) has the strongest predictability .
- In the later stage of experimentation, it was observed that by using the resonance tool as a means in identifying the MOE of finger jointed laminates involved the travelling of dynamic frequencies across the medium, in this case, are the constituted shooks with varied MOEs and across the finger joints jointed using adhesive. It was confirmed through experimentations that the process of resonance travelling resonance across the finger jointed samples was too complicated. As a

result, irregular test results were observed and the correlation between shook MOEs and the corresponding finger jointed MOE were less favourable.

- It is concluded that measurement of local bending MOEs using static bending method was more suitable and reliable than using the resonance method. Thus static bending method was chosen as the preferred measuring method in the achieving the subsequent objectives.
- A decisive model in describing the relationship between shook MOE and the overall MOE of finger jointed timber could not be suggested using the probabilistic modelling method. The probabilistic modelling could only be used in demonstrating a modelling approach. The mode of measurement and modelling approach have been changed and achieved in Objective 2 and Objective 3.

Objective 2: To develop a theoretical model to find the relationships between the MOEs of individual shakes and the corresponding overall MOE of the constituted finger jointed timber.

- A deterministic model (Equation 4.50) that describes the relationship between shook MOE and the overall MOE of the corresponding finger jointed wood has been developed. The overall MOE is described as a function of shook MOEs and shook lengths in relation to the corresponding location along the bending span. The numerical modelling was rendered from the Moment-curvature equation and modified based on two essential parameters – the shook MOE and the shook length used in the corresponding finger jointed laminate.
- The basis of the model is simple. It is the summation of the bending moment as a function of shook MOE. The model was developed on the basis of a free-free simply supported bending configuration. The contributions of the bending moment of shakes vary increasingly from bending supports towards mid-span, and it apexes at mid-span where maximum loading occurred. The level of contribution from each shook is dependent on its position across the loading span. As such, the length of shook in the total mid-span had a significant effect on the model.

Objective 3: To validate the predictive model by performing experiments on finger jointed member made with combinations of different shook lengths and bending stiffness

- The developed model was able to predict the overall MOE and the model was validated on a wide range of shooks MOE compositions, arranged at different level of standard deviations in shook MOE combinations.
- The measured overall MOE from static bending test was used as the yardstick to bench mark against the predictive models. For such purpose, comparisons were made between the measured overall MOE and i) the overall MOE computed from the control model, and ii) the derived predictive model. In general, the study's model has better predictability than the arithmetic mean method. The predictability of the current model is especially higher in finger jointed timber made of high standard deviation shook MOE. The range of mean errors from the predictive model across all the groups was less than $\pm 10\%$ (excluding outliers). In comparison with using the arithmetic mean method, the error was as high as 42.5%. Thus, the predictability of the predictive model surpassed the arithmetic mean method was considered excellence in prediction. The predictability of the study model was found to be especially effective in predicting shook MOE combinations having large standard deviations combinations. The mean error for these shooks combinations were only 0.33% while the mean error from arithmetic mean method was 10.87%.
- The effect of shook arrangements in cost of production was examined through economic analysis. Results indicated the model was the most cost effective predictive model in comparison to using the arithmetic mean of shook MOEs and using the minimum shook MOE. It was found that the simulated selling price of finger jointed timber computed based on predicted MOE using the study's model can be three times greater than the arithmetic mean and the lowest shook MOE method. The minimum shook MOE method appeared to be least effective.

Contributions to knowledge:

1. A model that can be applied in the finger jointing industry has been developed.
2. Sustainable use of resources
 - There is a great potential in upgrading laminates to be made from lower grades of timbers and timber offcuts. This could open doors of opportunity in upcycling offcut and upgrading the value of lower grades timbers while been able to manipulate in maintaining the quality of targeted outputs.
3. Improve profitability and resource management
 - The model is able to effectively predict the overall MOE of finger jointed timbers based on MOEs of individual shooks. There is a great potential and opportunity in optimising shooks arrangements based on shooks MOE as the principle parameter in defining value of a piece of shook and not solely based on the grade of timber. Thus, this entailed a greater chance in utilisation of offcuts; at the same time encourage the practice of leaner and wiser use of shook with high MOE.
4. The model has been experimentally validated and found to be more effective in predicting the overall MOE based on shooks MOE than the arithmetic mean and the minimum shook MOE methods.
5. The concept of the derivation of the model is unique and simple. Despite that the ultimate form of the derivation shared similarity to the equation proposed by F.K. Bechtel (Appendix 4.1), the approach in the derivation and the course of derivation are different. Hence, this modelling approach is claimed to be novel and original contribution to knowledge.

6.2 Recommendations for Future Studies

The following areas are recommended for future studies:

- i. There were some difficulties in handling the FFT analyser during the resonance frequency measurements. Among the challenges including not being able to pick

up frequencies in some instances, some of the first mode frequencies were not within the acceptable frequency range and the harmonic mode were either insignificant or giving “twin peaks” signals. Measuring tasks had become difficult despite that measurement using a resonance tool should be simple and straight forward. Further investigation studies on these faulty experiences accompanied with explanations based on the fundamental science in acoustics would be helpful for future troubleshooting and improvements. In-depth study on how frequency is resonated across in homogeneous combination of shook MOEs, finger profiles and adhesive, followed by studies on developing correction factors or method for low l/d ratio measurements are plausible.

- ii. Shook MOEs measured from the non-destructive machine stress grader is readily available and would be worth further investigation on application of the study’s model.
- iii. Expansion on modelling in the aspect of a) effect of finger joints at various finger lengths, b) finger jointed wood made from other species of softwood and hardwood, c) combination of finger jointed member made from different shook species could be included for future studies. Further experimental validation and modification on the proposed modelling approach using different test configurations would also be useful in assisting real life applications.
- iv. Extensive studies on predicting the bending MOR based on the arrangements of shook MOEs could be further explored.

References

1. American, S., *Science desk reference - Everything you need to know about science from the origins of life to the ends of the universe*. 1999, United States of America: John Wiley & Sons, Inc.
2. Piter, J.C., R.L. Zerbino, and H.J. Blass, *Relationship between global and local modulus of elasticity in beams of Argentinean Eucalyptus grandis*. *Maderas Ciencia y tecnologia*, 2003. **5**(2): p. 107-116.
3. Buchanan, A., *Timber Design Guide*. Third Edition 2007 ed. 2007: New Zealand Timber Industry Federation Inc.
4. Anon *Radiata Pine "The Remarkable Pine"*. New South Wales Department of Primary Industry, 2005.
5. NZWood *Information Sheet-Structural Material Glue-laminated Timber Manufacture*.
6. Edlund, J., et al., *Modulus of elasticity of Norway spruce saw logs vs. structural lumber grade*. *Holz als Roh- und Werkstoff*, 2006. **64**(4): p. 273-279.
7. Bier, H., *Radiata pine plywood: An experimental study of the bending properties of structural plywood*, in *FRI Bulletin No. 531983*, Forest Research Institute, New Zealand.
8. Walford, B. and D. Gaunt. *Experience with performance-based visual grading of dimension lumber*. in *9th World Conference on Timber Engineering*. 2006. Portland, Oregon - USA.
9. Kennedy, R.W., *Coniferous wood quality in the future: concerns and strategies*. *Wood Science and Technology*, 1995. **29**(5): p. 321-338.
10. Lulay, R. and W.L. Galligan. *The impact of juvenile and compression wood on lumber from small logs*. in *32nd Western Dry Kiln Clubs Meeting*. 1981.
11. Danny, W., *Finger joint strength analysis of New Zealand radiata pine juvenile wood.*, in *School of Forestry*1988, University of Canterbury.
12. Senft, J.F., B. Bendtsen, and W.L. Galligan., *Weak wood fast-grown-trees make problem lumber*. *Journal of Forestry Science*, 1985. **83**(3): p. 477-484.
13. Jayawickrama, K.J.S., *Breeding radiata pine for wood stiffness:review and analysis*. *Australian Forestry Journal*, 2001. **64**(1): p. 51-56.
14. Corder, S.E. *Localized deflection related to bending strength of lumber*. in *Proceedings of the Second Symposium on Nondestructive Testing of Wood*. 1965. Spokane, Washington.
15. AS/NZS, *AS/NZS 1328.2:1998 Glued laminated structural timber. Part 2: Guidelines for AS/NZS1328 Part for the selection, production and installation of glued laminated structural timber.*, 1998, Standards Australia and Standards New Zealand: Australia and New Zealand.
16. Aasheim, E., et al. *Norwegian Bending Tests with Glued Laminated Beams-Comparative Calculations with the "Karlsruhe calculation model"*. in *CIB-W18: Proceedings of 26th meeting International council for building research studies and documentation working commission W18-Timber structures*. 1993. Athens, GA.: Publisher unknown.
17. Frese, M. and H.J. Blaß, *Beech Glulam Strength Classes*, in *International council for research and innovation in building and construction Working Commission W18-Timber Structure - MEETING THIRTY-EIGHT*2005, Universität Karlsruhe: Karlsruhe, Germany.

18. Yoshihara, H., *Influence of span/depth ratio on the measurement of mode II fracture toughness of wood by end-notched flexure test*. Journal of Wood Science, 2001. **47**: p. 8-12.
19. Hartley, A., *Shooks length for jointer*, S.S. How, Editor 2009: Canterbury.
20. Freas, A.D. and M.L. Selbo, *Fabrication and design of glued-laminated wood structural members*, in *USDA Technical Bulletin* 1954, U.S. Department of Agriculture: Washington D.C.
21. AS/NZS, *AS/NZS 1328.1:1988 Glued laminated structural timber. Part 1: Performance requirements and minimum production requirements*, 1998, Standards Australia and Standards New Zealand: Australia and New Zealand.
22. Forest-Products-Laboratory, *Wood Handbook - Wood as an engineering material*. 1999 ed. 1999, Madison, Wisconsin, USA: Forest Products Laboratory.
23. AS/NZS, *AS/NZS 1748:2006 Timber-Mechanically stress-graded for structural purpose*, 2006, Standards Australia and Standards New Zealand: New Zealand.
24. Stalnaker, J.J. and E.C. Harris, *Structural design in wood*. 2nd Edition ed. 1997, New York, USA: Chapman & Hall.
25. Lee, J.J., et al., *Prediction of bending properties for structural glulam using optimized distribution of knot characteristics and laminar MOE*. Journal of Wood Science, 2005. **51**: p. 640-647.
26. ASTM, *ASTM D3737-09 Standard practice for establishing allowable properties for structural glued laminated timber (Glulam)*, 2009.
27. Yang, T.-H., et al., *Effect of laminate configuration on the modulus of elasticity of glulam evaluated using a strain gauge method*. Journal of Wood Science, 2007. **53**: p. 31-39.
28. Govindarajoo, R., *Simulation modeling and analyses of straight horizontally laminated timber beams*, 1989, Purdue University: Purdue.
29. *APA Glulam Product Guide*. 2008.
30. Lee, J.-J. and G.-C. Kim, *Study on the estimation of the strength properties of structural glued laminated timber I: determination of optimum MOE as input variable*. Journal of Wood Science, 2000. **46**: p. 115-121.
31. Kline, D.E., F.E. Woeste, and B.A. Bendtsen, *Stochastic model for modulus of elasticity of lumber*. Wood and Fiber Science, 1986. **18**(2): p. 228-238.
32. Govindarajoo, R., R.F. Pellerin, and R.J. Ross, *Localized modulus-of-elasticity properties of E-rated spruce-pine laminating lumber*. Forests Products Journal, 1994. **44**(4): p. 25-32.
33. Woeste, F., et al., *Proof Loading to Assure Lumber Strength*. Wood and Fiber Science, 1987. **19**(3): p. 283-297.
34. Orosz, I., *Some nondestructive parameters for prediction of strength of structural lumber*, in *FPL Research Paper* 1968, USDA Forest Products Laboratory: Madison, Wisconsin.
35. Frese, M. *Computer-aided simulation of glulam strength parallel to grain*. in *IV European Conference on Computational Mechanics - May 16-21, 2010*. 2010. Palais des Congres, Paris, France.
36. Kass, A.J., *Middle ordinate method measures stiffness variation within pieces of lumber*. Forest Products Journal, 1975. **25**(3): p. 33-41.
37. Richburg, B.A. and D.A. Bender, *Localized tensile strength and modulus of elasticity of E-related laminating grades of lumber*. Wood and Fiber Science, 1992. **24**(2): p. 225-232.

38. Burk, A.G. and D.A. Bender, *Predicting finger joint performance based on localized constituent lumber properties*, 1988, American Society of Agricultural Engineers.
39. Lam, F., et al., *Modified algorithm to determine localized modulus of elasticity of lumber*. Wood Science and Technology, 1993. **27**: p. 81-94.
40. Ehlbeck, J., F. Colling, and R. Görlacher, *Influence of finger jointed lamellae on the bending strength of Glulam beams - Input data for computer model*. Holz als Roh- und Werkstoff, 1985. **43**: p. 369-373.
41. Ehlbeck, J., F. Colling, and R. Görlacher, *Influence of finger jointed lamellae on the bending strength of Glulam beams: Verification of the computer model by bending tests*. Holz als Roh- und Werkstoff, 1985. **43**: p. 439-442.
42. Foshi, R.O. and J.D. Barrett, *Glued-laminated beam strength : A model*. Journal of Structural Division ASCE, 1980. **106**(8): p. 1735-1754.
43. Bechtel, F.K. *Beam stiffness as a function of pointwise E with application to machine stress rating*. in *Symposium on Forest Products Research International - Achievements and the Future*. 1985. CSIR Conference Center, Pretoria, Republic of South Africa.
44. Zombori, B., *"In Situ" Nondestructive Testing of Built in Wooden Members*. NDT.net, 2001. **6**(3).
45. Ross, R.J., et al., *Inspection of timber bridges using stress wave timing nondestructive evaluation tools-A guide for use and interpretation*, 1999, USDA.
46. Chauhan, S.S., K.M. Entwistle, and J.C.F. Walker, *Differences in Acoustic Velocity by Resonance and Transit-time Methods in An Anisotropic Laminated Wood Medium*. Holzforschung, 2005. **59**: p. 428-434.
47. Rajeshwar, B., et al., *An Ultrasonic Technique for Predicting Tensile Strength of Southern Pine Lumber*. American Society of Agricultural Engineers, 1997. **40**(4): p. 1153-1159.
48. Hu, Y. *Nondestructive testing of mechanical parameters for wood-based materials*. in *17th World Conference on Nondestructive Testing, 2-28 Oct 2008*. 2008. Shanghai, China.
49. Speaks, C.E., *Introduction to sound-Acoustics for the hearing and speech sciences*. Third ed, ed. M.N. Hedge. 2005, USA: Thomson Delmar Learning.
50. Donohue, B. and S. Chauhan, *Choosing between longitudinal and flexural frequency?*, V. How, Editor 2010: Christchurch.
51. Chauhan, S.S., A. Karmarkar, and P. Aggarwal, *Evaluation of dynamic elastic properties of wood-filled polypropylene composites*. Journal of applied Polymer Science, 2006. **102**: p. 1706-1711.
52. Doyle, J.F., *Wave Propagation in Structures - Spectral Analysis using Fast Discrete Fourier Transforms*. Second ed. Mechanical Engineering Series, ed. F.F. Ling. 1997, New York: Springer-verlag.
53. Hearmon, F.S., *The fundamental frequency of vibration of rectangular wood and plywood plates*. Proceedings of Physical Society, 1945. **58**(1): p. 78-92.
54. Hearmon, R.F.S., *Theory of the vibration testing of wood*. Forest Products Journal, 1966. **16**(8).
55. Divos, F. and T. Tanaka, *Lumber strength estimation by multiple regression*. Holzforschung, 1997. **51**(5): p. 467-471.
56. Halabe, U.B., et al., *Nondestructive Evaluation of Green Wood Using Stress Wave and Transverse Vibration Technique*. Material Evaluation, 1997. **55**(9): p. 1013-1018.

57. Ayarkwa, J., Y. Hirashima, and Y. Sasaki, *Predicting Modulus of Rupture of solid and finger-jointed tropical African hardwood using longitudinal vibration*. Forest Products Journal, 2001. **51**(1): p. 85-92.
58. Vikram, V., et al., *Stiffness of Douglas-fir lumber: effects of wood properties and genetics*. Canadia Journal of Forestry Resources, 2011. **41**: p. 1160-1173.
59. Walford, G.B., *What timer, what grade, what size, what stresses?* NZ Timber Design Journal. **10**(3): p. 13-15.
60. Y, H., et al. *The effects of S2 microfibril angles and density on MOE in sugi tree logs*. in *IAWA/IUFRO International Workshop on the Significance of Microfibril Angle to Wood Quality*. 1997. Westport, New Zealand.
61. Ayarkwa, J., Y. Hirashima, and Y. Sasaki, *Predicting tensile properties of finger-jointed tropical African hardwoods using longitudinal vibration method*. Ghana Journal of Forestry, 2000. **9**: p. 45-56.
62. Haines, D.W., J.M. Leban, and C. Herbe, *Determination of Young's modulus for spruce, fir and isotropic materials by the resonance flexure method with comparisons to static flexure and other dynamic methods*. Wood Science and Technology, 1996. **30**: p. 253-263.
63. Hossein, M.A., M. Shaverdi, and M. Roohnia, *The Effect of Wood Knot as a Defect on Modulus of Elasticity (MOE) and Damping Correlation*. Notulae Scientia Biologicae, 2011. **3**: p. 145-149.
64. OSHA. *Sound Pressure Level*. Jan 2013]; Available from: https://www.osha.gov/dts/osta/otm/new_noise/appendixb.pdf.
65. Auty, D., *Non-destructive evaluation of Scots pine (Pinus sylvestris L.) to determine timber quality following conversion to continuous cover forestry systems*, 2006, University of Edinburgh: Edinburgh.
66. Kretschmann, D.E., *Stress Grades and Design Properties for Lumber, Round Timber, and Ties*, in *Wood Handbook*. 2010, FPL: Madison, WI, US.
67. Yang, J.-L., J. Ilic, and T. Wardlaw, *Relationships between static and dynamic modulus of elasticity for a mixture of clear and decayed eucalyt wood*. Australian Forestry Journal, 2003(September).
68. Sandoz, J.L., *Moisture content and temperature effect on ultrasound timber grading*. Wood Science and Technology, 1993. **27**(5): p. 373-380.
69. Kang, H. and R.E.Booker, *Variation of stress wave velocity with MC and temperature*. Wood Science and Technology, 2002. **36**: p. 41-54.
70. Hu, L.J. and W.E. Hsu. *Implementation of transverse simple beam vibration technique to determine MOE for wood based materials: Accuracy, comparability, and limitations*. in *10th international symposium on nondestructive testing of wood : International symposium on nondestructive testing of wood NDT*. 1996. Lausanne, Switzerland. .
71. Nakai, T., T. Tanaka, and H. Nao, *Fundamental vibration frequency as a parameter for grading sawn timber*, in *International council for building research studies and documentation working commission W18A-Timber structures* 1989, Meeting 22: Berlin.
72. Machek, L., H. Militz, and R. Sierra-Alvarez, *The use of an acoustic technique to assess wood decay in laboratory soil-based tests*. Wood Science and Technology, 2001. **34**: p. 467-472.
73. Ilic, J., *Dynamic MOE of 55 species using small wood beams*. Holz als Roh und Werkstoff, 2003. **61**: p. 167-172.
74. ASTM, *ASTM D198-05a Standard Test Methods of Static Tests of Lumber in Structural Sizes*, in *D198-05a2005*, ASTM International: United States.

75. Olson, J.R., *Measurement of growth ring orientation*. Forest Products Journal, 1986. **36**(3): p. 23-24.
76. Pilkey, W.D., *Formulas for Stress, Strain and Strutural Matrices*.
77. Timoshenko, S., *Vibration problems in engineering*. 1955, New York: D. Van Nostrand.
78. APA *Apparent and true (shear free) E*. Technical Topics, 2010.
79. AS/NZS, AS/NZS 4063:1992 *Timber - Stress-graded - In-grade Strength and Stiffness Evaluation*, in 4063:1992, AS/NZS.
80. Orosz, I., *Modulus of elasticity and bending strength ratio as indicators of tensile strength of lumber*. Journal of materials, JMLSA, 1969. **4**(4).
81. Orosz, I., *Relationship between apparent modulus of elasticity, gage length, and tensile strength of lumber*. Wood Science and Technology, 1976. **10**: p. 273-291.
82. Foschi, R.O., *A procedure for the determination of localized modulus of elasticity*. Holz als Roh- and Werkstoff, 1987. **45**: p. 257-260.
83. Gerhards, C.C., *Relationship of tensile strength of Southern Pine dimension lumber to inherent characteristics*, in *USDA Forest Service Research Paper*, F.P. Laboratory, Editor 1972, USDA: Madison. p. 32.
84. Suddarth, S.K. and F.E. Woeste, *Influences of variability in loads and modulus of elasticity on wood column strength*. Wood Science and Technology, 1977. **10**(12): p. 62-67.
85. Kim, K.-M., K.-B. Shim, and C. Lum, *Predicting Tensile and Compressive Moduli of Structural Lumber*. Wood and Fiber Science, 2011. **43**(1): p. 83-89.
86. Nocetti, M., et al., *Relationship between local and global modulus of elasticity in bending and its consequence on structural timber engineering*. European Journal of Wood Products, 2013. **71**(3): p. 297-308.
87. Standardization, C.E.C.f., *DIN EN 408:2003*, in *Timber structures: Structural timber and glued laminated timber - Determination of some physical and mechanical properties* 2003: Brussels. p. 30.
88. Woeste, F.E., S.K. Suddarth, and W.L. Galligan, *Simulation of correlated lumber properties data - a regression approach*. Wood Science, 1979. **12**(2): p. 73-79.
89. Bender, D.A., et al., *Reliability formulation for the strength and fire endurance of glued-laminated beams*, in *Research Paper FPL1985*, USDA Forest Products Laboratory: Wisconsin, Madison.
90. Burk, A.G. and D.A. Bender, *Simulating finger-joint performance based on localized constituent lumber properties*. Forest Products Journal, 1989. **39**(3): p. 45-50.
91. Taylor, S.E. and D.A. Bender, *Simulating correlated lumber properties using a modified multivariate normal approach*. American Society of Agricultural Engineers - Transactions of the ASAE, 1988. **31**(1).
92. Showalter, K.L., F.E. Woeste, and B.A. Bendtsen, *Effect of length on tensile strength in structural lumber*, in *FPL1987*, USDA.
93. Taylor, S.E. and B. Donald A., *Stochastic Model for Localized Tensile Strength and Modulus of Elasticity in Lumber*. Wood and Fiber Science, 1991. **23**(4).
94. Govindarajoo, N., *Stochastic analysis of Glulam beams*, in *Department of Civil Engineering* 1989, Purdue University: West Lafayette, Indiana.

95. Isaksson, T. *Modelling the variability of bending strength in structural timber - length and load configuration effects*. Structural Engineering [Dissertation] 1999 1999-04-13.
96. Isaksson, T., *System effect*, in *Nordic Wood - Reliability of timber structures* 2001.
97. Ehlbeck, J., F. Colling, and R. Görlacher, *Influence of finger jointed lamellae on the bending strength of glulam beams - Development of a computer model*. Holz als Roh- und Werkstoff, 1985. **43**: p. 333-337.
98. Ehlbeck, J., F. Collins, and R. Garlacher, *Influence of finger-jointed lamellae on the bending strength of glulam beams: Development of a computer model (english translation version)*. Holz als Roh- und Werkstoff, 1985. **43**(9): p. 369-373.
99. Hernandez, R., et al., *Probabilistic modeling of Glued-laminated timber beams*. Wood and Fiber Science, 1992. **24**(3): p. 294-306.
100. Colling, F. and R.H. Falk. *Investigation of laminating effects in glued-laminated timber*. in *CIB-W18: Proceedings of 26th Meeting; International council for building research studies and documentation working commission W18 - Timber structures; August. 1994*. Athens, GA.
101. Hernandez, R. and R.H. Falk. *Simulation Analysis of Norwegian Spruce Glued-Laminated Timber*. in *CIB-W18: Proceedings of 26th meeting; International council for building research studies and documentation working commission W18-Timber structures. 1993*. Athens, GA. . : Publisher unknown.
102. Hooper, J.A. and D.A. Bender, *Modeling finger joint tensile strength and MOE for E-rated laminating lumber*, in *International Winter Meeting of the American Society of Agricultural Engineers* 1988, American Society of Agricultural Engineers, ASAE.: Hyatt Regency, Chicago, Illinois Center. p. 11.
103. Thelandersson, S. and H.J. Larsen, *Timber Engineering*. 2003: Wiley. 71-78.
104. (ISO), I.O.o.s., *ISO 3349-75: Wood - Determination of modulus of elasticity in static bending*, 1975, ISO.
105. Standards, B., *Structural timber - Determination of characteristic values of mechanical properties and density*, 2010.
106. D198-09, A., *ASTM D198-09: Standard Test Methods of Static Tests of Lumber in Structural Sizes*, 2009.
107. Grant, D.J., *Effect of test span on the apparent modulus of elasticity of radiata pine timber in scantling sizes*, 1979, Forestry Commission of N.S.W.: Sydney 17. p. 17.
108. Kubojima, Y., T. Ohtani, and H. Yoshihara, *Effect of shear deflection on bending properties of compressed wood*. Wood and Fiber Science, 2004. **36**(2): p. 210-215.
109. Fellmoser, P. and H.J. Blass *Influence of rolling shear modulus on strength and stiffness of structural bonded timber elements*. International Council for Research and Innovation in Building and Construction - Working commission W18: Timber Structures. Meeting 37, Edinburg, U.K., 2004. **CIB-W18/37-6-5**.
110. Ltd., I.P. *Flexure Test*. 2013.
111. JIS, *JIS Z2101 Methods of test of woods*, 1994.
112. Ljunggren, S., *Airborne sound insulation of thick walls*. Journal of Acoustic Society of America, 1991. **89**(5): p. 2338-2345.

113. Sorn, S., R. Bajramovic, and V. Hadziabdic, *Examination of proper span/depth ratio range in measuring the bending strength of wood based on the elementary bending theory*, in *15th International Research/Expert Conference "Trends in the Development of Machinery and Associated Technology" TMT 2011* 2011: Prague, Czech Republic.
114. Yang, L., et al., *Measure strain distribution using Digital Image Correlation (DIC) for tensile tests*, 2010, The Advanced High Strength Steel Stamping Team of the Auto/Steel Partnership (A/SP) 2000 Town Center, Suite 320, Southfield, MI 48075-1123.
115. Serrano, E. and B. Enquist, *Assessment of the strain distribution in wood adhesive bonds by contact-free measurement and finite element analyses*, SP Technical Research Institute of Sweden: Sweden. p. 7.
116. Jeong, G.Y., A. Zink-Sharp, and D.P. Hindman, *Applying digital image correlation to wood strands: Influence of loading rate and specimen thickness*. *Holzforschung*, 2010. **64**: p. 729-734.
117. Oscarsson, J., A. Olsson, and B. Enquist, *Strain fields around a traversing edge knot in a spruce specimen exposed to tensile forces*, in *World Conference on Timber Engineering WCTE2010*.
118. Hosseini, A., D. Mostofinejad, and M. Hajialilue-Bonab, *Displacement measurement of bending tests using digital image analysis method*. *IACSIT International Journal of Engineering and Technology*, 2012. **4**(5).
119. Craig, R.R., *Mechanics of materials*. 2nd edition ed. 2000, New York: John Wiley & Sons, Inc.
120. Beer, F.P., et al., *Mechanics of materials*. 5th Edition ed. 2009, New York: McGraw-Hill.
121. Benham, P.P., R.J. Crawford, and C.G. Armstrong, *Mechanics of engineering materials* 2nd ed. 1996, U.K.: Pearson Education Ltd.
122. Anon. *Curvature*. Wolfram Maths World, 1999-2012.
123. Brancheriau, L., H. Bailleeres, and D. Guitard, *Comparison between modulus of elasticity values calculated using 3 and 4 point bending tests on wooden samples*. *Wood Science and Technology*, 2002. **36**: p. 367-383.
124. Chris Eberl, R.T., D. Gianola, and S. Bundschuh, *Digital Image Correlation and Tracking with Matlab*, 2006: Karlsruhe Institute of Technology, Germany & Johns Hopkins University, USA.
125. V., V., K. S., and J. Barboutis *Bending strength properties of some finger-jointed oakwoods*.
126. ASTM, *ASTM D143-09 Standard test methods for small clear specimens of timber*, 2009.
127. Jorissen, A., et al. *The influence of acetylation of Radiata pine in structural sizes on its strength properties*. in *European Conference on Wood Modification 2005*. 2005. Gottingen, Germany.
128. Wang, S.-Y. and C.-Y. Ko, *Dynamic modulus of elasticity and bending properties of large beams of Taiwan-grown Japanese cedar from different plantation spacing sites*. *Journal of Wood Science*, 1998. **44**: p. 62-68.
129. Bailleeres, H., G. Hopewell, and G. Boughton, *MOE and MOR assessment technologies for improving graded recovery of exotic pines in Australia*, 2009, Forest & Wood Products Australia (FWPA): Victoria, Australia.
130. Byeon, H.-S., et al., *Nondestructive evaluation of strength performance for finger-jointed wood using flexural vibration techniques*. *Forests Products Journal*, 2005. **55**(10): p. 37-42.

131. Cown, D.J., *Modelling Pinus radiata lumber characteristics Part 1: Mechanical properties of small clears*. New Zealand Journal of Forestry Science, 1999. **29**(2): p. 203-213.
132. Knowles, C.D., *Characterization of selected wood properties in commercially produced southern pine finger-jointed dimension lumber*. Forest Products Journal, 2006. **56**(9): p. 43-46.
133. Cavanagh, G., *Stress grading of timber-revision to standards*. NZ Timber Design Journal. **13**(4): p. 7-12.

Appendices

Appendix 3.1: Derivation of Flexural dynamic MOE

From Hearmon's [54] equation, we have

$$E_{f_Dym} = \frac{4\pi^2 L^4 f^2 \rho}{m^4 k^2} .$$

Equation A3.1

where L =sample length, f = frequency of the n^{th} mode of the flexural vibration, ρ = density, $m = (2n+1) \pi / 2$, k = radius of gyration of the cross-section ($k = \frac{d}{\sqrt{12}}$ for rectangle section & d = thickness).

Substitute into [Equation A3.1](#), we get

$$E_{f_Dym} = \frac{0.9607 L^4 f^2 \rho}{d^2} .$$

Alternatively, m can be adapted as the λ coefficient based on testing boundary condition [76]:

Boundary condition	λ_1	λ_2
Free-free	4.730041	4.694091
Fixed-free	1.875104	4.694091
Pinned-pinned	$i\pi$	

Under free-free support on the harmonic mode, we have

$$E_{f_Dym} = \frac{0.9464 L^4 f^2 \rho}{d^2} .$$

Equation A3.2

Appendix 3.2: Density Distribution for Experiment I

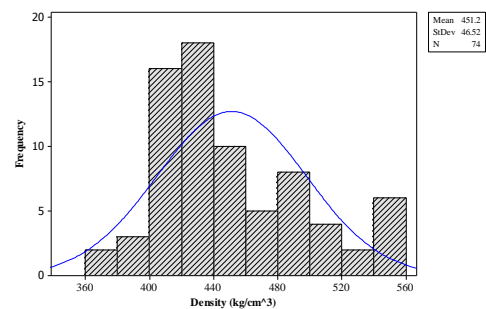


Figure A1: Density distribution for Experiment I

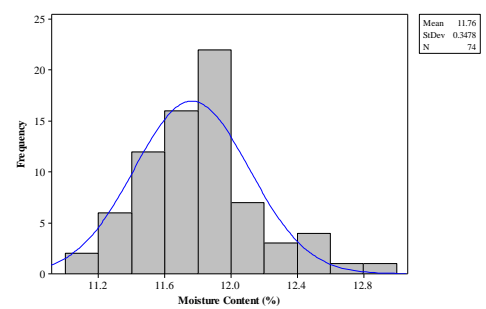


Figure A2: Moisture content distribution for Experiment I

Appendix 4.1: Derivation of Model by F. Bechtel [43]

The slope $S(x)$ of a simply-supported beam at any point x along the beam was given by Bechtel in the expression of u . The point x herein was referred to at any point; hence it was not restricted by boundary limits in an indefinite integral condition. The constant $S(0)$ was assumed by the author to be zero.

$$S(x) = \frac{1}{I} \int_0^x \frac{M(u)}{E(u)} du + S(0) \quad (\text{Eq. A4.1})$$

By changing the parameter from u to v , we get

$$S(u) = \frac{1}{I} \int_0^u \frac{M(v)}{E(v)} dv + S(0) \quad (\text{Eq. A4.2})$$

The conventional way in getting deflection $\Delta(x)$ is by integrating the radius of curvature twice and separately.

By integrating Eq. A4.2, we will get deflection $\Delta(x)$:

$$\begin{aligned} \Delta(x) &= \int_0^x \left[\frac{1}{I} \int_0^u \frac{M(v)}{E(v)} dv + S(0) \right] du + C \\ \Delta(x) &= \int_0^x \frac{1}{I} \int_0^u \frac{M(v)}{E(v)} dv du + \int_0^x S(0) du + C \end{aligned} \quad (\text{Eq. A4.3})$$

Since $S(0)$ is a constant, it can be written as follow:

$$\int_0^x S(0) du = \frac{x}{L} \int_0^L S(0) du$$

(Eq. A4.4)

where $\frac{x}{L}$ is a ratio in a constant form that can be cancelled off after substitution of the boundary condition x .

When we substitute Eq. A4.4 we get:

$$\Delta(x) = \int_0^x \frac{1}{I} \int_0^u \frac{M(v)}{E(v)} dv du + \frac{x}{L} \int_0^L S(0) du + C$$

In a simply-supported system, we know that zero deflections occurred at the reaction points.

Hence, when $x = 0$,

$$\Delta(0) = \int_0^0 \frac{1}{I} \int_0^u \frac{M(v)}{E(v)} dv du + \frac{0}{L} \int_0^L S(0) du + C$$

(Eq. A4.5)

We get $C = 0$

When $x=L$:

$$\Delta(L) = \int_0^L \frac{1}{I} \int_0^u \frac{M(v)}{E(v)} dv du + \int_0^L S(0) du$$

Thus,

$$\int_0^L S(0) du = - \int_0^L \frac{1}{I} \int_0^u \frac{M(v)}{E(v)} dv du ,$$

$$\int_0^L S(0) du = - \int_0^L \frac{1}{I} \int_0^u \frac{M(v)}{E(v)} dv du$$

(Eq. A4.6)

Substitute C and Eq. A4.6 into Eq. A4.3, we get:

$$\Delta(x) = \frac{1}{I} \int_0^x \int_0^u \frac{M(v)}{E(v)} dv du - \frac{x}{LI} \int_0^L \int_0^u \frac{M(v)}{E(v)} dv du$$

Over here, the author had divided x into v and u to incorporate the function in the form of a double integration so he could reduce the double integration into a single function by using the interchange of order method in the subsequent derivations.

From Eq. A4.1, the parameter u was changed to v and we get:

$$S(x) = \frac{1}{I} \int_0^x \frac{M(v)}{E(v)} dv + S(0)$$

When integrate the slope $S(x)$, we get

$$\Delta(x) = \int_0^x \left(\frac{1}{I} \int_0^u \frac{M(v)}{E(v)} dv + S(0) \right) du + C$$

$$\Delta(x) = \frac{1}{I} \int_0^x \int_0^u \frac{M(v)}{E(v)} dv du - \frac{x}{LI} \int_0^L \int_0^u \frac{M(v)}{E(v)} dv du$$

(Eq. A4.2)

By interchanging the order of integration on Eq. A4.2, we get:

$$\Delta(x) = \frac{1}{I} \int_0^x \frac{(x-v) M(v)}{E(v)} dv - \frac{x}{LI} \int_0^L \frac{(L-v) M(v)}{E(v)} dv$$

At mid-span where $x = L/2$,

$$\Delta(L/2) = \frac{1}{I} \int_0^{L/2} \frac{(L/2-v) M(v)}{E(v)} dv - \frac{x}{LI} \int_0^L \frac{(L-v) M(v)}{E(v)} dv$$

(Eq. A4.3)

In a simply-supported centre loading system, the moment is as follow:

$$M(v) = -\frac{Pv}{2}, \quad 0 < v < L/2$$

and

$$M(v) = -\frac{PL}{2}, \quad L/2 < v < L.$$

When substitute into Eq. A4.3, we have:

$$\Delta(L/2) = \frac{P \left[\int_0^{L/2} \frac{v^2}{E(v)} dv + \int_{L/2}^L \frac{(L-v)^2}{E(v)} dv \right]}{4I}.$$

(Eq. A4.4)

Recall from the conventional equation for a single point load as:

$$\Delta(L/2) = \frac{P L^3}{48 E_{overall} I}.$$

Equate with Eq. A4.2 we can rearrange and simplify to as follow:

$$E_{overall} = \frac{L^3/12}{\int_0^{L/2} \frac{v^2}{E(v)} dv + \int_{L/2}^L \frac{(L-v)^2}{E(v)} dv}.$$

(Eq. A4.5)

Appendix 5.1

Table A5.1 (1): Group B - Analysis of predicted integrated segments

	Integrated segments [N/mm ²]						SD of shook MOE s
	S1	S2	S3a	S3b	S4	S5	
B01	84.926	1549.002	2535.115	2535.115	1714.474	85.911	0.556
B02	83.438	1520.468	2469.136	2469.136	1696.021	83.542	0.542
B03	86.693	1525.822	2496.626	2496.626	1701.014	86.693	0.502
B04	83.963	1544.860	2481.556	2481.556	1701.014	83.647	0.566
B05	89.366	1532.567	2481.556	2481.556	1706.037	84.282	0.554
B06	84.818	1542.112	2491.582	2491.582	1711.089	88.535	0.540
B07	86.356	1542.112	2486.559	2486.559	1714.474	87.489	0.522
B08	84.175	1528.513	2484.055	2484.055	1714.474	84.282	0.544
B09	83.857	1513.828	2474.089	2474.089	1702.685	83.752	0.516
B10	84.926	1547.619	2501.690	2501.690	1711.089	84.282	0.532

Table A5.1 (2): Group C - Analysis of predicted integrated segments

	Integrated segments [N/mm ²]						SD of shook MOE s
	S1	S2	S3a	S3b	S4	S5	
C01	133.333	2773.333	3440.260	3440.260	2773.333	132.802	0.927
C02	131.492	2884.082	3425.926	3425.926	2850.877	131.492	0.882
C03	125.078	2795.699	3411.710	3411.710	2795.699	124.378	0.780
C04	129.702	2786.710	3459.561	3459.561	2804.746	129.199	0.836
C05	133.067	2786.710	3430.691	3430.691	2809.292	126.984	0.870
C06	124.378	2760.085	3454.715	3454.715	2670.776	130.463	0.835
C07	125.786	2751.323	3421.174	3421.174	2687.339	128.205	0.843
C08	126.984	2687.339	3351.449	3351.449	2764.487	123.229	0.855
C09	123.457	2791.197	3306.524	3306.524	2782.236	123.229	0.842
C10	124.611	2679.031	3365.166	3365.166	2679.031	124.378	0.844

Table A5.1 (3): Group D- Analysis of predicted integrated segments

	Integrated segments [N/mm ²]						SD of shook MOEs
	S1	S2	S3a	S3b	S4	S5	
D/01	162.999	2800.215	4913.679	4913.679	4248.366	132.802	0.869
D/02	160.643	2777.778	4894.180	4894.180	4301.075	129.955	0.892
D/03	160.643	2746.962	4808.317	4808.317	4176.707	129.955	0.893
D/04	160.643	2823.018	4808.317	4808.317	4196.933	128.949	0.838
D/05	155.039	2738.283	4645.323	4645.323	4031.008	123.686	0.854
D/06	152.555	2729.659	4680.582	4680.582	4320.988	126.502	0.831
D/07	157.233	2760.085	4671.717	4671.717	4088.050	127.959	0.852
D/08	155.400	2773.333	4771.115	4771.115	4156.675	128.949	0.839
D/09	161.812	2755.697	4817.708	4817.708	4207.120	130.208	0.899
D/10	156.128	2755.697	4743.590	4743.590	4059.329	127.714	0.838

Table A5.1 (4): Group E- Analysis of predicted integrated segments

	Integrated segments [N/mm ²]						SD of shook MOEs
	S1	S2	S3a	S3b	S4	S5	
E/01	88.889	1822.643	3284.510	3284.510	1822.643	88.652	1.095
E/02	88.183	1809.325	3275.786	3275.786	1807.438	87.951	1.111
E/03	88.183	1801.802	3249.890	3249.890	1798.064	88.652	1.136
E/04	86.468	1788.786	3199.308	3199.308	1779.603	86.468	1.098
E/05	87.719	1796.200	3228.621	3228.621	1790.634	86.919	1.111
E/06	87.146	1777.778	3207.629	3207.629	1799.931	87.032	1.109
E/07	85.034	1756.163	3126.320	3126.320	1757.945	85.034	1.100
E/08	85.911	1768.707	3170.523	3170.523	1774.139	85.911	1.106
E/09	88.417	1794.341	3241.349	3241.349	1792.485	84.495	1.095
E/10	87.835	1788.786	3249.890	3249.890	1786.942	87.835	1.153

Table A5.1 (5): Group F-Analysis of predicted integrated segments

	Integrated segments [N/mm ²]						SD of shook MOEs
	S1	S2	S3a	S3b	S4	S5	
F/01	147.493	3405.370	3071.814	3071.814	3412.073	145.879	1.463
F/02	136.893	3198.032	2936.508	2936.508	3198.032	136.612	1.480
F/03	141.543	3198.032	2971.888	2971.888	3192.142	140.647	1.484
F/04	144.928	3221.809	3045.267	3045.267	3209.877	143.678	1.437
F/05	144.928	3314.213	3015.485	3015.485	3198.032	144.928	1.485
F/06	140.351	3392.042	2997.165	2997.165	3392.042	138.600	1.478
F/07	148.148	3466.667	3075.644	3075.644	3459.747	147.820	1.481
F/08	146.520	3359.173	3008.130	3008.130	3352.676	146.520	1.526
F/09	140.351	3314.213	2975.472	2975.472	3314.213	139.762	1.492
F/10	146.199	3289.058	3019.176	3019.176	3289.058	146.199	1.498

Table A5.1 (6): Group G - Analysis of predicted integrated segments

	Integrated segments [N/mm ²]						SD of shook MOEs
	S1	S2	S3a	S3b	S4	S5	
G/01	73.992	2027.290	3067.993	3067.993	1917.404	87.604	0.622
G/02	73.584	2036.819	3056.588	3056.588	1917.404	87.374	0.620
G/03	73.502	2034.429	3064.182	3064.182	1908.957	87.260	0.632
G/04	73.341	1985.491	3041.513	3041.513	1906.857	87.374	0.643
G/05	73.099	2036.819	3022.876	3022.876	1896.426	88.300	0.673
G/06	72.701	2020.202	3019.176	3019.176	1890.222	87.146	0.657
G/07	71.917	2017.850	3083.333	3083.333	1865.806	84.495	0.669
G/08	73.502	2013.163	3083.333	3083.333	1904.762	87.146	0.646
G/09	71.839	1971.938	2975.472	2975.472	1867.816	86.133	0.665
G/10	71.149	1967.461	2957.634	2957.634	1845.935	85.911	0.697

Table A5.1 (7): Group H - Analysis of predicted integrated segments

	Integrated segments [N/mm ²]						SD of shook MOEs
	S1	S2	S3a	S3b	S4	S5	
H/01	91.701	1896.426	3297.683	3297.683	1890.222	92.081	1.004
H/02	89.726	1840.057	3319.874	3319.874	1838.105	89.726	1.093
H/03	89.969	1843.972	3310.962	3310.962	1843.972	89.606	1.077
H/04	91.075	1859.800	3360.581	3360.581	1857.806	90.827	1.091
H/05	93.371	1884.058	3435.469	3435.469	1847.903	93.110	1.168
H/06	89.969	1840.057	3310.962	3310.962	1840.057	89.847	1.092
H/07	90.090	1855.817	3328.835	3328.835	1853.832	90.212	1.065
H/08	92.721	1875.902	3388.278	3388.278	1896.426	92.464	1.076
H/09	92.208	1847.903	3397.612	3397.612	1869.831	91.954	1.139
H/10	91.199	1863.799	3356.009	3356.009	1849.875	91.075	1.100

Table A5.1 (8): Group I - Analysis of predicted integrated segments

	Integrated segments [N/mm ²]						SD of shook MOEs
	S1	S2	S3a	S3b	S4	S5	
I/01	68.027	4490.501	2283.951	2283.951	1457.808	137.741	3.642
I/02	67.137	4467.354	2279.729	2279.729	1467.683	137.741	3.634
I/03	67.820	4525.675	2279.729	2279.729	1470.172	137.741	3.633
I/04	67.682	4513.889	2277.624	2277.624	1457.808	136.893	3.652
I/05	70.249	4513.889	2286.067	2286.067	1478.953	136.612	3.563
I/06	67.682	4585.538	2286.067	2286.067	1494.253	136.333	3.588
I/07	67.340	4344.194	2248.557	2248.557	1503.325	136.054	3.544
I/08	67.340	4366.079	2248.557	2248.557	1475.177	135.227	3.595
I/09	67.137	4421.769	2250.608	2250.608	1495.542	135.227	3.574
I/10	67.613	4444.444	2248.557	2248.557	1450.488	135.777	3.665

Table A5.1 (9): Group J - Analysis of predicted integrated segments

	Integrated segments [N/mm ²]						SD of shook MOEs
	S1	S2	S3a	S3b	S4	S5	
J/01	157.978	4684.685	2198.455	2198.455	4710.145	157.604	3.259
J/02	149.813	4421.769	2148.664	2148.664	4399.323	151.172	3.274
J/03	164.609	4814.815	2240.388	2240.388	4882.629	164.609	3.228
J/04	150.150	4377.104	2161.846	2161.846	4377.104	151.172	3.236
J/05	157.604	4647.006	2202.381	2202.381	4622.222	157.233	3.235
J/06	156.495	4659.498	2163.743	2163.743	4597.701	155.763	3.316
J/07	154.679	4585.538	2186.761	2186.761	4585.538	155.763	3.249
J/08	152.555	4573.439	2188.702	2188.702	4722.979	152.905	3.246
J/09	149.477	4388.186	2190.645	2190.645	4433.078	149.142	3.170
J/10	148.810	4410.517	2161.846	2161.846	4399.323	148.478	3.232

Table A5.1 (10): Group K- Analysis of predicted integrated segments

	Integrated segments [N/mm ²]						SD of shook MOEs
	S1	S2	S3a	S3b	S4	S5	
K/01	65.104	1692.708	2401.818	2401.818	2095.929	80.515	1.082
K/02	64.475	1673.102	2380.952	2380.952	2070.888	79.650	1.086
K/03	63.918	1661.873	2364.973	2364.973	2048.857	78.802	1.079
K/04	64.164	1666.667	2367.242	2367.242	2065.952	79.460	1.103
K/05	63.857	1655.524	2360.447	2360.447	2048.857	78.802	1.092
K/06	63.613	1676.338	2364.973	2364.973	2065.952	79.460	1.111
K/07	64.977	1689.409	2404.159	2404.159	2080.832	79.650	1.046
K/08	65.041	1652.367	2364.973	2364.973	2063.492	79.554	1.099
K/09	65.104	1676.338	2390.181	2390.181	2142.563	79.177	1.127
K/10	65.295	1696.021	2411.209	2411.209	2088.353	80.515	1.057

Table A5.1 (11): Group L - Analysis of predicted integrated segments

	Integrated segments [N/mm ²]						SD of shook MOEs
	S1	S2	S3a	S3b	S4	S5	
L/01	54.600	3680.113	5225.989	5225.989	3641.457	96.339	3.242
L/02	53.591	3809.524	5409.357	5409.357	3784.571	96.200	3.415
L/03	53.548	3581.267	5138.889	5138.889	3611.111	95.923	3.308
L/04	53.079	3573.883	4993.252	4993.252	3494.624	95.923	3.310
L/05	54.780	3809.524	5281.941	5281.941	3695.807	95.785	3.268
L/06	54.825	3687.943	5171.209	5171.209	3664.553	95.923	3.220
L/07	55.051	3626.220	5160.391	5160.391	3618.650	95.374	3.177
L/08	55.142	3618.650	5493.690	5493.690	3618.650	95.785	3.212
L/09	55.188	3596.127	5106.970	5106.970	3559.206	95.648	3.138
L/10	55.325	3530.210	5013.550	5013.550	3494.624	95.374	3.086

Table A5.1 (12): Group M - Analysis of predicted integrated segments

	Integrated segments [N/mm ²]						SD of shook MOEs
	S1	S2	S3a	S3b	S4	S5	
M/01	172.712	1551.776	2260.923	2260.923	2479.733	143.988	3.422
M/02	169.635	1551.776	2331.443	2331.443	2483.286	143.678	3.322
M/03	174.520	1551.776	2318.296	2318.296	2486.848	142.450	3.358
M/04	170.940	1555.955	2327.044	2327.044	2545.277	142.450	3.325
M/05	167.084	1558.753	2338.073	2338.073	2483.286	142.755	3.279
M/06	182.149	1562.970	2333.649	2333.649	2486.848	143.678	3.371
M/07	182.149	1564.380	2344.740	2344.740	2504.817	144.613	3.364
M/08	182.149	1564.380	2346.971	2346.971	2587.065	144.928	3.372
M/09	187.266	1565.793	2349.206	2349.206	2618.328	145.243	3.400
M/10	190.476	1570.048	2349.206	2349.206	2650.357	147.820	3.428

Table A5.1 (13): Group N - Analysis of predicted integrated segments

	Integrated segments [N/mm ²]						SD of shook MOEs
	S1	S2	S3a	S3b	S4	S5	
N/01	94.697	2437.881	3430.691	3430.691	1635.220	62.834	1.913
N/02	91.827	2404.068	3425.926	3425.926	1615.409	62.247	1.915
N/03	91.954	2387.511	3392.939	3392.939	1590.214	62.657	1.925
N/04	91.575	2361.490	3356.009	3356.009	1584.400	62.305	1.917
N/05	90.580	2355.072	3346.902	3346.902	1590.214	61.671	1.913
N/06	90.457	2345.512	3378.995	3378.995	1607.916	61.162	1.910
N/07	90.090	2342.342	3293.280	3293.280	1578.628	62.073	1.881
N/08	90.580	2336.029	3324.349	3324.349	1615.409	62.131	1.824
N/09	89.246	2320.393	3297.683	3297.683	1578.628	62.131	1.854
N/10	93.240	2420.857	3306.524	3306.524	1622.971	62.364	1.882

Table A5.1 (14): Group O - Analysis of predicted integrated segments

	Integrated segments [N/mm ²]						SD of shook MOEs
	S1	S2	S3a	S3b	S4	S5	
O/01	84.926	1549.002	2535.115	2535.115	1714.474	85.911	1.490
O/02	83.438	1520.468	2469.136	2469.136	1696.021	83.542	1.496
O/03	86.693	1525.822	2496.626	2496.626	1701.014	86.693	1.623
O/04	83.963	1544.860	2481.556	2481.556	1701.014	83.647	1.448
O/05	89.366	1532.567	2481.556	2481.556	1706.037	84.282	1.620
O/06	84.818	1542.112	2491.582	2491.582	1711.089	88.535	1.582
O/07	86.356	1542.112	2486.559	2486.559	1714.474	87.489	1.591
O/08	84.175	1528.513	2484.055	2484.055	1714.474	84.282	1.496
O/09	83.857	1513.828	2474.089	2474.089	1702.685	83.752	1.522
O/10	84.926	1547.619	2501.690	2501.690	1711.089	84.282	1.467

Appendix 5.2

Table A5.2 (1): Group B – Comparison between model error calculated using arithmetic mean and the study's model and measured overall MOE

	Measured MOE [GPa]	Arithmetic Mean		PhD Model	
		Arithmetic Mean [GPa]	Arithmetic Mean Error [%]	Predicted Overall MOE [GPa]	Model Error [%]
B01	7.249	6.614	-8.760%	7.005	-3.363%
B02	7.130	6.654	-6.676%	7.032	-1.374%
B03	7.100	6.694	-5.718%	7.055	-0.637%
B04	6.971	6.630	-4.892%	7.016	0.641%
B05	7.096	6.652	-6.257%	7.039	-0.796%
B06	6.990	6.670	-4.578%	7.055	0.935%
B07	7.024	6.716	-4.385%	7.081	0.808%
B08	6.997	6.726	-3.873%	7.112	1.637%
B09	7.435	6.740	-9.348%	7.101	-4.492%
B10	6.851	6.742	-1.591%	7.105	3.707%

Table A5.2 (2): Group C – Comparison between model error calculated using arithmetic mean and the study's model and measured overall MOE

	Measured MOE [GPa]	Arithmetic Mean		PhD Model	
		Arithmetic Mean [GPa]	Arithmetic Mean Error [%]	Predicted Overall MOE [GPa]	Model Error [%]
C01	6.495	5.938	-8.576%	6.723	3.506%
C02	6.493	5.886	-9.349%	6.641	2.277%
C03	6.852	6.064	-11.500%	6.738	-1.662%
C04	6.329	5.966	-5.736%	6.683	5.587%
C05	6.529	5.968	-8.592%	6.710	2.771%
C06	6.859	6.076	-11.416%	6.775	-1.223%
C07	6.433	6.092	-5.301%	6.808	5.823%
C08	6.833	6.148	-10.025%	6.879	0.673%
C09	6.588	6.142	-6.770%	6.863	4.180%
C10	6.659	6.196	-6.953%	6.917	3.869%

Table A5.2 (3): Group D – Comparison between model error calculated using arithmetic mean and the study's model and measured overall MOE

	Measured MOE [GPa]	Arithmetic Mean		PhD Model	
		Arithmetic Mean [GPa]	Arithmetic Mean Error [%]	Predicted Overall MOE [GPa]	Model Error [%]
D/01	5.198	4.880	-6.118%	4.969	-4.398%
D/02	5.326	4.918	-7.661%	4.973	-6.620%
D/03	5.318	4.974	-6.469%	5.070	-4.663%
D/04	5.444	4.944	-9.184%	5.042	-7.393%
D/05	5.211	5.126	-1.631%	5.223	0.226%
D/06	5.385	5.116	-4.995%	5.113	-5.059%
D/07	5.385	5.050	-6.221%	5.179	-3.825%
D/08	5.710	5.010	-12.259%	5.093	-10.814%
D/09	5.151	4.954	-3.825%	5.052	-1.918%
D/10	5.235	5.050	-3.534%	5.145	-1.721%

Table A5.2 (4): Group E – Comparison between model error calculated using arithmetic mean and the study's model and measured overall MOE

	Measured MOE [GPa]	Arithmetic Mean		PhD Model	
		Arithmetic Mean [GPa]	Arithmetic Mean Error [%]	Predicted Overall MOE [GPa]	Model Error [%]
E/01	7.979	8.310	4.148%	8.212	2.915%
E/02	8.220	8.368	1.800%	8.249	0.355%
E/03	8.251	8.386	1.636%	8.304	0.639%
E/04	8.044	8.512	5.818%	8.416	4.619%
E/05	8.320	8.448	1.538%	8.351	0.369%
E/06	8.245	8.476	2.802%	8.393	1.796%
E/07	8.394	8.660	3.169%	8.588	2.306%
E/08	8.034	8.574	6.721%	8.486	5.627%
E/09	8.159	8.474	3.861%	8.331	2.112%
E/10	7.696	8.432	9.563%	8.324	8.163%

Table A5.2 (5): Group F – Comparison between model error calculated using arithmetic mean and the study's model and measured overall MOE

	Measured MOE [GPa]	Arithmetic Mean		PhD Model	
		Arithmetic Mean [GPa]	Arithmetic Mean Error [%]	Predicted Overall MOE [GPa]	Model Error [%]
F/01	6.631	5.458	-17.690%	6.438	-2.909%
F/02	5.580	5.798	3.907%	6.803	21.926%
F/03	6.623	5.720	-13.634%	6.764	2.126%
F/04	6.994	5.624	-19.588%	6.661	-4.761%
F/05	6.914	5.606	-18.918%	6.649	-3.826%
F/06	6.695	5.602	-16.326%	6.535	-2.386%
F/07	6.535	5.408	-17.246%	6.381	-2.361%
F/08	6.326	5.526	-12.646%	6.553	3.595%
F/09	6.760	5.654	-16.361%	6.636	-1.837%
F/10	6.868	5.566	-18.957%	6.610	-3.750%

Table A5.2 (6): Group G – Comparison between model error calculated using arithmetic mean and the study's model and measured overall MOE

	Measured MOE [GPa]	Arithmetic Mean		PhD Model	
		Arithmetic Mean [GPa]	Arithmetic Mean Error [%]	Predicted Overall MOE [GPa]	Model Error [%]
G/01	8.421	8.450	0.344%	8.331	-1.063%
G/02	7.953	8.462	6.400%	8.343	4.902%
G/03	8.281	8.472	2.306%	8.339	0.706%
G/04	8.241	8.530	3.507%	8.419	2.157%
G/05	8.004	8.496	6.147%	8.415	5.137%
G/06	8.338	8.548	2.519%	8.442	1.243%
G/07	7.992	8.608	7.708%	8.360	4.611%
G/08	8.418	8.486	0.808%	8.329	-1.056%
G/09	8.935	8.676	-2.899%	8.577	-4.003%
G/10	8.570	8.734	1.914%	8.632	0.723%

Table A5.2 (7): Group H – Comparison between model error calculated using arithmetic mean and the study's model and measured overall MOE

	Measured MOE [GPa]	Arithmetic Mean		PhD Model	
		Arithmetic Mean [GPa]	Arithmetic Mean Error [%]	Predicted Overall MOE [GPa]	Model Error [%]
H/01	8.187	8.060	-1.551%	8.076	-1.351%
H/02	7.910	8.228	4.020%	8.129	2.769%
H/03	7.908	8.220	3.945%	8.135	2.873%
H/04	8.099	8.130	0.383%	8.035	-0.795%
H/05	7.827	8.012	2.364%	7.909	1.048%
H/06	7.750	8.224	6.116%	7.765	0.198%
H/07	8.039	8.178	1.729%	7.585	-5.652%
H/08	7.931	8.012	1.021%	7.453	-6.028%
H/09	7.936	8.078	1.789%	7.479	-5.763%
H/10	7.478	8.130	8.719%	7.542	0.849%

Table A5.2 (8): Group I – Comparison between model error calculated using arithmetic mean and the study's model and measured overall MOE

	Measured MOE [GPa]	Arithmetic Mean		PhD Model	
		Arithmetic Mean [GPa]	Arithmetic Mean Error [%]	Predicted Overall MOE [GPa]	Model Error [%]
I/01	7.952	8.238	3.597%	7.959	0.085%
I/02	7.923	8.256	4.203%	7.976	0.663%
I/03	7.745	8.222	6.159%	7.930	2.388%
I/04	7.904	8.256	4.453%	7.952	0.603%
I/05	7.998	8.144	1.825%	7.922	-0.952%
I/06	7.584	8.182	7.885%	7.861	3.646%
I/07	8.023	8.258	2.929%	8.090	0.835%
I/08	7.958	8.304	4.348%	8.095	1.727%
I/09	7.717	8.266	7.114%	8.034	4.114%
I/10	8.068	8.318	3.099%	8.054	-0.176%

Table A5.2 (9): Group J – Comparison between model error calculated using arithmetic mean and the study's model and measured overall MOE

	Measured MOE [GPa]	Arithmetic Mean		PhD Model	
		Arithmetic Mean [GPa]	Arithmetic Mean Error [%]	Predicted Overall MOE [GPa]	Model Error [%]
J/01	5.721	5.410	-5.436%	6.049	5.731%
J/02	5.902	5.640	-4.439%	6.359	7.742%
J/03	6.433	5.252	-18.358%	5.882	-8.565%
J/04	6.368	5.636	-11.495%	6.378	0.158%
J/05	6.314	5.430	-14.001%	6.100	-3.388%
J/06	6.092	5.486	-9.947%	6.140	0.795%
J/07	5.987	5.486	-8.368%	6.159	2.873%
J/08	6.109	5.492	-10.100%	6.104	-0.077%
J/09	6.403	5.610	-12.385%	6.320	-1.289%
J/10	7.553	5.650	-25.195%	6.354	-15.881%

Table A5.2 (10): Group K – Comparison between model error calculated using arithmetic mean and the study's model and measured overall MOE

	Measured MOE [GPa]	Arithmetic Mean		PhD Model	
		Arithmetic Mean [GPa]	Arithmetic Mean Error [%]	Predicted Overall MOE [GPa]	Model Error [%]
K/01	9.717	9.460	-2.645	9.766	0.503
K/02	9.796	9.560	-2.409	9.865	0.705
K/03	9.965	9.642	-3.241	9.942	-0.234
K/04	9.420	9.598	1.890	9.910	5.203
K/05	9.737	9.656	-0.832	9.960	2.286
K/06	9.830	9.606	-2.279	9.905	0.761
K/07	9.581	9.496	-0.887	9.782	2.102
K/08	9.001	9.590	6.544	9.934	10.361
K/09	9.622	9.482	-1.455	9.760	1.430
K/10	9.415	9.448	0.351	9.749	3.553

Table A5.2 (11): Group L – Comparison between model error calculated using arithmetic mean and the study's model and measured overall MOE

	Measured MOE [GPa]	Arithmetic Mean		PhD Model	
		Arithmetic Mean [GPa]	Arithmetic Mean Error [%]	Predicted Overall MOE [GPa]	Model Error [%]
L/01	5.050	6.664	31.960%	4.761	-5.728%
L/02	4.640	6.612	42.500%	4.597	-0.925%
L/03	4.912	6.768	37.785%	4.843	-1.403%
L/04	5.403	6.852	26.818%	4.960	-8.198%
L/05	5.000	6.608	32.160%	4.684	-6.329%
L/06	5.340	6.662	24.757%	4.782	-10.454%
L/07	4.924	6.690	35.865%	4.817	-2.179%
L/08	4.885	6.624	35.599%	4.644	-4.937%
L/09	5.232	6.714	28.326%	4.871	-6.908%
L/10	5.337	6.766	26.775%	4.960	-7.055%

Table A5.2 (12): Group M – Comparison between model error calculated using arithmetic mean and the study's model and measured overall MOE

	Measured MOE [GPa]	Arithmetic Mean		PhD Model	
		Arithmetic Mean [GPa]	Arithmetic Mean Error [%]	Predicted Overall MOE [GPa]	Model Error [%]
M/01	9.442	7.512	-20.441%	9.620	1.889%
M/02	8.930	7.460	-16.461%	9.470	6.043%
M/03	9.068	7.456	-17.777%	9.490	4.651%
M/04	9.252	7.426	-19.736%	9.410	1.704%
M/05	9.126	7.462	-18.234%	9.452	3.573%
M/06	8.825	7.386	-16.306%	9.436	6.929%
M/07	8.838	7.358	-16.746%	9.392	6.272%
M/08	8.780	7.310	-16.743%	9.303	5.959%
M/09	9.168	7.268	-20.724%	9.260	1.006%
M/10	9.060	7.218	-20.331%	9.218	1.745%

Table A5.2 (13): Group N – Comparison between model error calculated using arithmetic mean and the study’s model and measured overall MOE

	Measured MOE [GPa]	Arithmetic Mean		PhD Model	
		Arithmetic Mean [GPa]	Arithmetic Mean Error [%]	Predicted Overall MOE [GPa]	Model Error [%]
N/01	7.668	8.510	10.981%	7.693	0.329%
N/02	7.288	8.622	18.304%	7.740	6.198%
N/03	7.701	8.664	12.505%	7.816	1.489%
N/04	7.750	8.722	12.542%	7.893	1.840%
N/05	7.870	8.760	11.309%	7.908	0.477%
N/06	7.978	8.748	9.652%	7.855	-1.537%
N/07	8.717	8.802	0.975%	8.005	-8.165%
N/08	8.068	8.732	8.230%	7.936	-1.638%
N/09	7.845	8.826	12.505%	8.016	2.176%
N/10	7.725	8.628	11.689%	7.892	2.163%

Table A5.2 (14): Group O – Comparison between model error calculated using arithmetic mean and the study’s model and measured overall MOE

	Measured MOE [GPa]	Arithmetic Mean		PhD Model	
		Arithmetic Mean [GPa]	Arithmetic Mean Error [%]	Predicted Overall MOE [GPa]	Model Error [%]
O/01	9.528	9.328	-2.099%	10.034	5.309%
O/02	9.975	9.516	-4.602%	10.254	2.800%
O/03	9.945	9.362	-5.862%	10.167	2.229%
O/04	9.973	9.452	-5.224%	10.187	2.147%
O/05	10.103	9.356	-7.394%	10.189	0.847%
O/06	10.041	9.332	-7.061%	10.147	1.056%
O/07	9.391	9.322	-0.735%	10.154	8.129%
O/08	9.507	9.442	-0.684%	10.184	7.116%
O/09	9.652	9.502	-1.554%	10.241	6.105%
O/10	9.936	9.390	-5.495%	10.121	1.862%

Table A5.2 (15): Overall MOE for measured, predicted, and arithmetic mean for Group P

Group P	Integrations						Measured MOE [GPa]	Arithmetic Mean		PhD Model	
	Shook 1	Shook 2	Shook 3a	Shook 3b	Shook 4	Shook 5		Arithmetic Mean [GPa]	Arithmetic Mean Error [%]	Predicted Overall MOE [GPa]	Model Error [%]
P/M1/3	174.417	2319.544	2954.787	2938.156	2281.380	173.770	5.673	5.382	-5.130	5.364	-5.454
P/M1/5	162.326	2289.389	2574.585	2704.728	2155.293	162.326	5.868	5.78	-1.500	5.787	-1.379
P/M2/1	172.490	2414.721	2715.273	2852.527	2273.069	172.173	5.757	5.466	-5.055	5.486	-4.708
P/M2/2	182.577	2554.569	2894.534	3040.849	2423.135	182.577	5.36	5.148	-3.955	5.156	-3.803
P/M2/4	177.055	2501.450	2839.400	2982.928	2381.517	177.055	5.38	5.272	-2.007	5.258	-2.264

Table A5.2 (16): Overall MOE for measured, predicted, and arithmetic mean for Group Q

Group Q	Integrations						Measured MOE [GPa]	Arithmetic Mean		PhD Model	
	Shook 1	Shook 2	Shook 3a	Shook 3b	Shook 4	Shook 5		Arithmetic Mean [GPa]	Arithmetic Mean Error [%]	Predicted Overall MOE [GPa]	Model Error [%]
Q/M1/1	61.502	1604.822	2283.785	2283.785	1593.297	61.502	5.928	5.546	-6.444	5.538	-6.572
Q/M1/2	59.157	1546.109	2204.072	2204.072	1548.807	59.674	6.316	5.738	-9.151	5.732	-9.242
Q/M1/3	60.413	1590.442	2259.273	2259.273	1587.597	60.735	6.213	5.606	-9.770	5.589	-10.049
Q/M1/4	57.658	1489.038	2119.016	2119.016	1491.541	57.560	6.289	5.944	-5.486	5.957	-5.272
Q/M1/5	57.560	1489.038	2115.466	2115.466	1491.541	57.560	6.345	5.948	-6.257	5.963	-6.016
Q/M2/1	39.598	1021.250	1461.728	1461.728	1024.788	39.506	8.409	8.650	2.866	8.654	2.914
Q/M2/2	38.965	1009.632	1436.784	1436.784	1010.782	38.876	8.446	8.780	3.955	8.788	4.045
Q/M2/3	40.110	1033.139	1445.004	1445.004	1037.973	39.969	8.397	8.586	2.251	8.667	3.212
Q/M2/4	39.144	1017.737	1448.318	1448.318	1017.737	39.099	8.775	8.722	-0.604	8.720	-0.626
Q/M2/5	38.095	987.171	1407.952	1407.952	988.270	38.053	8.998	8.974	-0.267	8.976	-0.244

Table A5.2 (17): Overall MOE for measured, predicted, and arithmetic mean for Group R

Group R	Integrations						Measured MOE [GPa]	Arithmetic Mean		PhD Model	
	Shook 1	Shook 2	Shook 3a	Shook 3b	Shook 4	Shook 5		Arithmetic Mean [GPa]	Arithmetic Mean Error [%]	Predicted Overall MOE [GPa]	Model Error [%]
R/M1/1	44.1192	2318.122	2757.108	3653.408	1421.822	44.276	6.138	5.66	-7.788	5.680	-7.469
R/M1/3	42.902	2246.917	2686.17	3559.41	1380.504	42.755	6.038	5.832	-3.412	5.839	-3.290
R/M2/1	39.310	2083.376	2462.323	3262.792	1265.822	39.186	6.404	6.348	-0.874	6.353	-0.789
R/M2/2	38.639	2031.934	2427.965	3217.265	1252.085	38.639	6.802	6.452	-5.146	6.457	-5.077
R/M2/3	38.819	2035.075	2435.517	3227.272	1255.979	38.759	6.445	6.432	-0.202	6.439	-0.095
R/M2/4	38.880	2057.333	2450.763	3247.474	1263.841	38.880	6.494	6.396	-1.510	6.392	-1.565
R/M2/5	39.002	2080.084	2458.457	3257.67	1279.865	40.005	6.657	6.322	-5.032	6.352	-4.583

Table A5.2 (18): Overall MOE for measured, predicted, and arithmetic mean for Group S

Group S	Integrations						Measured MOE [GPa]	Arithmetic Mean		PhD Model	
	Shook 1	Shook 2	Shook 3a	Shook 3b	Shook 4	Shook 5		Arithmetic Mean [GPa]	Arithmetic Mean Error [%]	Predicted Overall MOE [GPa]	Model Error [%]
S/M1/1	28.244	1492.850	1775.553	1775.553	1492.850	28.244	9.153	8.816	-3.682	8.820	-3.639
S/M1/2	28.180	1486.110	1773.542	1773.542	1486.110	28.180	8.633	8.842	2.421	8.844	2.439
S/M1/3	27.990	1479.431	1757.618	1757.618	1472.811	27.990	8.764	8.906	1.620	8.914	1.715
S/M1/4	27.710	1469.524	1749.762	1749.762	1466.251	27.834	8.730	8.966	2.703	8.959	2.625
S/M1/5	28.800	1508.240	1820.974	1820.974	1506.514	28.833	8.666	8.668	0.023	8.661	-0.059
S/M2/1	30.911	1633.615	1945.388	1945.388	1631.590	30.872	7.441	8.058	8.292	8.057	8.276

Appendix 5.3

Table A5.3 (a): Location, mode of rupture, MOR and predicted MOE for Group B

#	No. of Rupture	MOR (MPa)	Pred. MOE (GPa)	Outside Loading Zone?	S1 6.0	S2 7.0	S3 7.0	S4 7.0	S5 6.0	Mode of Failure		
										Wood	Wood/Joint	Joint
B/01	1	38.35	7.00				/			/		
B/02	2	42.51	7.03			/		/		//		
B/03	2	39.50	7.05				/	/		/		
B/04	2	40.44	7.02				//			//		
B/05	2	32.19	7.05				//			/	/	
B/06	1	43.20	7.06				/				/	
B/07	2	38.00	7.09			/		/		/		
B/08	1	34.58	7.12				/			/		
B/09	1	43.84	7.11				/				/	
B/10	1	39.43	7.10				/					/

Table A5.3 (b): Location, mode of rupture, MOR and predicted MOE for Group C

#	No. of Rupture	MOR (MPa)	Predicted MOE (GPa)	Outside Loading Zone?	S1 5.0	S2 6.0	S3 7.0	S4 6.0	S5 5.0	Mode of Failure		
										Wood	Wood/Joint	Joint
C/01	1	23.95	6.73					/		/		
C/02	2	40.35	6.64				//			/	/	
C/03	1	31.34	6.74					/		/		
C/04	1	34.16	6.68				/			/		
C/05	2	43.68	6.71				//			/	/	
C/06	2	38.22	6.78				/	/		/	/	
C/07	1	31.37	6.81	Y				/		/		
C/08	2	40.43	6.88				/	/		/	/	
C/09	2	40.76	6.86			/		/		//		
C/10	1	32.25	6.91				/				/	

Table A5.3 (c): Location, mode of rupture, MOR and predicted MOE for Group D

#	No. of Rupture	MOR (MPa)	Pred. MOE (GPa)	Outside Loading Zone?	S1 4.0	S2 6.0	S3 5.0	S4 4.0	S5 5.0	Mode of Failure		
										Wood	Wood/Joint	Joint
D/01	2	29.16	4.97			/		/		/		
D/02	1	35.99	4.78	Y				/		/		
D/03	2	35.43	5.07				/	/		//		
D/04	2	111.77	5.04			/		/		//		
D/05	2	74.17	5.22			/		/		//		
D/06	1	36.58	5.21				/			/		
D/07	1	36.25	5.18					/		/		
D/08	2	34.54	5.09			/		/		//		
D/09	1	30.53	5.05				/			/		
D/10	1	34.77	5.10				/			/		

Table A5.3 (d): Location, mode of rupture, MOR and predicted MOE for Group E

#	No. of Rupture	MOR (MPa)	Pred. MOE (GPa)	Outside Loading Zone?	S1 7.5	S2 9.5	S3 7.5	S4 9.5	S5 7.5	Mode of Failure		
										Wood	Wood/Joint	Joint
E/01	1	41.26	8.22				/			/		
E/02	1	38.62	8.24				/			/		
E/03	1	41.87	8.30			/				/		
E/04	1	44.72	8.41				/			/		
E/05	1	43.75	8.34				/			/		
E/06	1	49.92	8.39				/			/		
E/07	1	43.98	8.58				/			/		
E/08	2	42.97	8.49				/			/	/	
E/09	1	46.64	8.34		/							/
E/10	1	43.43	8.32				/					/

Table A5.3 (e): Location, mode of rupture, MOR and predicted MOE for Group F

#	No. of Rupture	MOR (MPa)	Pred. MOE (GPa)	Outside Loading Zone?	S1 4.5	S2 5.0	S3 8.0	S4 5.0	S5 4.5	Mode of Failure		
										Wood	Wood/ Joint	Joint
F/01	2	42.04	6.68				/	/		/	/	
F/02	1	39.02	6.80				/			/		
F/03	1	35.52	6.77					/		/		
F/04	2	38.05	6.66				/	/		/	/	
F/05	2	32.01	6.65	Y		/		/		//		
F/06	2	41.46	6.53	Y		/		/		//		
F/07	1	36.35	6.38			/				/		
F/08	2	37.99	6.38				/	/		/	/	
F/09	2	43.24	6.64	Y		/		/		//		
F/10	2	40.58	6.61			/		/		//		

Table A5.3 (f): Location, mode of rupture, MOR and predicted MOE for Group G

#	No. of Rupture	MOR (MPa)	Pred. MOE (GPa)	Outside Loading Zone?	S1 9.0	S2 8.5	S3 8.0	S4 9.0	S5 7.5	Mode of Failure		
										Wood	Wood/ Joint	Joint
G/01	2	51.25	8.13			/	/			/	/	
G/02	1	42.25	8.33				/			/		
G/03	1	48.54	8.35				/			/		
G/04	1	53.31	8.42				/				/	
G/05	1	48.51	8.41			/				/		
G/06	2	50.53	8.44	1 (Y)		/	/			//		
G/07	1	42.46	8.36				/				/	
G/08	1	48.16	8.33				/			/		
G/09	2	52.50	8.57			/	/			/		
G/10	2	50.75	8.62				//				//	

Table A5.3 (g): Location, mode of rupture, MOR and predicted MOE for Group H

#	No. of Rupture	MOR (MPa)	Pred. MOE (GPa)	Outside Loading Zone?	S1 7.0	S2 9.0	S3 7.0	S4 9.0	S5 7.0	Mode of Failure		
										Wood	Wood/ Joint	Joint
H/01	1	47.25	8.07				/				/	
H/02	1	46.29	8.13				/			/		
H/03	2	46.74	8.14			/	/			/	/	
H/04	2	42.77	8.03				//			//		
H/05	1	45.69	7.90				/			/		
H/06	1	35.07	8.14					/		/		
H/07	1	46.84	7.97				/			/		
H/08	1	49.72	7.94				/			/		
H/09	1	41.48	7.97				/			/		
H/10	1	42.57	8.04				/			/		

Table A5.3 (h): Location, mode of rupture, MOR and predicted MOE for Group I

#	No. of Rupture	MOR (MPa)	Pred. MOE (GPa)	Outside Loading Zone?	S1 9.5	S2 3.5	S3 10.5	S4 11.5	S5 4.5	Mode of Failure		
										Wood	Wood/ Joint	Joint
I/01	1	37.74	7.97			/				/		
I/02	1	63.80	7.97	Y		/				/		
I/03	1	35.04	7.93			/				/		
I/04	1	130.33	7.95				/				/	
I/05	1	41.37	7.92			/				/		
I/06	1	89.49	7.86				/			/		
I/07	1	41.39	8.09				/				/	
I/08	1	39.57	8.09			/				/		
I/09	1	36.36	8.03	Y		/				/		
I/10	1	38.13	8.06	Y		/				/		

Table A5.3 (i): Location, mode of rupture, MOR and predicted MOE for Group J

#	No. of Rupture	MOR (MPa)	Pred. MOE (GPa)	Outside Loading Zone?	S1 4.0	S2 3.5	S3 11.0	S4 3.5	S5 4.0	Mode of Failure		
										Wood	Wood/Joint	Joint
J/01	1	22.39	6.05			/				/		
J/02	1	22.45	6.36				/				/	
J/03	1	33.83	5.34			/				/		
J/04	1	36.38	6.38	Y		/				/		
J/05	2	34.37	6.10					//		/	/	
J/06	2	37.39	6.14	Y		/	/			/	/	
J/07	1	27.63	6.15	Y		/				/		
J/08	1	59.47	6.10					/		/		
J/09	1	-	6.28			/				/		
J/10	2	37.03	6.36			/		/		/		

Table A5.3 (j): Location, mode of rupture, MOR and predicted MOE for Group K

#	No. of Rupture	MOR (MPa)	Pred. MOE (GPa)	Outside Loading Zone?	S1 10.0	S2 10.0	S3 10.0	S4 8.0	S5 8.0	Mode of Failure		
										Wood	Wood/Joint	Joint
K/01	2	52.80	9.77				/	/		//		
K/02	1	57.17	9.87				/				/	
K/03	1	56.79	10.19				/			/		
K/04	1	52.46	9.90				/				/	
K/05	2	40.61	9.95			/	/			/	/	
K/06	1	56.43	9.91				/			/		
K/07	-	50.83	9.79									
K/08	2	48.49	9.95			/		/		//		
K/09	1	51.35	9.76			/				/		
K/10	2	46.89	9.76				//				//	

Table A5.3 (k): Location, mode of rupture, MOR and predicted MOE for Group L

#	No. of Rupture	MOR (MPa)	Pred. MOE (GPa)	Outside Loading Zone?	S1 12.0	S2 4.5	S3 4.5	S4 4.5	S5 6.5	Mode of Failure		
										Wood	Wood/Joint	Joint
L/01	2	25.80	4.76				//			/	/	
L/02	1	29.24	4.60			/				/		
L/03	1	32.31	4.84					/		/		
L/04	2	38.8	4.96			/	/			/	/	
L/05	2	30.69	4.69			/	/			/	/	
L/06	1	26.11	4.78				/			/		
L/07	-	33.46	4.82									
L/08	2	35.17	4.65			/		/		/		
L/09	1	32.21	4.87			/				/		
L/10	2	35.46	4.96			/		/			/	

Table A5.3 (l): Location, mode of rupture, MOR and predicted MOE for Group M

#	No. of Rupture	MOR (MPa)	Pred. MOE (GPa)	Outside Loading Zone?	S1 3.5	S2 11.0	S3 10.5	S4 6.5	S5 4.5	Mode of Failure		
										Wood	Wood/Joint	Joint
M/01	1	54.01	9.63	Y				/		/		
M/02	2	49.82	9.48			/	/				/	/
M/03	1	47.48	9.48				/			/		
M/04	3	47.59	9.39	Y		/	/		/	//	/	
M/05	1	41.21	9.43				/				/	
M/06	1	46.74	9.44				/			/		
M/07	1	50.54	9.40				/				/	
M/08	1	33.75	9.30					/		/		
M/09	3	49.16	9.26	Y	/			/	/	/	/	
M/10	1	43.47	9.22					/		/		

Table A5.3 (m): Location, mode of rupture, MOR and predicted MOE for Group N

#	No. of Rupture	MOR (MPa)	Pred. MOE (GPa)	Outside Loading Zone?	S1 7.0	S2 7.0	S3 7.0	S4 10.5	S5 10.5	Mode of Failure		
										Wood	Wood/Joint	Joint
N/01	1	42.34	7.69			/				/		
N/02	1	38.50	7.75				/				/	
N/03	1	43.45	7.82				/				/	
N/04	2	45.57	7.89				/			//		
N/05	1	45.42	7.90				/			/		
N/06	1	39.42	7.85				/			/		
N/07	1	37.28	7.99				/			/		
N/08	2	43.26	7.94			/	/			/		
N/09	1	36.28	8.00				/				/	
N/10	1	35.51	7.88				/			/		

Table A5.3 (n): Location, mode of rupture, MOR and predicted MOE for Group O

#	No. of Rupture	MOR (MPa)	Pred. MOE (GPa)	Outside Loading Zone?	S1 7.5	S2 11.0	S3 9.5	S4 10.0	S5 7.5	Mode of Failure		
										Wood	Wood/Joint	Joint
O/01	1	-	10.03				/				/	
O/02	-	52.53	10.25									
O/03	1	55.39	10.15				/			/		
O/04	1	48.58	10.20				/				/	
O/05	Tensile failure	53.52	10.19				/					
O/06	1	46.77	10.15				/			/		
O/07	1	52.27	10.15				/				/	
O/08	1	41.58	10.20				/				/	
O/09	1	50.61	10.26				/				/	
O/10	1	49.70	10.12				/				/	

Appendix 5.4

Table A5.4 (a): Projected pricing guide categorised by stiffness at 0.5 GPa intervals

MOE (GPa)	Price at (1200 x 20 x 1000) mm (NZ\$ per m)	300mm length Estimated Price (NZ\$)
3.0	1.00	\$0.30
3.5	1.25	\$0.38
4.0	1.50	\$0.45
4.5	1.75	\$0.53
5.0	2.00	\$0.60
5.5	2.25	\$0.68
6.0	2.50	\$0.75
6.5	2.75	\$0.83
7.0	6.00	\$1.80
7.5	6.90	\$2.07
8.0	7.80	\$2.34
8.5	8.10	\$2.43
9.0	8.40	\$2.52
9.5	8.70	\$2.61
10.0	9.00	\$2.70
10.5	9.50	\$2.85
11.0	10.00	\$3.00
11.5	10.50	\$3.15
12.0	11.00	\$3.30

Table A5.4 (b): Pricing analysis for Group AI

Groups	Shook MOE / Price per meter (NZ\$) / (Integrated value)					Model Overall MOE (GPa)	Model cost (NZ\$)	Model Selling Price (NZ\$)	Gross Profit (NZ\$)	Gross Profit (%)	Mean MOE (GPa)	Mean Selling Price (NZ\$)	Minimum shook MOE (NZ\$)
	Shook 1	Shook 2	Shook 3	Shook 4	Shook 5								
A1	5.0 \$0.60 (133.33)	6.0 \$0.75 (2888.89)	7.0 \$1.80 (3523.81)	6.0 \$0.75 (2888.89)	5.0 \$0.60 (133.33)	8.92	\$4.50	\$12.15	\$7.65	62.96	5.80	3.4	3.00
A2	5.0 \$0.60 (133.33)	6.0 \$0.75 (2888.89)	7.5 \$2.07 (3288.89)	6.0 \$0.75 (2888.89)	5.0 \$0.60 (133.33)	9.14	\$4.77	\$12.60	\$7.83	62.14	5.90	3.4	3.00
A3	5.0 \$0.60 (133.33)	6.0 \$0.75 (2888.89)	8.0 \$2.34 (3083.33)	6.0 \$0.75 (2888.89)	5.0 \$0.60 (133.33)	9.35	\$5.04	\$12.60	\$7.56	60.00	6.00	3.75	3.00
A4	5.0 \$0.60 (133.33)	6.0 \$0.75 (2888.89)	8.5 \$2.43 (2901.96)	6.0 \$0.75 (2888.89)	5.0 \$0.60 (133.33)	9.53	\$5.13	\$13.05	\$7.92	60.69	6.10	3.75	3.00
A5	5.0 \$0.60 (133.33)	6.0 \$0.75 (2888.89)	8.6 \$2.43 (2868.22)	6.0 \$0.75 (2888.89)	5.0 \$0.60 (133.33)	9.57	\$5.13	\$13.05	\$7.92	60.69	6.12	3.75	3.00
A6	5.0 \$0.60 (133.33)	6.0 \$0.75 (2888.89)	8.7 \$2.43 (2835.25)	6.0 \$0.75 (2888.89)	5.0 \$0.60 (133.33)	9.61	\$5.13	\$13.05	\$7.92	60.69	6.14	3.75	3.00
A7	5.0 \$0.60 (133.33)	6.0 \$0.75 (2888.89)	8.8 \$2.43 (2803.03)	6.0 \$0.75 (2888.89)	5.0 \$0.60 (133.33)	9.65	\$5.13	\$13.05	\$7.92	60.69	6.16	3.75	3.00
A8	5.0 \$0.60 (133.33)	6.0 \$0.75 (2888.89)	8.9 \$2.43 (2771.54)	6.0 \$0.75 (2888.89)	5.0 \$0.60 (133.33)	9.68	\$5.13	\$13.05	\$7.92	60.69	6.18	3.75	3.00
A9	5.0 \$0.60 (133.33)	6.0 \$0.75 (2888.89)	9.0 \$2.52 (2740.74)	6.0 \$0.75 (2888.89)	5.0 \$0.60 (133.33)	9.71	\$5.22	\$13.05	\$7.83	60.00	6.20	3.75	3.00

Table A5.4 (c): Pricing analysis for Group AII

Groups	Shook MOE / Price per meter (NZ\$) / (Integrated value)					Model Overall MOE (GPa)	Model Cost (NZ\$)	Model selling Price (NZ\$)	Gross Profit (NZ\$)	Gross Profit (%)	Mean MOE (GPa)	Mean MOE (NZ\$)	Minimum shook MOE (NZ\$)
	Shook 1	Shook 2	Shook 3	Shook 4	Shook 5								
B1	5.0 \$0.60 (133.33)	8.0 \$2.34 (2166.67)	7.0 \$1.80 (3523.81)	8.0 \$2.34 (2166.67)	5.0 \$0.60 (133.33)	10.50	\$7.68	\$14.25	\$6.57	46.11	6.60	\$4.15	\$3.00
B2	5.0 \$0.60 (133.33)	8.5 \$2.43 (2039.22)	7.0 \$1.80 (3523.81)	8.5 \$2.43 (2039.22)	5.0 \$0.60 (133.33)	10.84	\$7.86	\$14.25	\$6.39	44.84	6.80	\$4.15	\$3.00
B3	5.0 \$0.60 (133.33)	9.0 \$2.52 (1925.93)	7.0 \$1.80 (3523.81)	9.0 \$2.52 (1925.93)	5.0 \$0.60 (133.33)	11.70	\$8.04	\$15.75	\$7.71	48.95	7.00	\$9.00	\$3.00
B4	5.0 \$0.60 (133.33)	9.5 \$2.61 (1824.56)	7.0 \$1.80 (3523.81)	9.5 \$2.61 (1824.56)	5.0 \$0.60 (133.33)	11.47	\$8.22	\$15.00	\$6.78	45.20	7.20	\$9.00	\$3.00
B5	5.0 \$0.60 (133.33)	9.8 \$2.61 (1768.71)	7.0 \$1.80 (3523.81)	9.8 \$2.61 (1768.71)	5.0 \$0.60 (133.33)	11.65	\$8.22	\$15.75	\$7.53	47.81	7.32	\$9.00	\$3.00
B6	5.0 \$0.60 (133.33)	9.9 \$2.61 (1750.84)	7.0 \$1.80 (3523.81)	9.9 \$2.61 (1750.84)	5.0 \$0.60 (133.33)	11.70	\$8.22	\$15.75	\$7.53	47.81	7.36	\$9.00	\$3.00
B7	5.0 \$0.60 (133.33)	10.0 \$2.70 (1733.33)	7.0 \$1.80 (3523.81)	10.0 \$2.70 (1733.33)	5.0 \$0.60 (133.33)	11.76	\$8.40	\$15.75	\$7.53	46.67	7.40	\$9.00	\$3.00
B8	5.0 \$0.60 (133.33)	10.50 \$2.85 (1650.79)	7.0 \$1.80 (3523.81)	10.50 \$2.85 (1650.79)	5.0 \$0.60 (133.33)	12.03	\$8.70	\$16.50	\$7.80	47.27	7.60	\$10.35	\$3.00
B9	5.0 \$0.60 (133.33)	11.0 \$3.00 (1573.76)	7.0 \$1.80 (3523.81)	11.0 \$3.00 (1573.76)	5.0 \$0.60 (133.33)	12.29	\$9.00	\$16.50	\$7.50	45.45	7.80	\$10.35	\$3.00
B10	5.0 \$0.60 (133.33)	12.0 \$3.30 (1444.44)	7.0 \$1.80 (3523.81)	12.0 \$3.30 (1444.44)	5.0 \$0.60 (133.33)	12.78	\$9.60	\$16.50	\$6.90	41.82	8.20	\$11.70	\$3.00

Table A5.4 (d): Pricing analysis for Group AIII

Groups	Shook MOE / Price per meter (NZ\$) / (Integrated value)					Model Overall MOE (GPa)	Model Cost (NZ\$)	Model Selling Price (NZ\$)	Gross Profit (NZ\$)	Gross Profit (%)	Mean MOE (GPa)	Mean MOE (NZ\$)	Minimum Shook MOE (NZ\$)
	Shook 1	Shook 2	Shook 3	Shook 4	Shook 5								
C1	5.0 \$0.60 (133.33)	6.0 \$0.75 (2888.89)	7.0 \$1.80 (3523.81)	6.0 \$0.75 (2888.89)	5.0 \$0.60 (133.33)	8.92	\$4.50	\$12.15	\$7.65	62.96	5.80	\$3.40	\$3.00
C2	5.0 \$0.60 (133.33)	5.5 0.68 (3151.52)	7.0 \$1.80 (3523.81)	5.5 0.68 (3151.52)	5.0 \$0.60 (133.33)	8.68	\$4.36	\$12.15	\$7.79	64.12	5.60	\$3.40	\$3.00
C3	5.0 \$0.60 (133.33)	5.0 0.6 (3466.67)	7.0 \$1.80 (3523.81)	5.0 0.6 (3466.67)	5.0 \$0.60 (133.33)	8.16	\$4.20	\$11.70	\$7.50	64.10	5.40	\$3.00	\$3.00
C4	5.0 \$0.60 (133.33)	4.5 0.53 (3851.85)	7.0 \$1.80 (3523.81)	4.5 0.53 (3851.85)	5.0 \$0.60 (133.33)	7.60	\$4.06	\$10.35	\$6.29	60.77	5.20	\$3.00	\$2.65
C5	5.0 \$0.60 (133.33)	4.4 0.45 (3939.39)	7.0 \$1.80 (3523.81)	4.4 0.45 (3939.39)	5.0 \$0.60 (133.33)	7.48	\$3.90	\$9.00	\$5.10	56.67	5.16	\$3.00	\$2.25
C6	5.0 \$0.60 (133.33)	4.3 0.45 (4031.01)	7.0 \$1.80 (3523.81)	4.3 0.45 (4031.01)	5.0 \$0.60 (133.33)	7.37	\$3.90	\$9.00	\$5.10	56.67	5.12	\$3.00	\$2.25
C7	5.0 \$0.60 (133.33)	4.2 0.45 (4031.01)	7.0 \$1.80 (3523.81)	4.2 0.45 (4031.01)	5.0 \$0.60 (133.33)	7.25	\$3.90	\$9.00	\$5.10	56.67	5.08	\$3.00	\$2.25
C8	5.0 \$0.60 (133.33)	4.1 0.45 (4126.98)	7.0 \$1.80 (3523.81)	4.1 0.45 (4126.98)	5.0 \$0.60 (133.33)	7.12	\$3.90	\$9.00	\$5.10	56.67	5.04	\$3.00	\$2.25
C9	5.0 \$0.60 (133.33)	4.0 0.45 (4333.33)	7.0 \$1.80 (3523.81)	4.0 0.45 (4333.33)	5.0 \$0.60 (133.33)	7.00	\$3.90	\$9.00	\$5.10	56.67	5.00	\$3.00	\$2.25

Table A5.4 (e): Pricing analysis for Group BI

Groups	Shook MOE / Price per meter (NZ\$) / (Integrated value)					Model Overall MOE (GPa)	Model Cost (NZ\$)	Model selling Price (NZ\$)	Gross Profit (NZ\$)	Gross Profit (%)	Mean MOE (GPa)	Mean MOE (NZ\$)	Minimum MOE (NZ\$)
	Shook 1	Shook 2	Shook 3	Shook 4	Shook 5								
D1	5.0	7.0	8.0	7.0	5.0	10.28	\$7.14	\$13.50	\$6.36	47.11	6.40	\$3.75	\$3.00
	\$0.60	\$1.80	\$2.34	\$1.80	\$0.60								
	(133.33)	(2476.19)	(3083.33)	(2476.19)	(133.33)								
D2	5.0	6.5	8.0	6.5	5.0	9.83	\$5.20	\$13.05	\$7.85	60.15	6.20	\$3.75	\$3.00
	\$0.60	\$0.83	\$2.34	\$0.83	\$0.60								
	(133.33)	(2666.67)	(3083.33)	(2666.67)	(133.33)								
D3	5.0	6.0	8.0	6.0	5.0	9.35	\$5.04	\$12.60	\$7.56	60.00	6.00	\$3.75	\$3.00
	\$0.60	\$0.75	\$2.34	\$0.75	\$0.60								
	(133.33)	(2888.89)	(3083.33)	(2888.89)	(133.33)								
D4	5.0	5.5	8.0	5.5	5.0	8.84	\$4.90	\$12.15	\$7.25	59.67	5.80	\$3.40	\$3.00
	\$0.60	\$0.68	\$2.34	\$0.68	\$0.60								
	(133.33)	(3151.52)	(3083.33)	(3151.52)	(133.33)								
D5	5.0	5.4	8.0	5.4	5.0	8.73	\$4.74	\$12.15	\$7.41	60.99	5.76	\$3.40	\$3.00
	\$0.60	\$0.60	\$2.34	\$0.60	\$0.60								
	(133.33)	(3209.88)	(3083.33)	(3209.88)	(133.33)								
D6	5.0	5.3	8.0	5.3	5.0	8.63	\$4.74	\$12.15	\$7.41	60.99	5.72	\$3.40	\$3.00
	\$0.60	\$0.60	\$2.34	\$0.60	\$0.60								
	(133.33)	(3270.44)	(3083.33)	(3270.44)	(133.33)								
D7	5.0	5.2	8.0	5.2	5.0	8.52	\$4.74	\$12.15	\$7.41	60.99	5.68	\$3.40	\$3.00
	\$0.60	\$0.60	\$2.34	\$0.60	\$0.60								
	(133.33)	(3333.33)	(3083.33)	(3333.33)	(133.33)								
D8	5.0	5.1	8.0	5.1	5.0	8.41	\$4.74	\$11.70	\$6.96	59.44	5.64	\$3.40	\$3.00
	\$0.60	\$0.60	\$2.34	\$0.60	\$0.60								
	(133.33)	(3398.69)	(3083.33)	(3398.69)	(133.33)								
D9	5.0	5.0	8.0	5.0	5.0	8.30	\$4.74	\$11.70	\$6.96	59.49	5.60	\$3.40	\$3.00
	\$0.60	\$0.60	\$2.34	\$0.60	\$0.60								
	(133.33)	(3466.67)	(3083.33)	(3466.67)	(133.33)								

Table A5.4 (f): Pricing analysis for Group BII

Groups	Shook MOE / Price per meter (NZ\$) / (Integrated value)					Model MOE (GPa)	Model Cost (NZ\$)	Model Selling Price (NZ\$)	Gross Profit (NZ\$)	Gross Profit (%)	Mean MOE (GPa)	Mean MOE (NZ\$)	Minimum MOE (NZ\$)
	Shook 1	Shook 2	Shook 3	Shook 4	Shook 5								
E1	5.0	7.0	8.5	7.0	5.0	10.51	\$6.63	\$14.25	\$7.02	49.26	6.50	4.15	\$3.00
	\$0.60	\$1.80	\$2.43	\$1.80	\$0.60								
	(133.33)	(2476.19)	(2901.96)	(2476.19)	(133.33)								
E2	5.0	6.5	8.5	6.5	5.0	10.04	\$4.69	\$13.50	\$8.21	60.81	6.30	3.75	\$3.00
	\$0.60	\$0.83	\$2.43	\$0.83	\$0.60								
	(133.33)	(2666.67)	(2901.96)	(2666.67)	(133.33)								
E3	5.0	6.0	8.5	6.0	5.0	9.54	\$4.53	\$13.05	\$7.92	60.69	6.10	3.75	\$3.00
	\$0.60	\$0.75	\$2.43	\$0.75	\$0.60								
	(133.33)	(2888.89)	(2901.96)	(2888.89)	(133.33)								
E4	5.0	5.5	8.5	5.5	5.0	9.01	\$4.39	\$12.60	\$7.61	60.40	5.90	3.40	\$3.00
	\$0.60	\$0.68	\$2.43	\$0.68	\$0.60								
	(133.33)	(3151.52)	(2901.96)	(3151.52)	(133.33)								
E5	5.0	5.4	8.5	5.4	5.0	8.90	\$4.23	\$12.15	\$7.32	60.25	5.86	3.40	\$3.00
	\$0.60	\$0.60	\$2.4	\$0.60	\$0.60								
	(133.33)	(3209.88)	(2901.96)	(3209.88)	(133.33)								
E6	5.0	5.3	8.5	5.3	5.0	8.79	\$4.23	\$12.15	\$7.32	60.25	5.82	3.40	\$3.00
	\$0.60	\$0.60	\$2.43	\$0.60	\$0.60								
	(133.33)	(3270.44)	(2901.96)	(3270.44)	(133.33)								
E7	5.0	5.2	8.5	5.2	5.0	8.68	\$4.23	\$12.15	\$7.32	60.25	5.78	3.40	\$3.00
	\$0.60	\$0.60	\$2.43	\$0.60	\$0.60								
	(133.33)	(3333.33)	(2901.96)	(3333.33)	(133.33)								
E8	5.0	5.1	8.5	5.1	5.0	8.56	\$4.23	\$12.15	\$7.32	60.25	5.74	3.40	\$3.00
	\$0.60	\$0.60	\$2.43	\$0.60	\$0.60								
	(133.33)	(3398.69)	(2901.96)	(3398.69)	(133.33)								
E9	5.0	5.0	8.5	5.0	5.0	8.45	\$4.23	\$11.70	\$7.32	60.25	5.70	3.40	\$3.00
	\$0.60	\$0.60	\$2.43	\$0.60	\$0.60								
	(133.33)	(3466.67)	(2901.96)	(3466.67)	(133.33)								

Table A5.4 (g): Pricing analysis for Group BIII

Groups	Shook MOE / Price per meter (NZ\$) / (Integrated value)					Model MOE (GPa)	Model Cost (NZ\$)	Model Selling Price (NZ\$)	Gross Profit (NZ\$)	Gross Profit (%)	Mean MOE (GPa)	Mean MOE (NZ\$)	Minimum MOE (NZ\$)
	Shook 1	Shook 2	Shook 3	Shook 4	Shook 5								
F1	5.0 \$0.60 (133.33)	8.0 \$2.34 (2166.67)	9.0 \$2.52 (2740.74)	8.0 \$2.34 (2166.67)	5.0 \$0.60 (133.33)	11.63	\$8.40	\$15.75	\$7.35	46.67	7.00	\$9.00	\$3.00
F2	5.0 \$0.60 (133.33)	7.5 \$2.07 (2311.11)	9.0 \$2.52 (2740.74)	7.5 \$2.07 (2311.11)	5.0 \$0.60 (133.33)	11.18	\$7.86	\$15.00	\$7.14	47.60	6.80	\$4.15	\$3.00
F3	5.0 \$0.60 (133.33)	7.0 \$1.80 (2476.19)	9.0 \$2.52 (2740.74)	7.0 \$1.80 (2476.19)	5.0 \$0.60 (133.33)	10.72	\$7.32	\$14.25	\$6.93	48.63	6.60	\$4.15	\$3.00
F4	5.0 \$0.60 (133.33)	6.5 \$0.83 (2666.67)	9.0 \$2.52 (2740.74)	6.5 \$0.83 (2666.67)	5.0 \$0.60 (133.33)	10.23	\$5.38	\$13.50	\$8.12	60.15	6.40	\$3.75	\$3.00
F5	5.0 \$0.60 (133.33)	6.4 \$0.75 (2703.33)	9.0 \$2.52 (2740.74)	6.4 \$0.75 (2708.33)	5.0 \$0.60 (133.33)	10.13	\$5.22	\$13.50	\$8.28	61.33	6.36	\$3.75	\$3.00
F6	5.0 \$0.60 (133.33)	6.3 \$0.75 (2751.32)	9.0 \$2.52 (2740.74)	6.3 \$0.75 (2751.32)	5.0 \$0.60 (133.33)	10.03	\$5.22	\$13.50	\$8.28	61.33	6.32	\$3.75	\$3.00
F7	5.0 \$0.60 (133.33)	6.2 \$0.75 (2795.70)	9.0 \$2.52 (2740.74)	6.2 \$0.75 (2795.70)	5.0 \$0.60 (133.33)	9.92	\$5.22	\$13.05	\$7.83	60.00	6.28	\$3.75	\$3.00
F8	5.0 \$0.60 (133.33)	6.1 \$0.75 (2841.53)	9.0 \$2.52 (2740.74)	6.1 \$0.75 (2841.53)	5.0 \$0.60 (133.33)	9.83	\$5.22	\$13.05	\$7.83	60.00	6.24	\$3.75	\$3.00
F9	5.0 \$0.60 (133.33)	6.0 \$0.75 (2888.89)	9.0 \$2.52 (2740.74)	6.0 \$0.75 (2888.89)	5.0 \$0.60 (133.33)	9.71	\$5.22	\$13.05	\$7.83	60.00	6.20	\$3.75	\$3.00

Table A5.4 (h): Pricing analysis for Group BIV

Groups	Shook MOE / Price per meter (NZ\$) / (Integrated value)					Model MOE (GPa)	Model Cost (NZ\$)	Model Selling Price (NZ\$)	Gross Profit (NZ\$)	Gross Profit (%)	Mean MOE (GPa)	Mean MOE (NZ\$)	Minimum MOE (NZ\$)
	Shook 1	Shook 2	Shook 3	Shook 4	Shook 5								
G1	5.0 \$0.60 (133.33)	4.0 \$0.45 (4333.33)	5.0 \$0.60 (4933.33)	4.0 \$0.45 (4333.33)	5.0 \$0.60 (133.33)	6.15	\$2.70	\$3.75	\$1.05	28.00	4.60	\$2.65	\$2.25
G2	5.0 \$0.60 (133.33)	3.5 \$0.38 (4952.38)	5.0 \$0.60 (4933.33)	3.5 \$0.38 (4952.38)	5.0 \$0.60 (133.33)	5.76	\$2.56	\$3.40	\$0.84	24.71	4.40	\$2.25	\$1.90
G3	5.0 \$0.60 (133.33)	3.0 \$0.30 (5777.78)	5.0 \$0.60 (4933.33)	3.0 \$0.30 (5777.78)	5.0 \$0.60 (133.33)	5.18	\$2.70	\$3.00	\$0.30	10.00	4.20	\$2.25	\$1.50
G4	5.0 \$0.60 (133.33)	2.5 \$0.30 (6933.33)	5.0 \$0.60 (4933.33)	2.5 \$0.30 (6933.33)	5.0 \$0.60 (133.33)	4.54	\$2.40	\$2.63	\$0.25	9.43	4.00	\$2.25	\$1.50
G5	5.0 \$0.60 (133.33)	2.4 \$0.30 (7222.22)	5.0 \$0.60 (4933.33)	2.4 \$0.30 (7222.22)	5.0 \$0.60 (133.33)	4.40	\$2.40	\$2.25	-\$0.15	-6.67	3.96	\$1.90	\$1.50
G6	5.0 \$0.60 (133.33)	2.3 \$0.30 (7536.23)	5.0 \$0.60 (4933.33)	2.3 \$0.30 (7536.23)	5.0 \$0.60 (133.33)	4.27	\$2.40	\$2.25	-\$0.15	-6.67	3.97	\$1.90	\$1.50
G7	5.0 \$0.60 (133.33)	2.2 \$0.30 (7878.79)	5.0 \$0.60 (4933.33)	2.2 \$0.30 (7878.79)	5.0 \$0.60 (133.33)	4.12	\$2.40	\$2.25	-\$0.15	-6.67	3.88	\$1.90	\$1.50
G8	5.0 \$0.60 (133.33)	2.1 \$0.30 (8253.97)	5.0 \$0.60 (4933.33)	2.1 \$0.30 (8253.97)	5.0 \$0.60 (133.33)	3.98	\$2.40	\$1.90	-\$0.50	-26.32	3.84	\$1.90	\$1.50
G9	5.0 \$0.60 (133.33)	2.0 \$0.30 (8666.67)	5.0 \$0.60 (4933.33)	2.0 \$0.30 (8666.67)	5.0 \$0.60 (133.33)	3.83	\$2.40	\$1.90	-\$0.50	-26.32	3.80	\$1.90	\$1.50

Table A5.4 (i): Pricing analysis for Group BV

Groups	Shook MOE / Price per meter (NZ\$) / (Integrated value)					Model MOE (GPa)	Model Cost (NZ\$)	Model Selling Price (NZ\$)	Gross Profit (NZ\$)	Gross Profit (%)	Mean MOE (GPa)	Mean MOE (NZ\$)	Minimum MOE (GPa)
	Shook 1	Shook 2	Shook 3	Shook 4	Shook 5								
H1	5.0 \$0.60 (133.33)	5.0 \$0.60 (3466.67)	6.0 \$0.75 (4111.11)	5.0 \$0.60 (3466.67)	5.0 \$0.60 (133.33)	7.544	\$3.15	\$10.35	\$7.20	69.57	5.20	\$3.00	\$3.00
H2	5.0 \$0.60 (133.33)	4.5 \$0.53 (3851.85)	6.0 \$0.75 (4111.11)	4.5 \$0.53 (3851.85)	5.0 \$0.60 (133.33)	7.0632	\$3.01	\$9.00	\$5.99	66.56	5.00	\$3.00	\$2.65
H3	5.0 \$0.60 (133.33)	4.0 \$0.45 (4333.33)	6.0 \$0.75 (4111.11)	4.0 \$0.45 (4333.33)	5.0 \$0.60 (133.33)	6.542	\$2.85	\$4.15	\$1.30	31.33	4.80	\$2.65	\$2.25
H4	5.0 \$0.60 (133.33)	3.5 \$0.38 (4952.38)	6.0 \$0.75 (4111.11)	3.5 \$0.38 (4952.38)	5.0 \$0.60 (133.33)	5.975	\$2.71	\$3.40	\$0.69	20.29	4.60	\$2.65	\$1.90
H5	5.0 \$0.60 (133.33)	3.4 \$0.30 (5777.78)	6.0 \$0.75 (4111.11)	3.4 \$0.30 (5777.78)	5.0 \$0.60 (133.33)	5.356	\$2.55	\$3.00	\$0.45	15.00	4.56	\$2.65	\$1.50
H6	5.0 \$0.60 (133.33)	3.3 \$0.30 (5252.53)	6.0 \$0.75 (4111.11)	3.3 \$0.30 (5252.53)	5.0 \$0.60 (133.33)	5.734	\$2.55	\$3.40	\$0.85	25.00	4.52	\$2.65	\$1.50
H7	5.0 \$0.60 (133.33)	3.2 \$0.30 (6190.48)	6.0 \$0.75 (4111.11)	3.2 \$0.30 (6190.48)	5.0 \$0.60 (133.33)	5.092	\$2.55	\$3.00	\$0.45	15.00	4.48	\$2.25	\$1.50
H8	5.0 \$0.60 (133.33)	3.1 \$0.30 (5977.01)	6.0 \$0.75 (4111.11)	3.1 \$0.30 (5977.01)	5.0 \$0.60 (133.33)	5.225	\$2.55	\$3.00	\$0.45	15.00	4.44	\$2.25	\$1.50
H9	5.0 \$0.60 (133.33)	3.0 \$0.30 (5777.78)	6.0 \$0.75 (4111.11)	3.0 \$0.30 (5777.78)	5.0 \$0.60 (133.33)	5.356	\$2.55	\$3.00	\$0.45	15.00	4.40	\$2.25	\$1.50

Table A5.4 (j): Pricing analysis for Group BVI

Groups	Shook MOE / Price per meter (NZ\$) / (Integrated value)					Model MOE (GPa)	Model Cost (NZ\$)	Model Selling Price (NZ\$)	Gross Profit (NZ\$)	Gross Profit (%)	Mean MOE (GPa)	Mean MOE (NZ\$)	Minimum MOE (NZ\$)
	Shook 1	Shook 2	Shook 3	Shook 4	Shook 5								
I1	11.0 \$3.00 (60.61)	6.0 \$2.5 (2888.89)	11.0 \$3.00 (4484.85)	8.0 \$2.34 (2166.67)	9.0 \$2.52 (74.07)	8.82	\$13.36	\$12.15	-\$1.21	-9.96	9.0	\$12.60	\$3.75
I2	6.0 \$0.75 (111.11)	12.0 \$3.30 (1444.44)	11.0 \$3.00 (4484.85)	12.0 \$3.30 (1444.44)	5.0 \$0.60 (133.33)	11.20	\$10.95	\$15.00	\$4.05	27.00	9.2	\$12.60	\$3.00
I3	6.0 \$0.75 (111.11)	8.0 \$2.34 (2166.67)	12.0 \$3.30 (4111.11)	12.0 \$3.30 (1444.44)	5.0 \$0.60 (133.33)	10.71	\$10.29	\$14.25	\$3.96	27.79	8.6	\$12.15	\$3.00
I4	10.0 \$2.70 (66.67)	6.0 \$0.75 (2888.89)	10.0 \$2.70 (4933.33)	11.0 \$3.00 (1575.76)	5.0 \$0.60 (133.33)	8.89	\$9.75	\$12.15	\$2.40	19.75	8.4	\$11.70	\$3.00
I5	8.0 \$2.34 (83.33)	7.0 \$1.80 (2476.19)	9.0 \$2.52 (5481.48)	7.0 \$1.80 (2476.19)	9.0 \$2.52 (74.07)	8.06	\$10.98	\$11.70	\$0.72	6.15	8.0	\$11.70	\$9.00
I6	6.0 \$0.75 (111.11)	12.0 \$3.30 (1444.44)	11.0 \$3.00 (4484.85)	9.0 \$2.52 (1925.93)	9.0 \$2.52 (74.07)	10.61	\$12.09	\$14.25	\$2.16	15.16	9.4	\$12.60	\$3.75
I7	7.0 \$1.80 (95.24)	12.0 \$3.30 (1444.44)	8.0 \$2.34 (6166.67)	6.0 \$0.75 (2888.89)	7.0 \$1.80 (95.24)	7.98	\$9.99	\$10.35	\$0.36	3.48	8.0	\$11.70	\$3.75
I8	5.0 \$0.60 (133.33)	6.0 \$0.75 (2888.89)	12.0 \$3.30 (4111.11)	8.0 \$7.80 (2166.67)	4.0 \$0.45 (166.67)	9.01	\$12.90	\$12.60	-\$0.30	-2.38	7.0	\$9.00	\$2.25
I9	11.0 \$3.00 (60.61)	8.0 \$2.34 (2888.89)	12.0 \$3.30 (4111.11)	10.0 \$2.70 (2166.67)	6.0 \$0.75 (166.67)	9.08	\$12.09	\$12.60	\$0.51	4.05	9.4	\$12.60	\$3.75

